The University Of Sheffield.

The Involvement of P2X7R Signalling in LOX Mediated Formation of a Pre-Metastatic Niche in Bone

Iain D. Huggins

A thesis submitted in partial fulfilment of the requirements for the degree of

Doctor of Philosophy

The University of Sheffield

Faculty of Medicine, Dentistry, and Health

Department of Human Metabolism

Academic Unit of Bone Biology

Submitted February 2016

ACKNOWLEDGEMENTS

First and foremost, I would like thank my supervisor, Allie, for giving me the opportunity to undertake this PhD and for her support, patience, and reassurance throughout my studies in Sheffield. Without her guidance I would never have been able to complete this project and gain the valuable experiences that it has provided me. I'm particularly grateful for her organisation and encouragement to get involved with the STEM project, which was extremely rewarding. I would also like to thank Robin for stepping in as my second supervisor, for answering countless questions, and most importantly for keeping the now retired loading machine running just long enough to let me finish my work. I would also like to thank both Allie and Robin for their contribution to my research by undertaking all schedule 1 regulated activities in the *in vivo* work conducted in this thesis. I am also indebted to our collaborators, Janine Erler and Thomas Cox, from the University of Copenhagen for laying down the groundwork that made this project possible. Thanks are also due to Kim Naylor and Penelope Ottewell who performed the orthotopic tumour injections for this study, and Lang Yang for finite element analysis to calculate desired loading force.

I'm extremely grateful to the other members of the Gartland Bone Group, past and present, who've made my PhD so memorable and enjoyable. It has been a privilege and a pleasure to work alongside Karan, Ankita, Ning, Eric, and Magda. Special thanks also go to Zahra for teaching me how to Western Blot, Holly for training me in CT scanning and analysis, and to Gareth for sharing his extensive knowledge of myriad lab equipment, procedures, and techniques.

My time in Sheffield would not have been the same without the friendship of Aban, David, Karl, Lisa, and Sarah. Thanks for all the fun times we had away from the lab, and especially for good times at the Red Deer Pub Quiz. I'm sure we'll win next time! Also to Helen and Dea for livening up committee meetings and introducing me to Danish Christmas.

I would like to dedicate my thesis to Karima, my best friend throughout my time in Sheffield, who made the city a much brighter, colourful, and exciting place. She is sorely missed by all who knew her, and the place will never be the same without her.

Finally, I would like to extend my deepest thanks to my parents, David and Linda, for their belief and support all throughout my education, and particularly in the final months of my PhD. I couldn't have made it this far without your encouragement and your love. Thank you for all your patience.

ABSTRACT

Metastasis to bone seriously complicates treatment of cancer, resulting in an incurable and debilitating condition which can greatly decrease quality of life as a result of excessive bone destruction. Recent research has identified tumour secreted LOX as a contributor to cancer induced bone loss, by generating osteolytic lesions prior to cancer cell arrival, thus contributing to pre-metastatic niche formation, and enhancing metastatic cell recruitment and survival in bone. Previous research has also observed that LOX accumulates at areas of pressure, and is hypoxically regulated, highlighting a potential involvement with P2X7R, which contributes significantly to cancer cell survival and osteoclastic resorption of bone. This thesis builds on these observations by investigating the involvement of LOX and P2X7R in pre-metastatic modification of bone in a syngeneic BALB/c mouse/4T1 murine breast cancer model. Analysis of μCT data from the tibia of tumour bearing mice revealed significantly reduced bone destruction upon knockdown of LOX in the tumour, or knockout of P2X7R in the mouse, confirming an interaction. These observations were repeated in cancer cell free mice, receiving injections of conditioned medium from 4T1 cells grown *in vitro*, confirming that bone destruction and osteolytic lesion formation are the result of secreted factors from the primary tumour, and can occur prior to cancer cell arrival at the bone. The effect of mechanical loading upon LOX/P2X7R modification of pre-metastatic bone was also investigated by subjecting tumour bearing mice to non-invasive axial loading of the right hindlimb. Mechanical loading was found to have a mixed effect on bone, driving thickening of cortical and trabecular bone, but also osteolytic lesion formation. P2X7R contributed to bone response to loading, while tumour-secreted LOX had no effect. Taken together, mechanical loading and P2X7R inhibition were found to effectively combat tumour induced bone loss, identifying novel targets for future treatments of metastatic bone disease.

TABLE OF CONTENTS

LIST OF FIGURES

LIST OF TABLES

LIST OF ABBREVIATIONS

µCT	Micro computed tomography
ALP	Alkaline phosphatase
ATP	Adenosine triphosphate
BAPN	β-aminopropionitrile
BMDC	Bone marrow derived cells
BMP	Bone morphogenetic protein
BV/TV	Percentage bone volume (bone volume / tissue volume)
BzATP	2,3 (4-benzoyl) benzoyl adenosine triphosphate
cAMP	Cyclic adenosine monophosphate
CM	Conditioned medium
CRL	Cytokine receptor-like domain
DAO	Diamine oxidase
DMEM	Dulbecco's modified eagle medium
DPBS	Dulbecco's phosphate buffered saline
ECM	Extra-cellular matrix
FAK	Focal adhesion kinase
FBS	Foetal bovine serum
GSK	GlaxoSmithKline
HCl	Hydrochloric acid
HIF-1α	Hypoxia-inducible factor 1-α
IC_{50}	Half maximal inhibitory concentration
IGF	Insulin-like growth factor
IL	Interleukin
LOX	Lysyl oxidase
LOXL	Lysyl oxidase-like
LOX-PP	Lysyl oxidase propeptide
MAPK	Mitogen-activated protein kinases
M-CSF	Macrophage colony stimulating factor
MMP	Matrix metalloproteinase
mRNA	Messenger ribonucleic acid
MTS	[3-(4,5-dimethylthiazol-2-yl)-5-(3-carboxymethoxyphenyl)-2-(4-sulfophenyl)-2H-tetrazolium, inner salt]
NBF	Neutral buffered formalin
NFATc1	Nuclear factor of activated T-cells, cytoplasmic, calcineurin-dependent 1
nsd	no statistical difference
OD	Optical density
OIS	Oncogene induced senescence
OPG	Osteoprotegerin
P2X7R	P2X7 receptor
$P2Y_2R$	$P2Y_2$ Receptor
PBS	Phosphate buffered saline
PCR	Polymerase chain reaction
Pen-Strep	Penicillin - streptomycin
PDGF	Platelet derived growth factor
PlGF	Placental growth factor
proLOX	LOX proenzyme

PTHrP	Parathyroid hormone related peptide
RANK	Receptor activator of nuclear factor κ-B
RANKL	Receptor activator of nuclear factor κ-B ligand
rLOX	Recombinant LOX protein
RNA	Ribonucleic acid
ROI	Region of interest
RT	Reverse transcriptase
S100A8 / A9	Inflammatory S100 cytokine A8 / A9
SAA3	Serum amyloid A3
SDF	Stromal derived growth factor
shRNA	Short hairpin ribonucleic acid
SMI	Structure model index
SSAO	Semi-carbazide-sensitive amine oxidase
Tb No.	Trabecular number
Tb Th	Trabecular thickness
TGF-β	Tumour growth factor β
TNF-α	Tumour necrosis factor α
TRAP	Tartrate resistant acid phosphatase
VEGF	Vascular endothelial growth factor

CHAPTER 1:

INTRODUCTION

1.1 Introduction

Metastatic bone disease strongly contributes to mortality and morbidity among cancer patients, making treatment more difficult and causing multiple symptoms including weakened bone, pain, and potentially life-threatening levels of hypercalcaemia. Formation of a pre-metastatic niche in the secondary microenvironment to prime the area for cancer cell arrival is reported to be crucial for the development of metastases, and as such understanding the mechanisms by which this happens in bone will allow for the development of preventative treatments to combat the initial formation of metastases in bone. This is doubly important given the process known as "the vicious cycle of bone metastasis", a positive feedback cycle caused by metastatic destruction of bone, resulting in the release of a number of factors from the bone matrix which promote cancer cell recruitment, adhesion, and survival. It is therefore of paramount importance to prevent metastases as early as possible, as once established they can increase exponentially.

Lysyl Oxidase (LOX) has recently been identified as a novel contributor to the pre-metastatic niche in bone by promoting osteoclastic bone destruction and inhibiting osteoblastic bone growth, the net effect of which generates osteolytic lesions in bone, facilitating cancer cell colonisation and survival. While the mechanism by which LOX drives osteoclastic cell activity is partly understood, the exact mechanism by which LOX drives metastasis to bone remains unknown. This is of particular importance in metastatic bone disease, where current treatment is almost solely dependent on bisphosphonates to prevent osteoclastic bone destruction. Bisphosphonate treatment, however, has shown only limited effectiveness in combating skeletal related events (e.g. fractures). Furthermore, it does not repair bone loss sustained prior to the application of treatment, and more importantly has been shown to be ineffective in certain groups, such as pre-menopausal women. It is, therefore, highly important to identify new targets for the prevention of cancer cell metastasis to bone.

This introduction will provide a brief overview of the principles of bone remodelling and metastatic bone disease, and continue with a more in depth review of both LOX and P2X7R and their respective roles in bone, cancer, and their potential for interaction.

1.2 Bone Remodelling

Bone is a living, growing, tissue, constantly undergoing a process of remodelling via the coupling of osteoclast-mediated bone resorption, and osteoblast-mediated bone formation. The continual turnover of bone allows repair and replacement of damaged bone, as well as dynamic changes to bone structure and microarchitecture which alter bone to a form best able to withstand the local stresses and strains to which it is habitually subjected (Ruff et al. 2006). It is, therefore, important that a balance is maintained between osteoclastic and osteoblastic activity to ensure a net maintenance of bone mineral. Two inter-related metabolic pathways known to regulate the bone remodelling process are the Receptor Activator of Nuclear Factor κB (RANK)/RANK ligand (RANKL)/Osteoprotegerin (OPG) (RANK/RANKL/OPG) pathway, which regulates osteoclast activity (Boyce & Xing 2007); and the Wnt/β-catenin pathway which directly regulates osteoblast activity and indirectly regulates osteoclast activity via its actions on osteoblast cells (Roodman 2004; Boyce et al. 2005).

Receptor Activator of Nuclear Factor κB (RANK) and its ligand (RANKL) play a key role in the regulation of bone remodelling by driving the fusion of mononuclear osteoclast precursor cells to form mature, resorbing osteoclasts (Arai et al. 1999; Miyamoto et al. 2000). RANK is a transmembrane receptor protein expressed on a number of different cell types, including mature osteoclasts and their precursors. RANKL protein is found in numerous different cell types, including osteoblasts and T-lymphocytes, and may be expressed in either membrane-bound or soluble isoforms (Virk & Lieberman 2007). Stimulation of RANK by RANKL results in the activation of multiple intracellular signalling cascades within precursor osteoclast cells, which ultimately lead to the formation, maturation, and survival of osteoclasts, thereby increasing osteoclastic resorptive activity (Boyce & Xing 2007; Guise 2010). The final component of the RANK/RANKL/OPG pathway is osteoprotegerin (OPG), released from osteoblasts and stromal cells. OPG acts as a decoy receptor for RANKL, competitively antagonising RANKL/RANK signalling, and thus protecting bone from resorption by both reducing the rate of osteoclastogenesis, and increasing the rate of osteoclast apoptosis (Yasuda et al. 1998; Simonet et al. 1997).

The Wnt/β-catenin pathway is recognised as a substantial regulator of osteoblastic activity in the process of bone remodelling (Roodman 2004; Kramer et al. 2010). Current evidence shows that Wnt, signalling via β-catenin, commits mesenchymal cells to differentiate along the osteoblast cell lineage, promoting the production and maturation of osteoblasts (Boyce et al. 2005; Guise 2010). Wnt signalling has also been shown to interact with the RANK/RANKL/OPG pathway by directly promoting OPG expression in osteoblasts, thus the pathway is able to

simultaneously promote osteoblastogenesis while inhibiting osteoclast formation and survival. This results in a powerful shift towards bone formation in the process of bone remodelling.

Further evidence for the intertwined nature of both RANK/RANKL/OPG and Wnt/β-catenin pathways has recently been reported, with both pathways shown to be under regulation by parathyroid hormone (PTH), where continual dosage with PTH drives osteoclast activity, and intermittent dosage drives osteoblastic activity (Silva & Bilezikian 2015). A similar factor known to influence these bone remodelling pathways is parathyroid hormone related peptide (PTHrp). This is of particular importance in cancer, where release of TGF-β from tumour cells stimulates the release of PTHrp, increasing RANKL production while inhibiting that of OPG, causing a shift towards osteolysis (Guise 2010).

While there are many factors which contribute to bone remodelling in some manner or other, one recently discovered contributor, of interest to this study, is Lysyl Oxidase (LOX), which has recently been shown to regulate bone remodelling cell activity independent of the RANK/RANKL/OPG pathway. LOX has been shown to promote osteoclastogenesis and increase the resorptive activity of osteoclasts, while simultaneously reducing osteoblast proliferation and increasing terminal differentiation of osteoblasts (Cox et al. 2015). The intricacies of the mechanism by which LOX achieves this powerful shift towards bone breakdown are yet to be fully investigated, but H_2O_2 (a by-product of LOX enzymatic activity), driving translocation of NFATc1 (nuclear factor of activated T-cells, cytoplasmic, calcineurin-dependent 1), the master regulator of osteoclast cell function, to the osteoclast cell nucleus has been identified as a key step (Cox et al. 2015).

As is this case with other areas of metabolism, regulation of bone remodelling is mediated by a complex network of different signalling pathways, with further work required to map known pathways, and discover as yet unknown mediators. Regardless of the mechanisms involved, however, maintenance of homeostasis in bone remodelling is of paramount importance to ensure that bone mass remains constant, avoiding complications associated with excessive bone loss or gain, and ensuring healthy bone maintenance. This is particularly important in diseases which cause pathological bone destruction, such as osteoporosis and cancer induced bone disease.

1.3 Metastasis to Bone

1.3.1 The Metastatic Process

Metastatic disease is the leading cause of mortality and morbidity in cancer, with the majority of cancer patient's suffering resulting from the spread of cancer to distant secondary sites, rather than from the initial primary tumour (Chambers et al. 2002; Weigelt et al. 2005). Despite this observation, the majority of cancer research has historically focussed on the primary tumour, resulting in a better understanding of primary tumour growth than the conditions favouring metastasis (Peinado et al. 2011). It has also become increasingly understood that metastasis is a complex process, requiring the completion of a number of discrete steps before the successful colonisation of a secondary site by travelling tumour cells. These metastatic stages are thoroughly reviewed by Hanahan and Weinberg (2011). In order to successfully metastasise, cancer cells must detach from the primary tumour, invade local connective tissue, intravasate local vasculature, travel through the circulatory system, arrest in a distant capillary bed, extravasate, adhere to tissue at the secondary site, survive, and proliferate in their new microenvironment. All of these steps must be completed while also avoiding detection by the host immune system (Chambers et al. 2002; Guise 2010). While these challenges to metastasis seem thorough, it has been proposed that they can act like a form of natural selection, allowing only the fittest and most viable cells to form secondary tumours (Nguyen et al. 2009). Furthermore, the sheer number of cancer cells estimated to be shed ($1x10^6$ per gram of primary tumour per day) are proposed to contribute to metastatic success by overwhelming the seemingly insurmountable odds of metastasis with sheer numbers: while only a miniscule percentage of tumour cells may successfully metastasise, if enough are shed from the primary tumour a significant number will succeed in spreading to, and growing in, a secondary site (Chang et al. 2000).

In order to successfully achieve the final stages of this metastatic process, the local tissue microenvironment at the distant site must also be conducive to tumour cell survival and proliferation, highlighting the importance of metastatic site as well as metastatic cell. Despite the extensive and complex series of obstacles which a successfully metastasising cell must overcome, metastasis remains a persistent and challenging problem in cancer, contributing significantly to patient mortality and morbidity.

1.3.2 Metastatic Bone Disease

Metastatic bone disease is of particular concern due to the myriad complications it adds to an already serious disease. Once cancer has metastasised to bone it becomes more resistant to radiation, hormone and chemotherapies, to the extent that it is considered to be an incurable condition (Roodman 2004; Li et al. 2012). Surgical removal is also complicated, and more likely to leave physical disfigurement and disability. Bone is the most common metastatic site in cancer (Coleman 2006), and is of particular concern in breast and prostate cancers, the most common cancers affecting women and men, respectively, which are also the most common cancers to metastasise to bone. Around 70% of patients who die from breast and prostate cancer show evidence of metastatic bone disease (Coleman 2006; Rosen 2013) highlighting the prevalence of this secondary complication on top of the initial cancer. A study of 718 breast cancer patients found that over 50% developed skeletal complications, of whom 51% had more than one complication. The incidence of skeletal complications also increased to 80% when considering only women with metastases limited to the bone at first relapse (Domchek et al. 2000). These figures highlight the significant morbidity resultant from bone metastases.

Cancers of the bone may be segregated radiographically into those resulting in bone destruction, '*osteolytic*'; excess bone production, '*osteoblastic*'; or both osteolytic and osteoblastic activities, '*mixed*' (Roodman 2004). These classifications, however, have been described as overly simplistic, and it has been noted that most cancers affecting bone display a continuum of dysregulation in both bone resorption and formation, with patients exhibiting both remodelling activities to some degree (Bussard et al. 2008). The range of morbidities associated with bone metastatic disease are almost exclusively the result of interference in the bone remodelling process and the coupling of osteoclastic and osteoblastic activity. Specifically, the majority, if not all, bone metastatic disease morbidities result from problems associated with pathological bone destruction. Thus metastatic bone disease is a direct result of interactions between cancer cells and cells of the bone micro-environment, resulting in dysregulation of bone remodelling and an overall shift towards osteoclastic cell activity and bone destruction (Coleman 2002).

Skeletal complications from bone metastases may manifest in a number of different clinical features. One of the more prevalent features, having a considerably detrimental effect on quality of life, is pain. Bone metastases are the most common cause of cancer-related pain (Mercadante 1997), and while the mechanisms remain poorly understood, it is proposed that contributions from both the cancer cells themselves, and the increased osteolysis they cause, are responsible. Tumour cell production of growth factors and cytokines, coupled with direct infiltration of nervous tissue by secondary tumours are possible contributors to pain, as are

increased pressure in bone, either from the metastases themselves or the loss of load-bearing ability due to bone mineral destruction. Microfractures, stretching of the periosteum, and nerve compression by collapsed vertebrae are also listed as potential contributors (Coleman 2006; Mercadante 1997). While osteolysis has been argued to be a key contributor to cancer-related bone pain, one study has shown that while ~80% of patients with advanced stage breast cancer develop osteolytic bone metastases, almost two thirds of the metastatic sites are painless (Front et al. 1979). This suggests that osteolysis and the subsequent release of chemical messengers trapped in bone matrix is not essential for the development of pain, though does not rule it out as a contributing factor. The extent of cancer-related bone pain is often so severe that treatment with systemic opioids is contraindicated because the doses required to be effective carry unacceptable side-effects. As such low dose, single session radiotherapy (coupled with pharmacological management) is advised as the gold standard treatment for localised bone pain (Mercadante 1997; Schneider et al. 2012).

Other skeletal complications are more directly tied to the process of osteolysis, such as the weakening of bone resulting in microfractures which may progress to pathological long bone fracture as bone destruction continues, further reducing load bearing capability. In addition to long bone, fractures of the spinal column (the other major load bearing area of the skeleton) are also a danger, resulting in spinal cord compression, pain, and spinal instability (Domchek et al. 2000). There is relatively little published data on incidence of cancer induced fracture at specific skeletal sites, but a recent study of 151 cancer patients reported that 70.2% of the cohort presented with pathological fractures, of whom 52.7% had long bone fractures, 44.5% had fractures of the axial skeleton (i.e. skull, ribs, and spine), and 2.8% had fractures of both (Singh et al. 2014). These observations highlight both the high incidence of fracture in metastatic bone disease as well as the detrimental effect on the whole skeleton, with both long bones and the axial skeleton being similarly affected.

Finally, a further complication of osteolysis is the release of calcium from the bone matrix into the circulation, resulting in hypercalcaemia. Symptoms of this may include fatigue, weakness, anorexia, and confusion in the early stages; progressing to muscle spasms, bone pain, arrhythmias, coma, and death if left untreated (Cancer Research UK 2014).

It is evident that the incidence of skeletal complications in bone metastatic disease is correlated with mortality. A retrospective study of 859 patients with metastatic bone disease (secondary from breast cancer) allotted patients into four groups based on the presence of metastases: bone only; bone and soft tissue; bone and lung; and bone and liver (Plunkett et al. 2000). No difference was found between these groups in time to pathological long bone fracture, suggesting that metastases in sites other than bone do not affect development of

complications in bone. Patients with metastases limited to the bone had the longest survival rate of the groups (median 24 months), while those who also had liver metastases had the shortest survival (median 5 months). Subsequently, patients with bone only metastases had the highest rate of fracture (1 fracture to every 5.8 patients), and those with liver disease had the lowest fracture rate (1 fracture to every 22.2 patients). This disparity is likely a reflection of the mortality rates in the respective diseases. The shortest median time to first skeletal complication in patients with bone metastatic disease is reported to be 11 months (Domchek et al. 2000). As patients with bone and liver metastases survived only a median 5 months, the majority died before metastatic disease could progress sufficiently to cause long bone fracture. Patients with bone only metastases, however, survived longer and therefore the disease process had longer to manifest, resulting in the increased rate of pathological fracture.

As a result of the prolonged survival and increased morbidity associated with osteolytic bone metastases, current treatment focusses on the inhibition of osteoclast cell activity. This is achieved by treatment with bisphosphonates, which inhibit osteoclast activity and survival (Drake et al. 2008; Fleisch 2002), while also having antiproliferative and antiangiogenic effects (Coleman et al. 2012). Bisphosphonate treatment has been reported to greatly improve the systemic management of patients with advanced breast cancer as a result of its action in decreasing the frequency and morbidity of skeletal complications in bone metastatic disease (Blanchette & Pritchard 2015). Different bisphosphonates have been shown to reduce skeletal related events by between 20 and 40%, depending on the specific drug used and the population studied (Blanchette & Pritchard 2015). A meta-analysis of 9 studies (including 2806 patients overall), however, showed that bisphosphonate treatment resulted in an overall reduction of skeletal related events by only 15% compared to placebo control (Wong et al. 2012). It is therefore important to continue further exploratory research in order to identify new potential targets for the management of metastatic bone disease in order to compliment current treatment regimes, and prevent the establishment of bone metastases in the first instance.

1.3.3 Pre-Metastatic Niche Formation and The Vicious Cycle of Bone Metastases

While the majority of metastatic research has traditionally focussed on metastatic cells, it is becoming increasingly understood that the role of the metastatic site microenvironment is just as crucial to the success of metastasis as that of the metastatic cell itself (Guise 2010). The process of metastasis can be aided by modification of the secondary site microenvironment, prior to cell arrival, to prime the area to capture metastatic cells and increase their chances of survival. A micro-environment modified in this way is referred to as a 'pre-metastatic niche' (Kaplan et al. 2005). It has also been proposed that pre-metastatic priming is critical, rather than simply beneficial, for engraftment of metastasising cells (Psaila & Lyden 2009). A number of different factors and their pre-metastatic modifications at different sites have been discovered and are summarised below in table 1.1.

Table 1.1: Factors Involved in the Pre-Metastatic Niche

Factor	Name	Action
VEGFA	Vascular Endothelial Growth Factor	Upregulated in pre-metastatic sites, leading to the clustering of bone marrow derived haematopoietic progenitor cells.
PlGF	Placental Growth Factor	
TGFβ	Transforming Growth Factor-Beta	
S100A8 S100A9	Inflammatory S100 chemokines	
SAA3	Serum Amyloid A3	
Platelet-deployed SDF1	Stromal derived growth factor 1	Chemotactic for CXCR4+ haematopoietic stem cells, and metastatic tumour cells.
TNF-α	Tumour Necrosis Factor-alpha	Increases tumour cell proliferation, increases vascular permeability, recruits other host cells to niche
MMP9	Matrix metalloproteinase 9	Breakdown of basement membranes, allowing release of VEGFA and KIT ligand to attract c-Kit+ invasive cells
Fibronectin	Fibronectin	Promotes adhesion of cancer cells in secondary environment
LOX	Lysyl Oxidase	Promotes osteolysis, releasing tumour supporting factors stored in bone.

Once a migratory cancer cell successfully metastasises, the pre-metastatic niche is considered to progress to a '*micro-metastasis'*, which in turn will become a *'macro-metastasis'* upon the establishment of a blood supply to nourish the growing tumour. Progression through all three of these phases is critical for the establishment of a secondary cancerous growth (Guise, 2010).

The concept of the pre-metastatic niche is relatively novel, and more research is required to understand the intrinsic components which define it, the stages of its formation, and the factors involved in its genesis. It is believed that pre-metastatic niche formation is driven by chemical messengers released by the primary tumour (Hiratsuka et al., 2006, Hiratsuka et al., 2008, Kaplan et al., 2005), though whether this signal is released from the primary tumour itself, or by metastatic cells passing through the site of future metastasis, or both, is not known. It is also unclear whether pre-metastatic niches are formed *de novo*, or modified from existing physiological niches within the body (Psaila and Lyden, 2009) – a particularly important consideration for bone, housing the haematopoietic stem cell niche.

Another factor highlighting the considerable importance of the pre-metastatic niche for bone metastasis is the process known as 'The Vicious Cycle of Bone Metastasis', a positive feedback loop which exploits osteolytic bone resorption to fuel the growth of tumour cells (Bussard et al. 2008; Guise & Mundy 1998). This process involves the co-ordinated, reciprocal interaction of metastasised tumour cells, bone cells (osteoclasts and osteoblasts), and bone matrix (Virk and Lieberman, 2007). Tumour cells interfere with the RANK/RANKL/OPG pathway by secreting a number growth factors and cytokines, including interleukin-6 (IL-6) and tumour necrosis factor alpha (TNF-α), which induce osteolysis by upregulating RANKL expression in osteoblasts and stromal cells, promoting the formation of resorptive osteoclasts (Wittrant et al., 2004, Guise et al., 2005, Kitaura et al., 2005, Ara and DeClerck, 2011). The subsequent breakdown of bone matrix results in the release of growth factors stored therein, including Tumour Growth Factor beta (TGF-β) and bone morphogenetic protein (BMP) – both of which have been shown to promote an invasive phenotype in cancer cells (Taylor et al., 2011, Uzel et al., 2001). These released factors not only promote the initial growth of established metastatic tumour cells, but may also attract more metastasising tumour cells to the bone microenvironment (Feeley et al., 2005, Hauschka et al., 1986). The increased proliferation of the metastatic tumour leads to an increase in tumour mass, and a concordant increase in the release of pro-osteoclastic growth factors and cytokines, thus promoting further osteolysis and perpetuating a cycle of cancer growth and bone destruction. Table 1.2, below, gives a brief overview of some of the growth factors and cytokines involved in the vicious cycle, as listed by Virk and Lieberman (2007), while Figure 1.1 gives an overview of the vicious cycle process. As a result of the vicious cycle, osteolytic tumours become more debilitating, with increased tumour burden and acceleration

of bone loss. The positive feedback nature of this cycle highlights the importance of preventing the initial metastasis to bone, thereby removing any amplificatory effect produced by the vicious cycle.

Table 1.2: Summary of Factors and Cytokines Involved in the Vicious Cycle

	Name	Abbreviation
Growth Factors and Cytokines Released by Tumour Cells	Parathyroid Hormone Related Peptide	PTHrP
	Interleukin-1	IL-1
	Interleukin-6	Il-6
	Interleukin-8	Il-8
	Interleukin-11	Il-11
	Tumour Necrosis Factor-alpha	TNF-α
	Receptor Activator of nuclear factor κB ligand	RANKL
Growth Factors Released from Bone Matrix	Insulin-like Growth Factor	IGF
	Transforming Growth Factor-beta	TGF-β
	Bone Morphogenetic Protein	BMP
	Platelet Derived Growth Factor	PDGF
	Vascular Endothelial Growth Factor	VEGF

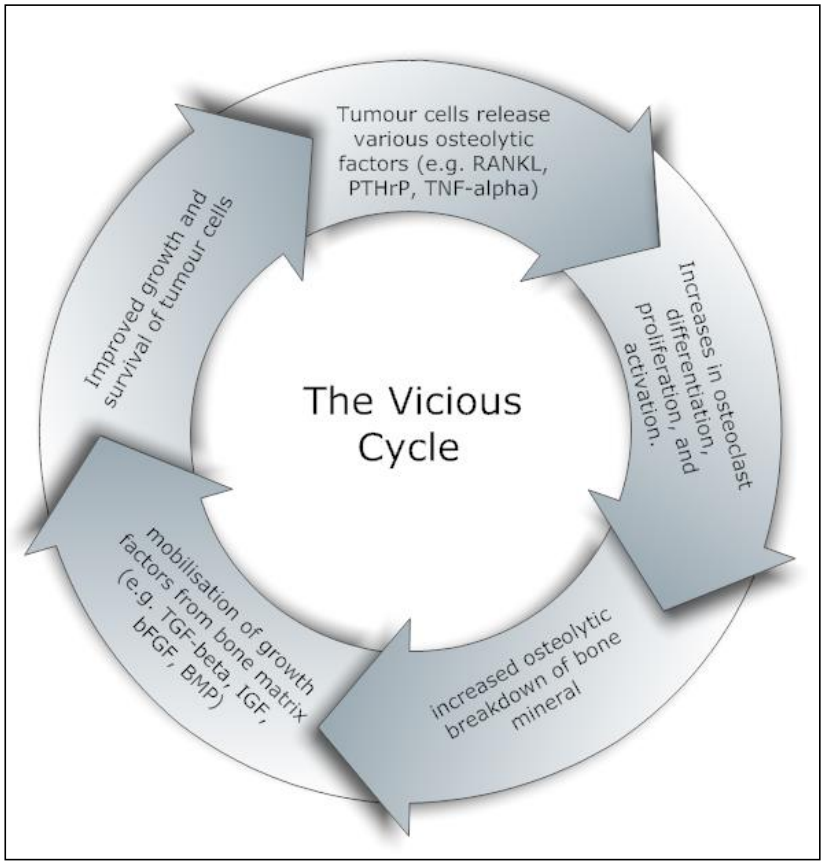

Figure 1.1: Overview of 'The Vicious Cycle' of Bone Metastasis. Representative overview of the vicious cycle of bone metastasis, a positive feedback cycle in which osteolytic factors released from cancer cells drive excessive osteoclastic bone resorption, releasing growth factors from the mineral matrix which potentiate cancer cell growth and survival (Guise 2010), in turn leading to a greater number of cancer cells releasing a greater volume of osteolytic factors, leading to yet further bone destruction.

1.4 Lysyl Oxidase

Lysyl Oxidase (LOX) is a copper-dependent amine oxidase, belonging to a family of enzymes which oxidise primary amine substrates to form reactive aldehydes (Csiszar, 2001). The LOX family is comprised of LOX and LOX-like proteins (LOXL, LOXL2, LOXL3, and LOXL4), and exists as a subgroup of the amine oxidase family, which is identifiable by the presence of topaquinone: a modified tyrosine side chain utilised as a redox cofactor (Csiszar 2001; Wang et al. 1996). Other amine oxidases include Diamine oxidase (DAO) and monoamine metabolising semi-carbazide-sensitive amine oxidase (SSAO) (Dove et al., 1996, Janes et al., 1992, Lyles, 1996). The LOX family are identifiable from these other enzymes by a highly conserved amino acid sequence, defining major structural and functional domains within the C-terminal of the molecule. In particular, the copper-binding domain encoded within this region is unique to the lysyl oxidase family, containing four histidines whereas other known copper-binding domains have only two or three (Csiszar, 2001). Other features encoded in this conserved C-terminal domain include a cytokine receptor-like domain, and residues for lysine tyrosylquinone cofactor formation (Csiszar 2001; Molnar et al. 2003).

The amino acid sequence, and hence structure, of LOX is highly conserved between a number of species, including: human, cow, mouse, rat, chick, fish, and drosophila (Csiszar, 2001, Kagan and Li, 2003, Langenau et al., 1999). LOXL proteins share the highly conserved C-terminal region with LOX, but differ distinctly in the N-terminal half of the protein, thus the LOXL proteins share the collagen-cross linking abilities of LOX (associated with the copper binding site), but with distinct, unique structures of their own (Fig. 1.2). The LOXL proteins are relatively recent discoveries and more research is required to understand how their physiological role may differ from that of LOX, however they have been shown to fulfil similar functions while displaying different expression patterns in various cancer cell lines (Wong et al., 2011).

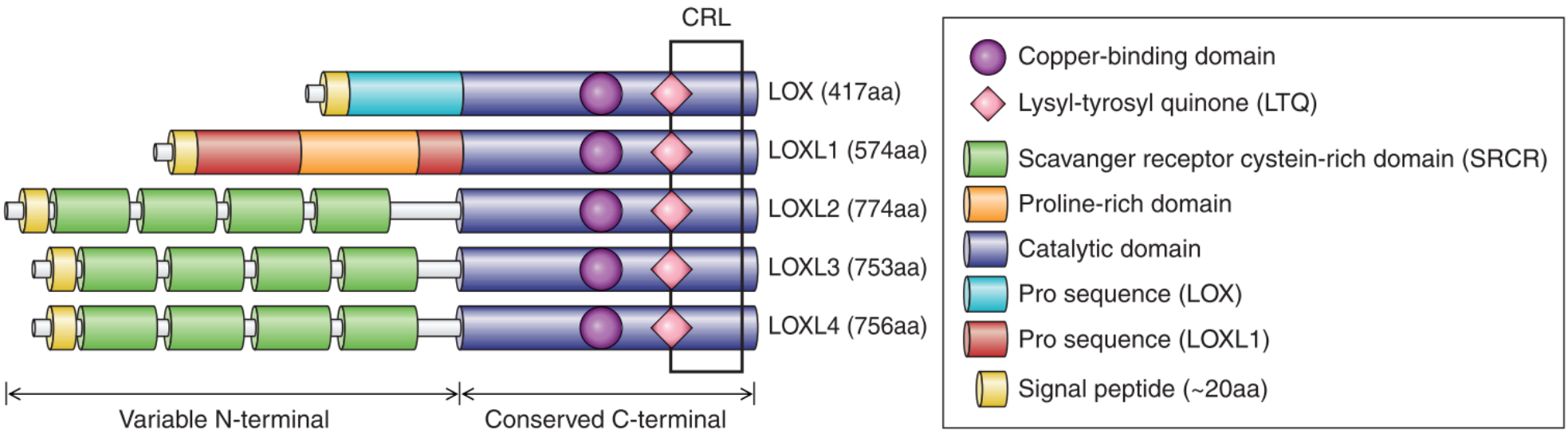

Figure 1.2: A Comparison of Conserved Domains within Human LOX and LOXL proteins: All LOX family members share a conserved C-terminus, containing a unique copper-binding domain; a cytokine receptor-like domain (CRL); and lysyl-tyrosyl quinone cofactor site (LTQ). The N-terminus varies between family members. The number of amino acids for each protein is also given in brackets for each protein. Reproduced from Figure 1 (Cox & Erler 2013), copyright © 2012, American Journal of Physiology- Gastrointestinal and Liver Physiology .

1.4.1 LOX Synthesis

LOX is first synthesised as a 46kDa preprotein, containing an N-terminal signal peptide sequence, contiguous with a propeptide domain, followed by the catalytic domain. The signal peptide is cleaved, and the propeptide domain N-glycosylated during passage through the Golgi apparatus. This process yields a 50kDa proenzyme (proLOX), which is secreted as a catalytically inactive protein (Panchenko et al., 1996, Trackman et al., 1992). A final proteolytic cleavage of the proLOX molecule, by pro-collagen C-proteinases (the most efficient of which is bone morphogenetic protein I (BMP-1)) occurs in the ECM and results in the mature, catalytically active 32kDa protein LOX (Uzel et al., 2001) and an 18kDa propeptide, lysyl oxidase propeptide (LOX-PP) (Vora et al., 2010). The synthesis and processing of LOX is summarised below in figure 1.3. A number of different factors have been found to regulate LOX expression, covering a vast array of responses from different cells and tissues, and these are reviewed by Csiszar (2001). Of particular interest from this review are prostaglandin E2, which reduces LOX enzyme activity in rat lung fibroblasts, contributes to osteoblastic and osteoclastic bone remodelling (Jee & Ma 1997; Norrdin et al. 1990) and bone response to loading (Li et al. 2005); and fibroblast growth factor (FGF), which affects LOX mRNA levels in mouse osteoblasts both positively and negatively, in a dose-dependent manner (Vora et al. 2010). Other factors of interest include: TGF-β, platelet derived growth factor (PDGF), cyclic adenosine monophosphate (cAMP), hypoxia-inducible factor 1 (HIF-1), and testosterone – all of which are involved with cancerous growth (Csiszar 2001; Erler et al. 2006; Taylor et al. 2011; Wong et al. 2011).

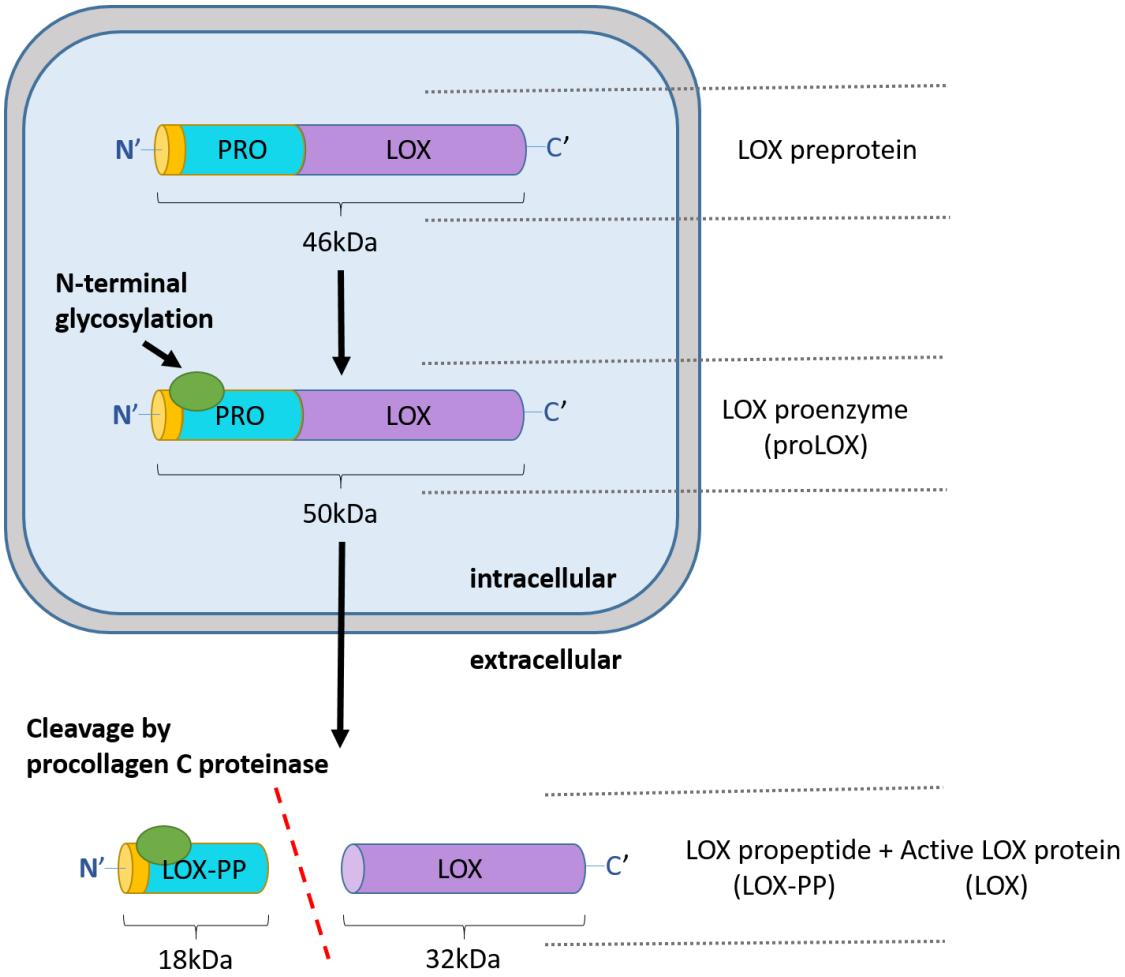

Figure 1.3: Synthesis and Processing of LOX. Lysyl Oxidase is initially synthesised as a 46kDa preprotein consisting of a catalytic domain (LOX, purple), propeptide domain (PRO, blue), and N-terminal signal peptide (yellow). The preprotein is N-glycosylated during passage through the Golgi apparatus, producing a catalytically inactive 50kDa proenzyme (proLOX). Following secretion through the cell membrane proLOX is cleaved by procollagen C-proteinases to yield an 18kDa LOX propeptide (LOX-PP) and the mature, catalytically active form of LOX at 32kDa.

1.4.2 LOX Enzymatic Action

LOX oxidatively deaminates the ε-amino group of specific peptidyl lysine and hydroxylysine residues at the surface of collagen and elastin fibrils. This results in the formation of peptidyl aldehydes which spontaneously condense with other nearby peptidyl aldehydes, or unreacted ε-amino groups, on other nearby side-chains; thus forming inter- or intra-molecular covalent cross-links between fibres (Knott & Bailey 1998; Oxlund et al. 1995; Panchenko et al. 1996). Figure 1.4 gives an overview of this process.

Increasing the number of cross-links between collagen or elastin fibres results in a more insoluble and increasingly stable matrix (Kagan & Li 2003). LOX activity therefore results in an increased tensile strength and structural integrity of the extra-cellular matrix, as well as the development of insoluble collagen. As such, LOX plays an essential role in the development, maintenance, and repair of structurally sound connective tissues, particularly important in the respiratory, cardiovascular, and musculoskeletal systems of the body (Csiszar 2001; Erler et al. 2006; Taylor et al. 2011; Wong et al. 2011).

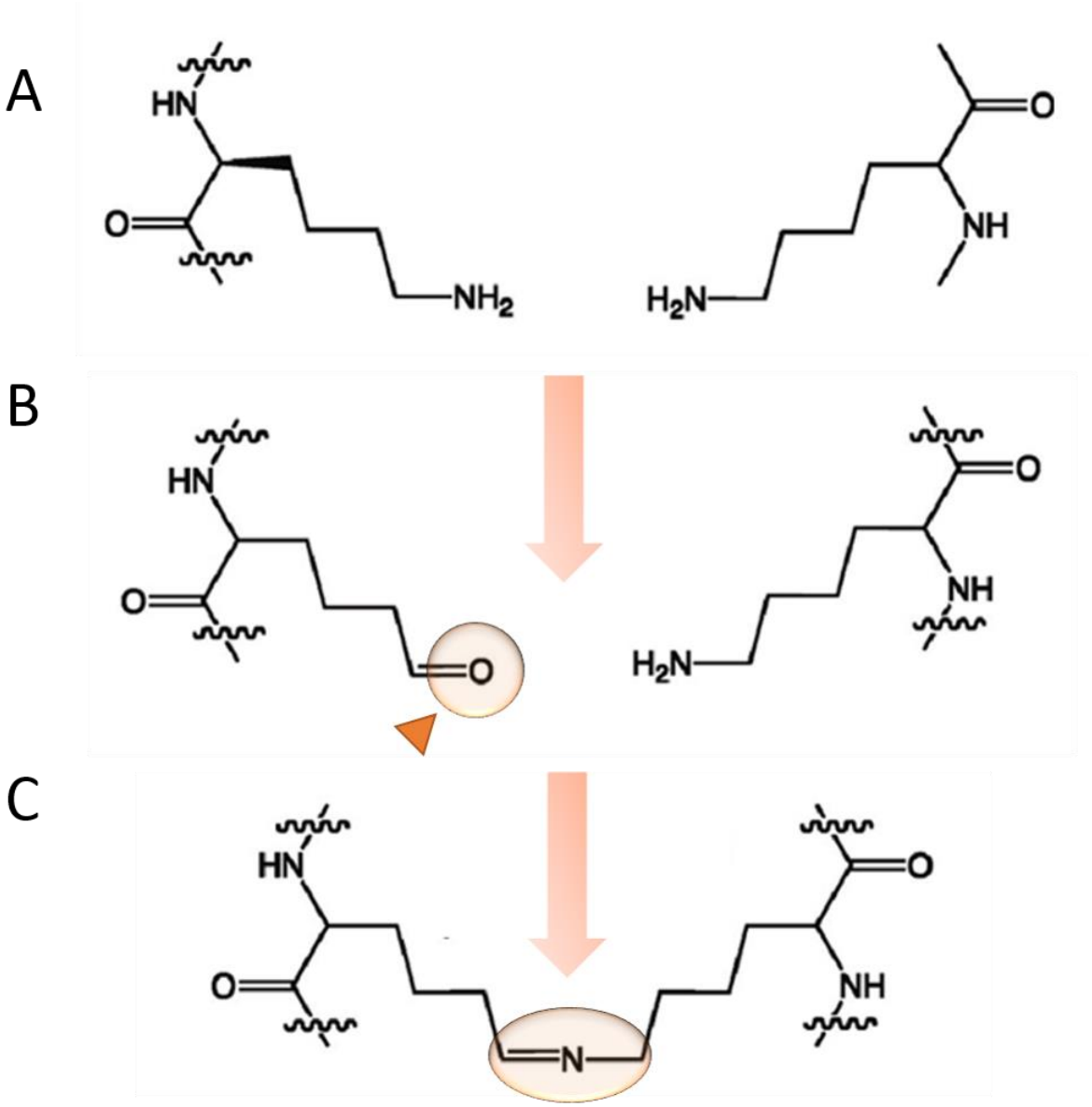

Figure 1.4: Diagram of Cross-Linking Reaction Catalysed by LOX. This diagram shows the cross-linking chemical reaction, catalysed by LOX, which results in covalent bonds between peptidyl lysine or hydroxylysine side chains on long chain collagen fibrils. **A** Two side chains are aligned but not bonded. **B** LOX cleaves the -NH_2 group, de-aminating the lysine side chain, leaving a double-bonded oxygen. **C** The deaminated side chain condenses with a neighbouring lysine side chain, covalently bonding the two fibrils. This bond may form between aminated or de-aminated lysine or hydroxylysine side chains, which may be present on the same or different collagen fibrils. Figure is modified with permission from Bakota et al. (2011). Copyright 2011 American Chemical Society.

1.4.3 LOX in Cancer

In addition to the traditional role of LOX as a cross-linker of collagen and elastin fibrils in the extra cellular matrix, it has also been shown to play a significant role in cancer biology, contributing to chemotaxis, metastasis, and bone tropism (Erler et al. 2006; Lazarus et al. 1995; Kirschmann et al. 2002; Cox et al. 2015). In addition, LOX has been identified as a crucial factor for the development of the pre-metastatic niche (Erler et al. 2009; Kaplan et al. 2006; Cox et al. 2015). Resultantly, expression of LOX is correlated with poorer survival rates in patients with ER- breast cancer, and patients with head and neck cancer (Erler et al. 2006). Thus LOX contributes to metastatic disease mortality by encouraging an invasive cancer cell phenotype, and priming the secondary microenvironment to promote survival of metastases, resulting in a poorer disease prognosis. The mechanisms by which LOX achieves this twofold promotion of metastasis are outlined further below in this section.

1.4.3.1 LOX and Cell Invasive Phenotype

LOX is known to be expressed in highly metastatic cancers in which it promotes an invasive cell phenotype, at least partly by driving remodelling of the actin cytoskeleton, and increased formation of stress fibres and focal adhesions required for chemotaxis (Erler et al. 2006). The highly invasive breast cancer cell lines (MDA-MB-231, Hs578T, and 4T1) show increased expression of LOX compared to poorly invasive breast cancer cell lines (MCF-7 and T47) (Kirschmann et al. 2002; Erler et al. 2006), with similar patterns also noted in melanoma (Hendrix et al. 1998) and prostate cancer cell lines (Luo et al. 1997). Inhibition of LOX with antisense oligonucleotides or β-aminopropionitrile (BAPN), a non-specific LOX-family inhibitor which irreversibly inhibits LOX enzyme activity, has been shown to significantly reduce cell invasion through a collagen IV/laminin/gelatine matrix *in vitro* (Kirschmann et al. 2002; Erler et al. 2006). Additionally, introduction of LOX expression to the poorly invasive MCF-7 cell line, which normally produces negligible quantities of LOX, increases invasion through matrix, and is dose-dependently reversible via treatment with BAPN (Kirschmann et al. 2002). This highlights the powerful role of LOX in generating an invasive cancer cell phenotype contributing towards metastasis.

1.4.3.2 LOX and Cell Adhesion

LOX is also known to contribute to metastatic potential by regulating cell adhesion. Both MDA-MB-231 (breast cancer) and SiHa (cervical cancer) cell lines expressing short hairpin RNA against LOX production (shLOX) displayed a decreased adhesion to collagen-I, which was restored via transfection with mature LOX (Erler et al. 2006). One proposed mechanism is that LOX enzymatic activity increases the availability of fibrillar collagen, which acts as a ligand for β_1 integrin (Taylor et al. 2011), a protein known to regulate focal adhesion kinase activation (Erler et al. 2006).

1.4.3.3 LOX and Metastatic Spread

As a result of LOX activity in generating an invasive, adhesive cell phenotype, it is not surprising that expression of LOX is linked to metastatic spread. Investigation into the potential of LOX as a novel target for future anti-cancer treatments showed that inhibition of LOX, via BAPN or anti-LOX antibody (LOX-Ab), eliminated metastatic spread to both the lung and liver in a mouse MDA-MB-231 breast cancer model, but did not affect primary tumour growth (Erler et al. 2006).

1.4.3.4 LOX and the Pre-Metastatic Niche

LOX enzymatic activity has been shown to be a crucial promoter of pre-metastatic niche formation in the lung, where it is essential for recruitment of CD11b+ bone marrow derived cells (BMDCs), a crucial early stage in pre-metastatic niche formation. Briefly, LOX enzymatic action results in cross-linking of collagen IV in the basement membrane, which allows transient CD11b+ BMDCs to adhere. Once adhered BMDCs release matrix-metalloproteinase II (MMP2), which cleaves collagen IV, resulting in the release of chemo-attractive collagen IV peptides, which in turn enhance the invasion and recruitment of yet more BMDCs and transiting metastatic cells (Erler et al. 2009), thus initiating a positive feedback cycle (Fig. 1.4).

Further evidence for LOX as a component in pre-metastatic niche formation is found in a study investigating the effects of hypoxia-inducible factor 1 (HIF-1), which regulates expression of all LOX family proteins, in breast cancer metastatic niche formation (Wong et al. 2011). Knockdown of HIF-1 reduced LOX expression in MDA-MB-231 and MDA-MB-435 breast cancer cell lines, and also reduced the invasion of BMDCs through Matrigel pre-treated with conditioned medium from the two breast cancer cell lines, supporting the role of LOX in pre-metastatic niche modification. In addition to LOX, this study also identified LOXL2 and LOXL4 as contributors to the pre-metastatic niche. This is not a surprising revelation given the importance attributed to enzymatic cross-linking in conditioning of the pre-metastatic niche, since the region of protein responsible for the enzymatic cross-linking action of LOX is highly conserved within the LOX family (Csiszar 2001).

More recently LOX has been confirmed to contribute to a pre-metastatic niche in bone. Tumour secreted LOX has been shown to imbalance bone remodelling in favour of osteolysis, generating osteolytic lesions in bone prior to cancer cell metastasis (Cox et al. 2015). Bone destruction is already known to release a number of pro-cancer factors which encourage the recruitment and growth of metastatic cells, in the process known as 'the vicious cycle' of bone metastasis (see section 1.3), but the effect of LOX mediated osteolytic lesions was assessed directly in this study. Mice were pre-conditioned with injections of LOX containing conditioned medium (CM) from 4T1 cells, prior to intra-cardiac injection of 4T1 cells expressing luciferase (4T1-Luc). Mice treated with 4T1 CM showed a significant increase in lesion number and tumour burden compared to those pre-treated with 4T1-shLOX CM or LOX-Ab. Furthermore, tumour burden was found to directly correlate to the number of osteolytic lesions present. This shows that osteolytic lesion formation by LOX directly results in a greater metastatic burden, and confirms that LOX plays a crucial role in pre-metastatic niche formation in bone.

1.4.4 LOX in Bone

A syngeneic mouse model, utilising the murine 4T1 breast cancer cell line and BALB/c mice, was used to investigate the effect of tumour secreted LOX on bone. LOX was shown to drive osteolysis, resulting in significant loss of both cortical and trabecular bone, as well as the development of the aforementioned osteolytic lesions. Bone loss was seen in both tumour bearing mice, and tumour free mice receiving intraperitoneal injections of 4T1 CM (Cox et al. 2015). The effects of LOX activity on the bone microenvironment are detailed below in figure 1.4.

The osteolytic imbalance created by LOX was found to be, at least in part, due to the direct effect of LOX on bone cells. Culture of pre-osteoclast cells showed LOX to be a potent stimulator of osteoclastogenesis, generating a higher number of mature osteoclasts, displaying greater resorptive capacity than control cultures grown with RANKL (Cox et al. 2015). Furthermore, the effects of LOX on osteoclasts were shown to occur in the absence of RANKL, identifying LOX as a novel mediator of bone remodelling with a separate pathway. Investigation of the mechanism behind the increased osteoclastogenesis seen in LOX treated cultures was found to involve translocation of NFATc1, the master regulator of osteoclastogenesis (Boyle et al. 2003), to the cell nucleus. Nuclear translocation of NFATc1 was, in turn, shown to be dependent on the reactive oxygen species by-product of LOX enzymatic activity, H_2O_2. Although the intricacies of this mechanism remain to be elucidated, H_2O_2 was shown to be crucial, with nuclear translocation of NFATc1 being prevented, in a dose-dependent manner, via the addition of catalase, which rapidly degrades H_2O_2. This exciting discovery details a new LOX activity dependent mechanism of *de novo* osteoclastogenesis (Cox et al. 2015).

In addition to promoting osteoclast cell formation and function, LOX was also found to inhibit the bone remodelling activities of osteoblast cells. Addition of recombinant LOX protein (rLOX) to primary calvarial mouse osteoblast cultures resulted in significant decreases in cellular proliferation as well as increasing terminal differentiation of cells in the osteoblast lineage. Thus the effect of LOX on osteoblasts was a combination of growth prevention and stimulation of terminal differentiation, preventing osteoblasts from contributing to the bone remodelling process. The effect of LOX on bone cells, therefore, is to promote the activity of those breaking down bone, and inhibit those that lay down new bone. This was confirmed *in vivo* where quantification of cell numbers on the endocortical surface of tibiae in mice with LOX secreting tumours were found to have more osteoclasts and fewer osteoblasts compared to controls, an imbalance which was partly removed by LOX interference via LOX-Ab or shLOX.

Finally, the functional consequence of LOX's ability to prime bone for metastatic cells was confirmed when it was shown that treatment with clinically relevant concentrations of the bisphosphonate zolendronic acid prevented lesion formation without affecting primary tumour growth. An experiment in which mice were primed for metastases by intraperitoneal injection of LOX containing conditioned medium, prior to an intra-cardiac injection of 4T1-Luc cells, showed that treatment with zolendronic acid alongside pre-conditioning CM significantly reduced the ability of 4T1-Luc cells to colonise bone. Zolendronic acid treated mice also showed significantly fewer metastases 5 weeks after tumour cell injection (Cox et al. 2015). Bisphosphonates broadly work by killing osteoclast cells, thus the mechanism for their protective action is the prevention of bone loss driven by LOX mediated osteoclastic activity, highlighting the necessity of LOX interaction with osteoclast cells in order to generate its pro-metastatic effect.

1.4.5 Intracellular activity of LOX

In addition to its aforementioned roles in the promotion of metastasis, there is growing evidence to support the role of LOX as a transcriptional regulator. Once LOX has been cleaved to its active form in the ECM, activated LOX is able to re-enter the cell where it localises at the nucleus (Li et al. 1997). It has been proposed that the enzymatic cross-linking activity of LOX can alter the macromolecular structure of histones located there, in turn affecting chromatin conformation and interfering with the process of transcription (Iturbide et al. 2015).

Recent research supports this role, identifying LOX as a novel regulator of bone remodelling, independent of RANKL, by driving nuclear localisation of NFATc1 (the master regulator for osteoclastogenesis) (Cox et al. 2015; Boyle et al. 2003). The mechanism by which this translocation occurs is currently unknown, but is reliant upon H_2O_2, a reactive oxygen species (ROS) which is a by-product of the LOX enzymatic cross-linking reaction. This supports previous reports of ROS as mediators of osteoclast differentiation and function (Garrett et al. 1990; Bax et al. 1992).

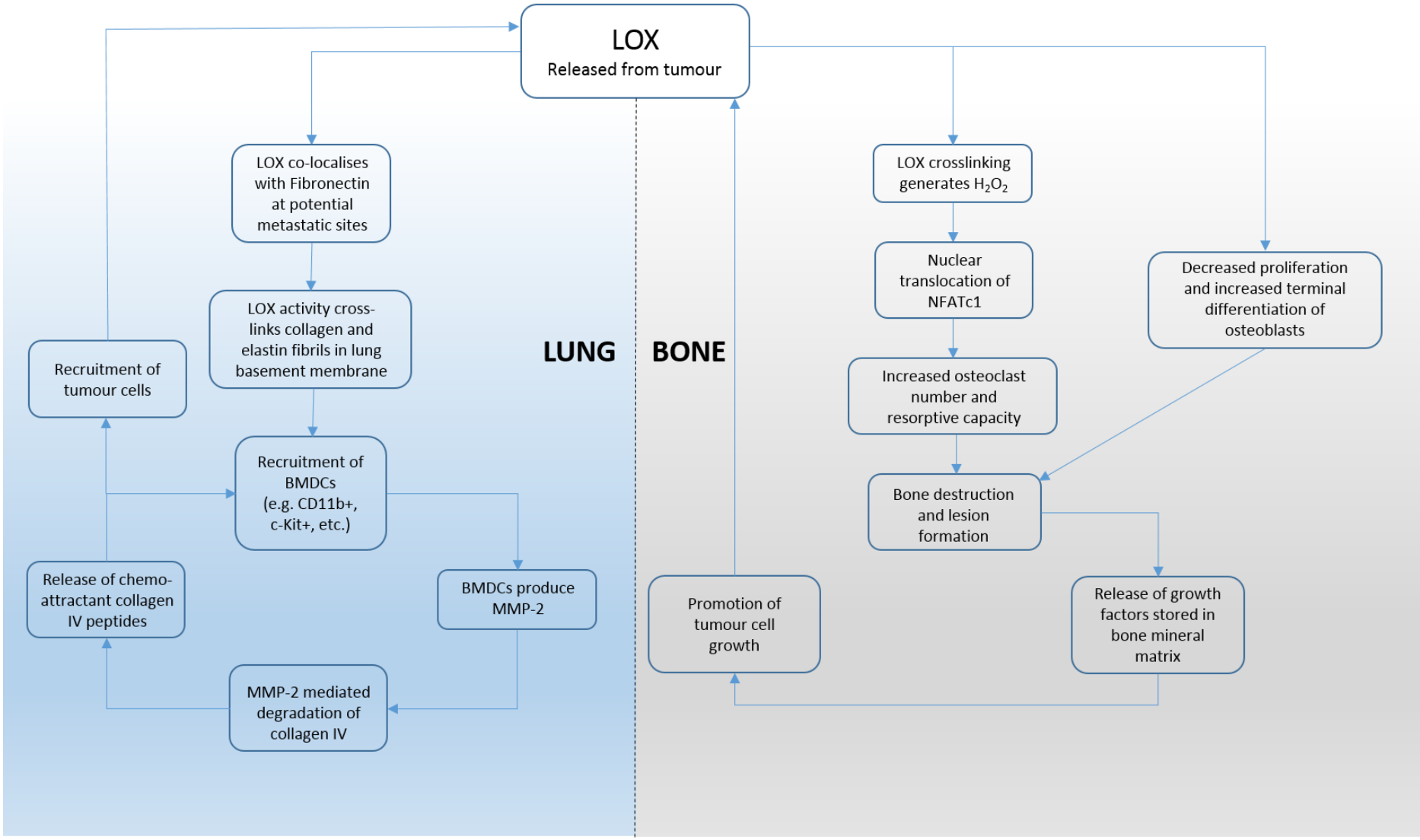

Figure 1.5: Roles for LOX in Pre-Metastatic Niche Formation in Lung and Bone. Presenting data for LOX involvement in formation of the pre-metastatic niche in lung (Erler et al. 2009) and bone (Cox et al. 2015).

1.5 The P2X7 Receptor

Purinergic receptors are divided into two broad groups: P1, stimulated by adenosine; and P2, stimulated by ATP and ADP (Burnstock 1978). P2 receptors are further divided into P2Y and P2X families based on their pharmacological properties. P2Y receptors are metabotropic G protein-coupled receptors , whereas P2X receptors are ligand-gated ion channels (Burnstock 2006). The P2X7 receptor (P2X7R) shares 35-40% structure identity with other P2X family members, but is considered to be the most unique in its family. The major structural difference in P2X7R is a large C-terminal chain which is 239 amino acids in length, compared to the 27-120 amino acids found in other P2X receptors (Rassendren et al. 1997). As with other P2X receptors, transient stimulation with ATP results in the activation of a selective cation channel permeable to small monovalent and divalent cations (Browne et al. 2010). In response to prolonged or repeated stimulation, however, P2X7R forms a large transmembrane pore, which allows the non-selective passage of molecules up to 900Da (Ralevic & Burnstock 1998). This feature is unique to P2X7R and appears to be dependent upon the receptors long C-terminus structure (North 2002; Rassendren et al. 1997). P2X7R is also pharmacologically distinct from other P2 family members in that it is more potently stimulated by 2,3(4-benzoyl)benzoyl ATP (BzATP), rather than ATP, which is the most potent stimulator of all other P2X receptors (Agrawal & Gartland 2015), and in that it requires a relatively higher concentration of ATP, upwards of 100μM, to activate (North 2002). Finally, stimulation of P2X7R is known to promote apoptosis, an activity not seen in other P2X receptors (Zheng et al. 1991).

P2X7R is expressed in a wide variety of cell types throughout the body, including bone cells, where its activity is implicated in a number of physiological processes, including but not limited to maturation and release of IL-1β (Chiozzi et al. 1997), ATP induced apoptosis via the caspase pathway (Humphreys et al. 2000), and cell fusion in macrophages and preosteoclasts (Chiozzi et al. 1997; Gartland et al. 2003a; Di Virgilio et al. 1999).

1.5.1 P2X7R in Cancer

P2X7R expression has been described in a number of different cancers, including: melanoma (White et al. 2005), non-melanoma skin cancer (Greig et al. 2003), intestinal (Coutinho-silva et al. 2005), lung (Schafer et al. 2003), breast (Slater et al. 2004; Jelassi et al. 2011; Dixon et al. 1997), prostate (Janssens & Boeynaems 2001), leukaemia (Adinolfi et al. 2002), and cervical cancers (Wang et al. 2004). Initial reviews of P2X7R function in cancer proposed that its activation led to a decrease in tumour cell number via the promotion of apoptosis (White & Burnstock 2006). More recent research, however, has shown that P2X7R expression may also promote cancer survival and growth (Adinolfi et al. 2012; Di Virgilio et al. 2009). While the molecular mechanisms conveying this growth advantage are not fully understood, it is likely that the complexity of P2X7R interaction with both cell growth and apoptosis is a result of its bifunctionality. Unchecked pore formation will undoubtedly result in cell death due to apoptosis, or simple inability to maintain a constant intracellular environment conducive to life, whereas channel formation (or even possibly controlled pore formation) can provide growth advantages by maintaining tonic intracellular Ca^{2+} levels (Di Virgilio et al. 2009). K562 (leukaemia) and LG15 (lymphoma) cell lines transfected with P2X7R showed no significant difference in growth rate from their mock-transfected (non-P2X7R expressing) controls when grown in normal culture medium, but when serum was removed from the culture medium, P2X7R transfected cell proliferation continued unabated, while mock transfected cell proliferation arrested (Di Virgilio et al. 2009). The molecular mechanisms behind this survivability are yet to be fully investigated, but potential growth advantages from P2X7R activation include increased efficiency of mitochondrial metabolism and ATP synthesis; increased MAP kinase pathway activity; and increased ability to release growth or survival promoting factors, or ATP (Di Virgilio et al. 2009). Further to this, a recent study has shown P2X7R growth promoting activity *in vivo*, where human embryonic kidney (HEK) cells expressing P2X7R were shown to display a more tumourigenic and anaplastic phenotype than control cells when inoculated in a mouse model (Adinolfi et al. 2012). The P2X7R expressing tumours displayed accelerated growth compared to controls, which was attributed to increased cellular proliferation, decreased apoptosis, and a high level of activation of the transcription factor NFATc1. The growth rate and overall size of tumours was also shown to be significantly reduced by intratumoural injection of oxidised ATP, a known inhibitor of P2X7R (Adinolfi et al. 2012).

In addition to contributions to cancer cell survival there is also evidence to support a role for P2X7R in the promotion of metastasis. P2X7R has been shown to be highly expressed and fully functional in the aggressively metastatic MDA-MB-435 breast cancer cell line, where its activation increases cell migration by 35%, and cell invasion through ECM by 150% (Jelassi et

al. 2011). This pro-migratory, invasive phenotype was found to be the result of morphological changes in the cell, notably the formation of neurite-like cell projections, which are possibly the same structures, identified as stress fibres and focal adhesions by Erler et al. (2006), seen in response to LOX stimulation. The formation of neurite-like cell projections occurred after stimulation of P2X7R with 1-3mM ATP, whereas stimulation with >3mM ATP resulted in mild levels of P2X7R dependent cell death. A further study found that ATP and BzATP stimulation of P2X7R in the T47D breast cancer cell line stimulated invasion and migration in a dose-dependent manner, possibly via activation of the AKT pathway and regulation of E-cadherin and MMP-13 expression (Xia et al. 2015).

While a great deal more research is required to investigate the roles of P2X7R in cancer, and even more to elucidate the mechanisms by which P2X7R activation may result in apoptosis, cell growth, or generation of a metastatic phenotype – it is clear that the level of P2X7R activation (as decreed by concentration of ATP agonist) is a crucial factor in determining resultant cell behaviour. High levels of ATP are known to occur in the tumour microenvironment, particularly in necrotic areas where it is directly released from dead cells, and as such there is no shortage of agonist for P2X7R, giving it the potential to be a crucial facilitator or inhibitor of cancer survival and spread.

1.5.2 P2X7R in Bone

P2X7R plays a substantial role in bone biology, and is known to be expressed and functionally active in the three major bone cell types: osteoclasts (Jørgensen et al. 2002; Naemsch et al. 2001), osteoblasts (Gartland et al. 2001; Ke et al. 2003; Panupinthu et al. 2008), and osteocytes (Li et al. 2005). The contribution of P2X7R towards homeostasis in bone remodelling is evident from the aberrant skeletal phenotypes seen in P2X7R$^{-/-}$ knockout mouse models

1.5.2.1 P2X7 in Bone Remodelling

There are presently two commercially available P2X7R$^{-/-}$ mouse models, GlaxoSmithKline (GSK) (Sim et al. 2004) and Pfizer (Solle et al. 2001). Both knockouts show signs of dysregulation in bone remodelling as a result of P2X7R knockout, however the observed changes differ between the two knockouts. The Pfizer knockout mouse phenotype mimics disuse of the skeleton and oestrogen deficiency, displaying a reduction in bone mineral content (Ke et al. 2003), resulting from a reduction in mineralising surface area, and bone formation (Li et al. 2005). The GSK knockout mouse, by contrast, displays an anabolic phenotype: increased thickness of cortical bone (Gartland et al. 2003a), increased bone strength, and increased bone mineral content

(Syberg et al. 2012). The differences between these two knockout models are believed to result from initial differences in the gene targeting construct, the genetic background of the mice used (Syberg et al. 2012), and the escape of the P2X7(k) splice variant from deletion in the GSK mouse (Nicke et al. 2009). Figure 1.6 illustrates the differences in structure between the P2X7 (a) and (k) splice variants. Regardless of the differences between the two knockout models, together they show that P2X7R is required for normal function of the bone remodelling process.

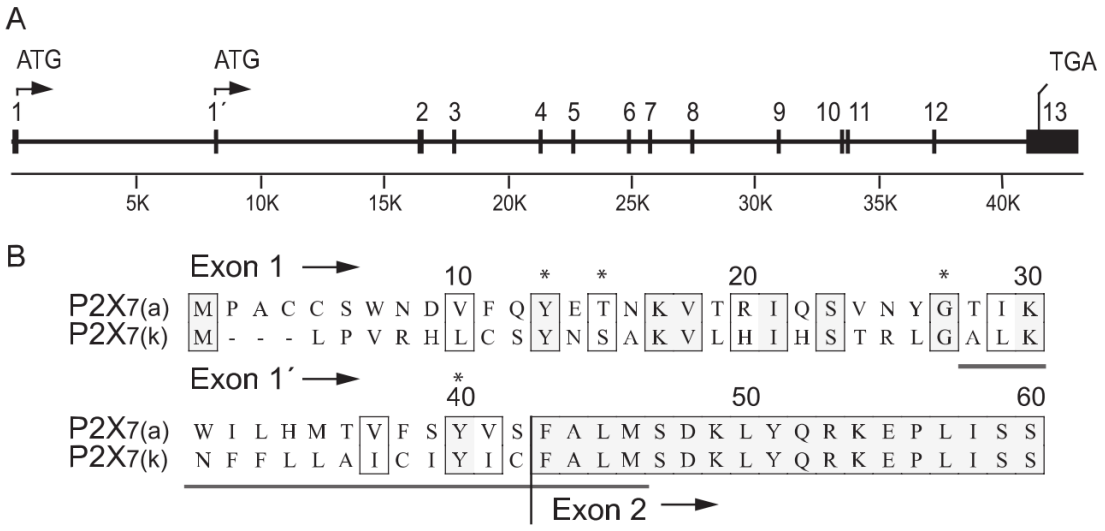

Figure 1.6 Structure and Amino Acid Sequence of P2X7R Splice Variants. A Genomic structure and dimensions of the *P2rx7* gene. Numbered bars represent exons. Positions of start and stop codons of the P2X7(a) and P2X7(k) variants are indicated. **B** Comparison of the amino acid sequence of exons 1 and 1' between P2X7(a) and P2X7(k) variants. Asterisks indicate residues that are conserved among all P2X subunits. Shaded and empty frames indicate identical and similar residues between both P2X7 variants, respectively. The underlined section indicates the presumed location of the transmembrane domain (TMD). Reproduced with permission from Figure 1, Nicke et al. (2009).

1.5.2.2 P2X7R in Bone Cells

The role of P2X7R in bone cells has been extensively researched, yet contradictory and conflicting reports mean that a comprehensive understanding of the effects and mechanisms of P2X7R signalling in bone cells remains elusive, highlighting its complexity.

As mentioned previously, P2X7R is expressed in osteoclasts (Hoebertz et al. 2000; Naemsch et al. 2001), osteoblasts (Gartland et al. 2001; Orriss et al. 2006), and osteocytes (Li et al. 2005), and there is evidence for it playing a functional role in regulation of bone remodelling in all three cell types (Agrawal & Gartland 2015). Evidence from cellular studies broadly suggests that P2X7R stimulation leads to an overall inhibition of osteoblastic activity, and stimulation of osteoclastic activity – although there are studies showing it to be involved in promoting osteoblastic activity under certain conditions. Considering the body of literature as a whole, it is clear that P2X7R plays a very complex role and is crucial for maintaining homeostasis in bone remodelling. This introduction will focus on the role of P2X7R in the osteoclast, as this is the cell of interest for the investigation into the formation of osteolytic lesions in bone. A brief discussion of the role of P2X7R in the osteoblast, however, highlights the importance of this receptor in the grand scheme of bone remodelling, as well as its role in the regulatory relationship between the two cell types.

1.5.2.3 P2X7R in Osteoblasts

Stimulation of P2X7R in various osteoblastic cells has shown that it induces cell death, with an increase in apoptosis noted in the SaOS-2 osteoblast cell line (Gartland et al. 2001), and induction of membrane blebbing, associated with apoptosis, in murine calvarial osteoblasts (Panupinthu et al. 2007). P2X7R stimulation has also been shown to inhibit bone mineralisation and alkaline phosphatase (ALP) levels (a marker of osteoblastic cell activity) *in vitro* (Orriss et al. 2013). In addition to direct effects upon osteoblast survival and activity, P2X7R is required for the propagation of intercellular Ca signalling between osteoblasts and osteoclasts (Jørgensen et al. 2002), thus highlighting its importance in the coupling of osteoblast and osteoclast cells for normal bone remodelling.

1.5.2.4 P2X7R in Osteoclasts

P2X7R is expressed by osteoclasts throughout all stages of development and there is evidence to suggest that P2X7R becomes more important as osteoclasts mature, with increased mRNA and protein expression noted in mature cells compared to precursors (Brandao-Burch et al. 2012). The major event in the formation of functional osteoclasts is the fusion of mononuclear precursor cells into mature multinucleated osteoclasts. Blockade of P2X7R has been shown to

inhibit the fusion of mononuclear osteoclast precursor cells *in vitro*, preventing the formation of mature cells, and thus inhibiting resorption (Gartland et al. 2003b; Agrawal et al. 2010). Studies *in vivo*, however have shown that P2X7R knockout mice retain the ability to form mature, multinucleated, resorptive osteoclast cells suggesting that there is a compensatory mechanism to overcome P2X7R blockade (Gartland et al. 2003c; Ke et al. 2003). One proposed mechanism by which P2X7R mediates cell fusion is by allowing ATP release from fusion competent cells. This released ATP is then degraded to yield an increased extracellular concentration of adenosine, which in turn drives cell fusion via the adenosine A2A receptor (Pellegatti et al. 2011).

In addition to driving osteoclast precursor cell fusion, P2X7R also influences the survival and resorptive activity of osteoclasts by regulation of genetic expression, with one study in particular showing that knockdown of P2X7R via siRNA resulted in reduced expression of a number of markers of osteoclast activity, including NFATc1, cathepsin K, and TRAP (Hwang et al. 2014). This regulation is at least in part the result of the role of P2X7R as a selective small cation channel. P2X7R mediated influx of Ca^{2+} is proposed to increase intracellular Ca^{2+} concentration ($[Ca^{2+}]_{ic}$) leading to activation of key signalling molecules, such as NF-κB (Korcok et al. 2004) and NFATc1 (Adinolfi et al. 2009), which are required for osteoclastogenesis and regulation of osteoclast differentiation, respectively (Iotsova et al. 1997; Takayanagi et al. 2002).

Stimulation of osteoclasts with high concentrations of ATP or BzATP, via P2X7R, has been shown to rapidly affect the cytoskeleton by disrupting filamentous actin belts (Armstrong et al., 2009, Hazama et al., 2009). Subsequent actin reorganisation was accompanied by microtubule deacetylation, which was shown to be crucial for the formation of sealing zones, structures which delimit the area of bone which the osteoclast proceeds to resorb (Hazama et al., 2009), thus describing a mechanism by which P2X7R signalling contributes to osteoclast cell function.

P2X7R is also known to contribute to cell response to mechanical loading, with P2X7R knockout mice displaying a reduction of up to 73% in sensitivity to mechanical loading, manifested as lower bone formation per unit of mechanical strain (Li et al. 2005). *In vitro* culture of human osteoclast cells has shown that blocking P2X7R activity inhibits mechanically induced intercellular calcium signalling between osteoclasts (Jorgensen et al., 2002), suggesting a potential mechanism for this observation.

Overall the stimulation of P2X7R in osteoclasts drives osteoclast cell formation, survival, maturation, and resorptive activity. While the intricacies of the mechanisms leading to these effects are extensively studied, more information is required to definitively map the effect of the receptor, but P2X7R cation channel formation allowing Ca^{2+} influx to the cell seems to be a key feature in a number of P2X7R's known roles in the osteoclast. Conversely, prolonged or excessive stimulation, leading to P2X7R pore formation, leads to apoptosis of the cells, which will inhibit resorptive activity. Thus P2X7R activity, while largely supportive of osteoclastic resorption, may also inhibit it, giving the receptor a complex relationship with the osteoclast.

1.6 Mechanical Loading

Mechanical loading is known to regulate bone remodelling, altering the structure of bone to best adapt to the forces to which it is subjected (Ruff et al. 2006). The effect of loading on bone is highly dynamic, depending on loading type and force, as well as the bone or cell type being affected. Ultimately, however, the effect of loading on bone remodelling comes down to the effect of loading on bone remodelling cells.

1.6.1 Effect of Mechanical Loading at the Cellular Level

Osteoblast cell cultures have shown that loading, generated by shear stress from fluid flow, results in increased cell proliferation and deposition of mineral matrix, as well as increases in alkaline phosphatase (ALP), a measure of osteoblast activity, and osteocalcin, a measure of terminal osteoblast differentiation (Ban et al. 2011).

One theory proposes that osteoclasts are passive in the process of bone response to loading, stating that osteoclasts continue to resorb bone until such a point as the stresses to which it is exposed reach a threshold whereupon the strain induced in the bone matrix initiates osteocyte signalling to promote osteoblastic activity. Osteoblasts are then recruited, inhibiting the activity of local osteoclasts, and laying down new bone to strengthen the area which initiated osteocyte signalling – thus coupling osteoclast and osteoblast activity to maintain a suitable level of bone mineral (Erben 2015). Prior research, however, has shown that mechanical loading does directly affect osteoclast cells, and is able to both promote and inhibit osteoclast cell activity depending on loading force, anatomical location, and maturity of the affected cell. A study by Rubin et al (1999) differentiated tartrate resistant acid phosphatase (TRAP) positive multinucleated cells (the classical description of osteoclast cell type) from primary bone marrow cells. Loading was applied to these cells by connecting the underside of the culture plate to a vacuum to distort the well bottom. Using this model they showed that subjecting the cells to strain inhibited osteoclast recruitment during early differentiation, resulting in a significant decrease in osteoclast number by the end of a 7 day culture if wells were subjected to strain during days 2-4 of the culture, but with negligible differences when strain was applied at a later timepoint. This demonstrates that the application of strain, at the right point in development, can impede osteoclastic activity.

A later study by Kurata et al. (2001) cultured osteoclasts on rectangular ivory plates, subjected to three point bending. They showed that stretching of the cells, by bending the ivory substrate on which they grew, increased mRNA expression of TRAP and cathepsin K, both marker enzymes for osteoclast cell type, and indicators of bone resorptive activity. Furthermore, the area of ivory substrate resorbed by osteoclast cells, and the number of resorption pits formed, significantly

increased in loaded cultures compared to non-loaded controls, thus providing compelling evidence to show that mechanical loading could also increase osteoclastic activity, contrary to the observations of Rubin et al. (1999).

More recently it was shown that the response of osteoclasts to loading was dependent upon the intensity of the strain generated. Xu et al. (2012) cultured cells from the RAW246.7 murine monocyte/macrophage cell line, which are known to differentiate into osteoclast-like cells in the presence of macrophage colony stimulating factor (M-CSF) and receptor activator of nuclear factor κ-B ligand (RANKL). These cells were differentiated into their osteoclast like form and culture plates were subjected to a 4 point bending regime designed to induce a uniaxial and homogenous mechanical strain. Application of low levels of strain (1000-1500με) resulted in a significant increase in apoptosis and concomitant reduction in cell number. Increasing strain to higher, though still physiologically normal, levels (2000-2500με) removed this apoptotic effect, resulting in a cell number not significantly different to non-loaded controls. Loading was also shown to cause changes in mRNA expression of two factors involved in osteoclastic activity: RANK, which is responsible for osteoclast differentiation and survival (see section 1.2); and matrix metalloproteinase-9 (MMP-9), required for osteoclastic resorption (Hill et al. 1994; Spessotto et al. 2002), as well as cell migration through collagen (Blavier & Delaissé 1995; Sato et al. 1998). At low levels of strain mRNA expression of both RANK and MMP-9 were reduced, indicating a reduction in osteoclastic cell activity. Increase of strain to higher (but still physiologically normal) levels reversed this with increases in mRNA levels of both RANK and MMP-9, suggestive of increased osteoclast cell activity. Increasing loading further (5000με), exceeding normal physiological levels, reversed mRNA expression, resulting in a reduction in RANK and MMP-9 mRNA compared to non-loaded controls. Taking these observations together, it can be concluded that low or exceedingly high levels of strain inhibit osteoclast cell survival and activity, while higher levels of strain, within physiological limits, stimulate osteoclast cell growth and activity. Thus regulation of osteoclast cell activity via loading is dependent upon the magnitude of strain generated at the cellular level.

1.6.2 P2X7R and Mechanical Loading

P2X7R is known to contribute significantly to bone response to loading, with a knockout mouse model showing a 61% reduction in new bone formation in female mice in response to loading when compared to WT controls (Li et al. 2005). P2X7R knockout also leads to a reduction in both mineral nodule formation and levels of ALP in cultures of calvarial osteoblasts (Panupinthu et al. 2008). Unfortunately, little is known about the role of P2X7R in osteoclast cell response to loading, perhaps as a consequence of the inherent difficulties in osteoclast cell culture and the lack of robust and representative cell lines. However, based on the general response to loading being osteogenic, P2X7R is more likely to inhibit osteoclast response to loading if involved at all.

1.7 Proposed Interaction between P2X7R and LOX

Previous research, discussed above, has highlighted the accumulation of LOX at future metastatic sites and its role in the generation of the premetastatic niche (Erler et al. 2009). Furthermore, our collaborators have noted that LOX accumulates in areas subjected to pressure within the body, for example areas of fluidic shearing stress at the bifurcation of arteries. ATP is also known to be released from certain cells, including bone cells, when subjected to pressure, and also in abundance from cancer cells. As such, it is proposed that LOX and ATP may co-localise in areas of high pressure, particularly within the tumour microenvironment and pre-metastatic niche in bone, a tissue known to be regulated by loading pressure. Given the aforementioned roles of P2X7R in the promotion of cancer growth and metastasis, in the bone remodelling process, and particularly in the osteoclast (especially in its response to mechanical loading); coupled with previous reports of purinergic signalling regulating LOX expression in hypoxic conditions (Joo et al. 2014), it is proposed that LOX interacts with purinergic signalling, via P2X7R, to induce osteoclastic resorptive activity.

Stimulation of P2X7R has been shown to cause nuclear translocation of NFATc1, independent of RANKL, via an increase in $[Ca^{2+}]_{ic}$ (Korcok et al. 2004; Adinolfi et al. 2009), and in response to hypoxia (Tafani et al. 2011). Activation of NFATc1, by high levels of intracellular calcium, is known to drive osteoclast differentiation (Takayanagi et al. 2002), thus contributing to bone resorption. Recently published research has shown that LOX also drives nuclear localisation of NFATc1 via an H_2O_2 dependent mechanism (Cox et al. 2015), thus presenting further evidence in support of potential interaction of P2X7R and LOX through a potential shared mechanism for osteoclast promotion.

1.8 Hypothesis and Aims

Tumour secreted LOX has previously been shown to contribute to the formation of a pre-metastatic niche in bone by driving the formation of osteolytic lesions, contributing to the vicious cycle of bone metastasis, and allowing tumour cells access to the haematopoietic stem cell niche within the medullary cavity. While the mechanism by which LOX influences osteoclast activity is partly understood, the mechanism by which it contributes to bone tropism in breast cancer metastasis remains unknown. Given the noted accumulation of LOX at areas of pressure within the body, and the propensity for cells to release ATP in response to loading, as well as the abundant release of ATP from cancer cells, it was hypothesised that P2X7R, which plays known roles in both cancer and bone biology, interacts with LOX activity to generate an osteolytic effect in bone. It was also hypothesised that mechanical loading would interact with LOX mediated bone destruction, either by driving further bone destruction through accumulation of LOX in the loaded limb; or alternatively by protecting against LOX mediated bone destruction by driving osteogenesis.

To test these hypotheses, the specific aims of this thesis are:

1) **To validate an experimental mouse model for the investigation of LOX/P2X7R activity in breast cancer metastasis to bone.** This will be achieved by utilising a previously confirmed $P2X7R^{-/-}$ BALB/c mouse strain in conjunction with the 4T1/4T1-shLOX murine breast cancer cell lines. Knockdown of LOX in the 4T1-shLOX cell line will be confirmed via Western blot of concentrated conditioned medium from cells grown *in vitro*. Thus identifying the validity of this cell line for the proposed experimental work. Expression of P2X7R in the 4T1 cell line shall also be investigated by PCR as well as culture in the presence of ATP and the specific competitive P2X7R antagonist A 438079 HCl. This will ascertain the possibility of LOX and P2X7R interaction at the level of the cancer cell, informing potential future research.

2) **To investigate the effects of LOX knockdown and P2X7R knockout in pre-metastatic niche formation in a validated mouse model.** This will be achieved by analysing µCT data from WT and $P2X7R^{-/-}$ mice with orthotopic 4T1 or 4T1-shLOX mammary tumours, or mice that received daily intraperitoneal injections of conditioned medium from 4T1 or 4T1-shLOX cells grown *in vitro*. Analysis of cortical thickness and trabecular variables will provide data on the effect of LOX/P2X7R on tumour mediated bone destruction, while quantification of osteolytic lesion formation will provide data on LOX/P2X7R effect on pre-metastatic niche formation. This will identify whether P2X7R is involved in tumour secreted LOX mediated alteration of bone.

3) **To investigate the effects of mechanical loading on LOX/P2X7R mediated bone destruction in a validated mouse model.** This will be achieved by subjecting the right hindlimb of age-matched and tumour bearing mice to non-invasive axial loading designed to engender a strain of 5000με in the tibia, in order to generate significant loading mediated effects in bone in the time allotted. Analysis of μCT will be conducted as above to investigate the effect of mechanical loading on LOX/P2X7R mediated bone destruction and osteolytic lesion formation. This will investigate whether mechanical loading contributes to LOX mediated bone destruction, via localisation of LOX at sites of loading; or protects against it by creating an osteogenic imbalance in bone homeostasis.

Completion of these aims will provide a better understanding of the mechanisms by which tumour secreted LOX is able to induce bone destruction and osteolytic lesion formation in the pre-metastatic niche, and will also help to identify new targets for potential anti-metastatic therapies to combat metastatic bone disease.

CHAPTER 2:

MATERIALS AND METHODS

2.1 Materials

2.1.1 Animals and Cell Lines

BALB/c WT mice were ordered from Charles River (Margate, UK.). P2X7R$^{-/-}$ BALB/c founding mice were kindly donated by Dr. Niklas Jørgensen, University Hospital of Copenhagen (Copenhagen, Denmark), while the colony is maintained at the University of Sheffield (Sheffield, UK).

Both the 4T1 and 4T1-shLOX cell line were kindly donated by Prof. Janine Erler (BRIC, University of Copenhagen, Copenhagen, Denmark).

2.1.2 Cell Culture

Reagent	Supplier
0.25% trypsin EDTA	25200, GIBCO, Life Technologies
Dulbecco's modified eagle medium (DMEM)	31966, GIBCO, Life Technologies
Dulbecco's modified eagle medium (Phenol-free)	31053, GIBCO, Life Technologies
Dulbecco's phosphate buffered saline (DPBS)	BR0014, Oxoid, Thermo Scientific
Foetal bovine serum (FBS)	10270, GIBCO, Life Technologies
Penicillin-streptomycin	15140, Invitrogen, Life Technologies
Phosphate buffered saline (PBS)	10010, GIBCO, Life Technologies

2.1.3 Fixatives

Reagent	Supplier
Disodium hydrogen orthophosphate	102494C, VWR
Formaldehyde (concentrate for NBF)	437533W, VWR
Hydrochloric acid (HCl^-)	10125, VWR
Industrial methylated spirits (IMS)	302434C, VWR
Paraformaldehyde (PFA)	P6148, Sigma-Aldrich
Sodium dihydrogen orthophosphate dihydrate	28011, VWR
Sodium hydroxide (NaOH)	28244, VWR

2.1.4 Western Blot

Reagent	Supplier
Ammonium persulphate	A3678, Sigma-Aldrich
β-mercaptoethanol	M6250, Sigma-Aldrich
Bovine serum albumin (BSA)	15561, Life Technologies
Bromophenol blue	0449, VWR
Coomassie brilliant blue G-250	20278, Thermo Scientific, Life Technologies
Ethanol	E/0065DF/17, Thermo Fisher Scientific
EZ-ECL colour substrate	Biological Industries Israel Beit-Haemek Ltd., Kibbutz Beit-Haemek, Israel.
N,N,N',N'-Tetramethylethylenediamine (TEMED)	T9281, Sigma-Aldrich
Non-fat dry milk powder	Tesco, UK.
Orthophosphoric acid	W290017, Sigma-Aldrich
Ponceau S	P7170, Sigma-Aldrich
Primary HRP-conjugated antibody against LOX	NOVUS, R&D systems Ltd., Abingdon, UK.
Protogel 30% acrylamide mix	EC-890, National Diagnostics
Sodium dodecyl sulphate (SDS)	71727, FLUKA, Sigma-Aldirch
TrailMIX™ HRP western blot kit markers	71048-3, Novagen®, Merck Millipore
TRI reagent®	T9424, Sigma-Aldrich
Tris (Base)	000000010708976001, Roche, Sigma-Aldrich
Tris HCl	RES3098T, Sigma-Aldrich
Tween-20	P9416, Sigma-Aldrich

2.1.5 PCR

Reagent	Supplier
Chloroform	C2432, Sigma Aldirch, St. Louis, MO, USA
Dnase I (Rnase-free)	New England Biolabs®, Ipswich, MA, USA
EDTA	15575, GIBCO, Life Technologies
High capacity RNA-to-cDNA™ Kit	Life Technologies Ltd., Paisley, UK.
Isopropyl alcohol	I1048, VWR
Nuclease free water	AM9937, Ambion®, Life technologies
Promega GoTaq® DNA polymerase kit	4387406, Life Technologies

2.1.6 Other Reagents

Reagent	Supplier
A438079 HCl	Tocris Bioscience, Bristol, UK
Adenosine 5'-triphosphate disodium salt hydrate	A7699, Sigma Aldrich
CellTiter 96® AQ_{ueous} non-radioactive cell proliferation assay	G5421, Promega
IsoFlo® isofluorane	05260-05, Abbot Animal Health

2.1.7 Laboratory Equipment

Device	Manufacturer
INSTRON 8511 loading machine	Instron, High Wycombe, UK.
Nanodrop 1000 spectrophotometer	Fisher Scientific, Loughborough, UK.
Skyscan 1172 µCT scanner	Skyscan, Kontich, Belgium.
Skyscan 1272 µCT scanner	Skyscan, Kontich, Belgium.
Spectramax M5e plate reader	Molecular Devices (UK) Ltd, Wokingham, Berkshire, UK.

2.1.8 Software

Name	Abbreviation	Publisher
CellD®	CellD	Olympus, UK
CT Analyzer v.1.11.4.2	CTAn	Skyscan, Kontich, Belgium
GOM Inspect v. 7.5 SR2	GOM	GOM mbH, Braunschweig, Germany
GraphPad Prism v. 6.04 for Windows	GraphPad	GraphPad Inc., La Jolla, CA, USA
Nrecon v. 1.6.5.8	Nrecon	Skyscan, Kontich, Belgium

2.1.9 Plastics and Disposables

Name	Manufacturer
96 well plate	Costar®, Corning, NY, USA.
Acrodisc® syringe filters with 0.2µm Supor® Membrane	PALL Corporation, Port Washington, NY, USA.
Cell scraper	ThermoFisher, Horsham, UK.
T75 flasks	Nunc™, Roskilde, Denmark
Vivaspin® 6 columns (10,000 Dalton MWCO)	VS0602, Sartorius, Goettingen, Germany

2.2 Culture of 4T1 Murine Breast Cancer Cell Line

The 4T1 cell line is a murine breast cancer cell line, originally derived from a spontaneous mammary tumour (Miller et al. 1983; Tao et al. 2008). LOX expression was previously knocked down in the 4T1-shLOX cell line by our collaborators, using infection with a retrovirus to stably express murine LOX shRNA (5'-TCTCTCCTCCTCCTTCTAC-3') as previously described (Erler et al. 2009). The 4T1 (originally sourced from the American Type Culture Collection) and 4T1-shLOX cell lines used in this study were a kind gift from Prof. Janine Erler (BRIC, University of Copenhagen, Copenhagen, Denmark), and were previously authenticated using short-tandem repeat analysis (Barker et al. 2013).

4T1 and 4T1 shLOX cell lines were cultured in T75 flasks containing 15ml DMEM, supplemented with FBS (10% of volume), penicillin (100 units/mL), and streptomycin (100µg/mL) - hereafter referred to as complete DMEM. Flasks were incubated at 37°C in a humidified atmosphere of 5% CO_2 and 95% air. Cells were passaged at a ratio of 1:10 when confluent, every 2-3 days. Cell passage was performed via trypsinisation with 0.25% Trypsin EDTA, pelleting by centrifugation at 1000rpm for 5 minutes, and resuspension in complete DMEM.

2.2.1 Generation of Conditioned Medium

Cells were cultured in T75 flasks in complete DMEM until 50-60% confluency. The flask was then washed twice with PBS to remove any cellular debris and residual FBS, and 10mL of serum and phenol free DMEM was added. Cells were then incubated for 24 hours before medium collection. Collected conditioned medium was centrifuged at 1000rpm for 5 minutes and sterile filtered using a 0.2µm membrane.

2.3 Western Blotting

2.3.1 Conditioned Medium Sample Preparation

Conditioned medium was generated as described above (Section 2.2.1) and concentrated by centrifugation using Vivaspin 6 (Sartorius AG, Goettingen, Germany.) concentration columns, spun at 3000rcf for 20 minutes at 25°C. Concentrated samples were aliquoted and stored at -80°C until needed. Samples were not subjected to more than one freeze thaw cycle.

2.3.2 Quantification of Protein in Concentrated Conditioned Medium Samples

Protein concentration in samples was assessed by Bradford Assay, which allows estimation of protein concentration based on the principle that the absorbance maximum of Coomassie Brilliant Blue G-250 in acidic solution shifts from 465nm to 595nm when bound to protein. Bradford reagent was made by dissolving 100mg Coomassie Brilliant Blue G-250 in 50mL of 95% ethanol, then adding 100mL 85% orthophosphoric acid. This solution was diluted with water to a final volume of 1 litre and filtered through Whatman #1 filter paper prior to use.

Using a 96 well plate, 5µL of protein sample and 250µL of Bradford reagent were added per well and incubated at room temperature for 5 minutes. Optical density of each well was measured on the Spectramax M5^{e} plate reader (Molecular Devices (UK) Limited, Wokingham, Berkshire, UK) at a wavelength of 595nm, and compared against a standard curve of known protein concentrations to calculate protein concentration of each of the samples. All samples were then diluted to a concentration of 1000µg/mL.

2.3.3 Preparation of Samples for Western Blotting

A 4X Laemmli blue loading buffer was made according to the following specifications: 8% sodium dodecyl sulphate (SDS), 20% β-mercaptoethanol, 40% glycerol, and 0.0008% bromophenol blue in a 250mM TrisHCl buffer with pH adjusted to 6.8.

Protein samples were diluted 3 parts sample to 1 part 4X Laemmli blue loading buffer and placed in a heating block at 95°C for 5 minutes to denature. Samples were then kept on ice until ready to use.

2.3.4 Gel Electrophoresis

Electrophoresis gels with a 12% polyacrimide resolving gel section were made according the specifications given in table 2.1 below and set at room temperature for use on the same day. A total volume of 20µL of the denatured sample was loaded per well. TrailMix™ HRP Western Blot Kit (Millipore, Watford, UK.) markers were used, following manufacturer's instruction.

The loaded gel was electrophoresed at 40mA for ~45 minutes until the sample could be seen to have passed through the stacking portion of the gel. The current was then increased to 80mA and run until the leading edge of the sample reached the end of the lane. The separated samples in the gel were then transferred to a nitrocellulose membrane using the wet transfer method. After transfer, the gel was stained with Coomassie Blue to visualise remaining protein bands and ensure that proteins in the sample had been separated as expected.

Table 2.1: Specifications for Electrophoresis Gel Preparation

Resolving gel (12%)		**Stacking gel**	
Water	3.3ml	Water	2.7ml
30% Acrylamide mix	4ml	30% Acrylamide mix	0.67ml
1.5M Tris (pH 8.8)	2.5ml	1M Tris (pH 6.8)	0.5ml
10% Sodium dodecyl sulphate	0.1ml	10% Sodium dodecyl sulphate	0.04ml
10% Ammonium Persulphate	0.1ml	10% Ammonium Persulphate	0.04ml
TEMED	0.004ml	TEMED	0.004ml

2.3.5 Antibody Incubation and Visualisation

Once the transfer process was complete the membrane was blocked with a solution of Tris-buffered saline with tween (TBST), using 1% bovine serum albumin (BSA) and 5% non-fat dry milk as blocking agents. Blocking was conducted at room temperature for 2 hours, using a plate shaker on a low setting to agitate gently.

A blocking buffer of TBST with 0.5% BSA, and 1% non-fat dry milk was made, and primary HRP-conjugated antibody against LOX (NOVUS, R&D Systems Ltd., Abingdon, UK.) added at a dilution of 1:1000 parts antibody to buffer. The membrane was incubated in 10mL of primary antibody blocking buffer in a 50mL Falcon tube, placed on a roller overnight at 4°C.

The transfer membrane was then washed in TBST on a plate shaker for 15 minutes, repeated 3 times at room temperature. Antibody-protein complexes were visualised using EZ-ECL colour substrate (Biological Industries Israel Beit-Haemek Ltd., Kibbutz Beit-Haemek, Israel), according to manufacturer's instructions. After one minute incubation in EZ-ECL at room temperature the membrane was imaged using radiographic film. Transfer membranes were then stained using Ponceau S to visualise protein in the nitrocellulose membrane, allowing assessment of whether protein had been equally loaded in all samples.

2.4 End-Point PCR

2.4.1 RNA extraction

Cells were grown to 50% confluency in a T75 flask in normal growth medium (DMEM +10% FBS, 100 U/mL penicillin, and 100µg/mL streptomycin). The flask was then washed twice with PBS and 1mL TRI-reagent (Sigma-Aldrich Company Ltd., Dorset, UK.) was pipetted over the cell monolayer, which was then agitated with a cell scraper to aid homogenisation. The homogenate was removed to a 1.5mL Eppendorf and incubated at room temperature for 5 minutes before 0.2mL of chloroform was added and the sample shaken vigorously for 15 seconds to initiate phase separation. The sample was then incubated at room temperature for a further 2-3 minutes and centrifuged at 12000rcf, 4°C, for 15 minutes to separate the different phases in the sample. The upper aqueous phase was carefully removed via pipette, taking care not to lift any genetic material from the interphase.

RNA was precipitated from the aqueous phase by adding 0.5mL of isopropyl alcohol and incubating at room temperature for 10 minutes. The sample was then centrifuged at 12000rcf, 4°C, for 10 minutes to pellet the RNA. The supernatant was removed and the pellet washed in 1mL of 75% ethanol to wash off salts, then centrifuged at 7500rcf and 4°C for 5 minutes. The supernatant was poured off and the pellet left to air dry at room temperature for up to 30 minutes, until it became transparent.

The dried pellet was then dissolved in nuclease free water, and RNA quantity and quality was assessed by Nanodrop 1000 Spectrophotometer (Fisher Scientific, Loughborough, UK).

2.4.2 DNAse Treatment

RNA samples were DNase treated, using DNase I (RNase-free) (New England BioLabs®, Ipswich, MA, USA), following manufacturer's instructions. Briefly, 10µg RNA was suspended in 1X DNase I reaction buffer to give a final volume of 100µL. Two units of DNase I were added to the suspension, which was then mixed and incubated for 10 minutes at 37°C. Finally, 1µL of 0.5M EDTA was added, and the suspension incubated at 75°C for 10 minutes to heat inactivate the enzyme.

2.4.3 cDNA Synthesis

First strand cDNA synthesis was performed using Applied Biosystems High-Capacity RNA-to-cDNA™ Kit (Life Technologies Ltd., Paisley, UK.), following manufacturer's instructions.

Two separate controls were used to check for sample contamination. Firstly, a no RNA control was used, substituting water for RNA, to check for contamination in the kit reagents. For each of the RNA samples run, a no RT (-RT) control was run to check for genomic DNA contamination in the RNA sample.

Reverse transcription of cDNA from RNA template was initiated by incubating the samples at 37°C for 60 minutes, followed by 95°C for 5 minutes to inactivate the reverse transcriptase enzyme. Samples were then held at 4°C until ready for use.

2.4.4 End-Point PCR

PCR was conducted using the Promega GoTaq® DNA polymerase kit. Each reaction was measured out following table 2.3 below. Primer sequences used are given in table 2.2, and thermocycling conditions are given in table 2.4. Primer sequences for the murine P2X7R splice variants were taken from Nicke et al. (2009). Each splice variant has a specific forward primer (mX7ex1Fv-a, for P2X7R(a), and mX7ex1Fv-k for P2X7R(k)), which binds to a region on the first exon, and a shared reverse primer (mX7ex4Rv), which binds to a common region on the fourth exon. Sequences for the GAPDH pan-species primers were kindly given by Dr. Gareth Richards (Mellanby Centre for Bone Research, University of Sheffield, Sheffield, UK.).

Table 2.2 Primer Sequences for End-Point PCR

P2X7 splice variants	
mX7ex1Fv-a	5'-CAC ATG ATC GTC TTT TCC TAC-3'
mX7ex1Fv-k	5'-GCC CGT GAG CCA CTT ATG C-3'
mX7ex4Rv	5'-GGT CAG AAG AGC ACT GTG C-3'
GAPDH	
pan-GAPDH-F	5'-TTG TCA GCA ATG CAT CCT GC-3'
pan-GAPDH-R	5'-GCT TCA CCA CCT TCT TGA TG-3'

Table 2.3: End-Point PCR Mix

Component	**Volume per reaction (µl)**
5X GoTaq® rxn buffer	2
dNTP mix (10mM stock)	0.2
Forward Primer (5µM stock)	0.4
Reverse Primer (5µM stock)	0.4
GoTaq® DNA polymerase	0.05
Nuclease-free Water	5.95
cDNA	1
TOTAL VOLUME	**10**

Table 2.4 Thermocycling conditions for End Point PCRs

	Temp	**No. of Cycles**	**Duration**
P2X7R splice variants			
Initial Denaturation	94°C	1	2 mins
Denaturation	94°C	35	40s
Annealing	58°C	35	40s
Extension	72°C	35	40s
Final Extension	72°C	1	10 mins
GAPDH			
Initial Denaturation	95°C	1	2 mins
Denaturation	95°C	35	40s
Annealing	64°C	35	40s
Extension	72°C	35	40s
Final Extension	72°C	1	10 mins

2.5 MTS Assay

MTS Assay was performed using the CellTiter 96®AQ_{ueous} Non-Radioactive Cell Proliferation Assay (Promega, Southampton, UK.) according to manufacturer's instructions. The MTS Assay is a colourimetric proliferation assay used to assess the number of viable cells in a sample. The assay is based upon the reduction of a novel tetrazolium compound [3-(4,5-dimethylthiazol-2-yl)-5-(3-carboxymethoxyphenyl)-2-(4-sulfophenyl)-2H-tetrazolium, inner salt] (MTS), into a soluble, purple, formazan dye product. The reaction is driven by dehydrogenase enzymes present in metabolically active cells, and occurs in the presence of the electron coupling reagent phenazine methosulphate (PMS). The quantity of formazan dye produced is directly proportional to the level of dehydrogenase enzyme activity, which is in turn proportional to the number of live cells in culture, and is identified by measuring the optical density (OD) of the sample at 490nm, using the Spectramax $M5^e$ plate reader (Molecular Devices (UK) Limited, Wokingham, Berkshire, UK).

PMS stock solution was prepared by dissolving 9.2mg PMS powder in 10mL Dulbecco's Phosphate Buffered Saline (DPBS). This solution was then sterile filtered using a 0.2µm syringe filter and stored at -20˚C in 1mL aliquots, wrapped in foil to protect from light. MTS stock solution was made by dissolving 42mg of MTS reagent powder in 21mL DPBS in a foil wrapped tube (to protect from light). The pH was adjusted to between 6.0 and 6.5 using 1N HCl, and sterile filtered with a 0.2µm syringe filter. 1mL PMS stock solution (thawed) was added to 20mL of the MTS solution – making a final 10X MTS stock, which was then stored at -20˚C in foiled wrapped 1mL aliquots.

For each assay timepoint, 1mL of 10X combined MTS and PMS stock solution was thawed and diluted to working concentration in 9mL of phenol-free DMEM (Gibco® Invitrogen, Paisley, UK). Medium was removed from the culture plate and the wells washed with PBS before 100µL of working MTS solution was added. MTS solution was also added to a column of empty wells for baseline reference. The plate was then wrapped in tinfoil to protect from light and incubated at 37°C (95% air, 5% CO_2) for 2 hours before recording OD at 490nm on the plate reader.

2.5.1 4T1 Cell Number MTS Assay Standard Curve

To assess the ability of MTS assay to determine cell number of *in vitro* cultures of 4T1 cells, known numbers of 4T1 cells, taken from 50% confluent flasks were plated in a 96 well plate in complete DMEM. The plate was incubated at 37°C (95% air, 5% CO_2) for one hour to allow cell adherence before continuing with the MTS assay, as described above. This data was used to generate a standard curve comparing known cell number with that predicted by assay.

2.6 Treatment of 4T1 Cell Culture with ATP

To investigate the effect of purinergic signalling on normal cell growth (in the presence of FBS) 4T1 cells were plated in a 96 well plate at a density of 3000 cells per well in DMEM +10%FBS. Cells were then incubated for 24 hours to allow adherence before wells were washed with PBS and medium was replaced with 180µL serum-free DMEM. Serial dilution of stock ATP solution (dissolved in serum-free DMEM) was conducted to generate 10X concentrations of all desired ATP concentrations (ranging from 0 to 5µM), and 20µL of the appropriate stock solution was added to each well as appropriate, resulting in 200µl total medium per well at the desired concentration of ATP. Cells were then incubated for 1 hour to allow ATP to activate the purinergic receptors. Wells were then washed again with PBS and medium changed to DMEM +0.5% FBS. Finally, cells were incubated for either 24 or 72 hours before MTS assay. In addition to the experimental groups dosed with ATP, a control group which was continually cultured in DMEM +0.5% FBS was included for use as a standard for normal cell growth.

To investigate the effect of purinergic signalling on 4T1 cells under the conditions of starvation (absence of FBS) cells were initially plated in DMEM +10% FBS and incubated for 24 hours to settle. Wells were then washed with PBS and serum free DMEM with ATP doses ranging from 0 to 5µM were added in the manner described above. Unlike in the normal culture, where the addition of FBS would lead to rapid catalysis of ATP from endonucleases present in the serum, there was no need to replace medium after ATP dosing. The ATP containing serum-free DMEM was, therefore, left on the cells for the full 24 or 72 hour incubation period. A control group of cells was cultured in DMEM +0.5% FBS, with no ATP stimulation as a standard for normal cell growth.

To determine the presence of functional P2X7R in the 4T1 cell line, a further series of cultures were conducted using ATP and A438079 HCl (Tocris Bioscience, Bristol, UK.), a competitive P2X7R antagonist, devoid of activity at other P2 receptors. Cells were cultured as described above in both normal (+FBS) and starvation (-FBS) culture conditions, with the addition of A438079 HCl at concentrations of IC_{50} (0.65µM) and 10X IC_{50} (6.5µM) in all ATP treatment groups. As A438079 HCl is a competitive antagonist, it was added to the wells of the culture prior to the ATP dose to maximise the chance for receptor binding and antagonism.

2.7 Murine Breast Cancer Model

2.7.1 P2X7R$^{-/-}$ BALB/c Mouse Model

WT BALB/c mice were purchased from Charles River (Margate, UK.). P2X7R$^{-/-}$ BALB/c mice were bred in house at The University of Sheffield (Sheffield, UK) from colony founders kindly donated by Dr. Niklas Rye Jørgensen (Research Centre for Ageing and Osteoporosis, Glostrup, Denmark).

The P2X7R$^{-/-}$ BALB/c mice used in this study were originally generated by backcrossing Glaxo P2X7R knockout C57BL/6 mice onto a BALB/c background (Chessell et al. 2005; Syberg et al. 2012) following published protocol (Conquet 1995). Briefly, partial sequencing of the 5' exons of the P2X7 gene allowed ligation of two fragments into a neomycin resistant plasmid, which served as a vector to disrupt the P2X7 gene via homologous recombination of the plasmid DNA into embryonic stem cells. This resulted in a targeted null mutation of the P2X7 gene. Chimaeric mice, with a transfected germline, were then crossed with C57BL/6J females to generate heterozygotes. The heterozygotes were then intercrossed to produce healthy mutant offspring with the expected Mendelian ratio. Successful homozygous knockout was confirmed with Southern and Western blots, PCR, and monitoring ATP activated YO-PRO-1 uptake in peritoneal macrophages (Chessell et al. 2005). Females from these C57BL/6 knockout mice were then crossed into a BALB/c inbred strain from Jackson Laboratories (Bar Harbor, ME, USA) for five generations. Founders for the P2X7R$^{-/-}$ BALB/c colony were then selected by PCR (Syberg et al. 2012).

All mice were housed in a 12 hour light/dark cycle and allowed free access to water and standard diet. After sacrifice the organs were removed and fixed for 48 hours in 4% paraformaldehyde (PFA), before switching to 70% industrial methylated spirits (IMS) for storage. Skeletons were fixed in 10% neutral buffered formalin (NBF). All procedures were conducted on female mice and complied with the UK Animals (Scientific Procedures) Act 1986 and were reviewed and approved by the local Research Ethics Committee of the University of Sheffield (Sheffield, UK).

2.7.2 Orthotopic Tumour Model

4T1 cells were cultured in complete DMEM to 70% confluency. Cells were then passaged as described above (Section 2.2), counted using a haemocytometer, and resuspended in PBS at a concentration of $2x10^6$ cells per mL. The cell suspension was then taken immediately to the treatment room for injection into the right mammary fat pad to simulate a primary breast tumour. The injection consisted of 50µl of cell suspension at $2x10^6$ cells/mL, resulting in a delivery of ~$1x10^5$ cancer cells to the mammary fat pad. After the injection process the remaining cell suspension was plated and cultured *in vitro* as normal to ensure cells remained viable at the time of injection.

Injections were administered at 9 weeks of age. Mouse weight and tumour size were monitored thrice weekly for 3 weeks before sacrifice. As the 4T1 cell line is derived from a spontaneous tumour originally found in a BALB/c mouse (Tao et al. 2008; Miller et al. 1983) this is a syngeneic model.

2.7.3 Cell Free Model

4T1 cells were plated in 6 well plates with 3mL complete DMEM per well. Various seeding densities were used to maximise the chance of wells at the desired confluency on the appropriate day. Cells were grown to 80% confluency, at which point the well was washed twice with PBS before 2mL of phenol-free DMEM (free from FBS, penicillin, and streptomycin) was added. The plate was then incubated as normal for 24 hours, after which the conditioned medium was collected, centrifuged and sterile-filtered through a 0.2µm membrane, as previously described (Section 2.2.1). The conditioned medium was taken directly to the treatment room for intraperitoneal injection.

Each mouse received a daily intraperitoneal injection of 300µL conditioned medium. Injections continued daily for 3 weeks. Mouse weight was monitored throughout the injection procedure and mice were sacrificed at 12 weeks of age.

2.8 Preparation of Fixatives

2.8.1 Paraformaldehyde (4% solution)

Paraformaldehyde (PFA) was prepared by dissolving 4g PFA powder in 90ml Dulbecco's Phosphate Buffered Saline (DPBS) heated to 60 ˚C with constant stirring and addition of 10N NaOH as needed to aid dissolution. The PFA solution was removed from heat and, where required, hydrochloric (HCl) acid added to reduce the pH to 7.2-7.4. The final volume of solution was brought to 100ml by the addition of DPBS, cooled to room temperature, and stored at 4˚C.

2.8.2 Neutral Buffered Formalin (10%)

Neutral buffered formalin (NBF) was prepared by dissolving 20g sodium dihydrogen orthophosphate dehydrate and 32.5g disodium hydrogen orthophosphate in a mix of 500ml concentrated formaldehyde and 500ml warm tap water. The solution was stored at room temperature until required.

2.9 Micro Computed Tomography (µCT)

The hindlimbs were dissected from fixed mice and enough musculature removed to allow full movement of the knee joint. Bones were scanned using either a Skyscan 1172 (Chapter 4), or Skyscan 1272 (Chapter 5) high resolution desktop Micro CT (µCT) scanner. For the Skyscan 1172 the following settings were used: Resolution 4.3µm, medium camera (2000x1024), 0.5 Al filter, 180° scan, 0.7 rotation, 2x averaging. The resultant image files were reconstructed, and the dynamic image range thresholded to 0-0.16 using the software package NRecon v.1.6.5.8 (Skyscan, Kontich, Belgium). Scans conducted with the Skyscan 1272 used the following settings: Resolution 4.3µm, medium camera (2016x1344), 0.5 Al filter, 0.7 rotation. Resultant images were reconstructed and the dynamic image range thresholded to 0-0.14, using NRecon as above. Scans from different machines were not included together in any analyses due to differing strengths in the power of the X-ray sources in each machine precluding compatibility.

2.9.1 Lesion Quantification

The software package CT Analyzer v.1.11.4.2 (Skyscan, Kontich, Belgium), hereafter referred to as CTAn, was used to generate 3D models of each bone from µCT data. The first break in the epiphyseal growth plate was identified as a landmark reference point. The region of interest (ROI) for 3D model generation included the epiphyseal head and a 2mm length of diaphysis, measured from the first break in the growth plate. The images comprising this ROI were thresholded to 70-255 greyscale and processed to remove white speckles with a volume of less than 10 voxels before being used to generate 3D models.

The resulting 3D model files were loaded into GOM Inspect v. 7.5 SR2 (available from http://www.gom.com/3d-software/gom-inspect.html), hereafter referred to as GOM, to allow visualisation of the model, and free movement of the model in virtual space. Each hole in the cortex with any dimension greater than 50µm was manually traced onto acetate, alongside a 50µm x 50µm scale box for reference. Once complete the acetate was scanned to PDF format and the area of the traced holes measured using the program CellD® (Olympus, UK). Any hole with an area less than 2500µm^2 was considered to be a normal physiological feature and removed from further analysis, any hole above this was considered to be a lesion.

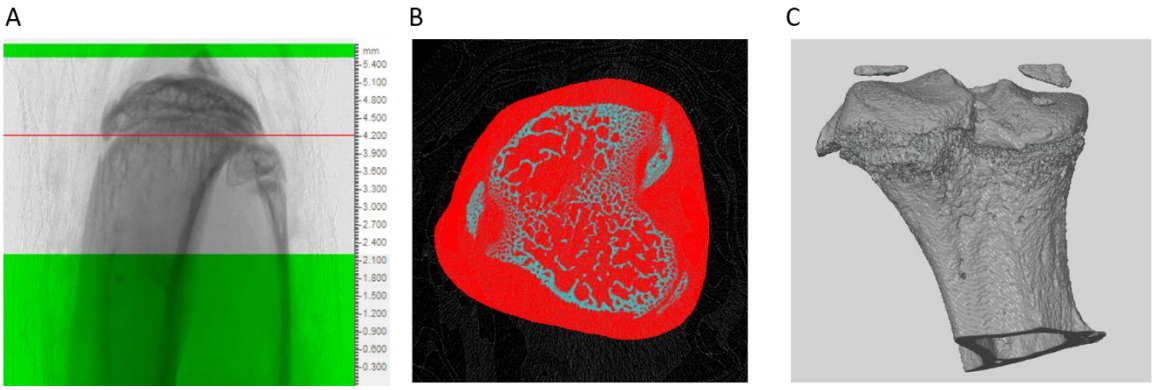

Figure 2.1: Lesion Analysis Region of Interest. **A:** Shadow projection showing area of bone included in ROI for lesion analysis. Green areas are excluded. Red line denotes level of first break in epiphyseal growth plate, and the plane of image in B. **B:** Cross-section of tibia. Red highlighted area denotes the ROI for 3D model generation. **C:** 3D model of tibia generated from µCT data and used to quantify osteolytic lesions.

2.9.2 Cortical Bone Analysis

Reconstructed µCT scans were loaded into CTAn and cortical thickness was manually measured at twelve equidistant points around the circumference of the diaphysis, at a distance of 0.75mm from the first break in the epiphyseal growth plate.

2.9.3 Trabecular Bone Analysis

Reconstructed µCT scans were loaded into CTAn where a 1mm section of diaphysis, offset from the growth plate break by 0.2mm, was selected for analysis. The medullary cavity was selected as the ROI by manually tracing around the inner cortical boundary. Image greyscale was thresholded to 70-255, and the mean greyscale for each ROI recorded. ROI images were then processed to remove white speckles under 10 voxels from the region of interest, and CTAn's 3D analysis run to output data on percentage bone volume (BV/TV), trabecular number (Tb No.), thickness (Tb Th), and structure model index (SMI). Bone Mineral Density (BMD) was calculated from mean greyscale using the following formula:

$$BMD = (0.0112\ x\ Mean\ Greyscale) - 0.2757$$

This formula was calculated from the equation of the line generated by plotting the greyscale values of two scanned phantoms of known densities against each other.

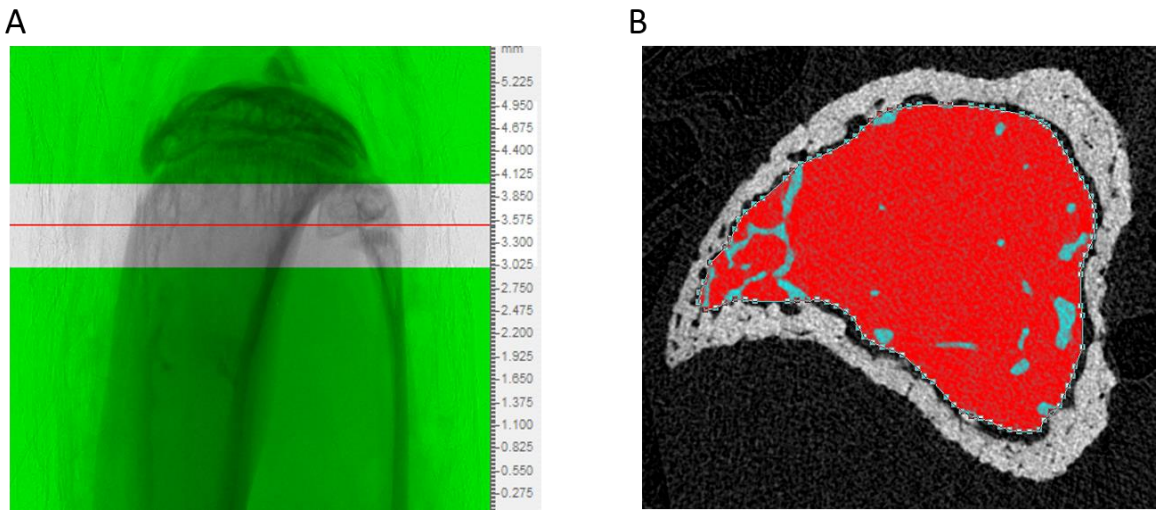

Figure 2.2: Trabecular Analysis Region of Interest. **A** Shadow projection showing 1mm section of tibia used for trabecular analysis. Green areas are excluded. Red line denotes plane of image in B. **B** Cross-section of tibia. Red area denotes ROI for conducting trabecular analysis.

2.10 Calculation of Tumour Volumes

Tumour volume was calculated from calliper measurements of the maximal and minimal diameter recorded at 17 days after initial injection of tumour cells to the mammary fat pad. Volume was calculated using the formula:

$$volume = \pi/6 \, [w_1 \, x \, (w_2)^2]$$

Where w_1 is the major diameter, and w_2 is the minor diameter (Adinolfi et al. 2015).

2.11 Mechanical Loading Procedure

2.11.1 Calculation of Appropriate Loading Force

Previously published research has shown that mechanical loading resulting in a strain of 5000 microstrain (με) is osteogenic in C57BL/6 mice (Wang et al. 2013). The requisite loading force to engender 5000με in a 10 week old female BALB/c mouse tibia was calculated as 8.3N, via Finite Element Analysis (FEA) of a whole bone CT scan, using previously published methods (Wang et al. 2013).

2.11.2 Mechanical Loading of Tibiae

Mice were subjected to mechanical loading using a previously reported non-invasive axial loading technique (De Souza et al. 2005a; Wang et al. 2013), using an INSTRON 8511 loading machine. The loading apparatus consisted of two loading cups: one fixed to the loading platform, the other to a hydraulic piston. A diagram of the device is given below in figure 2.3. Prior to loading, mice were anaesthetised with Isofluorane (IsoFlo®, Abbott, Maidenhead, UK). Once unconscious and unresponsive to pinch testing of the footpad, the ankle joint was placed into the lower loading cup and the knee joint flexed. The limb was then held in position as the piston was lowered into place and held at a force of 0.5N, cushioning the leg.

During each loading session a dynamic load of 7.8N was superimposed upon the 0.5N pre-load at a rate of 160000 N/s, giving a peak load of 8.3N. Each session delivered 40 trapezoidal waveform load cycles, with a 10s rest between each cycle. The left limb was left unloaded, and used as a contralateral control: previous research showing that functional adaptation to loading in both cortical and trabecular bone is controlled locally and thus confined to the loaded bone (Sugiyama et al. 2010; De Souza et al. 2005b). Mice were loaded every two days for a total of 6 loading sessions, then monitored for a further 4 days before euthanasia at 12 weeks of age.

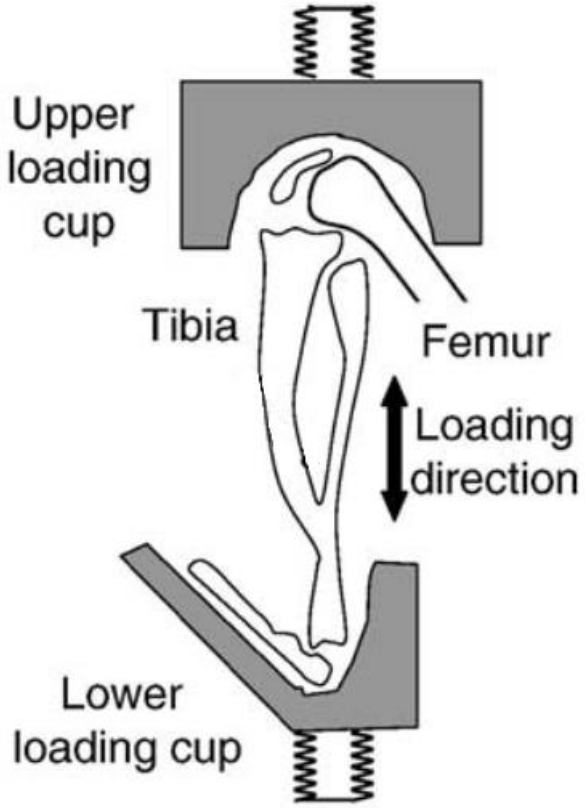

Figure 2.3: Axial loading schematic: Diagram displays position of mouse limb in loading apparatus. The upper loading cup is attached to a hydraulic piston exerting a constant force between 0.5 and 8.3N to load the tibia in the direction shown. Figure reproduced from De Souza et al. (2005a), with permission from publisher: Elsevier Science Ltd.

2.12 Statistical Analyses

All statistical analyses were carried out using GraphPad Prism v. 6.04 for Windows (GraphPad Inc., La Jolla, CA, USA). Dataset normality was assessed using the D'Agostino-Pearson omnibus normality test, and outliers were identified and removed as necessary using the Grubb's outlier test (http://graphpad.com/quickcalcs/Grubbs1.cfm). Where data were normally distributed, significant difference was assessed using either Student's t test for comparison of two groups, or one-way ANOVA, with Dunnett's multiple comparisons post-test, for more than two groups. Where data were not normally distributed, significant difference was assessed using the Mann-Whitney test for comparison of two groups, the Wilcoxon matched-pairs signed rank test for comparison of paired groups, or the Kruskall-Wallis test with Dunn's multiple comparison post-test, for comparison of more than two groups. Exact p-values are given where possible. Post-test analyses from one-way ANOVA and Kruskall-Wallis did not return exact p-values, and in these cases are reported by level of statistical significance (i.e. * $p<0.05$, ** $p<0.01$, *** $p<0.001$, **** $p<0.0001$). All data are plotted as mean values ± standard deviation from the mean (SD).

CHAPTER 3: VALIDATION OF P2X7R/LOX MURINE METASTATIC MODEL

3.1 Introduction

As discussed in the introductory chapter, we have proposed that LOX and P2X7R signalling interact to drive osteolytic lesion formation in bone, initiating a process which is able to increase metastasis, and contribute significantly to increased mortality and morbidity in cancer patients. In order to investigate the potential interaction of LOX and P2X7R signalling on metastasis to bone, a model had to be validated allowing the isolation of contributions from both LOX and P2X7R to this process. To meet these criteria a $P2X7R^{-/-}$ BALB/c mouse model (Hansen et al. 2011; Syberg et al. 2012) was used in conjunction with the 4T1 murine breast cancer cell line, which constitutively expresses LOX (Cox et al. 2015). 4T1 cells were originally derived from a spontaneous mammary tumour in a BALB/c mouse, thus making the model syngeneic (Tao et al. 2008; Miller et al. 1983). In order to ensure that the 4T1 cells used in this model were suitable for their intended purpose, a series of tests were run to investigate potential expression of both P2X7R and LOX in the cell line.

Interference with P2X7R activity in the devised experimental model was also carefully balanced. An important feature of this is that P2X7R is knocked out in the mouse, but remains unaltered in the 4T1 cancer cells. This allows investigation of how P2X7R may contribute to tumour related modification of the bone microenvironment to promote osteolytic lesion formation, and eventual metastasis in the host mouse, without affecting primary tumour growth or metastatic activity. This is an important consideration as P2X7R has previously been shown to contribute to cancer cell survival and metastasis (Adinolfi et al. 2012; Di Virgilio et al. 2009; Jelassi et al. 2011), as well as osteoclast cell activity. Previous research has also shown that P2X7R stimulation can lead to activation of NFATc1, the master regulator of osteoclastogenesis (Korcok et al. 2004; Adinolfi et al. 2009). As LOX has been shown to drive osteoclast activity via regulation of NFATc1 (Cox et al. 2015) this suggests a possible mechanism by which LOX and P2X7R may be interacting. If this hypothesis is correct then we would expect to see a reduction in osteolytic lesion formation in $P2X7R^{-/-}$ mice.

Characterisation of breast cancer cell lines has revealed that P2X7R drives an invasive cell phenotype, increasing formation of neurite-like cell projections which contribute to an increased invasion of the MBA-MB-435 breast cancer cell line through extra-cellular matrix (ECM) by up to 150% (Jelassi et al. 2011). P2X7R has also been shown to increase invasion and migration of the T47D breast cancer cell line via activation of the AKT pathway, and regulation of E-cadherin and MMP-13 (Xia et al. 2015). In addition to this metastatic activity, P2X7R is known to aid cancer cell survival, with activation having been shown to promote cancer cell proliferation and neoangiogenesis, while also inhibiting apoptosis (Adinolfi et al. 2012). As such it is important that P2X7R expression is unaltered in the breast cancer cell line used in this study's experimental

model to ensure that cancer growth and metastasis occurs as normal. Interference with normal P2X7R function in the 4T1 cell line may yield valuable information regarding LOX and P2X7R signalling in the primary tumour, but could potentially hinder metastasis to bone, thus making the model less suitable for the investigation of tumour secreted LOX on the bone microenvironment. This could subsequently inhibit potential effects of the cancer cell in generation of a pre-metastatic niche in bone, which is a primary aim of this study.

Despite being characterised in the MDA-MB-243 (Jelassi et al. 2011), and T47D breast cancer cell lines (Xia et al. 2015), a search of the literature returned no positive identification of whether or not the 4T1 cell line expressed P2X7R. Identifying the presence of P2X7R in the 4T1 cell line would identify the possibility of LOX and P2X7R interaction at the level of the cancer cell. While not an immediate aim of this study, identifying such a connection would inform potential future research, while also suggesting a possible mechanism for observations of increased primary tumour growth in LOX expressing tumours. To investigate whether 4T1 cells express P2X7R, end-point PCR was used to investigate P2X7R RNA expression. This was followed by *in vitro* culture of 4T1 cells in the presence of ATP (the agonist for P2X7R), and the specific P2X7R antagonist A438079 HCl, in order to ascertain whether a notable effect of P2X7R stimulation could be identified, thus providing evidence for the presence of functional P2X7R protein by the 4T1 cell. Together these investigations enabled an assertion of whether P2X7R was expressed by 4T1 cells, whether the expressed RNA was translated into functional protein, and therefore whether it could provide a potential mechanism for LOX contribution to metastatic activity in the 4T1 cell line.

While Western blotting would allow identification of P2X7R protein in 4T1 cells it would not offer insight into whether that protein was functional or not, necessitating the follow up *in vitro* culture already described. A positive identification of P2X7R stimulation on 4T1 cell growth in this culture would identify the presence of functional P2X7R protein, thus negating the need to check for protein expression by Western blot in the first instance. In addition, based on previous experience within the lab, commercially available P2X7R antibodies (required for Western blot) have been found to be neither particularly reliable nor specific. The fact that functional P2X7R protein, as a receptor, is bound within the cell membrane further complicates preparation of a suitable sample for Western blotting. Considering these factors, it was decided to use end-point PCR as the initial investigation as it is simpler, quicker, and more cost-effective than Western blot, and also does not rely on the performance of commercially available antibodies that have been found to be insufficient.

To investigate the role of tumour derived LOX in osteolytic lesion formation it was necessary to inhibit LOX production in 4T1 cells. Our collaborators have previously achieved this via insertion of a short hairpin RNA sequence against LOX (shLOX) into the 4T1 cell line (Erler et al. 2009). Short hairpin RNA works by using small antisense RNA molecules to target specific mRNA molecules for cleavage and degradation, thus preventing protein translation (Paddison et al. 2002; Rao et al. 2009). As this method of gene silencing targets mRNA which has already been expressed, and as it is not guaranteed to cleave 100% of expressed mRNA, shRNA is a method of genetic knockdown rather than knockout. It is, therefore, expected that there will be a reduced level of LOX production in the 4T1-shLOX cell line, rather than a complete removal.

Our collaborators kindly donated their modified cell line (4T1-shLOX) for use in this study. To confirm that the genetic manipulation of the 4T1-shLOX cell line remained functional, LOX knockdown in the 4T1-shLOX cell line was investigated using Western blot to assess protein concentration in conditioned medium from both 4T1 and 4T1-shLOX cells grown *in vitro.* This method is semi-quantitative allowing analysis of protein concentration from the intensity of the developed bands, assuming controls show equal protein loading in each sample. Confirming that LOX expression is reduced in the 4T1-shLOX cell line validates its use in the experimental model proposed above. It would have been beneficial to fully quantify LOX via ELISA, however attempts to do so with a commercially available ELISA were unsuccessful.

In summary, the experimental work detailed in this chapter investigates the presence of P2X7R in the 4T1 cell line to ascertain the possibility of direct effects of LOX stimulation of P2X7R at the cancer cell level, suggesting a further avenue of research to compliment that investigating the effect of LOX and P2X7R in the bone microenvironment, as investigated in this thesis. The efficacy of the shRNA knockdown of LOX in the 4T1-shLOX cell line, created by our collaborators, is also investigated to ensure that the genetic modification remains intact and functional, thus validating the cell line for use in the experimental work detailed later in this thesis.

3.2 Results

3.2.1 PCR for P2X7 in 4T1 cell lines

End-point PCR was used to show the presence of both A and K variants of P2X7R in the 4T1 cell line, confirming that the 4T1 cell line expresses both of these P2X7R splice variants. A PCR amplifying GAPDH was also run as a housekeeper to compare relative amounts of amplified product (Fig. 3.1).

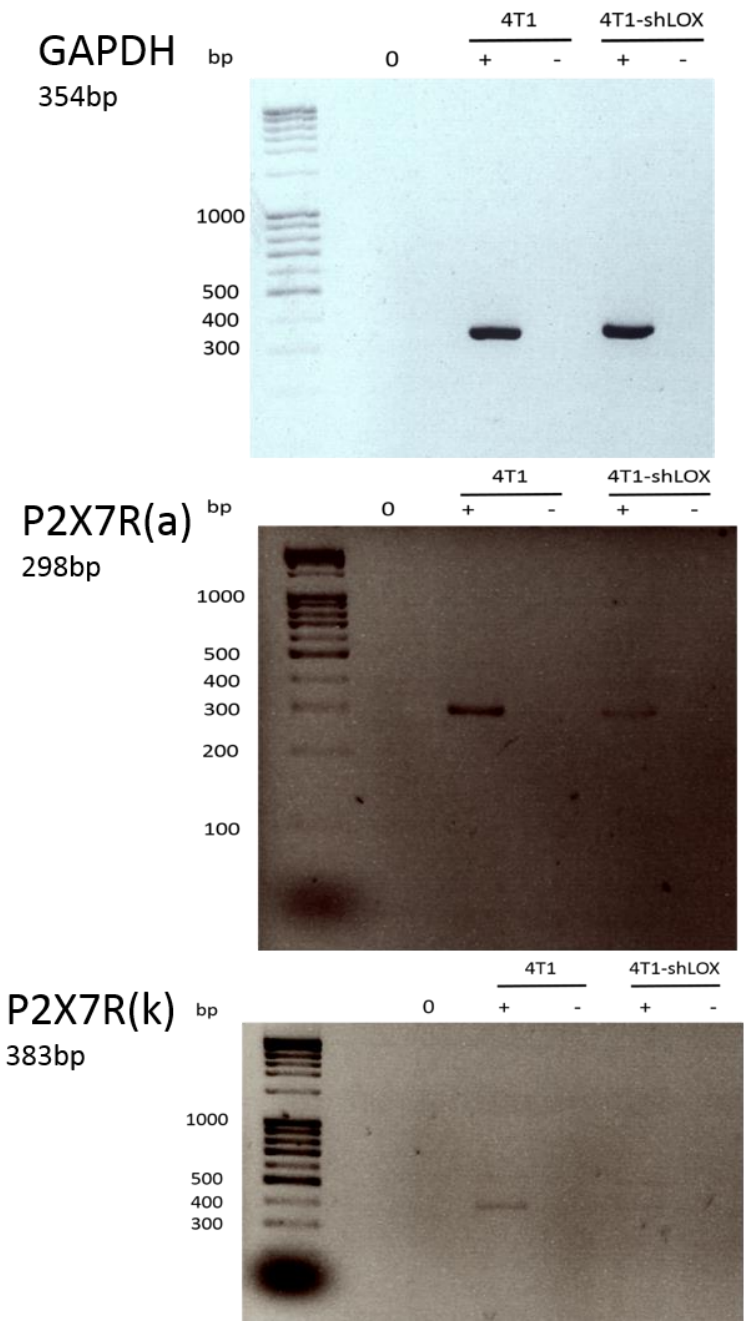

Figure 3.1 End-Point PCRs from 4T1 Cell Lines: Equal masses of RNA were amplified using specific forward primers for P2X7(a) and P2X7(k) variants, with a common reverse primer for both variants. GAPDH was used as a housekeeping gene to compare the relative amount of amplified product. The first lane (0) shows the no RNA control. Lanes 2 and 3 show the +RT and –RT reactions for 4T1 cell RNA; lanes 4 and 5 show the +RT and –RT reactions for 4T1-shLOX cell RNA. Expected product sizes are 354bp for GAPDH, 298bp for P2X7R(a), and 383bp for P2X7R(k).

3.2.2 P2X7R Functionality in 4T1 cell line

3.2.2.1 MTS Standard Growth Curve for 4T1 Cells

Known numbers of 4T1 cells, ranging from 1000 to 10000 cells per well, were plated in a 96 well plate and subjected to MTS assay one hour after plating. Plotting the raw optical density (OD) values obtained at 490nm revealed sequential increase in OD as cell number increased (Fig. 3.3). Linear regression was used to identify the best fit line, allowing an equation to approximate 4T1 cell number from MTS assay readouts:

$$Cell\ No. = \frac{OD - 0.1398}{0.00005629}$$

Although the MTS assay is strictly a measure of the metabolic activity of dehydrogenase enzymes found in proliferating cells, the clearly linear relationship between the MTS assay readout and known 4T1 cell number shows a strong correlation between the two variables (r^2=0.9964) proving it to be a reliable indicator of the number of metabolically active 4T1 cells.

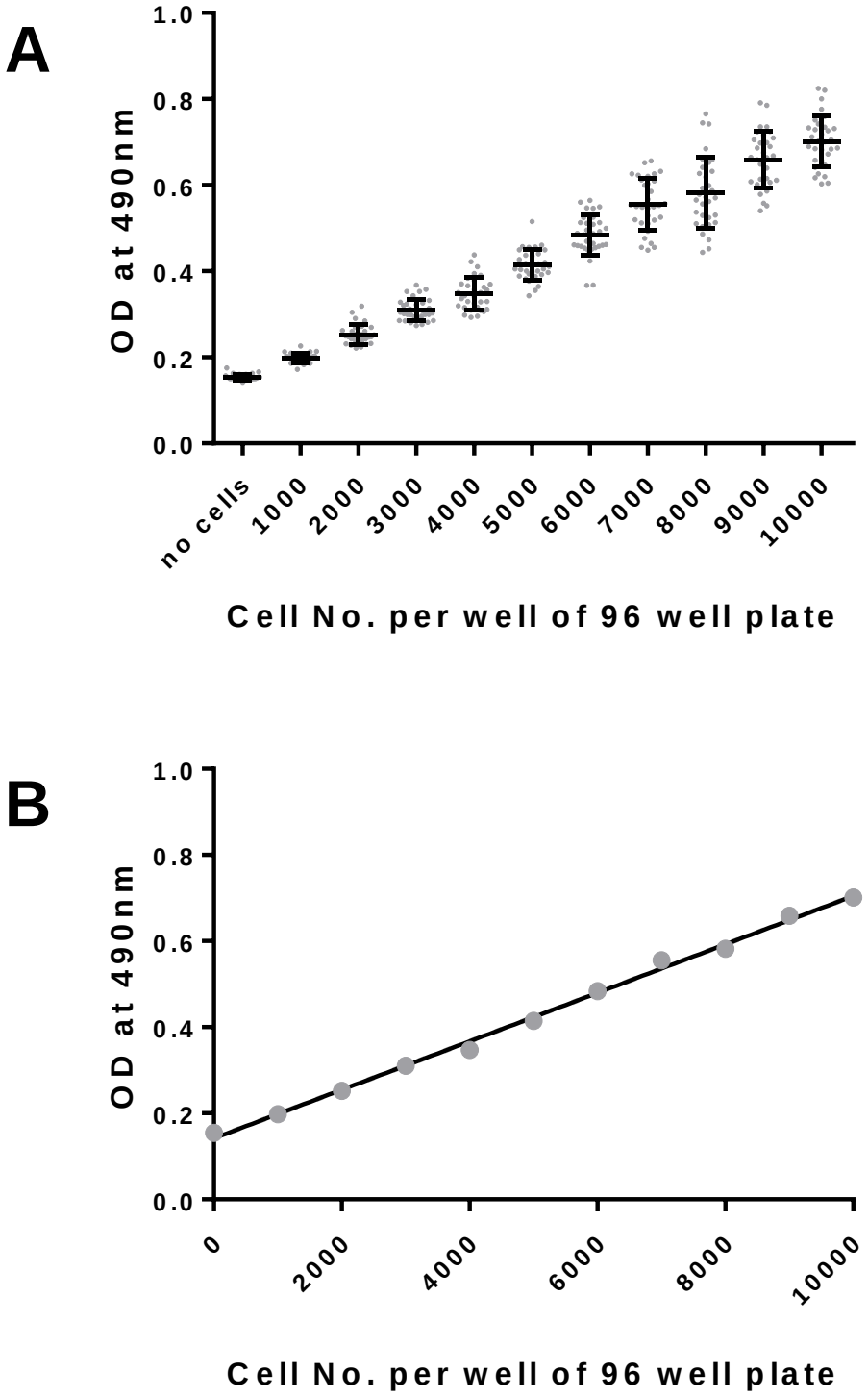

Figure 2.2: Standard Curve for Assessment of 4T1 Cell Number by MTS Assay. 4T1-WT cells were plated at between 1000 and 10000 cells per well and incubated for one hour to allow adherence to the plate. After incubation MTS assay reagent was added to each well. The plate was incubated at 37˚C for 2 hours before optical density (OD) at 490nm was measured. Data show **A** OD 490 raw values + SD for individual wells. **B** mean OD490 values plotted against the best fit line calculated by linear regression. Data from 3 cultures with n=10 for each treatment group per culture.

3.2.2.2 Effects of Purinergic Signalling on 4T1 Cell Number

To investigate the effect of purinergic signalling on 4T1 cancer cell number, 4T1 cells were cultured *in vitro* and stimulated for one hour with concentrations of ATP ranging from 0 to 5000μM. Cells were then returned to normal culture conditions (DMEM +0.5% FBS) for 24 or 72 hours before cell number was assessed by MTS assay. Under these conditions there were no statistically significant effects of ATP treatment on 4T1 cell number at either time point (Fig. 3.3).

At the 24 hour time point, the control group of cells (continually cultured in DMEM +0.5% FBS) showed a significant increase in OD490 fold change, representative of a greater number of cells in this group compared to those which were switched to serum-free DMEM for one hour during the ATP dosing phase. This difference was not present at the 72 hour time point, and suggests that removal of FBS from the culture medium for one hour had a significant effect on cell growth in the short term, but the deficit was recovered when cells had a longer period of time for catch-up growth.

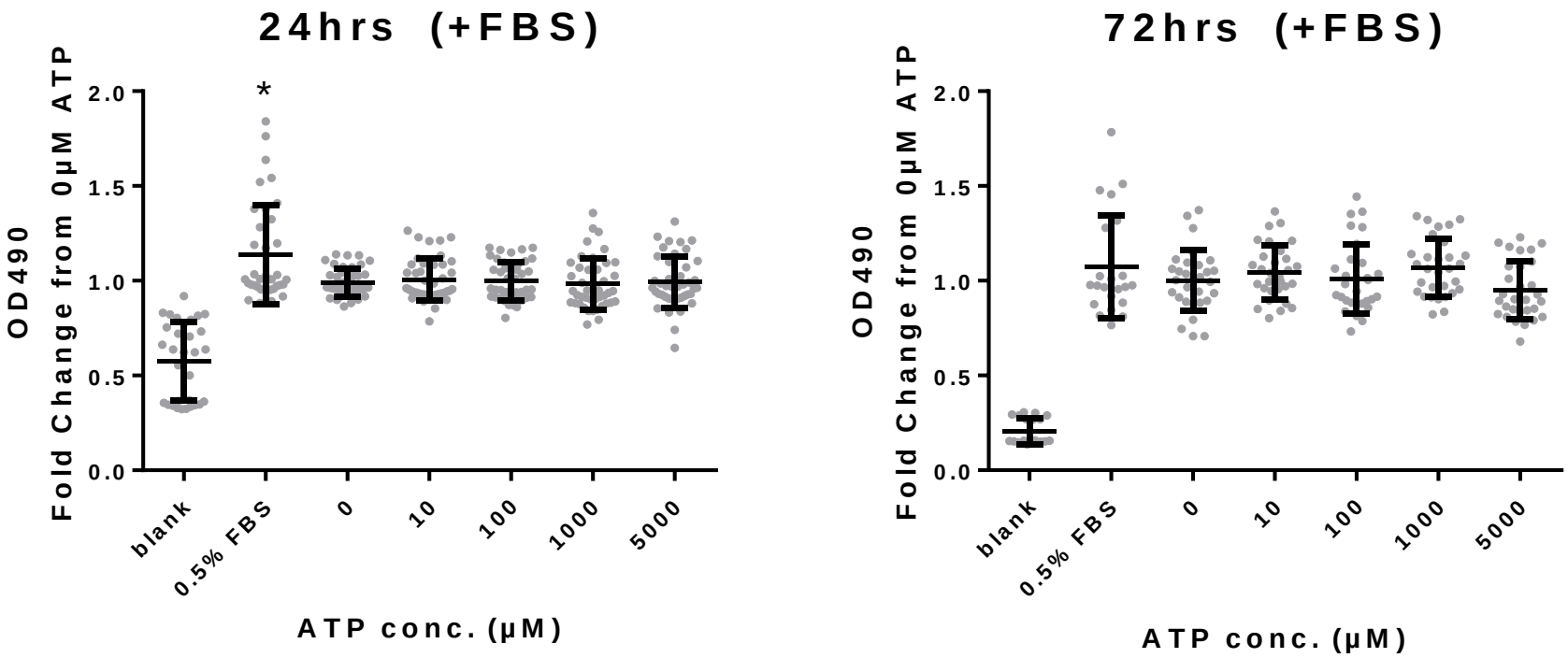

Figure 3.3: ATP Stimulation of 4T1 Cells in Normal Culture Conditions (+FBS). 4T1 cells were plated in DMEM +10%FBS at 3000 cells per well in a 96 well plate and left to incubate for 24 hours. Cells were subsequently dosed with ATP at a series of concentrations for one hour in serum-free DMEM before being returned to normal culture conditions (DMEM +0.5% FBS) for 24 or 72 hours prior to MTS assay. A control group were maintained in normal growth serum (0.5% FBS). Data shows fold change of OD490 (representative of total cell number) normalised to the 0µM ATP dose group for each culture ±SD. Data from 2 cultures with n=15 for each treatment group per culture. * denotes $p<0.05$ compared to 0 group, calculated by one-way ANOVA.

The effect of purinergic signalling on 4T1 cells was also investigated under starvation conditions (i.e. in the absence of FBS). At the 24 and 72 hr time-points there was a statistically significant reduction in cell number in the starved cells (0nM) compared to those cultured in normal growth conditions (0.5% FBS), showing that removal of FBS from the culture medium rapidly inhibited cellular growth and that the effects of starvation were noticeable in the time period chosen for the culture. Furthermore, the statistical significance of FBS removal increased as the culture progressed (24hrs, $p<0.001$; 72hrs $p<0.0001$).

Unlike in normal growth conditions, ATP was shown to have a significant effect on 4T1 cell culture when cells were starved. At the 24 hour time point cells dosed with either 10nM, 10µM or 3mM of ATP showed significant increases in cell number compared to the 0nM ATP group (10nM $p<0.05$; 10µM $p<0.01$; 3mM $p<0.001$, Fig. 3.4). Of these groups both 10µM and 3mM doses resulted in cell numbers not statistically different from the 0.5% FBS growth control group ($p>0.05$), while the 10nM group retained a statistically significantly lower cell number ($p<0.05$). Taken together this data shows that purinergic signalling in 4T1 cells is functional and allows at least short term maintenance of cellular proliferation during periods of nutrient deficiency at the doses listed above. By the 72 hour time point the pattern of ATP stimulation had changed, with all groups dosed at 100µM ATP or higher showing statistically significant reductions in cell number compared to the 0nM ATP group (100µ $p<0.001$; 1mM-5mM $p<0.0001$). This shows a detrimental effect of purinergic signalling on cell survival in starvation in the longer term.

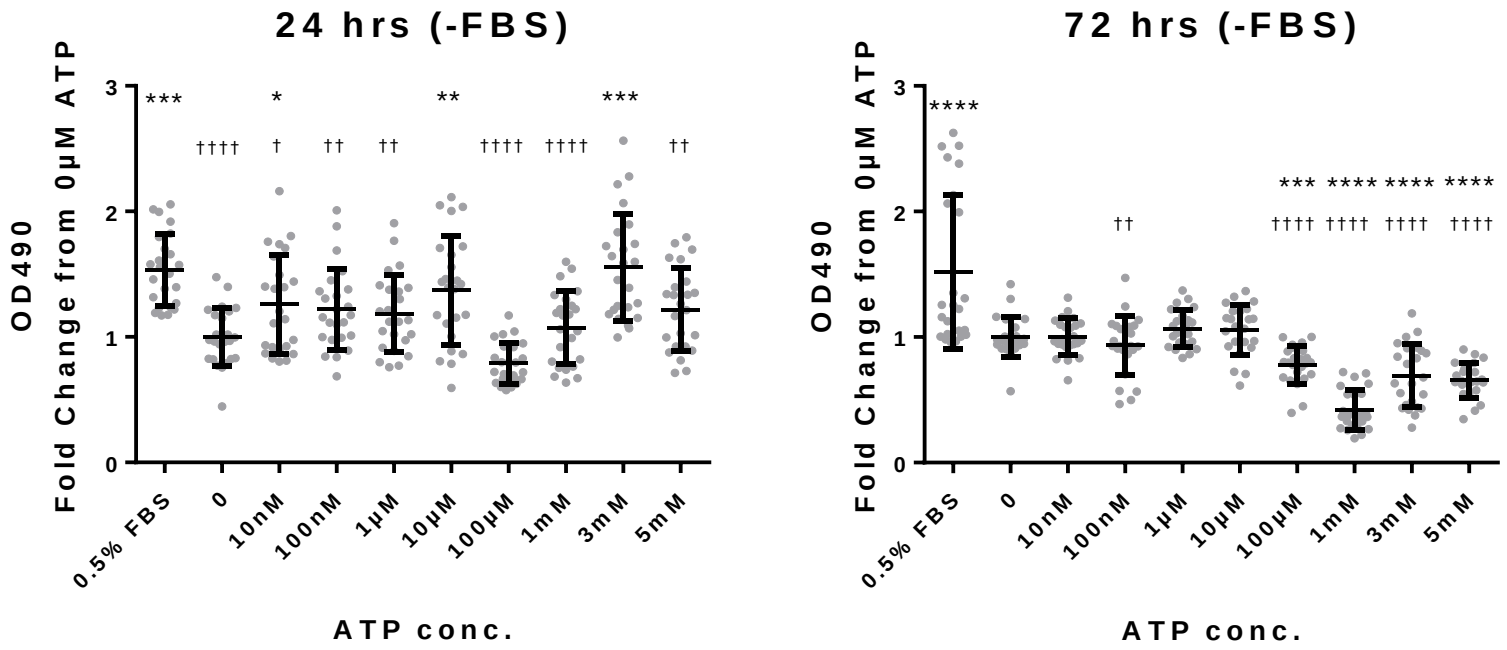

Figure 3.4: ATP Stimulation of 4T1 Cells in Starved Culture Conditions (-FBS). 4T1 cells were plated in DMEM +10% FBS at 3000 cells per well in a 96 well plate for 24 hrs before dosing with ATP at a series of concentrations in serum-free DMEM. Cells continued to be cultured in serum-free DMEM containing ATP for 24 or 72 hours before MTS assay. Data show fold change of OD490 (representative of total cell number) normalised to the 0µM ATP dose group for each culture +SD. Data from 3 cultures with n=8 for each treatment group per culture. * denotes statistical significance relative to 0nM, † denotes statistical significance relative to 0.5% FBS growth control, calculated by one-way ANOVA: * p<0.05, ** p<0.01, *** p<0.001, and **** p<0.0001.

3.2.2.3 Identification of Functional P2X7R expression in 4T1 cells

To identify whether P2X7R signalling was contributing to the purinergic signalling effects observed in the 4T1 cell culture described above, a further series of cultures were conducted with the addition of A438079 HCl, a competitive antagonist specific to P2X7R.

Cells were plated and incubated as described above (section 3.2.2.2), with the addition of A438079 HCl at concentrations of IC_{50} (0.65µM) and 10X IC_{50} (6.5µM). OD490 values from the cultures read after 24hrs and 72hrs were normalised to the 0µM ATP control of their appropriate antagonist dosage group to allow comparison of multiple cultures.

After 24 hours, under normal cell culture conditions, there was no significant effect of P2X7R antagonism on cell number in any of the ATP treatment groups. At the 72 hour time point P2X7R inhibition resulted in a significant increase in cell number when a 10X IC_{50} dose of antagonist was given to cells also treated with 10µM ATP. There were, however, no other significant differences resulting from P2X7R antagonism in any of the other ATP treatment groups at this timepoint (Fig. 3.5).

A repeat of the above experiment conducted under conditions of starvation (absence of FBS) revealed that inhibition of P2X7R showed no significant effect on cell number at any ATP concentration at either 24 hours or 72 hours (Fig. 3.6).

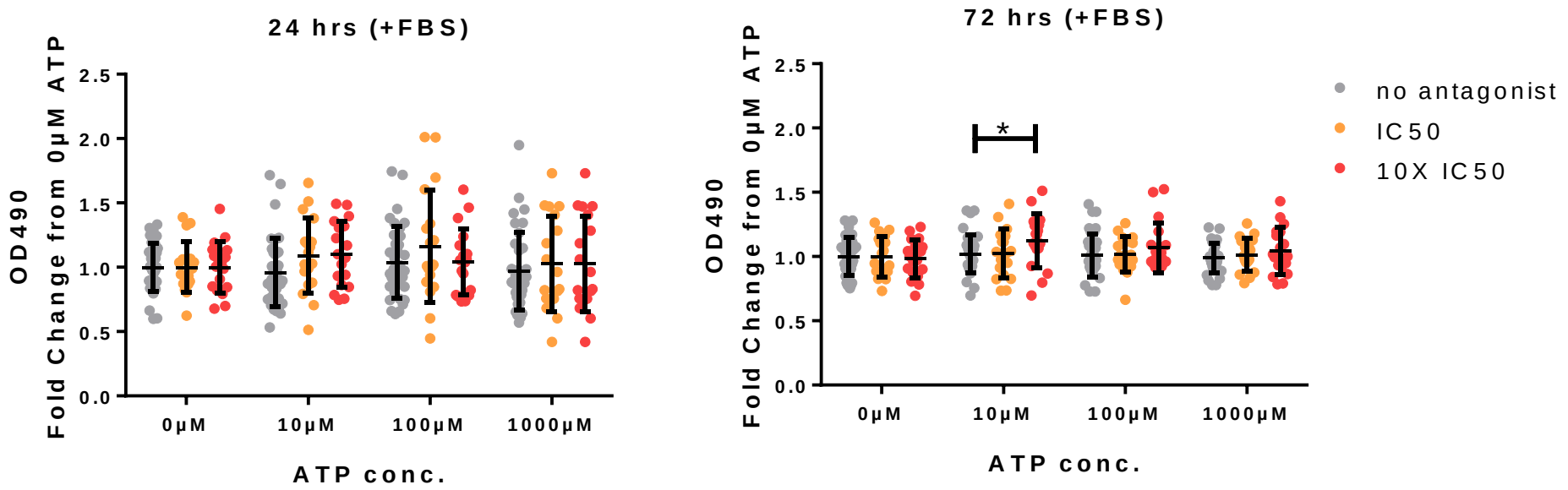

Figure 3.5: ATP Stimulation of 4T1 Cell in Normal Culture Conditions with P2X7R Inhibition (+FBS). 4T1 cells were initially plated in DMEM +10% FBS at 3000 cells per well in a 96 well plate and incubated for 24 hours to adhere. They were then dosed with A438079 HCl and ATP at a series of concentrations, for one hour, in serum-free DMEM before being returned to normal culture conditions (DMEM +0.5% FBS) for 24 or 72 hours prior to MTS assay. Data shows fold change of OD490 (representative of total cell number) normalised to the 0µM ATP dose group for each culture +SD. Data from 3 cultures with n=12 for each treatment group per culture. Statistical analysis conducted by one-way ANOVA within each ATP concentration group (0µM, 10µM, 100µ, and 1000µ).

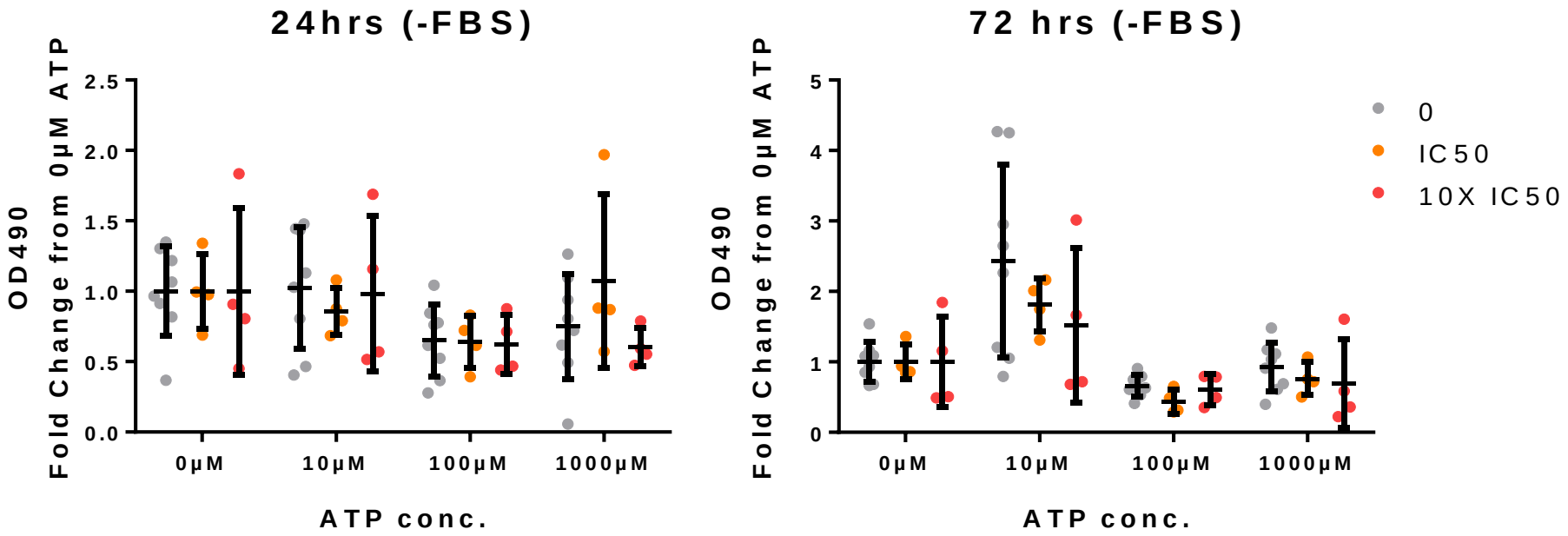

Figure 3.6: ATP Stimulation of 4T1 Cells in Starved Culture Conditions with P2X7R Inhibition (-FBS). 4T1 cells were plated in DMEM +10% FBS at 3000 cells per well in a 96 well plate for 24 hrs before dosing with ATP and A438079 HCl (where appropriate) at IC_{50} or 10X IC_{50} in serum-free DMEM. Cells continued to be cultured in ATP ± A438079 HCl containing serum-free DMEM for 24 or 72 hours before MTS assay. Data shows fold change of OD490 (representative of total cell number) normalised to the 0µM ATP dose group +SD. Statistical analysis conducted by one-way ANOVA within each ATP concentration group (0µM, 10µM, 100µ, and 1000µ).

3.2.3 Western Blot

To investigate the efficacy of LOX knockdown on levels of tumour secreted LOX in the 4T1-shLOX cell line, conditioned medium was collected from both 4T1 and 4T1-shLOX cells grown *in vitro*. Conditioned medium was concentrated by centrifugation using Vivaspin® 6 concentration columns and LOX protein content was assessed by Western Blot.

Active LOX protein (at 32kDa) was shown to be present in conditioned medium from both 4T1 and 4T1-shLOX samples, though the band for LOX produced by 4T1-shLOX conditioned medium was visibly smaller, consistent with a knockdown of LOX protein production (Fig. 3.7A). Ponceau S staining of total protein in the transfer membrane was conducted and showed consistent levels of protein loading in each of the lanes (Fig. 3.7B). Taken together this shows that secretion of LOX by the 4T1-shLOX cell line was successfully reduced.

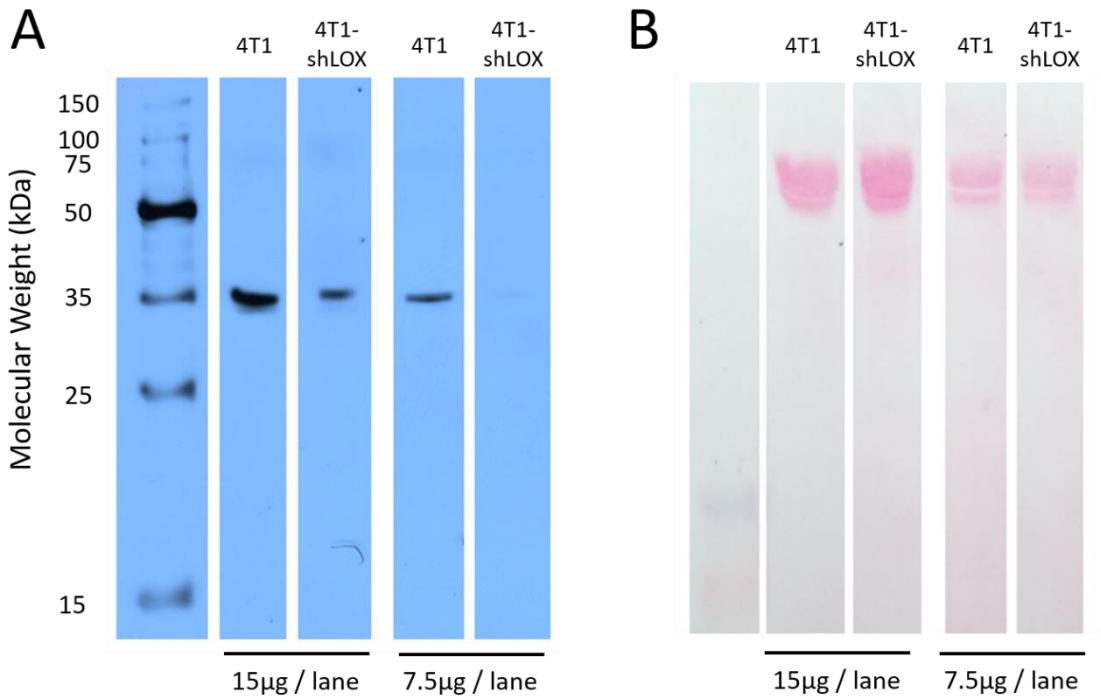

Figure 3.7: Western Blot for LOX in Conditioned Medium of 4T1 and 4T1-shLOX Cells: Conditioned medium (CM) was collected from 4T1 and 4T1-shLOX cells grown to 50% confluency in vitro. Secreted protein content in the samples was concentrated by centrifugation. Protein was loaded at either 15µg or 7.5µg/lane into a 12% acrylamide resolving gel and separated by electrophoresis. **A** Western blotting conducted using a primary HRP-conjugated antibody against LOX confirms reduced expression of active LOX protein (32kDa) in the 4T1-shLOX cell line. First lane shows protein marker, giving molecular weights in kDa. **B** Ponceau S staining for total protein in the transfer membrane confirms equal loading between samples.

3.3 Discussion

Validation of a model to study the effects of LOX and P2X7R in breast cancer metastasis to bone required confirmation that genetic manipulation of LOX expression in the 4T1 cell line had been successfully achieved by our collaborators. Furthermore, review of the literature revealed a lack of information regarding P2X7R expression or activity in the 4T1 cell line, and it was important to ascertain whether 4T1 cells expressed P2X7R, and if so whether P2X7R was functional and contributing to cancer cell activity.

3.3.1 P2X7R expression and activity in 4T1 cell lines

Expression of both P2X7R(a) and P2X7R(k) splice variants can clearly be seen in the 4T1 cell line, with clear bands at the expected base pair level for each receptor variant. Bands are also seen at the expected levels for both P2X7R(a) and P2X7R(k) variants in the 4T1-shLOX cell line, though they are fainter than those seen in the corresponding 4T1 cell line PCRs, particularly in the case of P2X7R(k) (see Fig. 3.1). As the GAPDH house keeping control shows strong bands for both 4T1 and 4T1-shLOX samples it is possible that the shRNA insertion may be inhibiting expression of P2X7R in the 4T1-shLOX cell line. Another potential explanation is that LOX expression in the 4T1 cell line is driving P2X7R expression, and thus when LOX expression is reduced so too is P2X7R. As P2X7R is linked to promotion of cancer cell survival (Adinolfi et al. 2012), this suggests that LOX could be an important mediator in tumour cell survival, as well as metastasis. Furthermore, it could also suggest a potential mechanism by which tumour secreted LOX drives osteoclastic bone destruction: whereby tumour secreted LOX could affect osteoclast cells to increase P2X7R expression, which in turn could drive osteoclast maturation and resorptive activity. It should, however, be noted that end-point PCR is not quantitative, and the fainter bands could be a sign of sample degradation rather than an actual reduction in gene expression. Nevertheless, these observations warrant further research before any conclusive link between tumour secreted LOX and P2X7R expression in either cancer or osteoclast cells can be confidently made.

Taken together, these results show that P2X7R is expressed in 4T1 cells, and thus stimulation of purinergic signalling has the potential to directly affect tumour cells, potentially promoting tumour cell survival and increasing chances of successful metastasis (Adinolfi et al. 2012; Adinolfi et al. 2009; Jelassi et al. 2011), which could in turn propagate an enhanced effect upon tumour induced bone destruction. LOX may play a contributory role in this process.

3.3.2 Purinergic Signalling in the 4T1 cell line

Though the 4T1 cell line was shown to express mRNA coding for P2X7R it was not known whether the cell line produced functional receptors. To investigate this 4T1 cells were cultured in the presence of varying concentrations of ATP, the ligand for P2 receptors, to assess the effect on cell growth, assessed by MTS assay.

Firstly, MTS assay was shown to be a reliable indicator of 4T1 cell number as the results from OD at 490nm (OD490) were shown to correlate linearly with known cell number (Fig. 3.2), thus OD490 values from MTS assay can be used as a proxy for cell number.

Cells cultured in normal growth conditions (in the presence of FBS) showed no effect of ATP stimulation on cell number (Fig. 3.3), but when cultured in starvation conditions (the absence of FBS) there were significant effects of ATP stimulation which differed depending on time-point (Fig. 3.4). In the short term, stimulation of purinergic signalling promoted cell survival, resulting in significant increases in cell number at ATP concentrations of 10nM, 10µM, and 3mM. In the longer term, stimulation of purinergic signalling pathways at ATP concentrations greater than or equal to 100µM caused a significant drop in cell number compared to the 0nM ATP control.

The P2X7 receptor is known to differ from other purinergic receptors in requiring a relatively high ATP concentration of 100µM upwards to activate (North 2002), thus the increased cell numbers noted 24 hours after stimulation with ATP in the starvation culture suggest that P2 receptors other than P2X7R are responsible, as significant effects are noted well below the 100µM threshold (Fig 3.4). The decrease in cell number at 72 hrs only in cultures treated with doses of ATP ≥100µM, however, suggests that activation of P2X7R alone is responsible for this decline. This is supported by previously published research which shows that P2X7R pore formation, which occurs at higher levels of stimulation, contributes towards pore formation, apoptosis, and cell death (Roger et al. 2014; Mackenzie et al. 2005).

Taken together these data show that purinergic signalling can affect 4T1 cell growth both positively and negatively, in a time dependent manner, when subjected to the conditions of starvation. Furthermore it suggests that P2X7R signalling may contribute to the mechanism for cell number reduction seen in cells treated with ATP at concentrations of 100µM or higher at the 72 hour timepoint, due to its known role in cell death and higher activation threshold of 100µM or greater (North 2002).

To test the hypothesis that P2X7R was contributing to the observed purinergic signalling in 4T1 cell culture, repeat 4T1 cultures were conducted with the addition of the specific competitive antagonist of P2X7R, A438079 HCl. In both normal and starvation culture conditions the only significant difference noted, in response to P2X7R antagonism, was in normal growth condition

wells dosed with 10X IC_{50} A4380279 HCl and 10µM ATP (Fig. 3.5). These wells showed a significant increase in cell number at 72 hrs compared to no antagonist controls. This is an unexpected finding given the total lack of significant differences in cell number in ATP dosed cultures conducted under normal growth conditions in the absence of A438079 HCl, and also as P2X7R antagonism appears to be exerting an effect at an ATP activation threshold 10 times below that reported for P2X7R activation (North 2002). Resultantly, this difference cannot be claimed to show an active effect of P2X7R on 4T1 cell number and it remains unclear as to whether or not P2X7R is active in the 4T1 cell line.

3.3.3 LOX knockdown in 4T1-shLOX cell line

Conditioned medium from the 4T1-shLOX cell line was shown to contain a lower level of secreted LOX protein than the naïve 4T1 cell line, as evidenced by the reduction in intensity of the band seen in 4T1-shLOX sample. In the lower protein load gel lanes (7.5µg protein) the band for LOX in the 4T1-shLOX lane is very faint, while the band in the 4T1 lane is clearly visible (Fig. 3.7). Thus it can be concluded that the shRNA insertion into the 4T1-shLOX cell line successfully reduced secretion of LOX, supporting a similar observation of reduced levels of circulating LOX in 4T1-shLOX tumour bearing mice compared to those with 4T1 tumours (Cox et al. 2015). Together these observations validate the use of the 4T1-shLOX cell line in experimentation to investigate the effect of LOX in breast cancer and its associated effects.

It is important to stress that shLOX inhibition reduces secreted LOX rather than completely removing it and as such LOX mediated effects are still expected to occur in mice with 4T1-shLOX tumours, although the magnitude of these effects is expected to be reduced.

3.4 Conclusion

Expression of P2X7R was confirmed in the 4T1 cell line, although it remains unclear whether the observed RNA expression results in translation of functional protein. Stimulation of 4T1 cultures with ATP showed that purinergic signalling does affect 4T1 cell growth, but was inconclusive with regards to a role for P2X7R in this. Given the observation of significant differences in the first starvation culture occurring predominantly at doses of 100μM ATP or above, and not at lower concentrations which would activate other P2 receptors, and also that the observed effect was a reduction in cell number, suggesting stimulation of some form of cell death for which P2X7R, alone of all P2 receptors, is known to promote, P2X7R remains a strong contender for the observed effects of purinergic signalling in the 4T1 cell line.

Genetic knockdown of LOX in the 4T1-shLOX cell line was found to be intact, with a reduction in tumour secreted LOX noted by Western blot, confirming observations of LOX reduction in the same 4T1-shLOX cell line in another publication (Cox et al. 2015). This validates the 4T1-shLOX cell line for use in this study to investigate the effects of LOX in breast cancer metastasis to bone, and its potential contribution to the formation of a pre-metastatic niche in bone.

Overall the experimental 4T1-BALB/c model used in this study is validated to be suitable for the investigation of the effects of tumour secreted LOX on breast cancer metastasis to bone. While the potential interaction of LOX and P2X7R is not able to be investigated in the primary tumour, as it remains unclear whether 4T1 cells express functional P2X7R or not, this does not hinder observations of LOX and P2X7R activity in the bone microenvironment of BALB/c mice, from which the effect of both LOX and P2X7R deletion is able to be investigated.

CHAPTER 4:

THE ROLE OF P2X7R IN LOX MEDIATED MODIFICATION OF PRE-METASTATIC BONE

4.1 Introduction

Lysyl Oxidase (LOX) is known to play a prominent role in metastatic disease, where its expression has been shown to increase the invasive properties of hypoxic cancer cells (Erler et al. 2006; Kirschmann et al. 2002), and to promote cancer cell adhesion (Erler et al. 2006; Taylor et al. 2011). LOX has also been identified as a crucial factor in the development of the pre-metastatic niche (Erler et al. 2009; Kaplan et al. 2005; Cox et al. 2015; Joo et al. 2014), and thus is able to promote metastatic cell release from the primary tumour while simultaneously preparing the secondary metastatic environment for cancer cell arrival. This is particularly important for metastasis to bone, where LOX activity has been shown to drive osteolytic lesion formation, with subsequently increased metastatic burden from primary breast tumours (Cox et al. 2015). Analysis of clinical data has highlighted the importance of LOX in metastatic disease as evidenced by clinical studies of patients with oestrogen receptor negative (ER-) breast cancer, or head and neck cancer. In both groups, patients with tumours expressing high levels of LOX were found to have significantly poorer survival rates than those with poorly LOX expressing tumours. This was the case for both metastasis-free and overall survival (Erler et al. 2006), highlighting the substantial effect of LOX upon mortality in metastatic disease.

The majority of research on the role of LOX in metastasis focuses on metastasis to the soft tissues of the liver and lung, however LOX is known to be expressed in cancers which preferentially metastasise to bone, and recent research has shown a strong correlation between the level of LOX expression and the affinity for bone metastasis (Cox et al. 2015). The underlying mechanism by which LOX promotes this affinity for bone, however, remains unclear. Our collaborators, Prof. Janine Erler and Dr. Thomas Cox (University of Copenhagen) have noted that LOX accumulates at areas of pressure within the body. Another molecule known to be released from cells in response to pressure, particularly from cancer cells, is ATP: the ligand for the purinergic P2 receptors, including the P2X7 receptor (P2X7R). Previous research has shown that expression of P2X7R can promote cancer cell survival and growth (Adinolfi et al. 2012; Di Virgilio et al. 2009), and is known to drive metastatic behaviour in the MDA-MB-435 and T47D breast cancer cell lines (Jelassi et al. 2011; Xia et al. 2015). Furthermore, P2X7R is also known to play a key role in bone remodelling where it is expressed in both bone-forming osteoblasts (Gartland et al. 2001; Ke et al. 2003) and bone-resorbing osteoclasts (Hoebertz et al. 2000; Naemsch et al. 2001; Agrawal et al. 2010). In osteoclasts P2X7R activation drives fusion of osteoclast precursors to form mature osteoclasts, capable of resorbing bone (Agrawal et al. 2010; Gartland et al. 2003a), and also regulates the cellular response to loading (Li et al. 2005; Jørgensen et al. 2002). Taken together, these factors qualify P2X7R as a contributor to the vicious cycle of bone

metastasis in which the breakdown of bone matrix results in release of growth factors to promote cancer cell growth.

A final consideration for the potential interaction of LOX and P2X7R is their respective relationships with hypoxia. Hypoxic MDA-MB-243 cancer cells have been shown to release ATP, stimulating the purinergic $P2Y_2$ receptor, resulting in expression of hypoxia-inducible factor 1-α (HIF-1α) and secretion of LOX, which in turn contributes to the formation of a pre-metastatic niche in the lung by cross-linking ECM to enhance recruitment of $CD11b^+$ bone marrow derived cells (Joo et al. 2014). HIF-1α has also been show to increase expression of P2X7R (Tafani et al. 2011), thus expression of P2X7R and secretion of LOX share a common hypoxic stimulus, further enhancing their co-localisation in the cancer microenvironment.

In summary, LOX and ATP are proposed to co-localise at areas of pressure, and areas of hypoxia. Hypoxia is also known to upregulate expression of P2X7R, which plays known roles in stimulating metastasis and in bone remodelling, particularly in the osteoclast. Purinergic signalling has also previously been shown to stimulate tumour secretion of LOX via the $P2Y_2$ receptor, setting a precedent for the possibility of P2X7R and LOX interaction promoting bone metastatic activity. This chapter tests the hypothesis that LOX interacts with P2X7R signalling in order to induce osteoclastic bone resorption. This would validate LOX as an important initial signalling molecule in the vicious cycle for bone metastasis, and would also identify LOX as a potential novel target for prophylactic cancer treatments, particularly important for those patients who do not respond to bisphosphonate treatment.

This chapter presents the results of μCT analyses investigating the effect of the 4T1 murine breast cancer cell line in BALB/c mice, from which the cell line initially arose (Tao et al. 2008; Heppner et al. 2000). The BALB/c mice used are either wild-type (WT), or have a null mutation of the *P2rx7* gene ($P2X7R^{-/-}$), which codes for the murine P2X7 receptor. Two separate models are used: the orthotopic model, in which mice receive an injection of 4T1 cells to simulate a primary breast tumour; and a cell-free model in which mice received daily injections of 4T1 conditioned medium. The effect of LOX in lesion formation will be investigated by comparing differences in lesion formation, cortical bone, and trabecular bone between mice injected with cells or CM from the 4T1 line, which constitutively express LOX, and those injected with the 4T1-shLOX line, in which LOX production has been genetically knocked down at the translational level. Similarly, the involvement of P2X7R will be investigated by comparing the effects of 4T1 and 4T1-shLOX tumours upon bone between WT and $P2X7R^{-/-}$ BALB/c mice.

4.2 Results

4.2.1 Effect of LOX and P2X7R on Osteolytic Lesion Formation in Tumour Bearing Mice

4.2.1.1 Lesion Quantification in Tumour Bearing WT BALB/c mice

Wild Type (WT) BALB/c mice received a single injection of $1x10^5$ 4T1 cells to the right mammary fat pad. One group received naïve 4T1 cells, which endogenously and constitutively express LOX, while another received 4T1-shLOX cells: cells expressing short hairpin RNA against LOX in order to knockdown LOX production. Mice were euthanised and fixed 3 weeks after injection, a timepoint selected to be within the pre-metastatic window (Tao et al. 2008). The hindlimbs were scanned using Skyscan 1172 high resolution desktop MicroCT (µCT, Sksycan, Kontich, Belgium).

Initial generation of 3D models from the µCT data showed that mice bearing 4T1 tumours developed a number of lesions in the cortical shaft (diaphysis) of the bone, while age matched mice had a solid cortex. The appearance of lesions was visibly reduced in mice bearing LOX knockdown 4T1-shLOX tumours (see Fig 4.1).

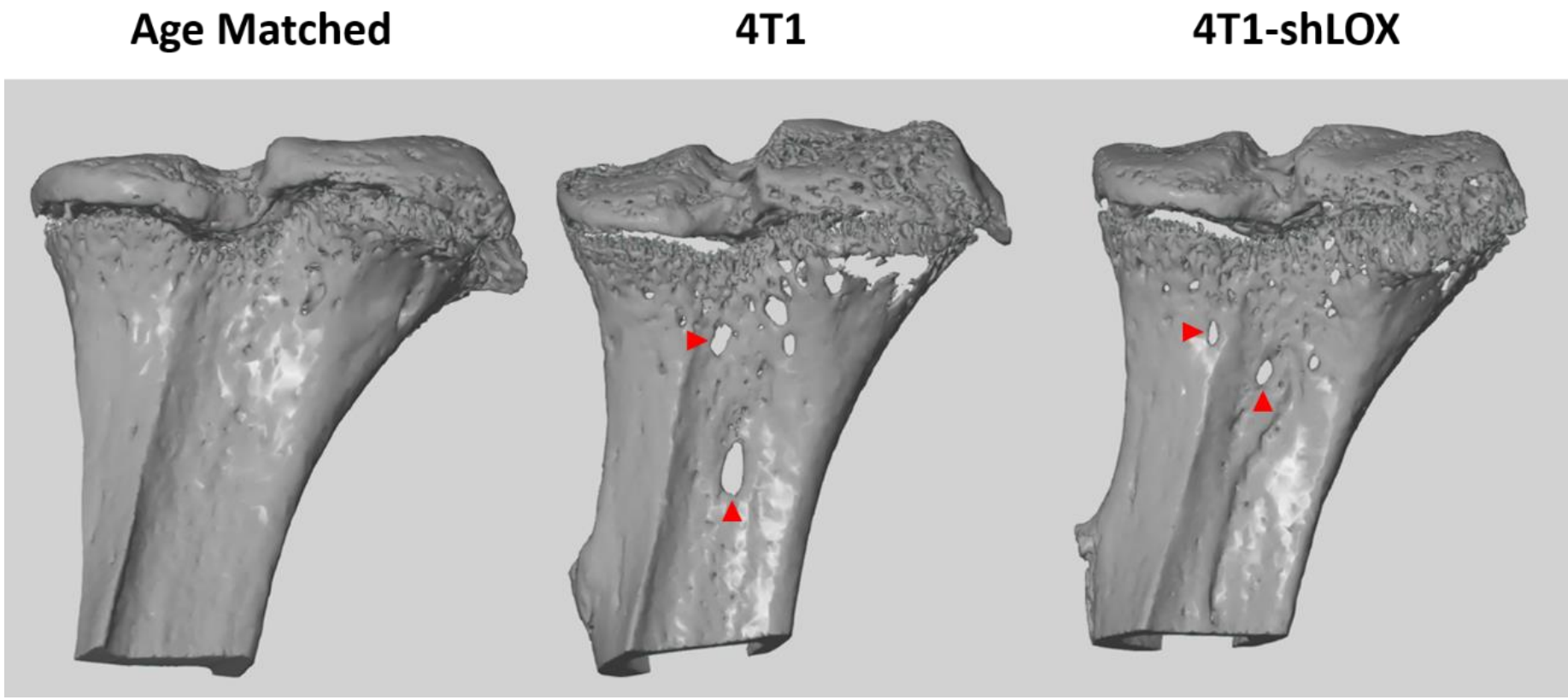

Figure 4.1: Representative 3D Models of WT BALB/c Mouse Tibiae. WT BALB/c mice received a single injection of either 4T1 (LOX expressing) or 4T1-shLOX (LOX knockdown) breast cancer cells to the mammary fat pad, to simulate a primary breast tumour. 4T1 tumour bearing mice display large lesions in the cortex of the tibia (indicated by arrows). Knockdown of LOX shows a marked reduction in lesion formation.

For the purposes of quantification, a lesion was defined as any hole perforating entirely through the cortical bone, with any dimension greater than 50µm, and an area >2500µm^2. These criteria did not exclude all naturally forming holes in either WT or P2X7R$^{-/-}$ age matched control mice, those representative of foramina for vasculature supplying the growing bone, or naturally porous regions of bone growth. Unfortunately there are no known consistent anatomical landmarks for blood vessel entry into bone, and thus these could not be confidently excluded from the dataset.

Quantification of lesion number and area revealed that WT BALB/c mice bearing 4T1 tumours developed a significantly greater number of lesions compared to age matched controls (Fig. 4.2 A), with a mean of 45.25 lesions per bone in 4T1 tumour bearing mice, compared to only 4 lesions per bone in age matched controls ($p<0.01$). 4T1-shLOX tumour bearing mice developed an average of 21.40 lesions per bone, significantly lower than 4T1 tumour bearing mice ($p=0.0427$), and not significantly different from age matched controls ($p>0.05$). These differences were reflected in total lesion area (Fig. 4.2 B), where 4T1 tumours resulted in a mean total lesion area of $1.02x10^6$ µm^2 per bone, which was significantly higher than both 4T1-shLOX tumour bearing mice ($0.275x10^6$ µm^2 per bone, $p=0.0275$), and age matched controls ($0.019x10^6$ µm^2, $p<0.05$). As with lesion number, 4T1-shLOX lesion area did not differ significantly from age-matched controls. Lesion number and area values are summarised in table 4.1, below.

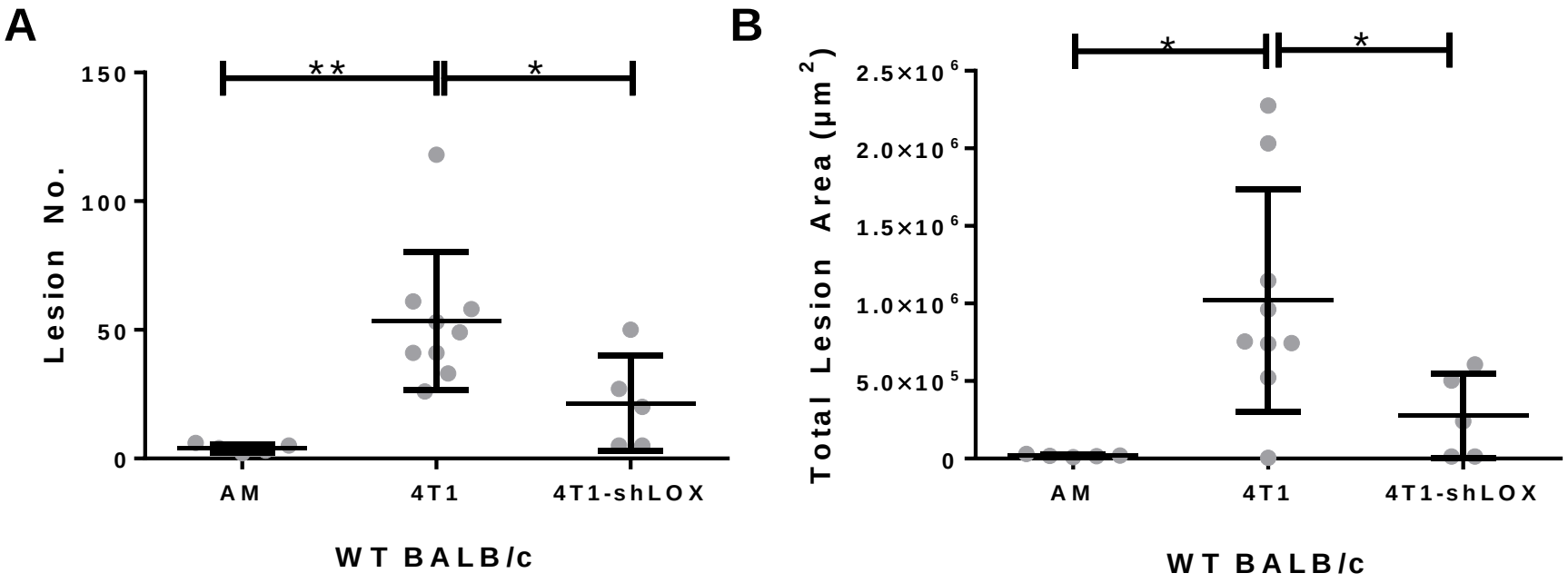

Figure 4.2: Quantification of Osteolytic Lesions in WT BALB/c mice. WT BALB/c mice received a single injection of 4T1 or 4T1-shLOX cells to the mammary fat pad. Mice were monitored for a period of 3 weeks before sacrifice. 3D models generated from µCT data of hindlimbs were used to assess lesion number and area in the cortical bone of the tibial diaphysis. **A** Total number of lesions per bone **B** Total lesion area per bone. Data shows individual values per tibia ± SD. AM n=5, 4T1 n=9, 4T1-shLOX n=5, where n= number of tibiae. * = $p<0.05$; ** $p<0.01$. Comparison to AM calculated by Kruskal-Wallis test, 4T1 vs. 4T1-shLOX comparison calculated by Mann-Whitney test.

4.2.1.2 Quantification of Lesions in Healthy Control WT and P2X7R$^{-/-}$ BALB/c mice

To compare normal porosity between WT and P2X7R$^{-/-}$ BALB/c mice µCT analysis of healthy, age-matched control mice was conducted. Holes in the cortical bone of these mice, meeting the definition of lesion as previously defined (Section 2.9.1), were then quantified. While these holes are not considered to be pathological, they are nevertheless referred to as 'lesions' for ease of comparison with tumour bearing mice, which display pathological lesion formation in response to tumour presence (see Fig. 4.1).

Comparison of age matched controls from the WT and P2X7R$^{-/-}$ BALB/c phenotypes revealed that P2X7R$^{-/-}$ mice had significantly more lesions in the cortex of the bone (Fig. 4.3 A), with an average of 9.82 per bone in P2X7R$^{-/-}$ mice, compared to 4.00 per bone in WT mice ($p=0.0005$). Total lesion area was also increased in P2X7R$^{-/-}$ mice (Fig. 4.3 B), with an average lesion area of 0.046×10^6 µm^2 in P2X7R$^{-/-}$ mice, compared to 0.019µm^2 in WT mice ($p=0.0005$). As these mice were healthy age matched controls, free from cancer cells or conditioned medium injections, these are considered to be naturally occurring pores in bone, most likely foramina for blood vessels or porous areas of new bone growth.

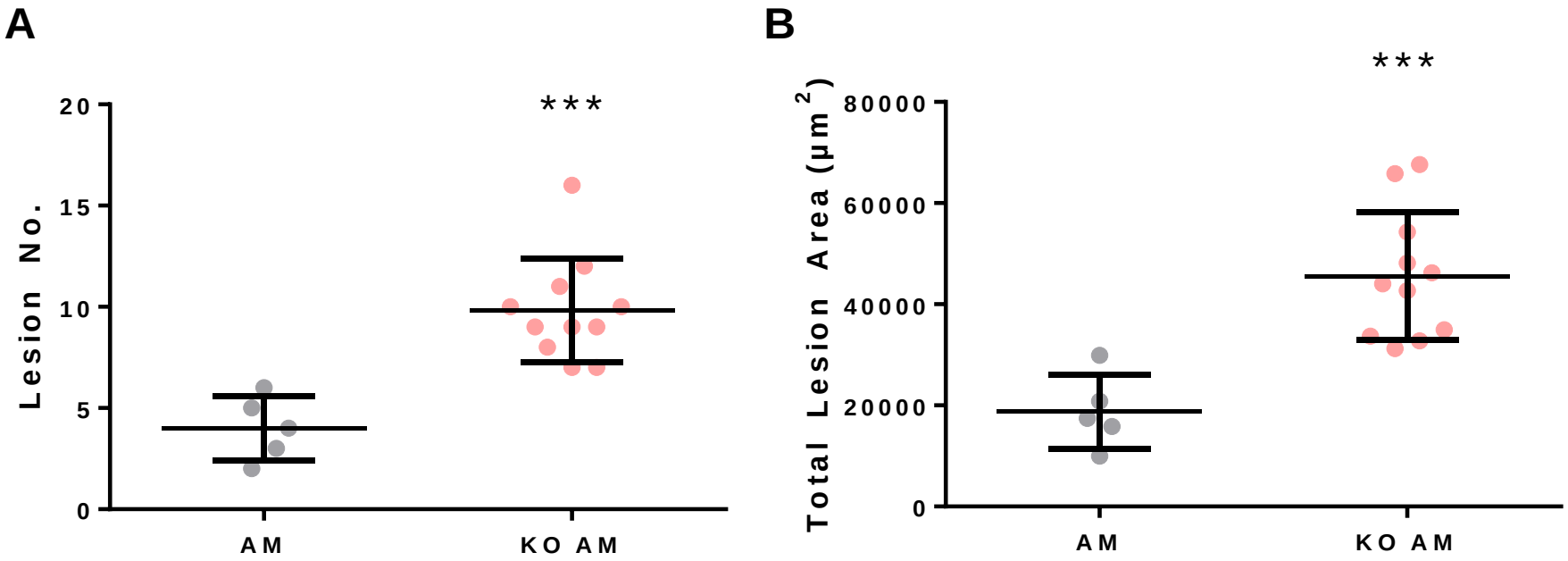

Figure 4.3: Comparison of WT and P2X7R$^{-/-}$ Cortical Bone Phenotypes. WT (grey, AM) and P2X7R$^{-/-}$ (pink, KO AM) age-matched BALB/c mice were sacrificed at 12 weeks of age. 3D models generated from µCT data of hindlimbs were used to assess lesion number and area in the cortical bone of the tibial diaphysis. **A** Total number of lesions per bone **B** Total lesion area per bone. Data shows individual values per tibia ± SD. AM n=5, KO AM n=11, where n= number of tibiae. * denotes statistical significance compared to AM, as calculated by Mann-Whitney test.

4.2.1.3 Lesion Quantification in Tumour Bearing P2X7R$^{-/-}$ BALB/c mice

Irrespective of the increased number of holes in the AM P2X7R$^{-/-}$ mice, orthotopic 4T1 tumour bearing P2X7R$^{-/-}$ mice, like their WT counterparts, developed a significant increase in lesion number (KO 4T1= 36.30 lesions, *cf* KO AM = 9.82 lesions $p<0.001$, Fig. 4.4 A, and table 4.1) and lesion area (KO 4T1= $0.344x10^6$ µm^2 *cf* KO AM = $0.046x10^6$ µm^2, $p<0.0001$, Fig. 4.4 B) compared to age-matched controls. Unlike in WT mice, knockdown of LOX in the tumours of P2X7R$^{-/-}$ mice did not significantly alter lesion formation as there was no significant difference in lesion number between 4T1 and 4T1-shLOX in P2X7R$^{-/-}$ mice (KO 4T1 = 36.30 lesions, *cf* KO 4T1-shLOX = lesions 38.40, $p=0.6142$, Fig. 4.4 A), and similarly no significant difference in total lesion area (KO 4T1 = $0.344x10^6$ µm^2, *cf* KO 4T1-shLOX = $0.297x10^6$ µm^2, $p=0.5389$, Fig. 4.4 B).

The 4T1-shLOX tumour bearing P2X7R$^{-/-}$ mice also showed a significant increase in lesion number compared to age matched controls (KO 4T1-shLOX = 38.40 lesions, *cf* KO AM = 9.82 lesion; $p=0.001$, Fig. 4.4 A) as well as lesion area (KO 4T1-shLOX = $0.297x10^6$ µm^2, *cf* KO AM =$0.046x10^6$ µm^2, $p<0.001$, Fig. 4.4 B).

Calculation of fold changes in lesion number and area (Table 4.1) allowed direct comparison of variables between WT and P2X7R$^{-/-}$ mice, normalising data to relevant age-matched controls to counter for the differences in lesion number and area previously noted between the two mouse strains (Fig. 4.4). Knockout of P2X7R significantly reduced lesion number fold change in 4T1 tumour bearing mice (4T1 = 11.1 *cf* KO 4T1 = 3.7, $p<0.0001$, Fig. 4.4C) as well as total lesion area fold change (4T1 = 54.34 *cf* KO 4T1 = 7.55, $p=0.0030$, Fig 4.4 C), but had no effect on fold change in either variable in mice with 4T1-shLOX tumours.

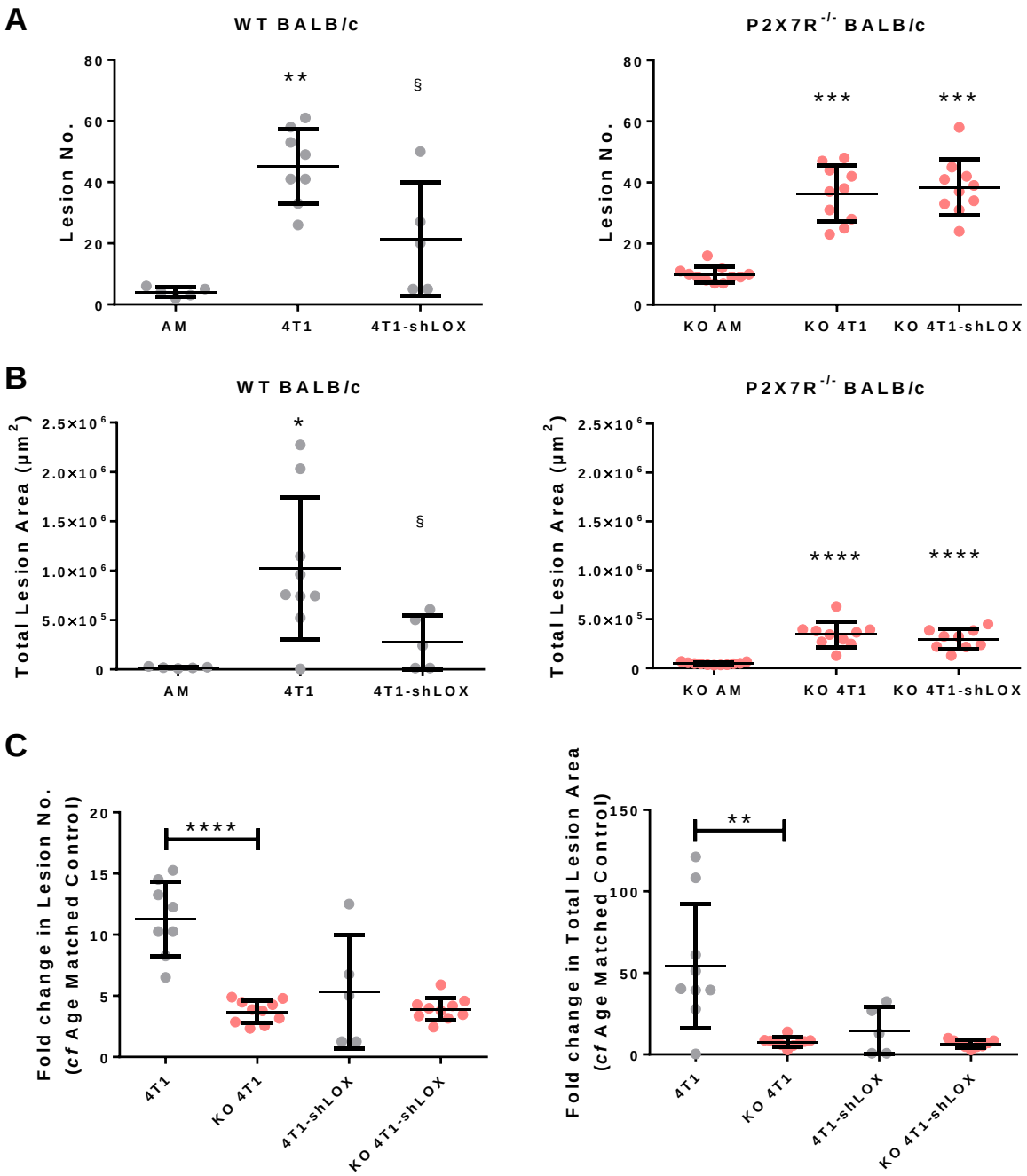

Figure 4.4: Quantification of Osteolytic Lesions in Tumour Bearing Mice. WT (grey) and P2X7R$^{-/-}$ (pink, KO) BALB/c mice received a single injection of 4T1 cells to the mammary fat pad. Mice were monitored for a period of 3 weeks before sacrifice. 3D models generated from µCT data of hindlimbs were used to assess lesion number and area in the cortical bone of the tibial diaphysis. A second group of mice were treated as above using 4T1 cells expressing shRNA (4T1-shLOX) to knockdown production of LOX. **A** Total number of lesions per bone **B** Total lesion area per bone **C** Comparison of fold change in variables between WT and P2X7R$^{-/-}$ mouse strains. Data shows individual values per tibia ± SD. AM n=5, 4T1 n=9, 4T1-shLOX n=5, KO AM n=11, KO 4T1 n=10, KO 4T1-shLOX n=10, where n= number of tibiae. * denotes statistical significance compared to relative age matched controls (Kruskall-Wallis test), unless otherwise indicated by line bar (Mann-Whitney test), § denotes statistical significance compared to relative 4T1 group (Mann-Whitney test). * p<0.05, ** p<0.01, ***p<0.001, **** p<0.0001.

Table 4.1: Summary of Lesion Numbers and Area in Tumour Bearing Mice.

Mouse Strain	Treatment Group	Mean Lesion No.	Mean Lesion No. Fold Change	Mean Summed Lesion Area (µm^2)	Mean Total Lesion Area Fold Change
WT BALB/c	*AM*	4.00	1.00	0.019×10^6	1.00
	4T1	45.25	11.31	1.020×10^6	54.34
	4T1-shLOX	21.40	5.35	0.275×10^6	14.67
P2X7R$^{-/-}$ BALB/c	*AM*	9.82	1.00	0.046×10^6	1.00
	4T1	36.30	3.70	0.344×10^6	7.55
	4T1-shLOX	38.40	3.91	0.297×10^6	6.51

Table shows mean values for each experimental group. AM = age-matched controls, 4T1 = 4T1 tumour bearing mice, 4T1-shLOX = 4T1-shLOX tumour bearing mice. Fold change for each variable is calculated against relative AM control. WT AM n=3, WT 4T1 n=11, WT 4T1-shLOX n=5, P2X7R$^{-/-}$ AM n=12, P2X7R$^{-/-}$ 4T1 n=12, P2X7R$^{-/-}$ 4T1-shLOX n=10.

4.2.2 Effect of LOX and P2X7R on Osteolytic Lesions in a Cancer Cell Free Model

To investigate the potential for LOX to exert an effect on bone independent of cancer cell presence in bone, WT and P2X7R$^{-/-}$ BALB/c mice received daily intraperitoneal injections of conditioned medium (CM) from LOX expressing 4T1 cells for a period of 3 weeks before sacrifice. 3D models were generated from μCT data and used to quantify osteolytic lesion formation as described above (section 4.2.1). WT mice injected with 4T1 CM developed a significantly greater number of lesions (4T1 CM = 12 lesions *cf* AM = 4 lesions, p=0.0079, Fig. 4.5 A) and also a significantly greater total lesion area (4T1 CM = 0.049x10^6 μm^2 *cf* AM = 0.019x10^6 μm^2, p=0.0079, Fig. 4.5 B) compared to age matched controls. Data are outlined in table 4.2.

P2X7R$^{-/-}$ mice repeated this pattern, with the CM injected mice developing a greater number of lesions (KO 4T1-CM = 15.5 lesions, *cf* KO AM = 9.8 lesions, p=0.0071, Fig. 4.5 A) and a greater total lesion area (4T1-CM KO = 0.058x10^6 μm^2 *cf* AM KO = 0.037x106 μm^2, p=0.0025, Fig. 4.5 B) compared to age matched controls.

Comparison of fold changes in lesion number and area between WT and P2X7R$^{-/-}$ mice revealed that knockout of P2X7R in 4T1 CM injected mice significantly reduced fold change in lesion number (4T1 CM = 3.000 *cf* KO 4T1 CM = 1.579, p=0.0016, Fig. 4.5 C). While there was a trend for a reduction in fold change of total lesion area in 4T1 CM injected P2X7R$^{-/-}$ mice compared to WT BALB/c, this did not achieve statistical significance (4T1 CM = 2.595 *cf* KO 4T1 CM = 1.684, p=0.0932, Fig. 4.5 C).

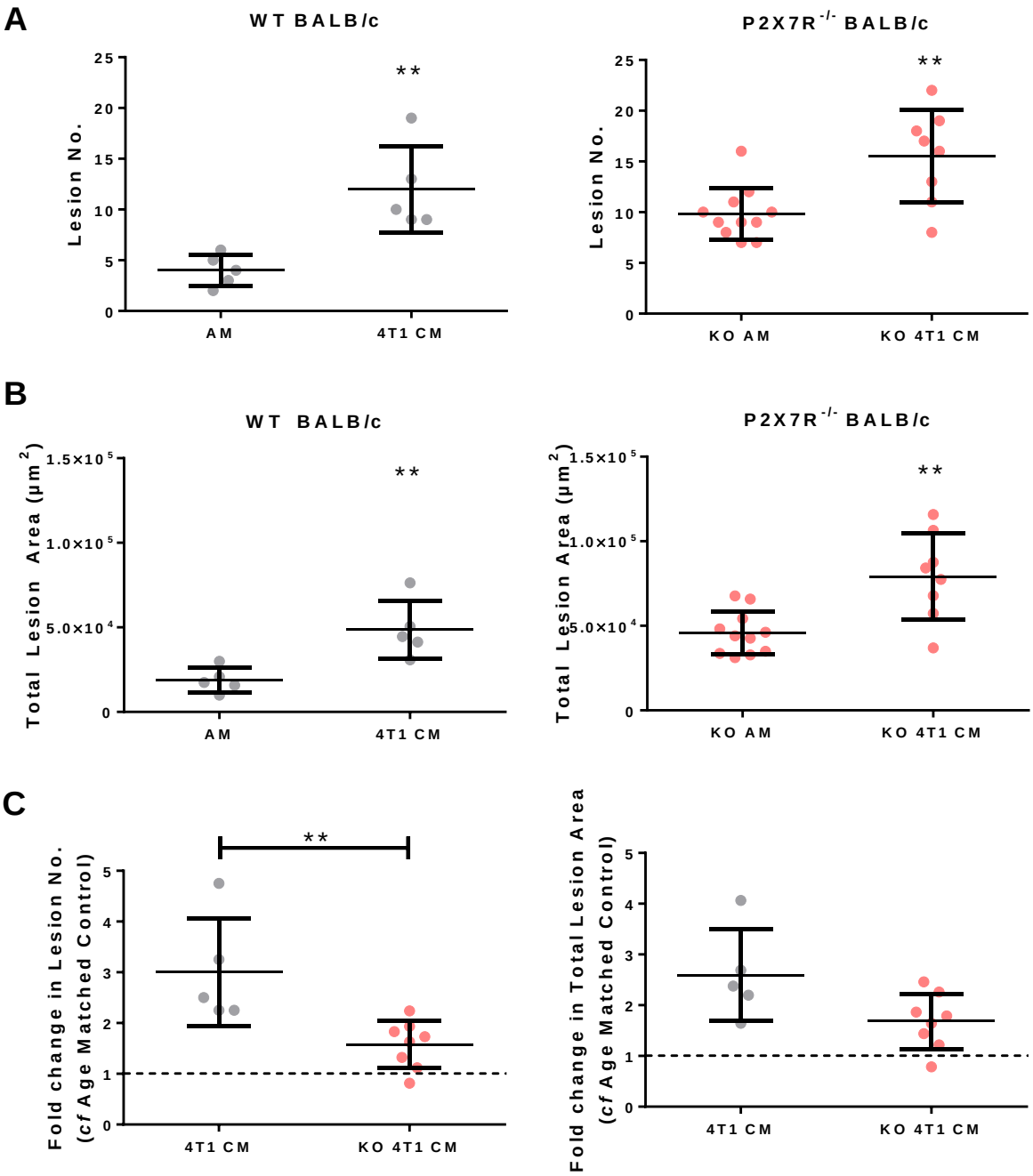

Figure 4.5: Quantification of Osteolytic Lesions in Conditioned Medium Injected Mice. WT (grey) and P2X7R$^{-/-}$ (pink, KO) BALB/c mice received daily intraperitoneal injections of conditioned medium from 4T1 cells for a period of 3 weeks before sacrifice. **A** Lesion number quantified from 3D models generated from µCT scans of mouse tibiae. **B** Total lesion area quantified from 3D µCT models of mouse tibiae. **C** Comparison of fold changes in lesion variables between WT and P2X7R$^{-/-}$ mouse strains. Data shows values for individual tibiae ± SD. AM n=5, 4T1 CM n=5, KO AM n=11, 4T1 CM KO n=8, where n= number of tibiae. * denotes statistical significance compared to relative age matched control, unless otherwise indicated by line bar. ** p<0.01, calculated by Mann-Whitney test.

Table 4.2: Summary of Lesion Numbers and Area in Conditioned Medium Injected Mice.

Mouse Strain	Treatment Group	Mean Lesion No.	Mean Lesion No. Fold Change	Mean Total Lesion Area (μm^2)	Mean Total Lesion Area Fold Change
WT BALB/c	*AM*	4.00	1.000	18776	1.000
	4T1 CM	12.00	3.000	48724	2.595
P2X7R$^{-/-}$ BALB/c	*AM*	9.82	1.000	45599	1.000
	4T1 CM	15.50	1.579	79192	1.684

Table shows mean values for lesion number and total lesion area. Fold change for each variable calculated against relative age-matched (AM) controls. AM = age-matched controls, 4T1-CM = mice injected with conditioned medium from 4T1 cells grown *in vitro*. WT AM n=5, WT 4T1 CM n=5, P2X7R$^{-/-}$ AM n=11, P2X7R$^{-/-}$ 4T1 CM KO n=8

4.2.3 Effect of LOX and P2X7 on Cortical Bone

Mice were injected with orthotopic 4T1 or 4T1-shLOX tumours as described previously (section 2.7.2). Cortical thickness was manually measured at twelve points around the circumference of the tibia at a location 0.75mm below the first break in the growth plate and the average of these values calculated. Data is summarised in figure 4.6 and table 4.3 below.

Analysis of cortical thickness in WT BALB/c mice showed no significant differences between age-matched controls and either 4T1 or 4T1-shLOX tumour groups, although 4T1-shLOX tumour bearing mice showed a significant reduction in cortical thickness when compared to 4T1 tumour bearing mice (4T1 = 0.12mm, 4T1-shLOX = 0.10mm; p=0.0317, Fig. 4.6 A).

Analysis of $P2X7R^{-/-}$ mice revealed that cortical thickness was significantly reduced in both 4T1 ($p<0.05$) and 4T1-shLOX ($p<0.01$) tumour bearing $P2X7R^{-/-}$ mice when compared to age-matched controls (Fig. 4.6 A). There was no significant effect of LOX knockdown in $P2X7R^{-/-}$ mice, with no significant difference in cortical thickness when comparing 4T1 and 4T1-shLOX tumour bearing knockout mice (p=0.1473).

Comparison of cortical thickness between WT and $P2X7R^{-/-}$ age-matched controls revealed that $P2X7R^{-/-}$ mice had significantly thicker cortical bone than WT mice (AM = 0.118mm *cf* KO AM = 0.155mm, p=0.0357, Fig. 4.6 B). In light of this difference, fold changes in cortical thickness relative to age-matched controls were calculated for tumour bearing mice to allow comparison of WT and $P2X7R^{-/-}$ data (Fig. 4.6C). Knockout of P2X7R was found to significantly reduce fold change in cortical thickness below 1.00 in both 4T1 and 4T1-shLOX tumour bearing mice, reflecting an increase in tumour induced cortical bone loss when P2X7R is knocked out.

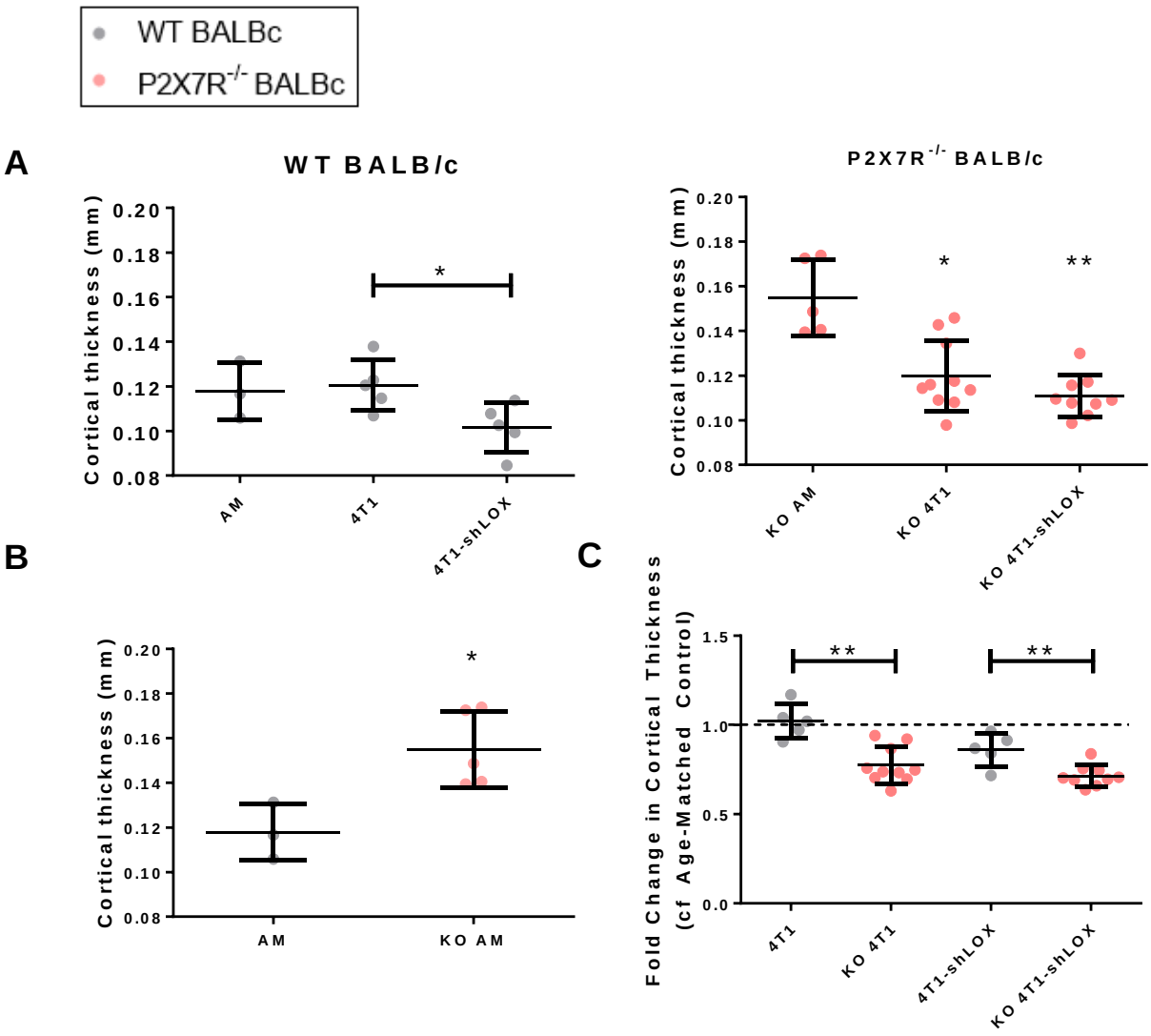

Figure 4.6: Effects of LOX and P2X7R on Cortical Thickness in Tumour Bearing Mice. WT (grey) and P2X7R$^{-/-}$ (pink) BALB/c mice each received a single injection of 1x10^5 4T1 cells to the mammary fat pad. A further group from each mouse strain were left untreated as age matched controls. Mice were sacrificed after a period of 3 weeks, and their hindlimbs scanned using high resolution desktop MicroCT (Sksycan, Kontich, Belgium). Cortical thickness was manually measured at twelve equidistant points around the circumference of the tibia at a section 0.75mm distal to the epiphyseal growth plate. **A** Comparison of cortical thickness in age matched controls alongside tumour bearing groups in both WT and P2X7R$^{-/-}$ mice. **B** Comparison of cortical thickness between WT and P2X7R$^{-/-}$ age-matched controls. **C** Comparison of fold change in cortical thickness between WT and P2X7R$^{-/-}$ tumour bearing mice. Data shows mean value for each tibia ± SD. AM n=3, 4T1 n=5, 4T1-shLOX n=5, KO AM n=5, KO 4T1 n=10, KO 4T1-shLOX n=9, where n= number of tibiae. * represents significance when compared to relevant age-matched control (Kruskal-Wallis test), unless otherwise indicated by line bar (Mann-Whitney test). *= p<0.05; **= p<0.01.

Table 4.3: Summary of Cortical Thicknesses of Tibiae in Experimental Mice.

Mouse Strain	Treatment Group	Mean Cortical Thickness (mm)	Sig. cf. AM	Sig. cf. 4T1
WT BALB/c	*AM*	0.118	n/a	nsd
	4T1	0.121	nsd	n/a
	4T1-shLOX	0.102	nsd	*
P2X7R$^{-/-}$ BALB/c	*AM*	0.155	n/a	*
	4T1	0.120	*	n/a
	4T1-shLOX	0.111	**	nsd

Table shows mean cortical thickness values for each experimental group. AM = age-matched controls, 4T1 = 4T1 tumour bearing mice, 4T1-shLOX = 4T1-shLOX tumour bearing mice. Sig. cf. = significance compared to. * denotes statistical significance. Comparison to AM calculated by Kruskall-Wallis test; comparison to 4T1 calculated by Mann-Whitney test. WT AM n=3, WT 4T1 n=11, WT 4T1-shLOX n=5, P2X7R$^{-/-}$ AM n=12, P2X7R$^{-/-}$ 4T1 n=12, P2X7R$^{-/-}$ 4T1-shLOX n=10. * = $p<0.05$, **= $p<0.01$, nsd = no significant difference.

4.2.4 Effect of P2X7R and LOX on Trabecular Bone

WT and P2X7R$^{-/-}$ BALB/c mice received either a single injection of 4T1 or 4T1-shLOX cells to the mammary fat pad; or received daily intraperitoneal injections of conditioned medium from 4T1 cells grown *in vitro*, as previously described (see Sections 2.2 and 2.7). The properties of the tibial trabecular bone were assessed in each treatment group by μCT analysis.

4.2.4.1 Comparison of WT and P2X7R$^{-/-}$ mouse trabecular bone phenotypes

Comparison of trabecular analysis results from age-matched mice of both genotypes of mice revealed that there were no significant differences attributable to P2X7R knockout in bone mineral density (BMD), percentage trabecular bone volume (BV/TV), trabecular number (Tb No.), or structural model index (SMI). P2X7R$^{-/-}$ mice, however, had significantly thicker trabeculae, with a mean thickness of 0.050mm, compared to WT mice with a mean thickness of 0.043mm (p=0.008, Fig. 4.7 D).

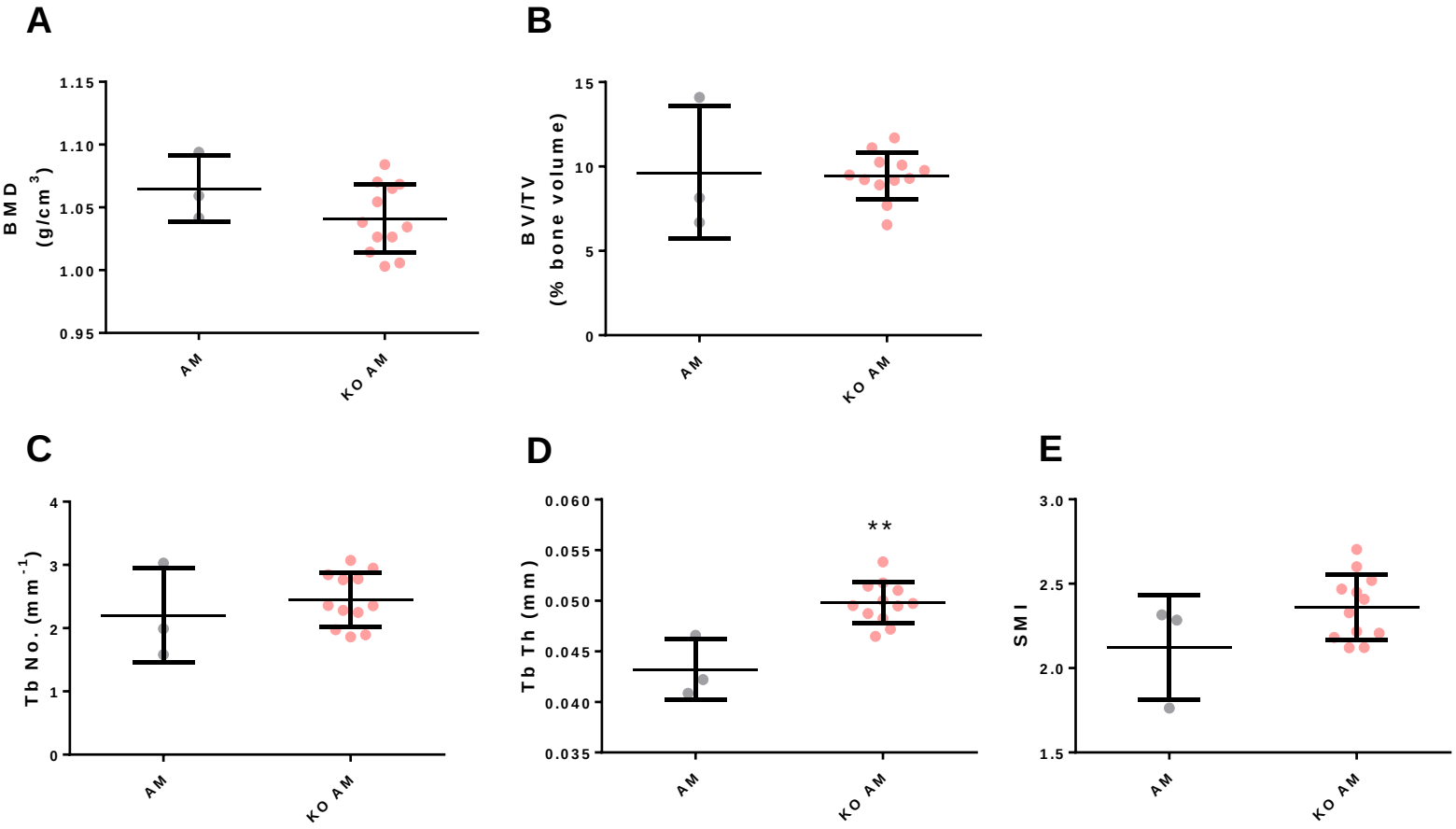

Figure 4.7: Comparison of WT and P2X7R$^{-/-}$ Mouse Trabecular Analyses. Age matched WT (grey) and P2X7$^{-/-}$ (pink) mice at 12 weeks of age had their tibiae subjected to µCT analysis of the trabecular cavity. **A** BMD values were calculated from mean greyscale values. **B** Percentage of the medullary cavity which is bone (Percentage Trabecular Bone Volume) **C** Number of trabeculae per mm of bone. **D** Mean thickness of individual trabeculae in mm. **E** Structural Model Index (SMI), a measure of morphology where 0 = ideal plate, 3 = ideal cylinder, 4 = ideal sphere. Data shows mean values for individual tibiae ± SD. * denotes statistical significance compared to WT mouse AM control. AM n=3, KO AM n=12. ** p<0.01, calculated by Mann-Whitney test.

4.2.4.2 Trabecular Analysis in Tumour Bearing Mouse Model

WT BALB/c mice

Trabecular BMD in WT mice bearing 4T1 tumours was significantly lower than age matched controls (AM mean = 1.065 g/cm^3, 4T1 mean = 0.9671 g/cm^3, $p<0.05$, Fig. 4.8 A). Knockdown of LOX protected against tumour induced bone loss, with 4T1-shLOX tumour bearing mice displaying a BMD which was significantly greater than that of 4T1 tumour bearing mice (4T1-shLOX mean = 1.035 g/cm^3, 4T1 mean = 0.9671 g/cm^3; $p=0.0133$, Fig. 4.8 A), and which did not differ significantly from age matched controls. BV/TV, however, showed no effect from either 4T1 or 4T1-shLOX tumours when compared to age matched controls (Fig. 4.8 B).

Tb No. reduced from 2.201 trabeculae/mm in age matched mice to 2.018 trabeculae/mm in 4T1 tumour bearing mice, and to 1.695 trabeculae/mm in 4T1-shLOX tumour bearing mice, however neither tumour group resulted in a value significantly different from age matched controls, nor did the tumour types differ significantly from each other (Fig. 4.8 C). Trabecular thickness displayed a statistically significant reduction in 4T1 tumour bearing WT mice, thinning from 0.043mm in age matched mice, to 0.038mm in 4T1 tumour bearing mice ($p<0.05$, Fig. 4.8 D). 4T1-shLOX tumour bearing mice had a mean trabecular thickness of 0.040mm, which did not differ significantly from either age matched controls or 4T1 tumour bearing mice.

SMI did not differ significantly from age-matched controls in either group of tumour bearing mice, nor was there any significant difference between tumour types (Fig. 4.8 E).

P2X7R$^{-/-}$ BALB/c mice

As visualised in figure 4.8, below, trabecular analysis of tumour bearing P2X7R$^{-/-}$ mice revealed no significant differences in BMD between any of the experimental groups: tumour presence did not affect BMD compared to age matched controls, and knockdown of LOX in the tumour had no effect (Fig. 4.8 A). Tumour bearing did, however, affect BV/TV in the trabecular cavity. P2X7R$^{-/-}$ mice bearing 4T1 tumours had a significant decrease in BV/TV from 9.4% in age matched mice to 7.9% in 4T1 tumour bearing mice ($p=<0.01$, Fig. 4.8 B). Knockdown of LOX protected against bone loss, resulting in an increase in trabecular bone volume to 11.1%, a value which was significantly increased compared to both age matched controls ($p>0.0001$) and 4T1 tumour bearing mice ($p<0.01$).

Trabecular number was significantly decreased in 4T1 tumour bearing P2X7R$^{-/-}$ mice, from a mean of 2.449 trabeculae/mm in age matched controls, to 1.836 trabeculae/mm in 4T1 tumour bearing mice ($p<0.0001$, Fig. 4.8 C). Knockdown of LOX resulted in a slightly higher value of 2.084 trabeculae/mm in 4T1-shLOX tumour bearing mice. This was still significantly lower compared to age matched controls ($p<0.05$, Fig. 4.8 C), and did not differ significantly from 4T1 tumour bearing mice. Trabecular Thickness was similarly affected with a thinning of trabeculae from a mean of 0.046mm in age matched mice, to 0.043mm in 4T1 tumour bearing P2X7R$^{-/-}$ mice ($p<0.0001$, Fig. 4.8 D). Knockdown of LOX had no effect on these results. 4T1-shLOX tumour bearing mice had a mean trabecular thickness of 0.045mm, which was significantly lower than the age matched controls ($p<0.001$, Fig. 4.8 D), but did not differ significantly from 4T1 tumour bearing mice.

Finally, 4T1 tumour bearing P2X7R$^{-/-}$ mice developed trabeculae with a structural model index (SMI) of 2.620, significantly higher than the age matched controls with a mean SMI of 2.360 ($p<0.01$, Fig. 4.8 E). Knockdown of LOX removed this effect, resulting in trabeculae with a mean SMI of 2.524, which was not significantly different from either other group.

A summary of the mean values for each variable for both genotypes of mice is presented in table 4.4 below.

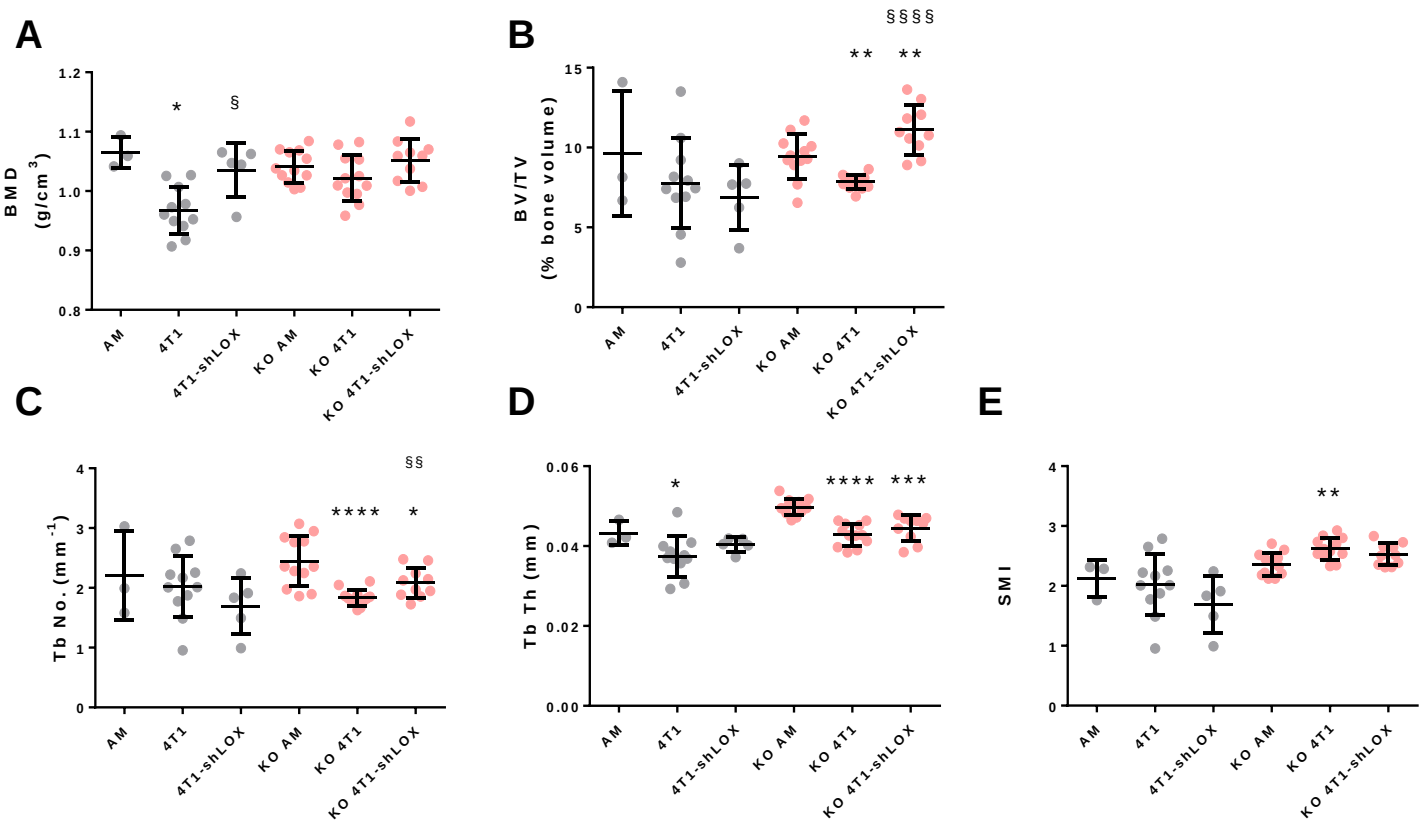

Figure 4.8: Trabecular Analysis of Tumour Bearing WT and P2X7R$^{-/-}$ Mice. WT (grey) and P2X7R$^{-/-}$ (pink, KO) BALB/c mice received a single injection of 4T1 cells to the mammary fat pad. Mice were monitored for a period of 3 weeks before sacrifice. Hindlimbs were dissected, and the tibiae subjected to µCT analysis of the trabecular cavity. **A** BMD values were calculated from mean greyscale values. **B** Percentage of the medullary cavity which is bone (Percentage Trabecular Bone Volume) **C** Number of trabeculae per mm of bone. **D** Mean thickness of individual trabeculae in mm. **E** Structural Model Index (SMI), a measure of morphology where 0 = ideal plate, 3 = ideal cylinder, 4 = ideal sphere. Data shows mean values for individual tibia ± SD. * denotes statistical significance compared to relative age matched controls (Kruskall-Wallis test). § denotes statistical significance relative to respective 4T1 group (WT data analysed by Mann-Whitney test, P2X7R$^{-/-}$ data analysed by unpaired t-test). AM n=3, 4T1 n=11, 4T1-shLOX n=5, KO AM n=12, KO 4T1 n=12, KO 4T1-shLOX n=10.

Table 4.4: Summary of Trabecular Analysis in WT and P2X7R$^{-/-}$ Tumour Bearing Mice.

	WT			P2X7R$^{-/-}$		
	AM	**4T1**	**4T1-shLOX**	**AM**	**4T1**	**4T1-shLOX**
BMD (g/cm^3)	1.065	0.967 *	1.035 §	1.041	1.022	1.052
BV/TV (%)	9.637	7.765	6.872	9.436	7.851 **	11.1 ** §§§§
Tb No. (mm^{-1})	2.201	2.018	1.695	2.449	1.836 ****	2.084 * §§
Tb Th (mm)	0.043	0.037 *	0.04	0.05	0.043 ****	0.045 ***
SMI	2.121	2.018	1.695	2.36	2.62 **	2.524

Table shows mean values for trabecular variables in each experimental group. AM = age-matched controls, 4T1 = 4T1 tumour bearing mice, 4T1-shLOX = 4T1-shLOX tumour bearing mice. * denotes statistical significance compared to relevant age matched control, calculated by Kruskall-Wallis test. § denotes statistical significance compared to 4T1 group, calculated by Mann-Whitney test for WT data, and by unpaired t-test for P2X7R$^{-/-}$ data. WT AM n=3, WT 4T1 n=11, WT 4T1-shLOX n=5, P2X7R$^{-/-}$ AM n=12, P2X7R$^{-/-}$ 4T1 n=12, P2X7R$^{-/-}$ 4T1-shLOX n=10. */§ = p<0.05, **/§§ = p<0.01, ***/§§§ = p<0.001, ****/§§§§=p<0.0001.

4.2.4.3 Trabecular Analysis in Cell-Free Mouse Model

Effect of 4T1 CM injection

As shown in figure 4.9, WT mice receiving daily intraperitoneal injections of conditioned medium from 4T1 cells show a significant reduction in BMD from 1.065g/cm^3 in age-matched controls, to 1.015g/cm^3 in 4T1 CM injected mice (p=0.0280, Fig. 4.9 A). SMI was also affected, rising from a mean of 2.121 in age matched mice, to 3.029 in 4T1 CM injected mice (p=0.0070, Fig. 4.9 E). WT mice displayed no significant change in BV/TV, Tb No., or Tb Th in response to 4T1 CM injection. All trabecular values, and associated statistical significances, are summarised below in table 4.5.

Injection of 4T1 CM in P2X7R$^{-/-}$ mice had a similar response to that seen in WT mice. P2X7R$^{-/-}$ mice injected with 4T1 CM showed a significant reduction in BMD from 1.041 g/cm^3 to 1.010 g/cm^3 (p=0.0205, Fig. 4.9 A), and an increase in SMI from 2.195 to 2.551 (p=0.0177, Fig. 4.9 E). There were no statistically significant effects of 4T1 CM injection on BV/TV or Tb No. in P2X7R$^{-/-}$ mice, however Tb Th was significantly reduced by 4T1 CM injection, from a mean of 0.05mm to 0.047mm (p=0.0088, Fig. 4.9 D).

Effect of P2X7R Knockout

Comparison of WT and P2X7R$^{-/-}$ BALB/c mice which received 4T1 CM injections revealed that knockout of P2X7R resulted in significant reductions in BV/TV (AM=9.436%, 4T1 CM=9.049%, p<0.0001, Fig. 4.9 B); Tb No. (AM=2.449/mm, 4T1 CM=2.091/mm, p<0.0001, Fig. 4.9 C); and SMI (AM=2.195, 4T1 CM=2.551, p=0.0196, Fig. 4.9 E). There was no statistically significant effect of P2X7R knockout in BMD or Tb Th in 4T1 CM injected mice.

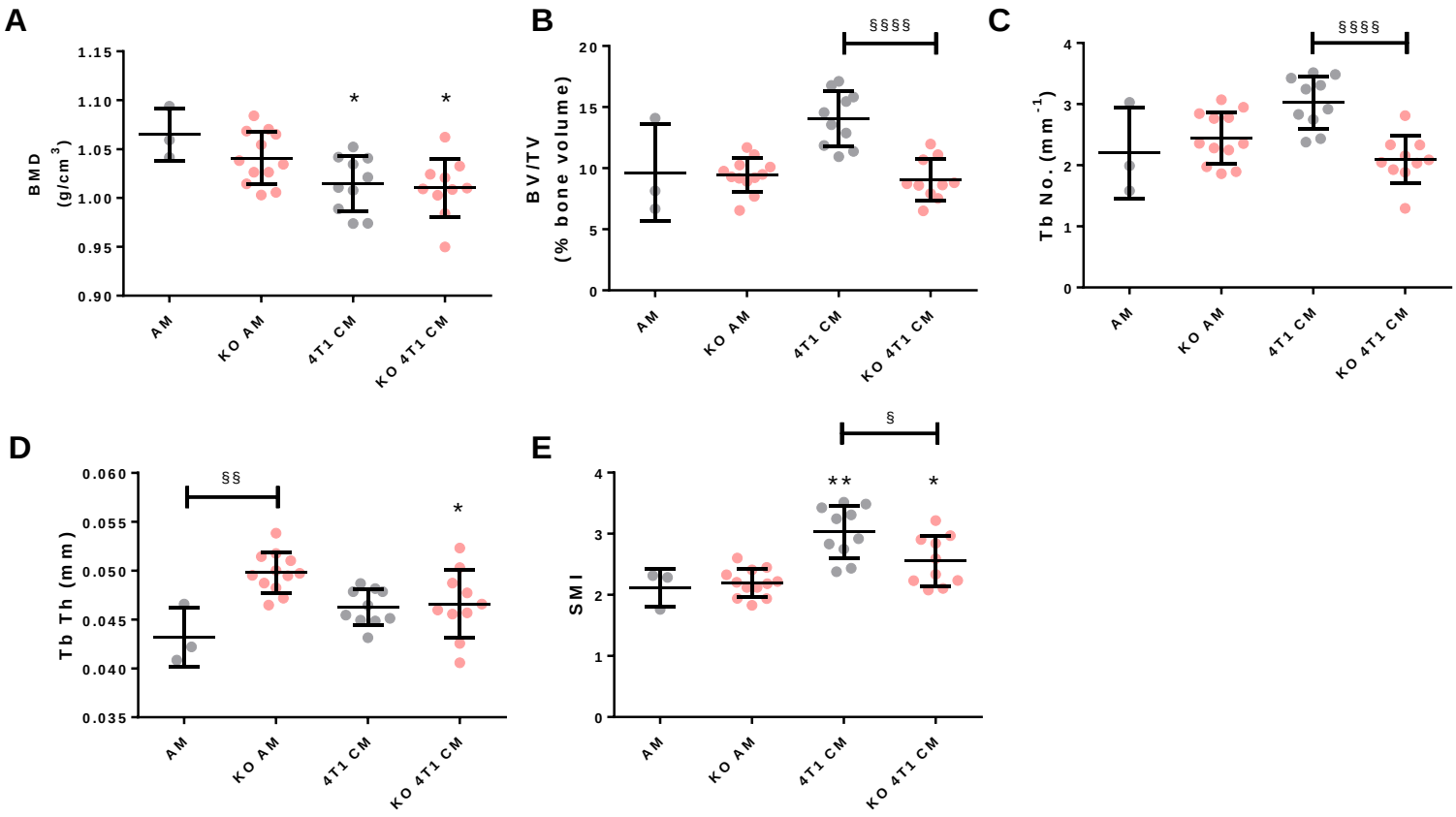

Figure 4.9: Trabecular Analysis of Conditioned Medium Injected WT and P2X7R$^{-/-}$ Mice. WT (grey) and P2X7R$^{-/-}$ (pink, KO) BALB/c mice received daily intraperitoneal injections of conditioned medium from 4T1 cells for a period of 3 weeks before sacrifice. Hindlimbs were dissected, and µCT analysis of the trabecular cavity of the tibiae conducted. **A** BMD values, calculated from mean greyscale values. **B** Percentage Trabecular Bone Volume (BV/TV) **C** Number of trabeculae per mm of bone. **D** Mean thickness of individual trabeculae in mm. **E** Structural Model Index (SMI), a measure of morphology where 0 = ideal plate, 3 = ideal cylinder, 4 = ideal sphere. Data shows mean values for individual tibia ± SD. * denotes statistical significance compared to relative age matched control, calculated by Mann-Whitney test for WT data, and unpaired t-test for P2X7R$^{-/-}$ data; § denotes statistical significance compared to WT control (as denoted by line bar), calculated by Mann-Whitney test. AM n=3, 4T1 n=10, KO AM n=12, KO 4T1 n=10. */§= $p<0.05$; **/§§ = $p<0.01$; ****/§§§§ = $p<0.0001$.

Table 4.5: Summary of Trabecular Analysis in WT and P2X7R$^{-/-}$ Conditioned Medium Injected Mice.

	WT		P2X7R$^{-/-}$	
	AM	**4T1-CM**	**AM**	**4T1-CM**
BMD (g/cm^3)	1.065	1.015 *	1.041	1.010 *
BV/TV (%)	9.637	14.03	9.436	9.049 §§§§
Tb No.. (mm^{-1})	2.201	3.029	2.449	2.091 §§§§
Tb Th (mm)	0.043	0.046	0.05 §§	0.047 *
SMI	2.121	3.029 **	2.195	2.551 * §

Table shows mean values for trabecular variables in each experimental group. AM = age-matched control, 4T1-CM = mice injected with conditioned medium from 4T1 cells cultured *in vitro*. * denotes statistical significance compared to relevant age matched control, calculated by Mann-Whitney test for WT data, and unpaired t-test for P2X7R$^{-/-}$ data. § denotes statistical significance compared to relevant WT BALB/c mouse group, calculated by Mann-Whitney test. */§ = $p<0.05$, **/§§ = $p<0.01$, ***/§§§ = $p<0.001$, ****/§§§§=$p<0.0001$.

4.2.5 Effect of LOX on Primary Tumour

Comparison of tumour volumes (calculated from calliper measurements, see section 2.10) in WT BALB/c mice revealed that genetic knockdown of LOX resulted in a significant reduction in tumour volume from 374.8mm^3 in 4T1 tumours, to 179.9mm^3 in 4T1-shLOX tumours (p=0.0043, Fig. 4.10). Knockdown of LOX also significantly reduced tumour size in P2X7R$^{-/-}$ mice, from 328.2mm^3 in 4T1 tumours, to 170.7mm^3 in 4T1-shLOX tumours (p=0.0390). Data are summarised below in figure 4.10 and table 4.7.

There were no significant differences in corresponding tumour volumes between WT and P2X7R$^{-/-}$ mouse strains, however it should be noted that knockdown of P2X7R$^{-/-}$ occurred only in the host mouse, and not in the 4T1 cell line. Thus this shows that host P2X7R activity did not contribute to tumour volume.

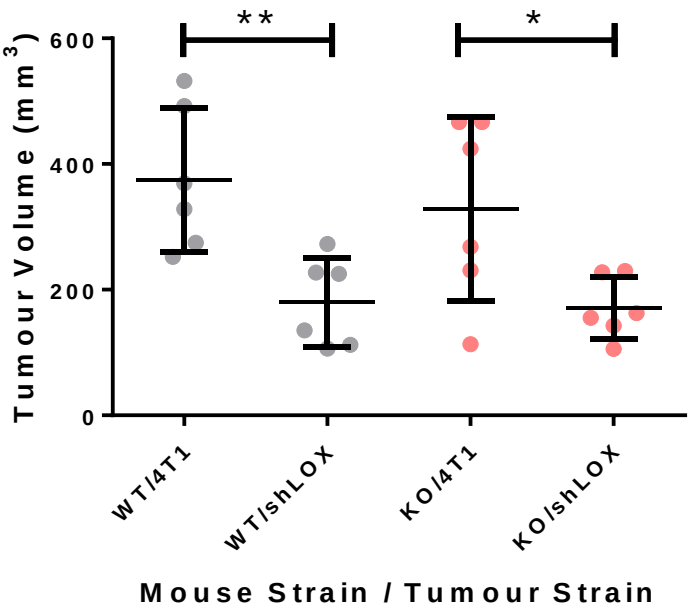

Figure 4.10: Effect of LOX on Primary Tumour Volumes. WT (grey) and P2X7R$^{-/-}$ (pink, KO) BALB/c mice (n=6) received a single injection of either 4T1 or 4T1-shLOX cells to the mammary fat pad. Maximal and minimal tumour diameters were recorded at day 17 after injection and used to calculate tumour volume. Data show tumour volume ± SD. * denotes statistical significance, calculated by Mann-Whitney test. * = p<0.05; ** = p<0.01.

Table 4.6: 4T1 and 4T1-shLOX Tumour Volumes in WT and P2X7R$^{-/-}$ BALB/c Mice.

	Tumour Volume (mm^3)		Sig.	p
	4T1	4T1-shLOX		
WT	374.8	179.9	**	0.0043
P2X7R$^{-/-}$	328.2	170.7	*	0.0390

Table shows tumour volumes for each of the tumour bearing experimental groups. 4T1 = 4T1 tumour bearing mice, 4T1-shLOX = 4T1-shLOX tumour bearing mice. Sig. = statistical significance between 4T1 and 4T1-shLOX groups, calculated by Mann-Whitney test. * = p<0.05, ** = p<0.01.

4.3 Discussion

LOX has previously been shown to contribute significantly towards the formation of osteolytic lesion formation in bone, driving formation of a pre-metastatic niche which generates favourable conditions for metastasis (Cox et al. 2015). Given the accumulation of LOX at areas of pressure, noted by our collaborators, and the role of P2X7R in bone remodelling and response to loading, we hypothesised that P2X7R was involved in LOX mediated lesion formation in the pre-metastatic bone microenvironment. To investigate this a syngeneic breast cancer mouse model was used to determine if knockout of P2X7R in the mouse affected tumour secreted LOX modification of bone.

4.3.1 Interaction of LOX and P2X7R signalling in osteolytic lesion formation

4.3.1.1 Orthotopic Mouse Model

The results of the orthotopic tumour model described above, in section 4.2.1, confirm that 4T1 tumours drive the formation of osteolytic lesions in mice. Furthermore, they show that LOX contributes significantly to the formation of these lesions as LOX knockdown in 4T1 tumours caused a significant reduction in both the number and area of osteolytic lesions formed in WT mice (Figs. 4.1 & 4.2), confirming previous observations (Cox et al. 2015). In addition, knockout of P2X7R has been shown to interfere with LOX mediated lesion formation: 4T1 tumour bearing $P2X7R^{-/-}$ mice developed both fewer lesions, and a smaller total lesion area compared to their WT counterparts (Fig. 4.4), despite having a higher number of natural 'lesions' in bone prior to tumour inoculation.

Interestingly, lesion formation in $P2X7R^{-/-}$ mice was unaffected by knockdown of LOX in the primary tumour, with both 4T1 and 4T1-shLOX tumour bearing groups developing similar levels of lesion number and area (Fig. 4.4), suggesting that P2X7R is necessary for LOX mediated lesion formation. This is compelling evidence for an interaction between LOX activity and P2X7R signalling, suggesting that breast cancer induced osteolytic lesion formation may be inhibited by interfering with either LOX activity or P2X7R signalling. Previous research by Tao et al. (2008) has shown, via luciferase imaging, that BALB/c mice with 4T1 orthotopic tumours in the mammary fat pad do not display signs of metastasis until 5-6 weeks after the introduction of the cancer cells. Mice in the current experiment were euthanised 3 weeks after 4T1 cell injection, meaning that observations in this study are in the pre-metastatic window, and the osteolytic lesions formed can be considered a pre-metastatic modification, forming in bone prior to the arrival of metastatic cells.

Neither knockout of P2X7R or knockdown of LOX completely prevented lesion formation in the tumour bearing model (Fig. 4.4), suggesting that there are other factors which may be contributing to osteolytic lesion formation. One possible contributory factor is the LOX like protein LOXL-2, which has previously been shown to drive osteolytic lesion formation in bone (Barker et al. 2011).

4.3.1.2 Cell-Free Mouse Model

The cell-free model (Section 4.2.2), in which tumour free mice received daily intra-peritoneal injections of conditioned medium, also led to the formation of osteolytic lesions in bone: confirming that it is possible for tumour secreted factors, such as LOX, to initiate lesion formation in the bone micro-environment prior to metastasis, and in the absence of cancer cells.

Knockout of P2X7R in the mice used in the conditioned medium injection experiment did not result in reductions in overall lesion number or area to the same extent observed in the orthotopic model. It is worth noting, however, that while CM injection does cause significant increases in lesion number and area (Fig. 4.5 A & B), the overall level of lesion formation (after 3 weeks) is much lower than that seen in tumour bearing mice at the same time point (Fig. 4.4 A & B); thus the cell-free model is shown to drive lesion formation at a slower rate than the orthotopic model. The level of osteolytic lesion formation generated by CM injection may not have been great enough to escape being masked by the naturally higher number and area of lesions observed in age-matched P2X7R$^{-/-}$ mice. To counter this effect data were normalised to their relevant age matched control in order to assess overall fold change in lesion number and area (Fig. 4.5 C). This revealed that while the 4T1 CM injected P2X7R$^{-/-}$ mice had more lesions than 4T1 CM injected WT mice, the number formed in P2X7R$^{-/-}$ mice amounted to a 1.6 fold increase, compared to a 3 fold increase in WT mice. Similarly, 4T1 CM injection led to a 1.7 fold change in total lesion area in P2X7R$^{-/-}$ mice, but a 2.6 fold increase in WT mice. When considering this normalised data, it becomes apparent that knockout of P2X7R is in fact reducing the effect of 4T1 CM injection induced osteolytic lesion formation, supporting the hypothesis that P2X7R does play a role in promoting potential pre-metastatic osteolytic lesion formation, and confirming observations made in tumour bearing mice.

The different levels of lesion formation between the orthotopic and cell free models could be explained by differences in LOX dosing. Tumour bearing mice would receive a constant supply of LOX from their tumour *in situ*, whereas those in the cell free model received a single dose of LOX at only one point each day. As a result, it is possible that mice in the cell free model received a lower overall dosage of LOX, resulting in less activation of the pathway (or pathways) responsible for osteolytic lesion formation.

4.3.2 Effects of LOX and P2X7 on Cortical Bone

4T1 tumour presence did not significantly affect cortical thickness in WT mice (Fig. 4.6A), suggesting that the observed lesion formation is occurring in bone at specific loci, rather than as the result of an overall thinning of the bone. Knockdown of LOX in the tumour caused a small decrease in mean cortical thickness (Fig. 4.6A), which was not significantly different from age matched controls, but significantly thinner than in mice with regular 4T1 tumours. Given that knockdown of LOX has been shown to protect against bone loss in other analyses conducted on these same samples it is likely that this apparent bone loss resulting from LOX knockdown is actually an artefact of small sample size. P2X7R$^{-/-}$ mice were found to have thicker cortical bone compared to WT mice (Fig. 4.6 B), corroborating the findings of previous studies investigating the skeletal phenotype of the Glaxo P2X7R$^{-/-}$ mice used in this study (Gartland et al. 2003c; Syberg et al. 2012). Knockout of P2X7R did, however, alter bone response to tumour presence with both 4T1 and 4T1-shLOX tumour bearing mice displaying significant reductions in cortical thickness compared to age matched controls (Fig. 4.6 A). In keeping with the findings of osteolytic lesion analysis, there was no significant effect of LOX knockdown in P2X7R$^{-/-}$ mice. Analysis of fold change data shows that the reductions in cortical thickness in tumour bearing mice are a genuine effect, and not just the result of P2X7R$^{-/-}$ mice having thicker cortical bone prior to tumour inoculation, as when normalised for cortical thickness P2X7R$^{-/-}$ tumour bearing mice display significant reductions in fold change, below 1.00, indicative of an increased level of cortical thinning in these mice (Fig. 4.6 C). It is possible that some feature of the bone in P2X7R$^{-/-}$ mice allowed for easier cortical thinning, perhaps the greater abundance of bone in the thicker cortices of P2X7R$^{-/-}$ mice providing more material for osteoclasts to adhere and develop upon *in vivo.* It is interesting to note that cortical thickness in tumour bearing P2X7R$^{-/-}$ mice reduced to levels similar to those found in all experimental groups in the WT mice, perhaps hinting that there is some mechanism preventing drop of cortical thickness below a certain level. Alternatively, given more time, it is possible that the P2X7R$^{-/-}$ cortices would have continued to thin.

4.3.3 Effects of LOX and P2X7 on Trabecular bone

The initial comparison of age-matched control mice from the WT and P2X7R$^{-/-}$ genotypes showed that the P2X7R$^{-/-}$ phenotype displayed thicker trabecular bone than WT (Fig. 4.7 D). This supports previous research, using the same (Glaxo) P2X7R$^{-/-}$ mouse strain, which reported increased Tb Th in the vertebrae, and a trend towards increased Tb Th in the proximal tibia (Syberg et al. 2012). Furthermore the general osteogenic effect of P2X7R$^{-/-}$ on trabecular bone supports wider research on the Glaxo P2X7R$^{-/-}$ mouse, describing an imbalance in bone homeostasis in favour of bone formation (Gartland et al. 2003c), although these observations were based on cortical bone and not trabecular.

Trabecular bone in tumour bearing WT mice showed significant changes which were attributable to LOX production from a primary mammary fat pad tumour. Both BMD and Tb Th were significantly reduced in 4T1 tumour bearing WT mice (Fig. 4.8 A & D), and in both cases these reductions were prevented by inhibiting LOX production via shRNA (i.e. no significant differences were noted between age matched controls and 4T1-shLOX tumour bearing WT mice in BMD or Tb Th).

In contrast to observations in osteolytic lesion formation and cortical bone thickness, where LOX expression by tumour cells was not shown to exert any significant effect in P2X7R$^{-/-}$ mice, there does appear to be some significant modification of trabecular bone in P2X7R$^{-/-}$ mice attributable to LOX. LOX was shown to drive a reduction in BV/TV and Tb No. in tumour bearing P2X7R$^{-/-}$ mice, indicating a potentiation of cancer induced bone loss which was reversed on genetic knockdown of LOX in the tumour (Fig. 4.8 B & C). Knockdown of LOX also prevented morphological changes to the trabeculae of tumour bearing P2X7R$^{-/-}$ mice. None of these variables showed significant change in relation to tumour presence (or LOX knockdown) in WT BALB/c mice, suggesting that P2X7R$^{-/-}$ mice maybe more susceptible to tumour (and LOX) induced trabecular bone loss, but more resistant to tumour induced cortical bone loss, as evidenced by the reduction in osteolytic lesion formation in cortical bone previously discussed (Section 4.3.1). Considering these two observations together it can be concluded that LOX interaction with P2X7R is required in order to drive substantial levels of osteolytic lesion formation in cortical bone, but that P2X7R is not required for LOX mediated remodelling in trabecular bone.

To understand the observed differences in LOX and P2X7R effect on bone between the cortical and trabecular compartments, the differences in bone remodelling and LOX activity between cortical and trabecular P2X7R$^{-/-}$ microenvironments must be considered. A review of the cellular mechanisms of bone remodelling by Eriksen (2010) highlights some important differences between remodelling of trabecular and cortical bone. Trabecular bone remodelling occurs

across the surface of trabeculae, which are located within the bone marrow cavity. As such they are immediately accessible to osteoprogenitor cells of the haematopoietic stem cell niche which reside therein. By contrast cortical bone remodelling occurs distal to the marrow cavity and must wait for osteoprogenitor cell arrival from the blood supply. This would suggest that trabecular bone remodelling is able to be more responsive to stimuli simply because it is nearer to the necessary cells, and supports the convention that cortical bone is typically less metabolically active than trabecular bone (Clarke 2008). Despite these observations, analysis of bone remodelling cycles has shown that cortical bone remodels more quickly than trabecular bone (Israel et al. 1994; Eriksen 2010). One cycle of trabecular bone remodelling (from resorption pit formation to the completion of new matrix deposition) takes on average 200 days (Eriksen 1986), compared to 120 days for cortical bone (Agerbaek et al. 1991). The reasons for this have not been conclusively investigated, but one possible explanation lies in the stimuli for bone remodelling. Cortical bone is largely stimulated to remodel in response to damage (i.e. microfractures), while trabecular bone remodels in response to stress, following the principles of Wolff's Law (Ruff et al. 2006). As microdamage occurs as discrete events, at singular points in time, it is perhaps a less constant stimulus than stress on the trabeculae from loading of the limb. Hence a continual signal to remodel in trabecular bone could result in a prolonged period of remodelling, and may in fact increase the quantity of remodelling conducted, while extending the time it takes to complete the cycle. Another feature to consider is disease state in the bone. Patients with osteoporosis (either postmenopausal or as a result of hypoparathyroidism) display an increased rate of bone remodelling compared to healthy controls (Israel et al. 1994). This rate increase, however, is only noted in cortical bone, not trabecular. This further suggests a higher rate of bone remodelling in cortical bone compared to trabecular, particularly in diseases of excess bone resorption, such as in the metastatic bone disease stimulated in this study secondary to breast cancer. Considering these factors together it is unlikely that the differences in LOX mediated change between cortical and trabecular bone noted in the $P2X7R^{-/-}$ mice (namely that there is no effect of LOX in osteolytic lesion formation in the cortical bone of $P2X7R^{-/-}$ mice, but there are notable effects upon BV/TV, Tb No., and SMI in trabecular bone) are the result of a greater rate of bone remodelling in the trabecular bone allowing LOX mediated differences to manifest within the time frame of the experiment, while those in cortical bone lagged behind. Rather, the biological processes driving bone remodelling in these two compartments must differ in some aspect other than rate.

LOX activity has been shown to drive osteoclast cell formation and activity (Cox et al. 2015), and while P2X7R stimulation in osteoclasts also drives osteoclast cell formation (Agrawal et al. 2010; Gartland et al. 2003a) it is as yet unknown whether LOX and P2X7R achieve this via the same or

different pathways. Given that LOX activity is shown to drive trabecular bone loss in the absence of P2X7R, this suggests that it either acts downstream of P2X7R or via a different pathway – and in either case does not require P2X7R to generate trabecular bone loss in metastatic bone disease. However, considering that LOX mediated osteolytic lesion formation is inhibited (though not entirely prevented) by knockout of P2X7R, it suggests that there is an effective interaction between LOX and P2X7R in cortical bone, if not in trabecular bone. As mentioned previously, one major difference between the cortical and trabecular microenvironments is proximity to osteoprogenitor cells. Thus one possibility is that LOX in the cortical bone microenvironment, signalling via P2X7R, drives the recruitment of osteoprogenitor cells to the cortical bone allowing bone remodelling to commence. In this case removal of P2X7R would retard cortical bone remodelling, but perhaps not effect trabecular bone remodelling which already occurs in the vicinity of the requisite cells, thus providing a possible explanation for the LOX mediated differences seen between the two compartments in $P2X7R^{-/-}$ mice.

A final point for consideration is the skeletal development of the mice. BALB/c Mouse skeletal development has been reported to have three phases: rapid bone growth, attainment of peak bone mass, and age related decline (Ke 2005). BALB/c mice have an initial skeletal growth period which ends at around 7 months. The mice used in this study were sacrificed at 3 months, thus putting them in the middle of the early rapid growth phase (Willingham et al. 2010). P2X7R has been reported to inhibit trabecular bone remodelling during the early growth phase of C57BL/6 mice (Ke 2005). Presuming the same function in BALB/c mice, this could explain why differences in this study are noted in the trabecular bone of $P2X7R^{-/-}$ mice, but not WT mice.

WT mice receiving 4T1 CM injection broadly reciprocated the results noted in tumour bearing mice (Fig. 4.9), though 4T1 CM injected mice showed a trend towards an increase in Tb Th as opposed to the significant decrease observed in 4T1 tumour bearing mice. Differences between the orthotopic and cell free models were more pronounced in $P2X7R^{-/-}$ mice, where BV/TV and Tb No. showed significant reductions in tumour bearing mice (Fig. 4.8 B & C), which were absent in CM injected mice (Fig. 4.9 B & C). Conversely CM injected $P2X7R^{-/-}$ mice showed a significant reduction in BMD (Fig. 4.9 A), which was not present in the orthotopic model. These differences, particularly those showing significant change in the orthotopic model, but not cell free model, are likely the result of difference in LOX dosage as previously discussed (section 4.3.1.2). Another consideration for analysis of data in the cell free model is the low number of samples in the WT age matched control group (n=3) which negatively affects the robustness of the data. Regardless of these limitations, the fact that the results in trabecular bone largely follow the pattern seen in the orthotopic model is encouraging, and demonstrates that trabecular bone can be altered

in the absence of cancer cell presence, confirming that it is possible for tumour secreted LOX to drive trabecular bone loss in the pre-metastatic environment.

4.3.4 Effects of LOX on Primary Tumour Volume

As discussed above LOX has been found to drive the development of metastatic bone disease by contributing to osteolytic lesion formation. One mechanism by which LOX could be, at least partially, responsible for this is by promoting growth of the primary tumour. This would result in an increased tumour mass and cell number, which could in turn release a greater volume of tumour secreted factors into the blood stream, potentiating the stimuli for the development of metastatic bone disease.

Comparison of tumour volumes between 4T1 and 4T1-shLOX tumours in both WT and P2X7R$^{-/-}$ mice in this study revealed that knockdown of LOX in the primary tumour resulted in a significant reduction in overall tumour volume (Fig. 4.10), suggesting that LOX expression promotes primary tumour growth. This observation is contrary to previous publications, using the same 4T1 cell line and shLOX construct, which have stated that LOX showed no significant effect on primary tumour growth (Erler et al. 2006; Erler et al. 2009). It does, however, support other studies reporting that LOX expression drives cancer cell growth (Baker et al. 2011; Baker et al. 2013; Wiel et al. 2013).

LOX enzymatic activity appears to be an important feature in the promotion of cancer cell growth, and stiffening of collagen in the immediate vicinity of tumour cells both *in vivo* and *in vitro* has been reported to potentiate colorectal cancer cell growth via a corresponding increase in FAK (focal adhesion kinase)/SRC signalling (Baker et al. 2013). FAK/SRC signalling is known to promote cell motility, cell cycle progression, and survival; allowing it to contribute to tumour growth and metastasis (Mitra & Schlaepfer 2006). LOX stimulation of FAK signalling has also been shown to counteract the cancer defence mechanism of oncogene induced senescence (OIS), whereby aberrant oncogenic signals drive cells into stable cell cycle arrest (Serrano et al. 1997). Constitutive expression of LOX in mammary human epithelial cells *in vitro,* and in transgenic a mouse model of pancreatic ductal adenocarcinoma, has been found to favour escape from OIS, while LOX inhibition stabilises OIS in both models (Wiel et al. 2013).

While it is possible that differences in tumour cell volume could occur as a result of experimental error in generating the correct number of 4T1 cells in solution for injection, the data in this study represent two separate sessions of injection, as WT and P2X7R$^{-/-}$ mice were inoculated on different days, thus making it unlikely that the observation of reduced tumour volume in 4T1-shLOX tumours is the result of such an error. Considering these observations together it is apparent that expression of LOX in the 4T1 mouse breast cancer model used in this study

supports a role for LOX mediated tumorigenesis, which may contribute, in part, to the observed increase in bone loss observed in these mice.

4.4 Conclusion

LOX, secreted from breast cancer cells, has been shown to drive osteolytic lesion formation in bone (Cox et al. 2015). This study supports these findings, and furthermore presents evidence to show that LOX driven lesion formation requires the P2X7 receptor, although the nature of this interaction and potential pathways activated remain unknown. Osteolytic lesion formation was shown to occur in the pre-metastatic window, as well as in the absence of cancer cells, supporting the hypothesis that LOX secreted from a primary tumour may induce osteolytic lesion formation in bone prior to cancer cell arrival, thus contributing to pre-metastatic modification of the bone microenvironment. Cortical thickness of bone was found to be unaffected by LOX secretion in WT mice but cause thinning in $P2X7R^{-/-}$ mice, suggesting that P2X7R has a protective effect against cortical thinning in tumour bearing mice. Trabecular bone was found to be more complex and displayed LOX mediated differences which occurred independent of P2X7R involvement.

This chapter provides evidence identifying P2X7R signalling as a key feature of the pathway by which LOX drives osteolytic lesion formation in bone, supporting the targeting of both LOX and P2X7R in future research for prophylactic treatments to combat breast cancer metastasis to bone.

CHAPTER 5:

THE EFFECT OF MECHANICAL LOADING ON LOX/P2X7R MODIFICATION OF PRE-METASTATIC BONE.

5.1 Introduction

The general rule of bone remodelling, referred to as Wolff's Law (Meakin et al. 2014) or Bone Functional Adaptation (Ruff et al. 2006), holds that bone adapts to the stresses under which it is placed: remodelling itself to a form which is best able to withstand the forces to which it is subjected. In this way cortical bone can become thicker to withstand increasing compressive forces from heavy use, such as those noted in studies of the serving arms of professional tennis players (Bass et al. 2002). Conversely disuse of bone will result in an overall loss of bone mineral, for example in cases of prolonged bedrest, paralysis, or in the low gravity conditions of space flight (Cazzaniga et al. 2014). This, however, is only a small part of the greater picture. In reality the way in which bone responds to loading depends on numerous different factors, such as loading type, intensity, and frequency. Furthermore, different bones are able to resist some forces better than others. The long bones, whose principal purpose is weight bearing, are well adapted to resist compression, to which they are commonly subjected, but less able to resist tension, to which they are less commonly subjected. While the concept of bone functional adaptation is widely accepted, the underlying mechanisms by which it is enacted are not fully understood.

A wealth of prior research using a variety of different loading models has highlighted the complexity of bone response to loading. Experimentation with *in vivo* models for whole bone mechanical loading have shown that axially compressing long bones, typically the ulna or tibia, results in osteogenesis of the cortical bone, and remodelling of the trabeculae to produce a more robust bone, better able to withstand this force (De Souza et al. 2005a; Robling & Turner 2002; Holguin et al. 2013; Li et al. 2005). Applying compression to other bones, however, has been shown to have an osteolytic effect. In an experiment to investigate whether mechanical loading could be a cause of bone loss in the maxilla following tooth loss, Fujiki et al. (2013) loaded the hard palate of rats. They found that loading of the hard palate resulted in a loss of cortical bone volume and an increase in cortical bone porosity in the areas under the loading contact, with 90% of the osteoclasts counted clustering in the areas of highest strain within the bone, possibly responding to the presence of microfractures in these areas. Thus mechanical loading can alter bone remodelling in either an osteoblastic or osteoclastic direction depending on which bone is being affected.

Bone response to loading has been shown to be a highly localised effect. In mice where one bone is loaded to induce new bone formation, the contralateral control limb shows no significant difference from non-loaded age-matched control mice. (Sugiyama et al. 2010). Thus the effect of loading is considered to be site specific, with bone responding to local stresses and strains.

The process of bone remodelling is ultimately mediated by cellular activity, that of the bone producing osteoblast, and the bone resorbing osteoclast. Indeed, it has been shown that loading has a direct effect upon the bone cells themselves. Experimentation with primary rat osteoblasts *in vitro* has shown that application of fluid sheer stress to the cells results in significant increases in cell proliferation, calcium deposition (mineralisation), and expression of the osteogenic markers alkaline phosphatase (ALP, a marker of osteoblast cell activity) and osteocalcin (a marker of terminal osteoblast differentiation) (Ban et al. 2011).

Recent research has also shown that osteoblasts respond to fluid sheer stress with a rapid influx of Ca^{2+}, and release of ATP (Sun et al. 2014; Li et al. 2005; Romanello et al. 2005; Romanello et al. 2001). ATP, the ligand for P2 receptors (including P2X7R), is known to play a prominent role in bone response to loading. Knockout of P2X7R in osteoblasts results in a significant reduction in mineral nodule formation and ALP activity *in vitro* (Panupinthu et al. 2008). Whole bone *in vivo* loading experiments have also shown that knockout of P2X7R in mice causes a substantial reduction in bone response to loading, with female mice displaying as much as a 61% reduction in loading mediated bone formation compared to WT controls (Li et al. 2005).

Loading experiments utilising osteoclast cell cultures are complicated by the lack of viable osteoclast cell lines, and difficulties in generating a primary culture of sufficient osteoclast cell purity. As a result, there is relatively little published literature regarding osteoclast cell response to loading, but what has been published shows that strain is able to both promote and inhibit osteoclast cell activity. Application of strain to the culture substrate on which osteoclasts are grown has been shown to impede osteoclast recruitment in the first few days of culture (Rubin et al. 1999), but also to promote osteoclast maturation and increase resorptive activity, as well as the number and area of resorptive pits formed (Kurata et al. 2001). Thus loading of osteoclasts can either drive or impede osteoclastic resorption. The level of strain generated by loading appears to be a key factor in determining how osteoclasts respond to loading. Osteoclast cells subjected to either low or excessively high levels of strain are less active and even apoptotic, while those exposed to higher physiological levels of strain have been shown to be more active and driven to resorb (Xu et al. 2012).

Osteoclasts *in vitro* have also been shown to respond to mechanical stimulation by release of ATP (Rumney et al. 2011). As previously mentioned, ATP is the ligand for P2 receptors which are known to play a prominent role in bone response to loading (Li et al. 2005; Panupinthu et al. 2008). Thus this observation suggests a potential mechanism for the observed effects of mechanical loading on osteoclasts. Culture of osteoclasts, derived from human peripheral blood monocytes, were subjected to mechanical stimulation by 80% fluid displacement by pipette. This was shown to drive ATP release from the cells, and resulted in a significant decrease in

resorption on day 14 of the culture, but not at day 21 (Rumney et al. 2011). There was no significant correlation between basal ATP release and osteoclast cell number, indicating that the reduced resorption was the result of a reduction in cell activity. This suggests that the osteoclast response to loading in this study was to inhibit cell activity. This would result in a shift towards bone growth, resulting in an osteogenic effect of loading, and supports a crucial role for purinergic signalling in bone response to loading, as previously proposed by Li et al. (2005).

In summary mechanical loading affects different bones in different manners, and the effect generated is dependent upon the nature and strength of the force applied. Axially loading long bones has been shown to imbalance bone remodelling homeostasis towards osteogenesis, however this likely involves the co-ordinated actions of both osteoclasts and osteoblasts working in tandem. To the author's knowledge no study has yet investigated the effect of loading upon osteolytic lesion formation, an important development in metastatic bone disease which greatly affects patient mortality and quality of life, and represents a key determinant in the decision to commence chemotherapy (Rajkumar et al. 2014). Formation of osteolytic lesions in bone has been shown to be a crucial factor in promoting cancer cell recruitment and survival at secondary metastatic sites, thus contributing to the pre-metastatic niche. Our previous study induced osteolytic lesions in mice via injection on conditioned medium from cancer cells grown *in vitro.* Mice that developed osteolytic lesions prior to inoculation with breast cancer cells showed that metastatic tumour burden directly correlates with the number of osteolytic lesions formed, demonstrating that lesion formation contributes significantly to the development of future metastases (Cox et al. 2015).

In addition to this, the bone loss associated with lesion formation also contributes to complications for the patient. Morbidities resulting from metastatic bone destruction include bone loss, increased fracture risk, pain, fatigue, and potentially life-threatening levels of hypercalcaemia (Mercadante 1997; Domchek et al. 2000; Cancer Research UK 2014). Current treatment for metastatic bone disease is almost completely limited to the administration of anti-resorptive bisphosphonates to prevent further bone loss by inhibiting osteoclast activity and survival (Drake et al. 2008; Fleisch 2002). While this treatment does reduce the frequency and morbidity of skeletal complications from metastases (Blanchette & Pritchard 2015), it does not repair lesions which have already formed prior to the course of medication, potentially leaving the patient at greater risk of relapse. Furthermore, a meta-analysis of 9 separate studies (comprising a total of 2806 patients overall) revealed that bisphosphonate treatment only reduced skeletal related events by 15% when compared to placebo control (Wong et al. 2012). Taken together this highlights the importance of understanding the underlying causes of

osteolytic bone destruction and lesion formation, in an effort to find new targets for anabolic treatments which are able to repair lesions already formed at the time of diagnosis.

Given the relationship of mechanical loading and ATP/P2X7R, and the newly discovered LOX mediated lesion formation pathway, it is highly plausible that these processes interact with each other to at least some degree, warranting research to discover new targets for future treatments. To that end, this chapter investigates the effect of mechanical loading on osteolytic lesion formation in a mouse model in which LOX and P2X7R are manipulated. We have previously shown in Chapter 4 that osteolytic lesion formation appears to be site specific, rather than arising from an overall thinning of cortical bone, thus it is not certain what effect mechanical loading (which increases overall cortical thickness) will have on lesion formation. P2X7R has also been shown to contribute significantly to LOX mediated lesion formation, where its deletion substantially reduced both lesion number and area (Chapter 4). Loading of bone causes release of ATP from cells, including osteoblasts (Romanello et al. 2001; Romanello et al. 2005) and osteoclasts (Rumney et al. 2011), which will propagate purinergic signalling, including that via P2X7R. It is hypothesised that increased activation of P2X7R signalling will allow for a greater effect of LOX driven osteolytic lesion formation. Alternatively, it is possible that increased cortical thickness from mechanical loading may mitigate lesion osteolysis, drive osteogenesis, and protect the bone from lesion formation.

5.2 Results

5.2.1 Effect of Mechanical Loading on Bone in Tumour Bearing Mice

The effects of mechanical loading on bone were investigated via µCT, in a mouse model of breast cancer metastasis to bone. Results for indices of loading effect on cortical and trabecular bone are given below.

5.2.1.1 Effects of Mechanical Loading on Cortical Thickness

Cortical Thickness was manually measured from µCT scans of tibiae in loaded (right) and non-loaded (left) hindlimbs of WT and P2X7R$^{-/-}$ mice. Statistical assessment between loaded and non-loaded limbs was conducted using Wilcoxon matched–pairs signed rank test (a non-parametric paired t-test). All cortical thickness data are summarised below in figure 5.1 and table 5.1.

Comparison of loaded and non-loaded tibiae within the same mouse in healthy age-matched controls revealed that mechanical loading at 8.3N resulted in a significant increase in tibial cortical thickness from 0.13mm to 0.15mm ($p=0.0313$, Fig. 5.1) in WT mice. In P2X7R$^{-/-}$ mice there was no significant difference between loaded and non-loaded tibiae, although there was a trend towards increased cortical thickness in the loaded limb, which increased from 0.15 to 0.18mm ($p=0.125$, Fig. 5.1).

Comparison of left and right tibiae in non-loaded control mice (both WT and P2X7R$^{-/-}$), showed no significant differences in cortical thickness associated with limb side (Fig. 5.1, Table 5.1). Thus the observed changes in loaded tibiae can be attributed to the mechanical loading procedure, rather than from preferential loading of a dominant limb during routine activities, such as running and jumping.

Cortical thickness was also assessed in tumour bearing groups (4T1 and 4T1-shLOX) in both WT and P2X7R$^{-/-}$ mice. Mechanical loading also resulted in significant increases in cortical thickness in both 4T1 and 4T1-shLOX tumour bearing WT mice. In P2X7R$^{-/-}$ mice mechanical loading significantly increased cortical thickness in 4T1 tumour bearing mice but not in 4T1-shLOX tumour bearing mice (Fig. 5.1, Table 5.1).

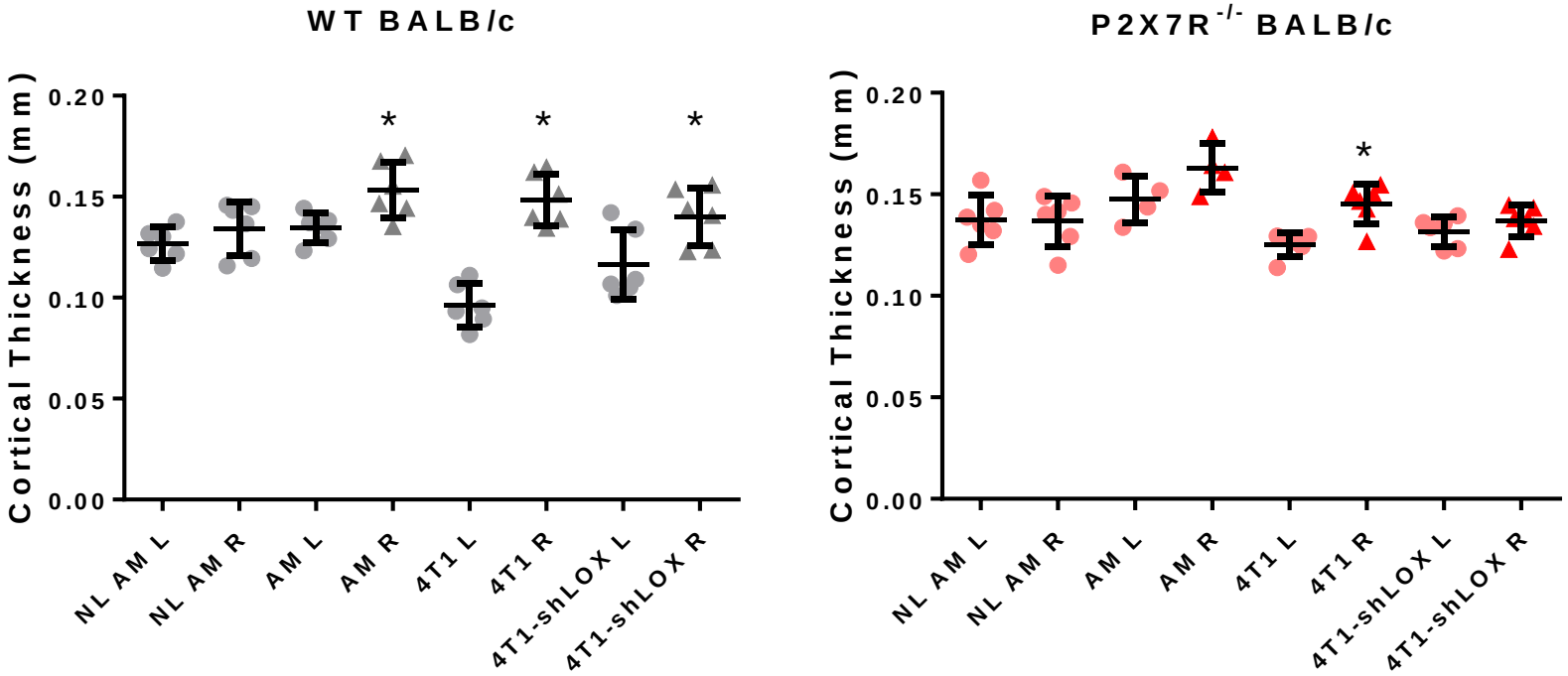

Figure 5.1: Effect of Mechanical Loading on Tibial Cortical Thickness. Mice were non-invasively mechanically loaded on their right (R) limb, with the left (L) limb used as a non-loaded contralateral control. Mice were divided into three experimental groups: age matched controls (AM); 4T1 tumour bearing mice (4T1); or 4T1-shLOX tumour bearing mice (4T1-shLOX). A further group of mice were not subjected to loading and used as non-loaded age-matched controls (NL AM). Data shows mean values ± SD. *denotes significance compared to left (L, non-loaded) limb, calculated by Wilcoxon test. * = $p < 0.05$, n=6 for all groups, except KO AM L and KO AM R, where n=4.

Table 5.1: Cortical Thickness in Loaded and Unloaded Tibiae.

	Group	Cort Th. (mm)	SD	Sig.	p
WT BALB/c	NL AM L	0.127	0.008	nsd	p=0.0938
	NL AM R	0.134	0.013		
	AM L	0.135	0.135	*	p=0.0313
	AM R	0.153	0.153		
	4T1 L	0.096	0.096	*	p=0.0313
	4T1 R	0.149	0.149		
	4T1-shLOX L	0.116	0.116	*	p=0.0313
	4T1-shLOX R	0.140	0.140		
P2X7R$^{-/-}$ BALB/c	KO NL AM L	0.138	0.012	nsd	p=0.8438
	KO NL AM R	0.137	0.013		
	KO AM L	0.148	0.010	nsd	p=0.125
	KO AM R	0.177	0.032		
	KO 4T1 L	0.125	0.006	*	p=0.0313
	KO 4T1 R	0.145	0.010		
	KO 4T1-shLOX L	0.132	0.007	nsd	p=0.5625
	KO 4T1-shLOX R	0.137	0.008		

Table shows cortical thicknesses ± SD for left (L) and right (R) limbs for experimental groups in both WT and P2X7R$^{-/-}$ BALB/c mice. NL AM = non-loaded age-matched controls, AM = age-matched loaded controls, 4T1 = 4T1 tumour bearing loaded mice, 4T1-shLOX = 4T1-shLOX tumour bearing loaded mice. Mice in loaded groups subjected to mechanical loading on their right (R) leg, with left (L) leg used as a non-loaded internal control. Statistical significance (and p-values) presented show difference between left and right limbs in each group, as calculated by Wilcoxon test. * = $p<0.05$, nsd = no significant difference. n=6 for all groups, except KO AM L and KO AM R, where n=4.

5.2.1.2 LOX and Cortical Thickness Response to Loading

To compare the effects of tumour secreted LOX, in combination with mechanical loading, between WT and P2X7R$^{-/-}$ mice, fold changes in cortical thickness (calculated relative to the non-loaded limb of age-matched loaded mice) were analysed using a Kruskall-Wallis test, with Dunn's multiple comparisons post-test to compare experimental groups against each other. Analysis of fold change data showed no significant effect of mechanical loading, or of either tumour type, on cortical thickness when compared to external non-loaded controls (i.e. healthy, non-loaded mice). Mechanical loading did, however, significantly increase cortical thickness in 4T1 tumour bearing mice, increasing fold change from 0.714 in non-loaded 4T1 tumour bearing WT mice limbs to 1.103 in their loaded counterparts ($p<0.05$, Fig. 5.2 A). Thus application of mechanical loading of WT mice with 4T1 tumours reversed the trend of bone loss seen in response to 4T1 tumour bearing, resulting in a net increase in cortical thickness (a fold change >1), albeit this increase was not significant compared to controls. There was no statistically significant effect of tumour bearing or mechanical loading on cortical thickness fold change in P2X7R$^{-/-}$ mice.

Knockdown of LOX in 4T1 tumours showed a trend to mitigate tumour induced loss in cortical thickness, though this was not statistically significant. There was no significant effect of LOX knockdown on cortical thickness fold change in response to loading in WT or P2X7R$^{-/-}$ mice. Data are summarised below in figure 5.2 and table 5.2.

5.2.1.3 P2X7R and Cortical Thickness Response to Loading

Comparison of loaded and non-loaded limbs in WT mice with their corresponding P2X7R$^{-/-}$ counterparts, using Wilcoxon matched–pairs signed rank test, revealed that knockout of P2X7R showed no statistically significant effect of mechanical loading in age-matched mice ($p=0.8286$, Fig. 5.2 C), but did significantly inhibit changes in cortical thickness in both 4T1 tumour bearing mice, and 4T1 tumour bearing mice subjected to mechanical loading (Fig. 5.2 C). In both groups P2X7R$^{-/-}$ mice displayed fold changes in cortical thickness which were closer to age-matched controls. Results are summarised in figure 5.2 and table 5.3 below.

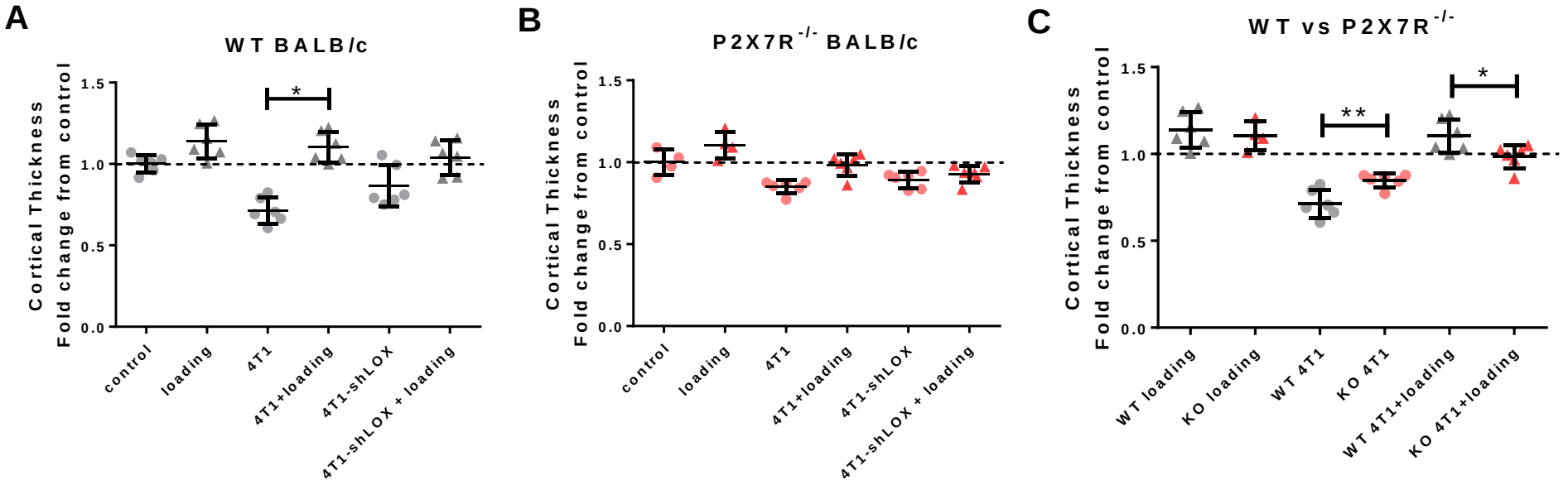

Figure 5.2: Fold Change in Cortical Thickness - Mechanical Loading and Tumour Effect. WT and P2X7R$^{-/-}$ mice were mechanically loaded on their right limb, with the left limb used as a contralateral non-loaded control. Data shows fold change in cortical thickness relative to non-loaded age-matched controls ± SD. **A** Data from WT mice. **B** Data from P2X7R$^{-/-}$ mice. **C** Comparison of WT and P2X7R$^{-/-}$ mouse data. Dotted line denotes mean value of control. Points above this line represent increase in cortical thickness, points below indicate decrease in cortical thickness * denotes statistical significance compared to control (Kruskal-Wallis test), unless otherwise indicated by line bar (Mann-Whitney test). *= $p<0.05$, **= $p<0.01$.

Table 5.2: Cortical Thickness Fold Change Values – Effect of LOX and Mechanical Loading.

	Group	Fold Change	Sig. cf. control	p	Sig. cf.4T1	p
WT BALB/c	Loading	1.138	nsd	>0.05	nsd	>0.05
	4T1	0.714	nsd	>0.05	n/a	>0.05
	4T1 + loading	1.103	nsd	>0.05	*	<0.05
	4T1-shLOX	0.864	nsd	>0.05	nsd	>0.05
	4T1-shLOX + loading	1.040	nsd	>0.05	nsd	>0.05
P2X7R$^{-/-}$ BALB/c	Loading	1.105	nsd	>0.05	nsd	>0.05
	4T1	0.849	nsd	>0.05	n/a	>0.05
	4T1 + loading	0.984	nsd	>0.05	nsd	>0.05
	4T1-shLOX	0.892	nsd	>0.05	nsd	>0.05
	4T1-shLOX + loading	0.927	nsd	>0.05	nsd	>0.05

Table shows mean fold change data for each experimental group, calculated from non-loaded controls. 'Sig. cf. control' and 'Sig. cf. 4T1' display statistical significance between each experimental group and the respective variable, as calculated by Kruskall-Wallis test. * = p<0.05, nsd = no significant difference. n=6 for all groups, except 'P2X7R$^{-/-}$ Loading' where n=4.

Table 5.3: Cortical Thickness Fold Change Values – Effect of P2X7R Knockout.

	Strain	Fold Change	Sig.	p
loading	WT	1.138	nsd	0.8286
	P2X7R$^{-/-}$	1.105		
4T1	WT	0.714	**	0.0087
	P2X7R$^{-/-}$	0.849		
4T1 + loading	WT	1.103	*	0.0411
	P2X7R$^{-/-}$	0.984		

Table shows mean fold change data for each experimental group, arranged for comparison between WT and P2X7R$^{-/-}$ mouse strains. Fold change is calculated relative to respective non-loaded controls. 'Sig.' displays statistical significance between WT and P2X7R$^{-/-}$ groups for each experimental group, calculated by Mann-Whitney test. * = p<0.05, ** = p<0.01, nsd -= no significant difference.

5.2.1.4 Effect of Mechanical Loading on Trabecular Bone

Loading effect on trabecular bone was assessed by comparing raw trabecular variables from the right (loaded) limb with the left (non-loaded) limb within the same mouse, using Wilcoxon matched–pairs signed rank test (a non-parametric paired t-test). Analysis of loaded heathy age-matched control mice revealed no statistically significant differences resulting from loading in any of the recorded trabecular variables: bone mineral density (BMD), percentage bone volume (BV/TV), trabecular number (Tb No.), trabecular thickness (Tb Th), or structure model index (SMI). This was the case for both WT and P2X7R$^{-/-}$ mice. Tumour bearing mice, however, displayed loading mediated changes in BV/TV, Tb Th, and SMI. All data herein is summarised in figure 5.3 and statistically significant variables are summarised in table 5.4, below.

Mechanical loading caused a significant increase in BV/TV in WT mice bearing either 4T1 ($p=0.0313$, Fig. 5.3) or 4T1-shLOX tumours ($p=0.0313$, Fig. 5.3). P2X7R$^{-/-}$ mice also displayed a significant increase in BV/TV in the loaded limbs of mice with 4T1-shLOX tumours ($p=0.0313$, Fig. 5.3), but not those with 4T1 tumours ($p=0.0625$, Fig. 5.3).

Trabecular thickness displayed the same pattern seen in BV/TV, with mechanical loading resulting in significant increases in trabecular thickness in WT mice with 4T1 ($p=0.0313$, Fig. 5.3) or 4T1-shLOX ($p=0.0313$, Fig. 5.3) tumours, and in P2X7R$^{-/-}$ mice with 4T1-shLOX tumours ($p=0.0313$, Fig. 5.3) but not 4T1 tumours ($p=0.125$, Fig. 5.3).

Finally, mechanical loading was also found to significantly increase SMI in P2X7R$^{-/-}$ mice with 4T1 tumours ($p=0.0313$, Fig. 5.3). No effect from loading was noted in age-matched or 4T1-shLOX tumour bearing P2X7R$^{-/-}$ mice, nor in any of the experimental groups of WT mice.

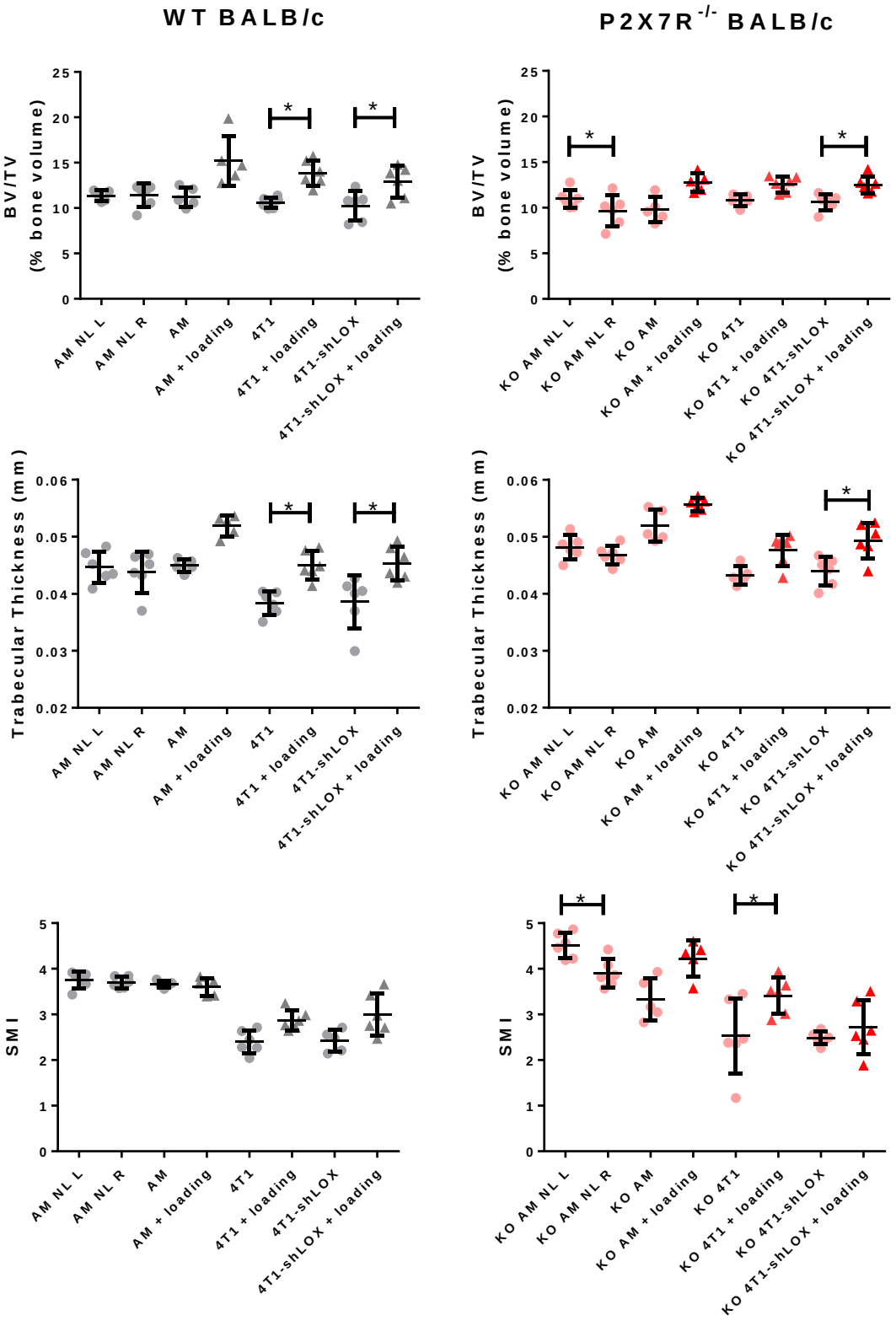

Figure 5.3: Trabecular Analysis – Comparison of Loaded and Non-Loaded Limbs. WT (grey) and P2X7R$^{-/-}$ (KO, red/pink) BALB/c mice received a single injection of 4T1 or 4T1-shLOX cells to the mammary fat pad, or were left as age-matched controls. After an initial period of one week mice had their right (R) limb loaded every 2 days, for a total of 6 periods of loading prior to sacrifice. The left (L) limb was not loaded and used as a contralateral non-loaded control. A further group of age-matched mice were not subjected to loading and used as controls (AM NL). Tibiae were subjected to µCT analysis of the trabecular cavity. Data shows raw values for each variable + SD; n=6 for each groups, except AM where n=5. * = p<0.05, calculated by Mann-Whitney test.

Table 5.4 Trabecular Analysis of Loaded Limbs vs. Contralateral Non-Loaded Controls.

		BMD	*Sig.*	*p*	**BV/TV**	*Sig.*	*p*	**Tb Th**	*Sig.*	*p*	**Tb No.**	*Sig.*	*p*	**SMI**	*Sig.*	*p*
WT BALB/c	NL AM L	1.31	nsd	0.1563	11.360	nsd	0.8125	0.045	nsd	0.1875	2.672	nsd	0.6875	3.755	nsd	0.5625
	NL AM R	1.30			11.420			0.044			2.609			3.700		
	AM L	1.35	nsd	0.0625	11.210	nsd	0.625	0.045	nsd	0.0625	2.497	nsd	0.125	3.656	nsd	0.625
	AM R	1.38			15.210			0.052			2.691			3.604		
	4T1 L	1.32	nsd	0.1875	10.590	*	0.0313	0.038	*	0.0313	2.763	nsd	0.0938	2.398	nsd	0.0625
	4T1 R	1.34			13.840			0.045			3.076			2.865		
	4T1-shLOX L	1.35	nsd	>0.9999	10.250	*	0.0313	0.039	*	0.0313	2.731	nsd	0.4375	2.421	nsd	0.0625
	4T1-shLOX R	1.32			12.890			0.045			2.850			2.994		
P2X7R$^{-/-}$ BALB/c	NL AM L	1.37	nsd	0.6875	10.030	*	0.0313	0.050	nsd	0.3125	1.723	*	0.0313	2.927	*	0.0313
	NL AM R	1.36			8.839			0.049			2.071			2.532		
	AM L	1.40	nsd	0.6250	9.784	nsd	0.0625	0.052	nsd	0.0625	1.898	nsd	0.0625	3.332	nsd	0.0625
	AM R	1.39			12.730			0.056			2.290			4.224		
	4T1 L	1.34	nsd	0.3125	10.800	nsd	0.0625	0.043	nsd	0.125	2.503	nsd	0.1325	2.527	*	0.0313
	4T1 R	1.37			12.540			0.048			2.648			3.408		
	4T1-shLOX L	1.36	nsd	>0.9999	10.600	*	0.0313	0.044	*	0.0313	2.414	nsd	0.2188	2.484	nsd	0.4375
	4T1-shLOX R	1.37			12.510			0.049			2.545			2.714		

Table shows mean values for trabecular variables in each experimental group. NL AM = non-loaded, age-matched control; AM = loaded age-matched control; 4T1 = loaded 4T1 tumour bearing mice; 4T1-shLOX = loaded 4T1-shLOX tumour bearing mice. Mice in loaded groups subjected to mechanical loading on their right (R) leg, with left (L) leg used as a non-loaded internal control. 'Sig'. displays results of statistical analysis comparing right (R) and left (L) limbs, calculated by Wilcoxon test. * = $P<0.05$, nsd = no significant difference. n=6 for all groups, except P2X7R$^{-/-}$ AM L & R, where n=5.

5.2.1.5 Effect of Mechanical Loading and LOX in Trabecular Bone

To investigate the influence of LOX and mechanical loading in WT and P2X7R$^{-/-}$ mice, the fold change in trabecular variables, relative to the non-loaded limbs of loaded age matched mice from each genotype, were calculated and analysed using a Kruskall-Wallis test, with Dunn's multiple comparisons post-test to compare each experimental group to age-matched controls. Fold change data for trabecular analysis is presented below in figure 5.4 and table 5.5.

Analysis of fold change in trabecular variables revealed no significant effect of mechanical loading or tumour presence in fold change of BMD in either WT or P2X7R$^{-/-}$ mice, although there was a trend towards BMD loss in tumour bearing mice, which was lost upon loading in WT, and reduced upon loading in P2X7R$^{-/-}$ mice (Fig. 5.4 A).

BV/TV fold change showed a trend towards increase in response to loading in WT mice, and there was no notable change in response tumour bearing. P2X7R$^{-/-}$ mice were found to have a significant increase in BV/TV fold change in response to loading in both age-matched and 4T1 tumour bearing groups, with a trend towards increase in 4T1-shLOX tumour bearing mice. There was also no notable effect of tumour bearing upon BV/TV in P2X7R$^{-/-}$ mice (Fig. 5.4 B).

There was a notable trend towards increase of Tb Th in response to loading (1.115 fold change), and decrease in Tb Th in response to tumour bearing in WT mice (0.869 fold change), though neither were statistically significant (Fig. 5.4 C). Mechanical loading is seen to counteract the effect of tumour bearing, returning a fold change close to controls in the mechanically loaded limbs of tumour bearing mice (1.005 fold change). P2X7R$^{-/-}$ mice with 4T1 tumours showed a significant reduction in Tb Th fold change (0.0833 fold change, $p<0.05$, Fig. 5.4 C) which was returned to a level not significantly different from control (0.917 fold change, $p>0.05$, Fig. 5.4 C) upon application of mechanical loading. Knockdown of LOX in the 4T1 tumour also altered fold change to a level not significantly different from controls (0.846, $p>0.05$, Fig. 5.4 C), though the mean fold change in 4T1-shLOX tumour bearing P2X7R$^{-/-}$ mice was very close to that in 4T1 tumour bearing P2X7R$^{-/-}$ mice, suggesting this may be an artefact of small sample size.

Trabecular number showed no significant fold change in any treatment group in WT mice (Fig. 5.4 D). While both 4T1 and 4T1-shLOX tumour bearing mice showed a trend towards increasing fold change in Tb No. in P2X7R$^{-/-}$ mice, neither of these increases were statistically significant (Fig, 5.4 D). Loading also showed a slight trend towards increased fold change in trabecular number in P2X7R$^{-/-}$ mice, but again this wasn't significant. The combined effect of mechanical loading and 4T1 tumour bearing, however, significantly increased trabecular number fold change (Fig. 5.4 D). While the same pattern was present in 4T1-shLOX tumour bearing mice, the

combined effect of tumour bearing and loading failed to achieve statistical significance in this group.

Finally, WT mice with either 4T1 or 4T1-shLOX tumours showed a significant reduction in SMI fold change compared to controls (Fig. 5.4 E). Mechanical loading in these mice had no significant effect on age-matched controls, but did increase SMI in both tumour bearing groups to levels not significantly different to controls. There was no statistically significant effect of either tumour bearing or mechanical loading on SMI fold change in $P2X7R^{-/-}$ mice, however there was a trend towards increased SMI in response to loading, and reduced SMI in response to tumour bearing, with the combination of both factors resulting in a fold change close to control (Fig. 5.4 E).

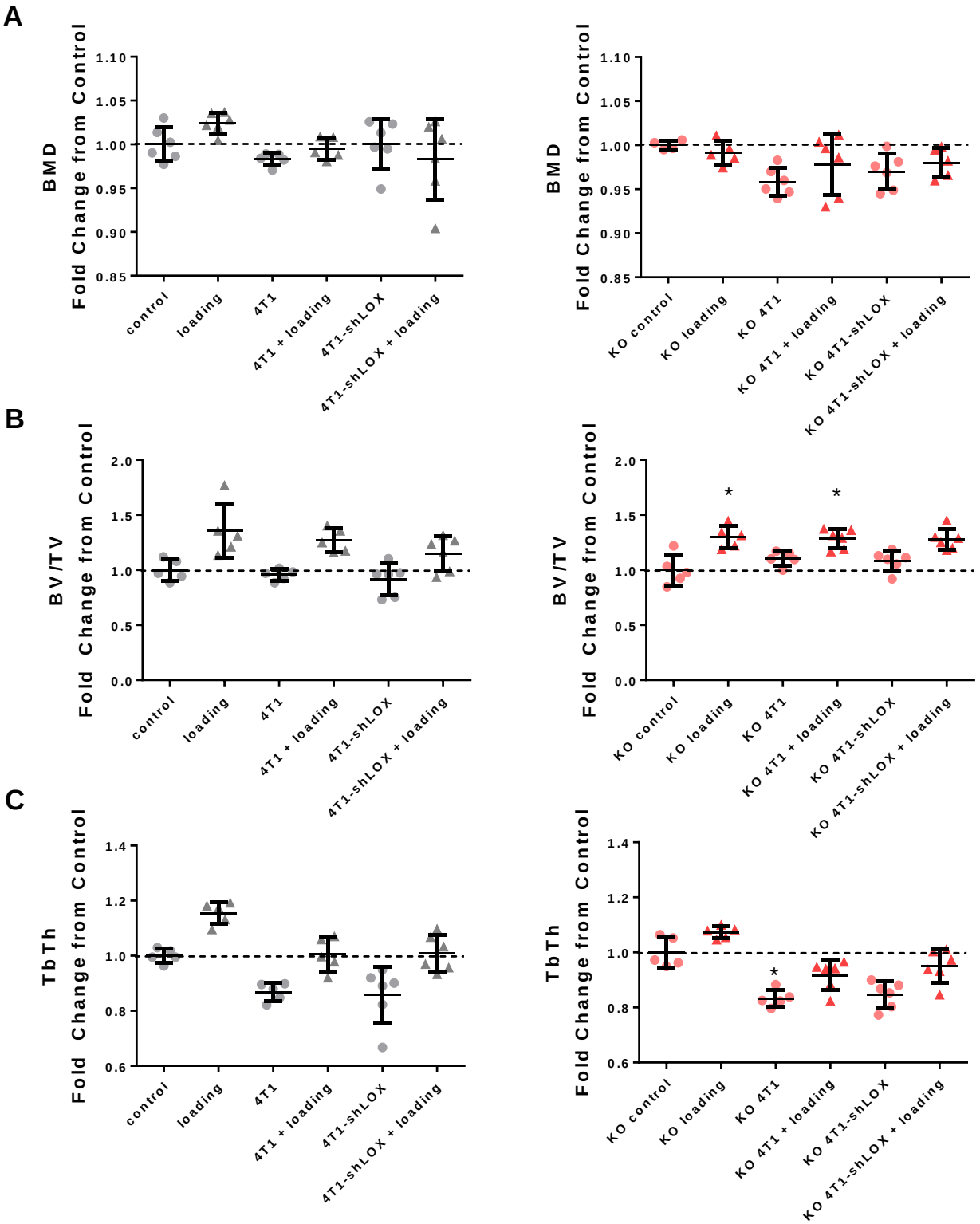

Figure 5.4: continued on next page.

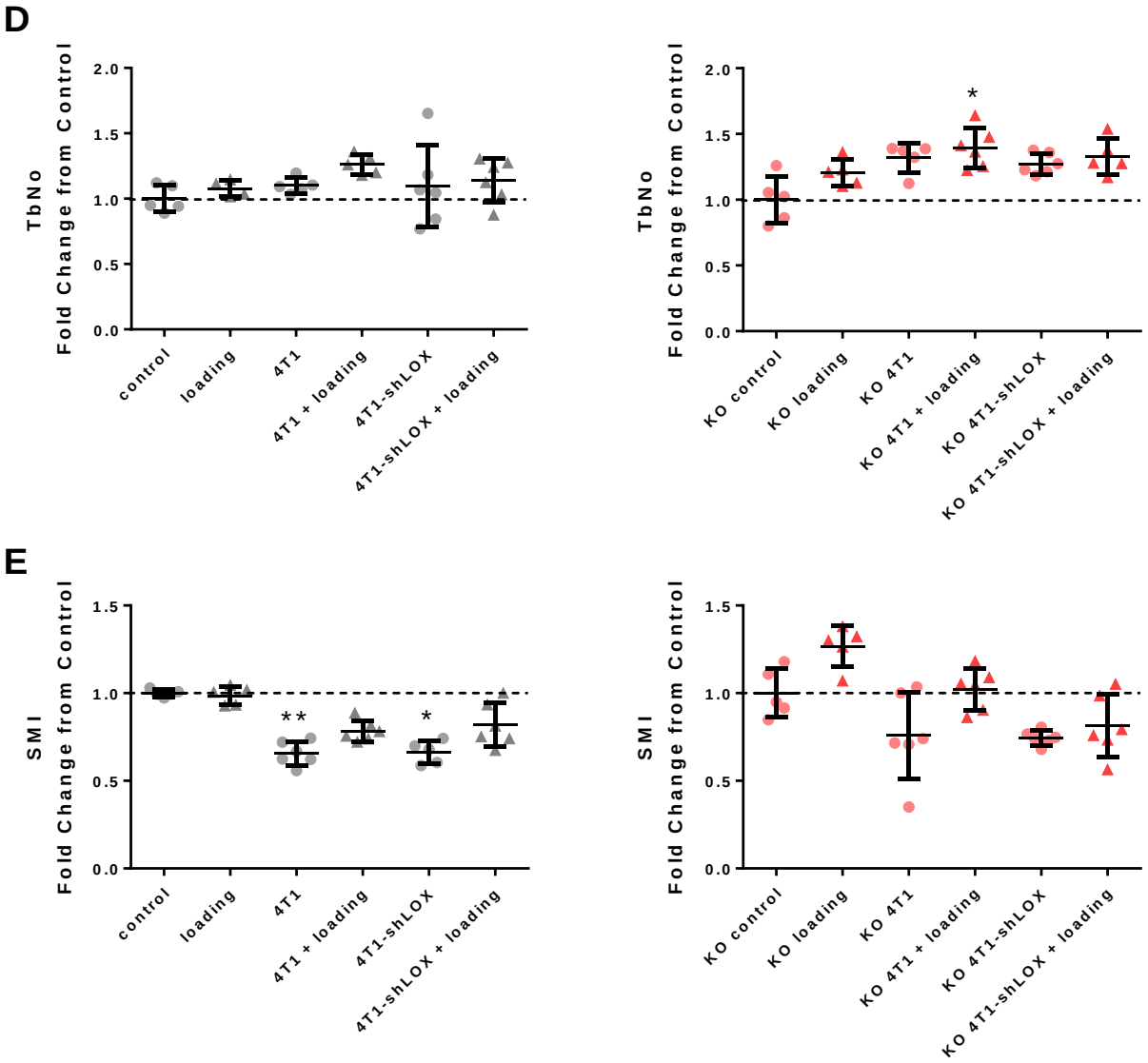

Figure 5.4: Effects of LOX and Mechanical Loading on Trabecular Variable Fold Change. Age-matched and 4T1 tumour bearing WT and P2X7R$^{-/-}$ (KO) mice were non-invasively mechanically loaded on their right limb. Data were normalised to the non-loaded (left) limb of age-matched controls of the appropriate genotype and show fold change relative to non-loaded age-matched controls ± SD. **A** BMD **B** BV/TV **C** Tb Th **D** Tb No. **E** SMI. * denotes statistical significance relative to control, calculated by Kruskal-Wallis test: * = p<0.05, ** = p<0.01. n=6 for all groups, except KO loading, where n=5.

Table 5.5: Fold Change in Trabecular Variables Relative to Non-Loaded Age-Matched Controls.

		BMD		BV/TV		Tb Th		Tb No.		SMI	
WT BALB/c	loading	1.024	nsd	1.356	nsd	1.155	nsd	1.078	nsd	0.986	nsd
	4T1	0.983	nsd	0.956	nsd	0.869	nsd	1.100	nsd	0.656	**
	4T1+loading	0.995	nsd	1.268	nsd	1.005	nsd	1.261	nsd	0.784	nsd
	4T1-shLOX	1.000	nsd	0.914	nsd	0.858	nsd	1.094	nsd	0.662	*
	4T1-shLOX + loading	0.983	nsd	1.150	nsd	1.010	nsd	1.142	nsd	0.819	nsd
P2X7R$^{-/-}$ BALB/c	loading	0.991	nsd	1.302	*	1.073	nsd	1.206	nsd	1.268	nsd
	4T1	0.958	nsd	1.104	nsd	0.833	*	1.319	nsd	0.758	nsd
	4T1+loading	0.978	nsd	1.282	*	0.917	nsd	1.395	*	1.023	nsd
	4T1-shLOX	0.970	nsd	1.083	nsd	0.846	nsd	1.272	nsd	0.746	nsd
	4T1-shLOX + loading	0.980	nsd	1.278	nsd	0.950	nsd	1.328	nsd	0.815	nsd

Table shows mean fold change values for each trabecular variable calculated relative to non-loaded age-matched controls. 'loading' = age-matched loaded mice; 4T1 = 4T1 tumour bearing mice; 4T1-shLOX = 4T1-shLOX tumour bearing mice. * denotes statistical significance relative to non-loaded age-matched controls, as calculated by Kruskall-Wallis test. * = $p<0.05$, ** = $p<0.01$, nsd = no significant difference. n=6 for all groups, except P2X7R$^{-/-}$ loading, where n=5.

5.2.1.6 Effect of P2X7R in Mechanical Loading and Trabecular Bone

Analysis of fold change calculated from the non-loaded limbs of loaded age-matched controls allowed direct statistical comparison of trabecular variables between WT and P2X7R$^{-/-}$ mice, using Wilcoxon matched–pairs signed rank test. Data from these comparisons is summarised below in figure 5.5 and table 5.6, revealing a role for P2X7R in trabecular bone response to loading.

Analysis of fold changes revealed that P2X7R$^{-/-}$ mice displayed a significant reduction in BMD response to loading, showing a 0.991 fold change upon loading, compared to a 1.024 fold change in WT mice (p=0.0087, Fig. 5.5). P2X7R$^{-/-}$ mice also showed a greater susceptibility to tumour induced BMD loss, displaying a 0.958 fold change in BMD when bearing a 4T1 tumour, compared to 0.983 fold change in WT mice (p=0.0173, Fig. 5.5). Application of mechanical loading to tumour bearing mice increased BMD, as discussed above (see 5.2.1.5), and counteracted tumour induced BMD loss in both WT and P2X7R$^{-/-}$ mice, resulting in fold changes which were not significantly different between the two mouse strains.

Knockout of P2X7R had no statistically significant effect on response to loading in BV/TV in either age-matched or tumour bearing mice (Fig. 5.5). P2X7R$^{-/-}$ mice, however, showed a significant increase in BV/TV fold change in tumour bearing mice compared to WT counterparts (4T1 = 0.956, KO 4T1=1.104; p= 1.104, Fig. 5.5).

Tb Th response to loading was significantly impaired by knockout of P2X7R, with the loading induced fold change of 1.155 in WT age-matched controls reduced to 1.073 in P2X7R$^{-/-}$ mice (p=0.0159, Fig. 5.5). There was, however, no statistically significant effect of P2X7R knockout on loading response in tumour bearing mice, nor on Tb Th fold change response to tumour presence.

There were no statistically significant differences in Tb No. fold change in response to loading between WT and P2X7R$^{-/-}$ mice, in either age-matched or tumour bearing groups, though P2X7R$^{-/-}$ mice show a trend towards increased sensitivity to loading in this variable (Fig. 5.5). P2X7R$^{-/-}$ mice were also found to be more responsive to tumour induced change in Tb No., with a fold change of 1.319 in P2X7R$^{-/-}$ mice, compared to 1.100 in WT mice (p=0.0159, Fig. 5.5).

Finally, knockout of P2X7R$^{-/-}$ was found to significantly increase SMI response to loading in age-matched and 4T1 tumour bearing mice. Age-matched P2X7R$^{-/-}$ mice subjected to mechanical loading showed a 1.268 fold change in SMI compared, to 0.986 in WT mice ($p=0.0079$, Fig. 5.5). Loaded P2X7R$^{-/-}$ mice bearing 4T1 tumours showed a 1.023 fold change in SMI compared to 0.784 in their WT counterparts ($p=0.0043$, Fig. 5.5). There was no notable effect of P2X7R knockout on SMI fold change in response to tumour bearing, with both WT and P2X7R$^{-/-}$ mice showing similar fold changes (Fig. 5.5).

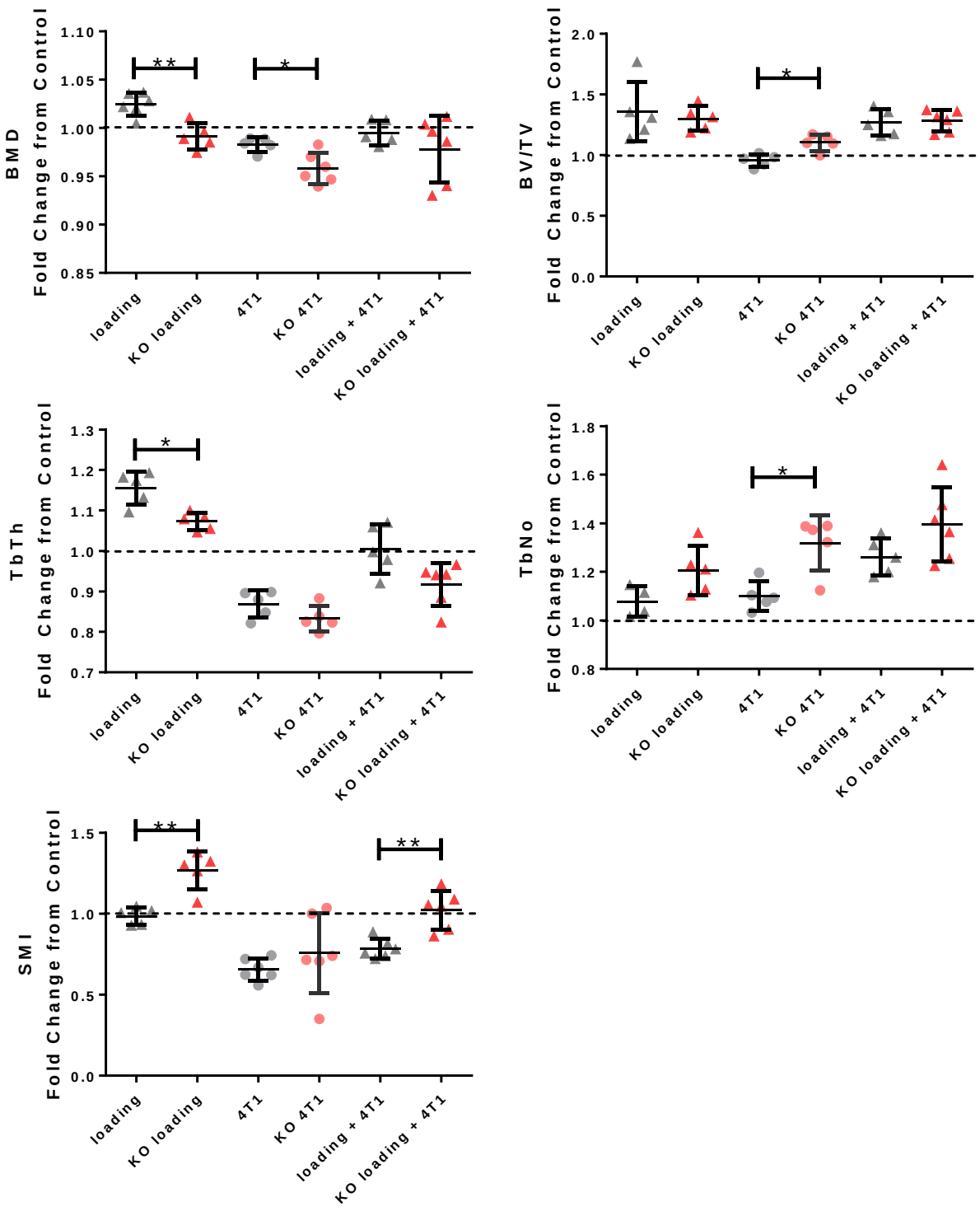

Figure 5.5: Effect of P2X7R on Loading Mediated Trabecular Change. Age-matched and 4T1 tumour bearing WT and P2X7R$^{-/-}$ (KO) mice were non-invasively mechanically loaded on their right limb with the left limb used as a non-loaded contralateral control. Data were normalised to the non-loaded limb of age-matched controls of the appropriate genotype and shows fold change relative to non-loaded age-matched controls ± SD. * = $p<0.05$, ** = $p<0.01$, calculated by Mann-Whitney test. n=6 for all groups, except 'KO loading', where n=5.

Table 5.6: Comparison of fold changes in trabecular variables between WT and P2X7R$^{-/-}$ Mice.

		WT	P2X7R$^{-/-}$	Sig.	P
BMD	*Loading*	1.024	0.991	**	0.0087
	4T1	0.983	0.958	*	0.0173
	Loading + 4T1	0.995	0.978	nsd	0.6494
BV/TV	*Loading*	1.356	1.302	nsd	0.9444
	4T1	0.956	1.104	*	0.0159
	Loading + 4T1	1.268	1.282	nsd	0.7489
Tb Th	*Loading*	1.155	1.073	*	0.0159
	4T1	0.869	0.833	nsd	0.2222
	Loading + 4T1	1.005	0.917	nsd	0.0519
Tb No.	*Loading*	1.078	1.206	nsd	0.1111
	4T1	1.100	1.319	*	0.0159
	Loading + 4T1	1.261	1.395	nsd	0.1255
SMI	*Loading*	0.986	1.268	**	0.0079
	4T1	0.656	0.758	nsd	0.3052
	Loading + 4T1	0.784	1.023	**	0.0043

Table displays mean fold change data for each trabecular variable, calculated relative to non-loaded, age-matched controls. 'Sig.' column shows statistical significance between each experimental group and non-loaded age-matched controls, as calculated by Kruskall-Wallis test. * = $p<0.05$, ** = $p<0.01$, nsd = no significant difference. n=6 for all groups, except P2X7R$^{-/-}$ loading, where n=5.

5.2.2 Effect of Mechanical Loading on Pre-Metastatic Niche Formation

Osteolytic lesion formation has previously been shown to contribute to pre-metastatic niche formation in breast cancer metastasis to bone (Cox et al. 2015). The effect of mechanical loading on pre-metastatic niche formation was, therefore, investigated in this study by monitoring its effect on osteolytic lesion formation. Non-invasive mechanical loading was used to investigate whether the observed osteolytic lesion promoting effect of LOX, possibly acting via P2X7R signalling, could be influenced by bone response to loading pathways.

5.2.2.1 Comparison of Loaded and Non-Loaded Models

To compare the effects of tumour inoculation on lesion formation in mice used in the loading experiment with those from the previous chapter (which were subjected to the same tumour injection routine but were not loaded) lesion data from the non-loaded limbs of the mice used in the loading experiment were pooled and analysed (Fig. 5.6). WT mice replicated the pattern observed in the previous chapter, with 4T1 tumours resulting in significant increases in lesion number and area, and knockdown of LOX in the tumour reducing this increase. P2X7R$^{-/-}$ mice, however, displayed a different pattern. Those with 4T1 tumour showed a trend towards increase in lesion number and area, which was further increased upon knockdown of LOX in the primary tumour, in contrast to the previous chapter where LOX knockdown had no effect on lesion formation in P2X7R$^{-/-}$ mice.

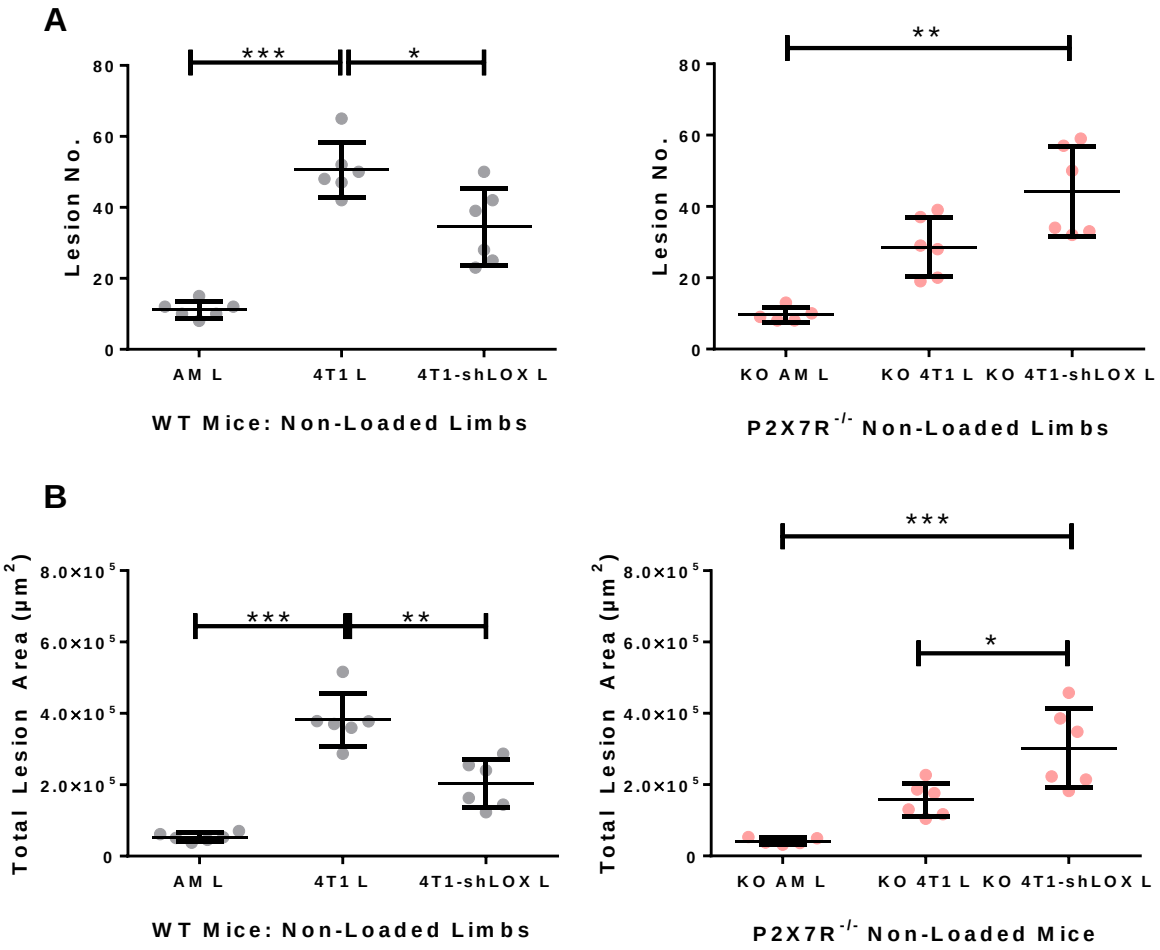

Figure 5.6: Tumour effect on Osteolytic Lesion Formation in Non-Loaded Limbs of Loaded WT and P2X7R$^{-/-}$ Mice. WT and P2X7R$^{-/-}$ (KO) Mice were non-invasively mechanically loaded on their right limb with the left (L) limb used as a non-loaded contralateral control. Mice were divided into loaded age matched controls (AM); 4T1 tumour bearing mice (4T1); or 4T1-shLOX tumour bearing mice (4T1-shLOX). Data shows raw values for non-loaded (L) tibiae only ± SD. **A** Lesion Number Data. **B** Total Lesion Area Data. * p<0.05, ** p<0.01, *** p<0.001, n=6 for all groups. Comparison with age-matched controls (AM L) conducted by Kruskall-Wallis test, comparison of 4T1 and 4T1-shLOX groups conducted by Mann-Whitney test.

5.2.2.2 Effect of Mechanical Loading on Osteolytic Lesion Formation

Analysis of raw data from non-loaded age-matched mice, using Wilcoxon matched–pairs signed rank test, returned no significant differences in lesion number or area between the left and right limbs in either non-loaded WT or P2X7R$^{-/-}$ strain mice (Fig. 5.7), therefore changes noted in lesion number between limbs in loaded mice can be attributed to the effects of mechanical loading.

Mechanical loading of healthy age-matched WT mice resulted in a significant increase in lesion number from a mean of 11.17 to 26.33 ($p=0.0043$, Fig. 5.7 A). In P2X7R$^{-/-}$ mice, while loading did cause an increase in lesion number, from a mean of 9.6 to 17.8, this did not achieve statistical significance ($p=0.0952$, Fig. 5.7 A).

Lesion area reciprocated the pattern noted in lesion number. Mechanical loading caused a significant increase in lesion area in healthy age-matched WT mice, from $0.053x10^6$ µm^2 to $0.149x10^6$ µm^2 ($p=0.0313$, Fig. 5.7 B). Loading in P2X7R$^{-/-}$ mice resulted in an increase in lesion area from $0.042x10^6$ µm^2 to $0.080x10^6$ µm^2 but, as with lesion number, this increase was not statistically significant ($p=0.1250$, Fig. 5.7 B).

Analysis of lesion data in non-loaded limbs of tumour bearing mice showed that primary breast tumours contributed significantly to lesion formation, as observed in Chapter 4, confirming that mechanical loading of the contralateral limb did not affect the ability of tumour cells to metastasise to bone in this model. WT mice with 4T1 tumours showed a significant increase in lesion number and area compared to age-matched controls and genetic knockdown of LOX or knockout of P2X7R prevented this increase in 4T1 tumour bearing mice, replicating the results from the previous chapter (See Figure 5.6). P2X7R$^{-/-}$ mice, however, showed a different pattern to that previously observed, with an increase in lesion formation upon knockdown of LOX in the primary tumour, resulting in 4T1-shLOX tumour bearing mice returning significant increases in both lesion number ($p<0.01$) and area ($p<0.01$) compared to age-matched controls.

Application of mechanical loading to the limbs of tumour bearing mice revealed that while mechanical loading of WT mice generated increases in mean lesion number and area in both 4T1 and 4T1-shLOX tumour bearing mice, these increases were not statistically significant when compared to contralateral non-loaded controls (Fig. 5.7). Mechanical loading showed no effect on lesion formation in tumour bearing P2X7R$^{-/-}$ mice, where comparison of loaded and non-loaded limbs in 4T1 and 4T1-shLOX tumour bearing mice revealed no significant differences between loaded and non-loaded limbs (Fig. 5.7). Unlike in their WT counterparts, however, lesion number and area in the loaded limbs of tumour bearing P2X7R$^{-/-}$ mice closely matched those of the non-loaded limb with no visible trend. Lesion data are summarised below in table 5.7.

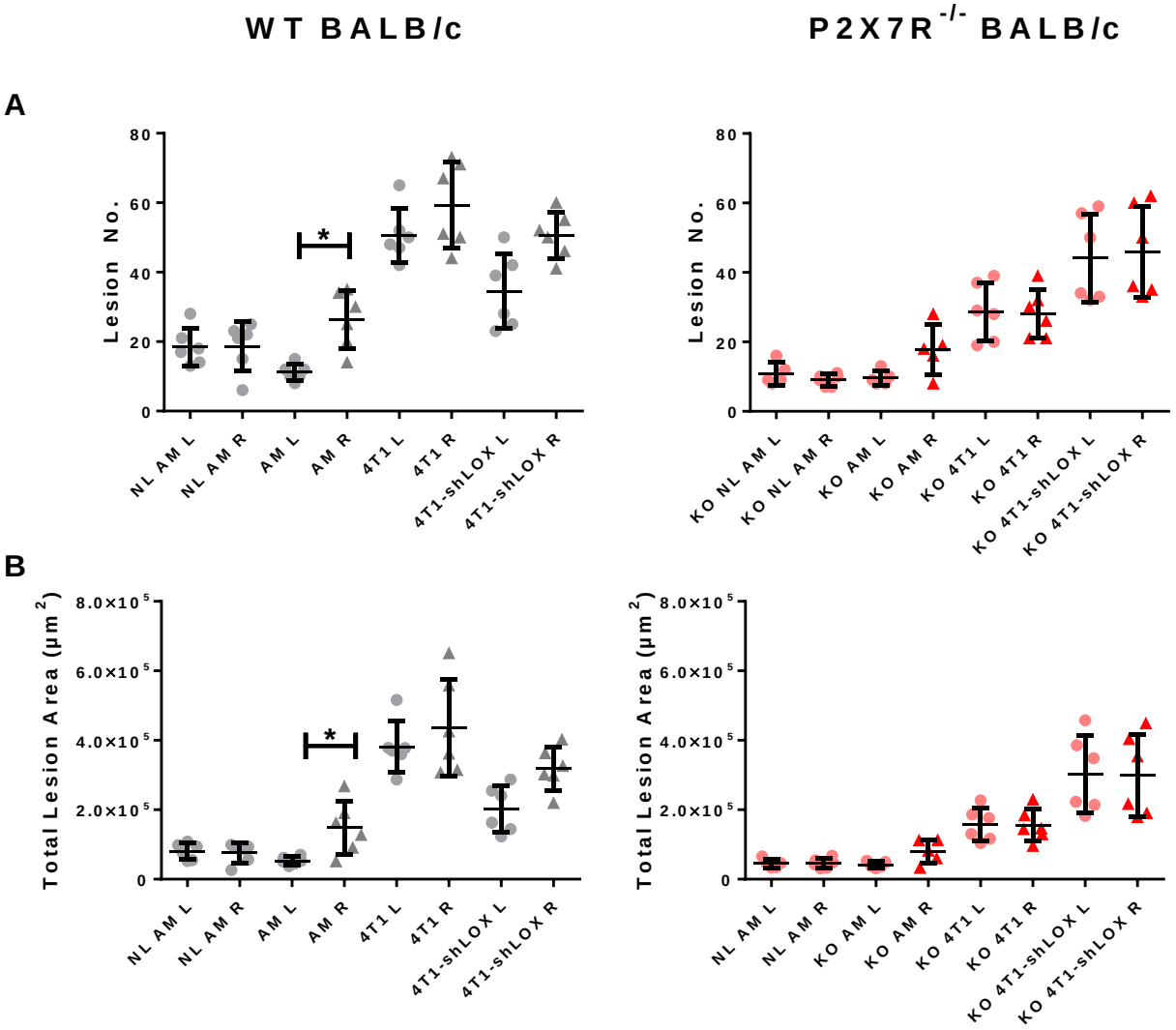

Figure 5.7: Effect of Mechanical Loading on Osteolytic Lesion Formation. WT and P2X7R$^{-/-}$ (KO) Mice were non-invasively mechanically loaded on their right (R) limb with the left (L) limb used as a non-loaded contralateral control. Mice were divided into four experimental groups: non-loaded age-matched controls (NL AM), loaded age matched controls (AM); 4T1 tumour bearing mice (4T1); or 4T1-shLOX tumour bearing mice (4T1-shLOX). **A** Lesion number **B** Total lesion area. Data shows raw values per tibia ± SD. *denotes significance compared to relative contralateral non-loaded control. * denotes statistical significance, calculated by Mann-Whitney test. * = $p < 0.05$, n=6 for all groups, except KO AM L and KO AM R, where n=5.

Table 5.7: Summary of lesion quantification in loaded and unloaded WT and P2X7R$^{-/-}$ mice.

	Group	Lesion No.	*Sig.*	*p*	Lesion Area	*Sig.*	*p*
WT BALB/c	NL AM L	18.50	nsd	>0.999	8.05E+04	nsd	0.688
	NL AM R	18.67			7.57E+04		
	AM L	11.17	*	0.031	5.32E+04	*	0.031
	AM R	26.33			1.49E+05		
	4T1 L	50.67	nsd	0.188	3.82E+05	nsd	0.438
	4T1 R	59.33			4.36E+05		
	4T1-shLOX L	34.50	nsd	0.156	2.02E+05	nsd	0.094
	4T1-shLOX R	50.67			3.19E+05		
P2X7R$^{-/-}$ BALB/c	KO NL AM L	10.80	nsd	0.500	4.50E+04	nsd	0.500
	KO NL AM R	9.00			4.61E+04		
	KO AM L	9.60	nsd	0.125	4.15E+04	nsd	0.125
	KO AM R	17.80			8.02E+04		
	KO 4T1 L	28.67	nsd	>0.999	1.57E+05	nsd	0.688
	KO 4T1 R	28.17			1.55E+05		
	KO 4T1-shLOX L	44.17	nsd	0.688	3.02E+05	nsd	0.844
	KO 4T1-shLOX R	46.00			2.99E+05		

Table shows mean lesion number and area data for each experimental group. NL AM = non-loaded, age-matched control; AM = loaded age-matched control; 4T1 = loaded 4T1 tumour bearing mice; 4T1-shLOX = loaded 4T1-shLOX tumour bearing mice. Mice in loaded groups subjected to mechanical loading on their right (R) leg, with left (L) leg used as a non-loaded internal control. 'Sig.' column presents statistical significance of loaded vs. non-loaded limbs within each experimental group, as calculated by Wilcoxon test. * = $p<0.05$, nsd = no significant difference. n=6 for each group, except for 'KO AM' where n=5.

5.2.2.3 Effect of Mechanical Loading and LOX on Lesion Formation

Calculation of fold change in lesion number and area, relative to non-loaded age-matched controls, allowed direct comparison of loading and tumour effect on lesion formation between WT and P2X7R$^{-/-}$ mice. Statistical significance was calculated using a Kruskall-Wallis test, with Dunn's multiple comparisons post-test to compare experimental groups against each other. Fold change data is summarised below in figure 5.8 and table 5.8.

Analysis of fold changes in WT mice revealed that mechanical loading in age-matched mice resulted in a 2.358 fold change in lesion number compared to non-loaded controls, though this increase was not statistically significant (Fig. 5.8 A). Non-loaded limbs of WT mice with 4T1 tumours showed a statistically significant 4.537 fold change in lesion number compared to age matched controls ($p<0.01$, Fig. 5.8 A). Mechanical loading of WT mice with 4T1 tumours further increased lesion number fold change to 5.313, which was significantly greater than non-loaded age matched controls ($p<0.001$, Fig. 5.8 A) but not to non-loaded 4T1 tumour bearing WT mice.

Knockdown of LOX in the 4T1 tumour reduced fold change in lesion number to 3.09, which was not statistically different from 4T1 tumour bearing WT mice, but also not significantly different from age-matched controls (Fig. 5.8 A). Addition of mechanical loading to 4T1-shLOX tumour bearing WT mice increased lesion number fold change to 4.537, which remained significantly greater than age-matched controls (1.00, $p<0.01$, Fig. 5.8 A), but was not significantly different to non-loaded 4T1-shLOX tumour bearing WT mice.

Mechanical loading of age-matched P2X7R$^{-/-}$ mice revealed a 2.358 fold change in lesion number compared to non-loaded controls, though this difference was not statistically significant. P2X7R$^{-/-}$ mice bearing 4T1 tumours displayed a 2.986 fold change in lesion number compared to age-matched controls, which was also not statistically significant (Fig. 5.8 A). Applying mechanical loading to 4T1 tumour bearing P2X7R$^{-/-}$ mice showed no discernible effect, generating a fold change of 2.934 which was not statistically significant from either age-matched or 4T1 tumour bearing non-loaded controls (Fig. 5.8 A).

Knockdown of LOX in the 4T1 tumour returned significant increases in lesion number in P2X7R$^{-/-}$ mice, resulting in a lesion number fold change of 4.601, which was highly significant compared to non-loaded age-matched controls ($p<0.01$, Fig. 5.8 A). Application of mechanical loading to 4T1-shLOX tumour bearing P2X7R$^{-/-}$ mice slightly increased the observed lesion number fold change to 4.792, which remained highly significantly different to non-loaded age-matched controls ($p<0.01$, Fig. 5.8 A) but did not differ from non-loaded 4T1-shLOX tumour bearing controls.

Analysis of fold change in summed lesion area largely repeated the pattern observed in fold change of lesion number. Mechanical loading of age-matched WT mice resulted in a 2.794 fold increase in lesion area, which was not statistically significant compared to controls (Fig. 5.8 B).

WT Mice with 4T1 tumours showed a 7.174 fold change in lesion area which was significantly greater than controls (1.00, $p<0.001$, Fig. 5.8 B) and mechanical loading further increased this to 8.198, which remained significantly greater than non-loaded age-matched controls (1.00, $p<0.001$, Fig. 5.8 B), as well as loaded age-matched controls (2.794, $p<0.05$, Fig. 5.8 B) but did not significantly differ from non-loaded 4T1 tumour bearing mice.

WT mice with 4T1-shLOX tumours displayed a 3.799 fold change in lesion area, which was not significantly different to 4T1 tumour bearing mice, but also not significantly different from age-matched controls (Fig. 5.8 B). Application of mechanical loading increased lesion area fold change in 4T1-shLOX WT mice to 5.988, which was significantly greater than non-loaded age-matched controls ($p<0.05$, Fig. 5.8 B) but not to non-loaded 4T1-shLOX tumour bearing WT mice.

Analysis of lesion area fold change in $P2X7R^{-/-}$ mice showed no significant effect of 4T1 tumour bearing, mechanical loading, or the combination of both (Fig. 5.8 B). $P2X7R^{-/-}$ mice with 4T1-shLOX tumours, however, showed a statistically significant 7.264 fold increase in lesion area compared to non-loaded age-matched controls ($p<0.01$, Fig. 5.8 B). Mechanical loading of 4T1-shLOX tumour bearing $P2X7R^{-/-}$ mice resulted in a 7.191 fold increase in lesion area, which did not differ significantly from the non-loaded 4T1-shLOX tumour bearing controls, and remained significantly greater than non-loaded age-matched controls ($p<0.01$, Fig. 5.8 B).

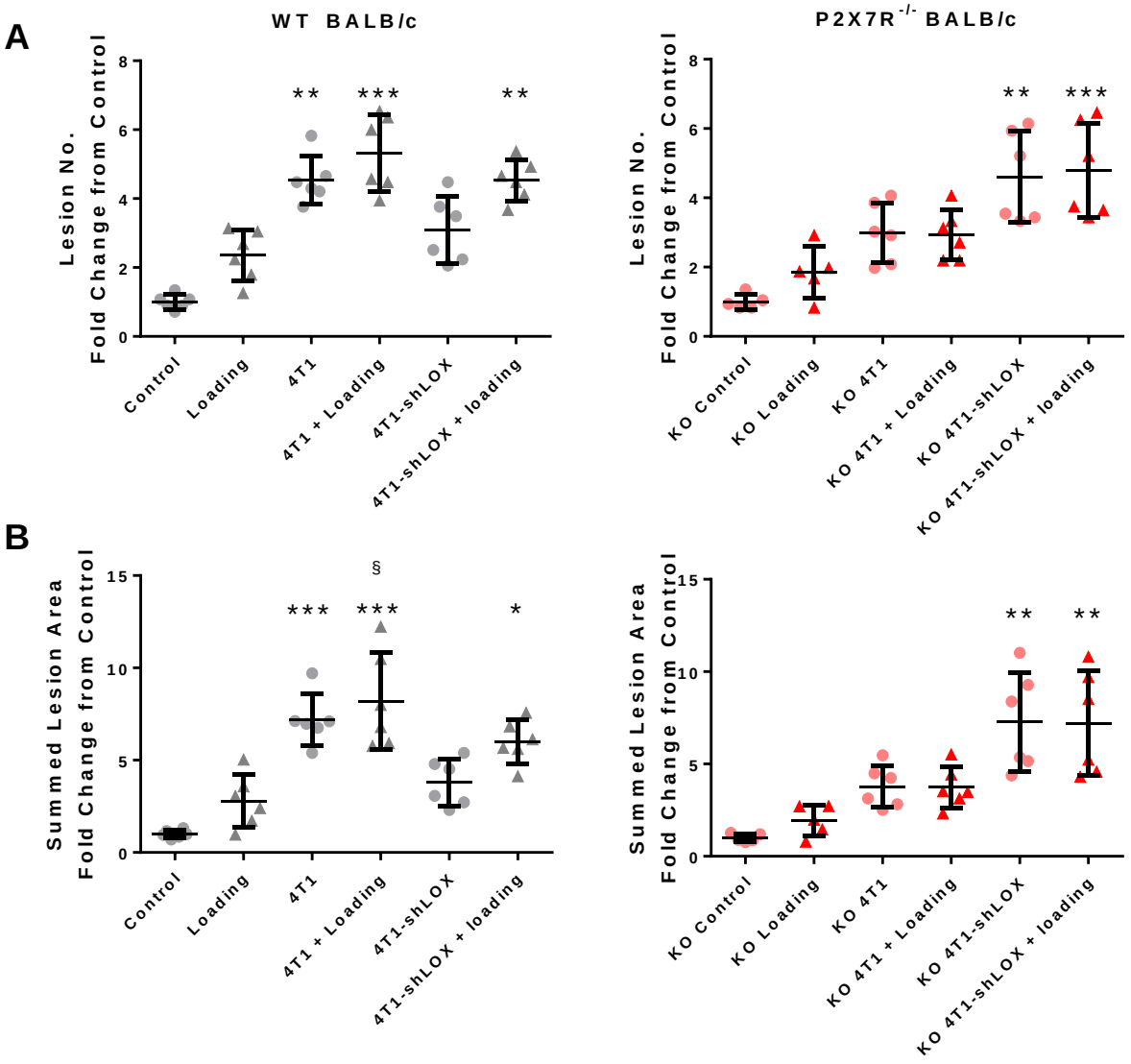

Figure 5.8: Effects of LOX and Mechanical Loading on Lesion Number and Area Fold Change. Age-matched and 4T1 tumour bearing WT and P2X7R$^{-/-}$ (KO) mice were non-invasively mechanically loaded on their right limb. Data were normalised to the non-loaded (left) limb of age-matched controls of the appropriate genotype (i.e. control / KO control) and show fold change relative to non-loaded age-matched controls ± SD. **A** Fold change in lesion number. **B** Fold change in total lesion area. * denotes statistical significance relative to control, calculated by Kruskal-Wallis test: ** = $p<0.01$, *** = $p<0.001$. § denotes statistical significance relative to loading, calculated by Mann-Whitney test: § = $p<0.05$. n=6 for all groups, except KO loading, where n=5.

Table 5.8: Fold Changes in Lesion Number and Area in Response to Tumour Presence and Mechanical Loading.

		WT	Sig. cf. Control	p	P2X7R$^{-/-}$	Sig. cf. Control	p
Lesion Number Fold Change	Loading	**2.358**	*nsd*	*>0.05*	**1.854**	*nsd*	*>0.05*
	4T1	**4.537**	***	*<0.01*	**2.986**	*nsd*	*>0.05*
	4T1 + loading	**5.313**	***	*<0.001*	**2.934**	*nsd*	*>0.05*
	4T1-shLOX	**3.090**	*nsd*	*>0.05*	**4.601**	***	*<0.01*
	4T1-shLOX + loading	**4.537**	***	*<0.01*	**4.792**	***	*<.001*
Summed Lesion Area Fold Change	Loading	**2.794**	*nsd*	*>0.05*	**1.932**	*nsd*	*>0.05*
	4T1	**7.174**	***	*<0.001*	**3.78**	*nsd*	*>0.05*
	4T1 + loading	**8.198**	***	*<0.001*	**3.734**	*nsd*	*>0.05*
	4T1-shLOX	**3.799**	*nsd*	*>0.05*	**7.264**	***	*<0.01*
	4T1-shLOX + loading	**5.988**	*	*<0.05*	**7.191**	***	*<0.01*

Table shows mean fold change in lesion number and area for each experimental group, calculated relative to non-loaded age-matched controls. 'Loading'= mechanical loading, 4T1 = 4T1 tumour bearing mice, 4T1-shLOX = 4T1-shLOX tumour bearing mice. 'Sig. cf. Control' displays significant differences between each experimental group and non-loaded, age-matched controls as calculated by Kruskall-Wallis test. * = $p<0.05$, ** = $p<0.01$, *** = $p<0.001$, nsd = no significant difference. n=6 for all groups, except P2X7R$^{-/-}$ loading, where n=5.

5.2.2.4 Effect of P2X7R on Loading Mediated Lesion Formation

Direct comparison of fold changes between WT and P2X7R$^{-/-}$ mice using Wilcoxon matched–pairs signed rank test allowed direct statistical assessment of the effect of P2X7R knockout in osteolytic lesion formation in response to both tumour bearing and mechanical loading.

Comparison of fold changes in lesion number between WT and P2X7R$^{-/-}$ age-matched mice showed no significant difference in response to loading (See Fig. 5.9 and table 5.9). Analysis of 4T1 tumour bearing mice, however, revealed that knockout of P2X7R inhibited tumour mediated lesion formation, repeating observations from the previous chapter (Fig. 5.9). WT mice with 4T1 tumours showed a 4.537 fold increase in lesion number compared to a 2.986 fold increase in P2X7R$^{-/-}$ mice (p=0.009, Fig. 5.9 A). This was also the case for mechanically loaded mice with 4T1 tumours, where a 5.313 fold increase in WT mice was reduced to 2.934 in P2X7R$^{-/-}$ mice (p=0.004, Fig. 5.9 B).

Analysis of the fold change in summed lesion area data repeated the pattern observed in lesion number. Knockout of P2X7R had no significant effect on lesion area fold change in age-matched mice subjected to mechanical loading (p=0.320, Fig. 5.9 B), but did significantly reduce fold change in 4T1 tumour bearing mice from 7.174 in WT to 3.780 in P2X7R$^{-/-}$ (p=0.004, Fig. 5.9 B), and in mechanically loaded 4T1 tumour bearing mice from 8.198 in WT to 3.734 in P2X7R$^{-/-}$ (p=0.002, Fig. 5.9 B).

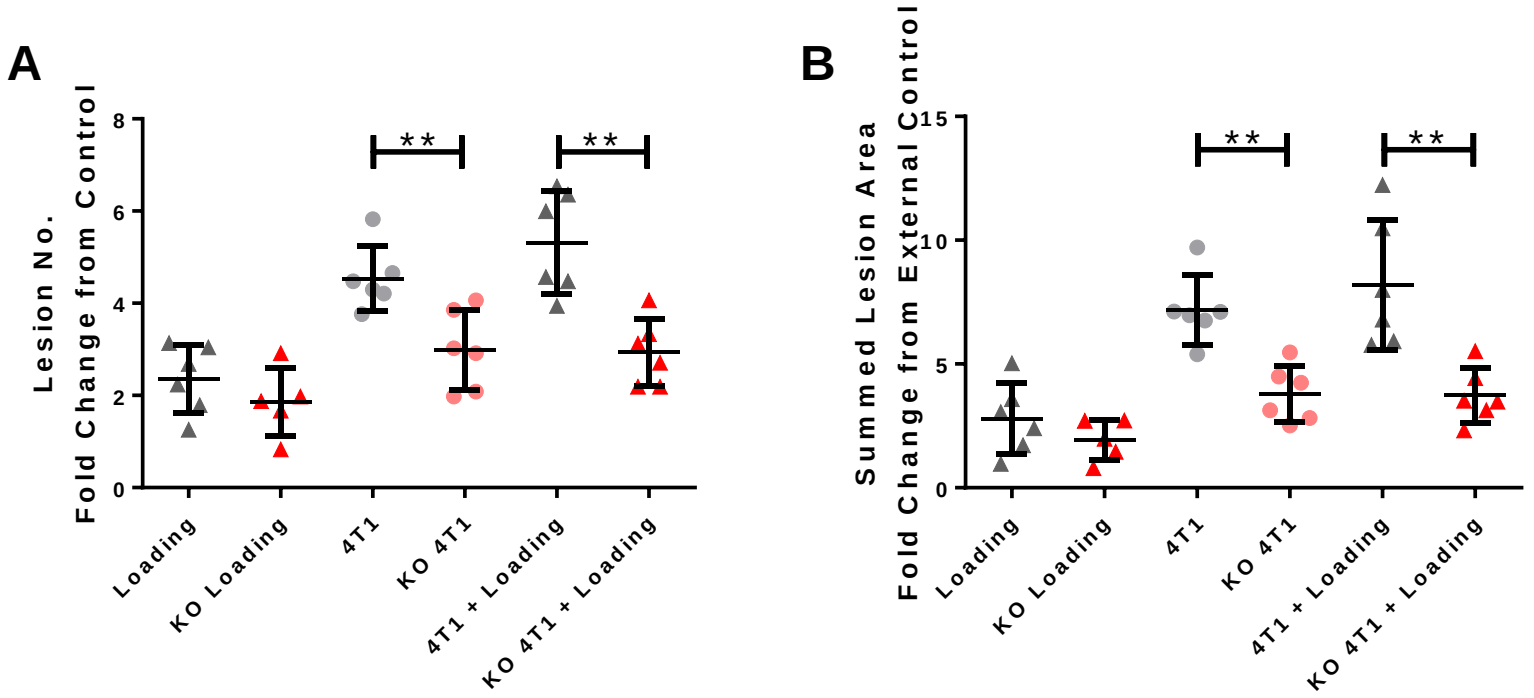

Figure 5.9: Effect of P2X7R on Loading Mediated Lesion Formation. Age-matched and 4T1 tumour bearing WT and P2X7R$^{-/-}$ (KO) mice were non-invasively mechanically loaded on their right limb with the left limb used as a non-loaded contralateral control. Data were normalised to the non-loaded limb of age-matched controls of the appropriate genotype and shows fold change relative to non-loaded age-matched controls ± SD. **A** Fold change in lesion number. **B** Fold change in total lesion area. * denotes statistical significance calculated by Mann-Whitney test. ** = p<0.0. n=6 for all groups, except KO loading, where n=5.

Table 5.9: Comparison of fold changes in lesion number and area between WT and P2X7R$^{-/-}$ Mice

		WT	P2X7R$^{-/-}$	Sig.	p
Lesion No. FC	*Loading*	2.358	1.854	nsd	0.320
	4T1	4.537	2.986	**	0.009
	4T1 + loading	5.313	2.934	**	0.004
Summed Lesion Area FC	*Loading*	2.794	1.932	nsd	0.320
	4T1	7.174	3.780	**	0.004
	4T1 + loading	8.198	3.734	**	0.002

Table shows mean fold change in lesion number and area for each experimental group, calculated relative to non-loaded, age-matched controls. 'Loading' = mechanical loading, 4T1 = 4T1 tumour bearing mice. 'Sig.' displays statistical significance of WT vs. P2X7R$^{-/-}$ genotypes, calculated by Mann-Whitney test. ** = $p<0.01$. n=6 for all groups, except P2X7R$^{-/-}$ loading, where n=5.

5.3 Discussion

Tumour induced bone loss is the most common cause of morbidity in metastatic disease, with the potential to substantially reduce quality of life. Current treatment with bisphosphonates is not effective in all patients, and does not repair bone loss caused by tumour activity prior to the start of treatment. In addition, as noted in the previous chapter, LOX and P2X7R interact to drive osteolytic lesion formation in bone, forming a pre-metastatic niche which can potentiate the vicious cycle of bone disease. Mechanical loading has previously been shown to have an osteogenic effect on bone, and is implicated in accumulation of LOX and activation of P2X7R, providing a potential stimulus for LOX mediated lesion formation. Thus the effects of mechanical loading on metastasis to bone warrant further investigation from the dual perspective of providing an osteogenic treatment to combat tumour induced bone loss, and understanding how mechanical loading may be contributing to pre-metastatic niche formation by interacting with LOX and P2X7R mediated osteolytic lesion formation.

5.3.1 Effect of Mechanical Loading on Bone in Tumour Bearing Mice

5.3.1.1 Effect of Mechanical Loading on Cortical Bone Thickness

The mechanical loading regime implemented in this study was found to generate significant change in both cortical and trabecular bone. Loading of the tibia drove cortical bone growth, resulting in significant increases in cortical thickness in both healthy and tumour bearing mice (Figs. 5.1 and 5.2). This supports previous studies which have reported osteogenic responses in the cortex of long bones, typically either the tibia (De Souza et al. 2005b; Holguin et al. 2013; Wang et al. 2013) or ulna (Robling & Turner 2002; Li et al. 2005).

The osteogenic effect of loading was also found to sufficiently counteract the reduction in cortical thickness caused by tumour presence in both 4T1 and 4T1-shLOX tumour bearing mouse groups, with mechanical loading entirely reversing tumour induced bone loss, resulting in a net gain in cortical thickness in the loaded limbs of tumour bearing mice (Fig. 5.2).

5.3.1.2 Effect of LOX and Mechanical Loading on Cortical Thickness

LOX expression in the primary tumour contributed to cortical bone loss, repeating observations seen in non-loaded mice in the previous chapter (chapter 4). The greatest change in cortical thickness in response to loading was seen in 4T1 tumour bearing mice (in both WT and $P2X7R^{-/-}$ genotypes, Fig. 5.2), however this is likely to be the result of increased bone loss in the non-loaded limb, against which the loaded limb is compared, rather than an amplification of bone response to loading being driven by LOX. There is no notable difference in cortical thickness between the loaded limbs of 4T1 tumour bearing mice and the loaded limbs of age-matched controls, supporting this observation (Fig. 5.2).

5.3.1.3 Effect of P2X7R and Mechanical Loading on Cortical Thickness

P2X7R contributed to both tumour mediated bone loss, and loading mediated bone growth. Knockout of P2X7R reduced LOX mediated bone loss (Fig. 5.2C), repeating observations from the previous chapter (chapter 4), but also reduced bone response to loading in tumour bearing mice. This supports previous studies which have shown reductions of up to 61% in bone response to loading in female mice upon knockout of P2X7R (Li et al. 2005). Interestingly, despite a reduced loading response, the combined effect of mechanical loading and P2X7R knockout in 4T1 tumour bearing mice was a mean cortical thickness almost identical to that of healthy controls (fold change of 0.984). Thus mechanical loading is shown to successfully combat tumour mediated loss of cortical bone, even in the absence of P2X7R.

5.3.1.4 Effect of Mechanical Loading on Trabecular Bone

Mechanical loading was also found to have an osteogenic effect in trabecular bone, specifically increasing raw values for both BV/TV and Tb Th, but not affecting BMD or Tb No. (Fig. 5.3), suggesting that mechanical loading resulted in a thickening of existing trabecular architecture, rather than remodelling new structures. While statistically significant differences in loading response were only noted in tumour bearing mice, there was a trend to increase in both BV/TV and Tb Th in age-matched controls in response to loading (Fig. 5.3). It is likely that, while slight, the reduction in BV/TV and Tb Th in the non-loaded limb, as a result of tumour presence, increased disparity between the loaded and non-loaded limbs enough to generate a statistical significance between them.

Given that the principle role of trabecular bone is to provide structural support to resist the forces to which the whole bone is subjected, and trabecular microarchitecture remodels to a configuration best able to resist these stresses (van Oers et al. 2008), then this osteogenic response to loading is expected. Mechanical loading of the limb in this study induced a compressive force in the tibia, similar to that engendered by weight bearing during normal locomotion, but with a greater force, generating greater strain. As a result, the existing architecture was likely already configured to best resist the direction of this force, and the thickening of trabecular architecture enabled endurance of higher strains in the same plane. Similar osteogenic responses in trabecular bone have previously been reported at lower induced strains of 1700-2400με in 8 week old C57BL/6 mice (Berman et al. 2015), and at 5000με in 16 week old C57BL/6 mice (Wang et al. 2012). While there was no thickening of the trabeculae in mice subjected to 1700-2400με by Berman et al. (2015), the density of the trabecular bone was seen to increase, effecting a similar functional response in trabecular bone, allowing the bearing of greater loads. Loading at 5000με by Wang et al. (2013), using the same loading protocol and

apparatus as the present study, induced increases in BMD, BV/TV, Tb Th, and Tb No., exceeding the effects seen in this study.

It is likely that differing genetic background, mechanical loading regimes, and skeletal maturity of the mice contributed to the differences in trabecular responses observed between these studies. Indeed both genetic background (Robling & Turner 2002) and loading waveform (Holguin et al. 2013) have previously been shown to influence bone response to loading. There is also evidence to suggest a significant effect of skeletal maturity in bone response to loading. BALB/c mice are reported to have two stages of skeletal development: a skeletal growth phase occurring between 2-7 months, characterised by a rapid increase in cortical bone cross-sectional area; and an 'ageing' phase from 7-20 months, characterised by plateauing and maintenance of cortical bone area (Willingham et al. 2010). By contrast C57BL/6 mice display 3 stages of skeletal maturity: a rapid growth period between months 1-3; attainment of peak bone mass between months 6-9; and age-related decline from 12 months onwards (Ke 2005). The BALB/c mice used in this study were 3 months old at sacrifice, placing them in the first half of the skeletal growth period according to the BALB/c maturity timeline. The C57BL/6 mice used by Wang et al. (2013) were 4 months old at time of sacrifice, placing them in between the rapid growth and plateauing phases for C57BL/6 mice, suggesting a slowing down of bone growth and balancing of bone resorption and formation. Thus it is possible that mechanical loading was unable to induce significant change in the trabecular bone of age-matched BALB/c mice used in this study because the process of bone remodelling was still at a developmental stage where it was rapidly laying down new bone, and mechanical loading was unable to increase the rate of this process further. The C57BL/6 mice used by Wang et al. (2013), however, were more mature, and the rate of laying down new bone could have decreased enough to allow effects of mechanical loading to manifest significant change in trabecular bone. This explanation is supported by research in C57BL/6 mice which has shown that trabecular bone is less responsive to mechanical loading in young mice (10 weeks) than it is in older mice (26 weeks), indicating an age-related effect upon potential trabecular bone growth (Willie et al. 2013).

The fact that mice in all three studies responded to loading by reinforcing trabecular bone is, however, encouraging and suggests that even though the specific way in which trabecular bone responds to loading in different genetic backgrounds, loading regimes, and skeletal maturities may differ, the end result is a reinforcement of existing microarchitecture to compensate for the increased loading experienced.

5.3.1.5 Effect of LOX and Mechanical Loading on Trabecular Bone

Analysis of fold change in trabecular variables calculated relative to the non-loaded limb of loaded mice revealed a subtle pattern of interaction in tumour effects and mechanical loading upon trabecular bone. The effect of 4T1 tumours was generally osteolytic, showing a statistically significant reduction in SMI (Fig. 5.4 E), representing a shift towards a more rod-like morphology, and trends towards reduction in BMD and Tb Th in tumour bearing WT mice (Fig. 5.4 A and C, respectively). Of these variables, only BMD displayed a response to LOX knockdown, which returned BMD back to levels comparable to healthy controls (Fig. 5.4 A). Resultantly LOX does not appear to contribute substantially to tumour mediated change in trabecular bone, but may contribute to a loss of trabecular BMD. This partly reciprocates results from the previous chapter (Chapter 4) in non-loaded mice, where tumour secreted LOX was found to contribute to significant reductions in BMD and Tb Th.

As in age-matched controls, mechanical loading was generally osteogenic in tumour bearing mice, with trends towards increase in BMD, BV/TV, and Tb Th (Fig.5.4). Interestingly BV/TV displayed no response to tumour bearing, but was increased by mechanical loading nonetheless (Fig. 5.4 B). The magnitude of effect of mechanical loading in tumour bearing mice reverted the trends for decrease in BMD and Tb Th, returning both to levels comparable with healthy age-matched controls (Fig. 5.4). Thus mechanical loading is shown to be capable of maintaining normal levels of BMD and Tb Th in metastatic bone disease.

5.3.1.6 Effect of P2X7R and Mechanical Loading on Trabecular Bone

Consideration of both raw variables and fold change data revealed that P2X7R$^{-/-}$ mice responded differently to tumour bearing and mechanical loading than their WT counterparts. In general, P2X7R$^{-/-}$ mice appeared to be marginally more susceptible to tumour induced trabecular bone loss and less responsive to mechanical loading. Despite the smaller magnitude of changes seen in raw data for P2X7R$^{-/-}$ mice when compared to WT mice (Fig. 5.4), they generated statistically significant effects in fold change data, which show significant increases in BV/TV (Fig. 5.4 B) and Tb No. (Fig. 5.4 D) fold change in response to loading, and significant reductions in Tb Th fold change in response to tumour presence (Fig. 5.4 C). None of these fold change variables display significant differences in WT mice. It should, however, be noted that the overall pattern within each variable is largely similar between WT and P2X7R$^{-/-}$ mouse strains (i.e. tumour induces bone loss and loading induces bone growth) despite the differences observed in variables achieving statistical significance. It is, therefore, possible that the perceived increase of loading and tumour effect upon fold changes in P2X7R$^{-/-}$ mice is an artefact of small sample size.

Direct assessment of the effect of P2X7R knockout, by comparing fold changes in $P2X7R^{-/-}$ limbs with those in their WT counterparts revealed significant effects of P2X7R knockout in at least one group for each trabecular variable (Fig. 5.5). Knockout of P2X7R reduced loading induced response in BMD and Tb Th, suggesting P2X7R is required for normal response to loading, supporting previous research (Li et al. 2005). Knockout of P2X7R also induced a significant increase in SMI fold change in response to loading, indicating more plate-like trabeculae, in both tumour bearing mice and controls, which was not seen in WT mice (Fig. 5.5). This suggests that P2X7R may contribute to maintenance of trabecular morphology in loaded WT mice.

As well as influencing bone response to loading, P2X7R also influenced trabecular bone response to primary tumour. Knockout of P2X7R increased the severity of tumour induced BMD loss, while increasing Tb No. (Fig. 5.5). Both of these changes are arguably representative of bone loss, as resorption of existing trabeculae can split one trabeculum into two or more parts, if osteoclasts resorb completely through the bony strut. P2X7R is thus shown to protect against tumour induced loss of trabecular bone. Conversely, P2X7R knockout appears to increase BV/TV in tumour bearing mice (Fig. 5.5), though there is no marked reduction in WT tumour bearing mice and so it is doubtful that P2X7R knockout would have any real effect on bone in the context of structural compromise from metastatic bone loss. Taken together P2X7R is shown to play roles in both trabecular bone response to loading and, to a lesser extent, resistance to tumour induced trabecular bone loss.

5.3.1.7 Summary of the Effect of Mechanical Loading on Bone in Tumour Bearing Mice

Mechanical loading exhibits osteogenic effects in both cortical and trabecular bone, supporting previous research which shows osteogenic effects from loading of long bones (De Souza et al. 2005a; Robling & Turner 2002; Holguin et al. 2013; Wang et al. 2012; Li et al. 2005). More importantly, the extent of the osteogenic effect of loading in tumour bearing mice was great enough to counteract tumour induced bone loss in both cortical and trabecular bone, in some cases completely reversing bone loss and resulting in a net gain. This highlights the potential for mechanical loading as a therapy to combat cancer-induced bone loss, and its associated morbidities.

5.3.2 Effect of Mechanical Loading on Pre-Metastatic Niche Formation

In the previous chapter tumour secreted LOX, acting via P2X7R, was shown to contribute to the formation of osteolytic lesions. Knockdown of LOX in the tumours of these mice reduced lesion formation to levels not significantly different from healthy age-matched controls (see section 4.2.1). Osteolytic lesion formation was also observed to occur in a cancer cell free model, being induced by injections of conditioned medium from 4T1 cells grown *in vitro* (see section 4.2.2), and confirming that lesion formation can occur prior to metastasis. Generation of osteolytic lesions in this manner has been shown to significantly enhance the ability of metastatic cells to colonise bone, with the recorded metastatic burden showing a positive correlation with lesion number (Cox et al. 2015). Thus osteolytic lesion formation can be considered a key contributor to the pre-metastatic niche in bone.

Given the positive feedback nature of the vicious cycle of bone metastases, in which growth factors released from resorbed bone mineral matrix drive further bone loss and tumour cell survival (Guise 2010), it is highly important that metastasis to bone be prevented as soon as feasibly possible. Inhibition of the formation of a pre-metastatic niche in bone, by inhibiting osteolytic lesion formation, is a key feature for this strategy. It is, therefore, important to understand the mechanisms driving lesion formation in order to develop therapies to combat it. Mechanical loading has been shown to be osteogenic, driving cortical bone growth as evidenced by the increases in cortical bone thickness observed previously in this study (Section 5.2.1.1, Fig. 5.1) and widely in the literature (De Souza et al. 2005a; Robling & Turner 2002; Holguin et al. 2013; Li et al. 2005). It is thus logical to assume that mechanical loading of bone may hinder lesion formation by rebalancing bone remodelling in favour of osteogenesis. Conversely, as LOX has been reported to accumulate at areas of high pressure within the body, it is possible that mechanical loading could lead to an increase in LOX levels in the loaded limb, driving greater lesion formation. To further investigate the effects that mechanical loading, LOX, and P2X7R exert upon osteolytic lesion formation, fold changes in lesion number and area, relative to non-loaded age-matched controls, were calculated. Normalising datasets between WT and $P2X7R^{-/-}$ mice in this manner allows direct statistical analysis between the two genotypes.

5.3.2.1 Effect of Mechanical Loading on Osteolytic Lesion Formation

Mechanical loading was found to drive the formation of holes in the bone of healthy, tumour-free WT mice. As these holes match the definition of "lesion" used in this study (i.e. holes penetrating the cortical bone with a dimension greater than 50μm, and an area >2500μm^2), they shall, in the interest of a simplified discussion, be referred to as 'lesions', despite not being caused by cancer. Considering that these healthy, age-matched mice show an increased cortical thickness as a result of mechanical loading, this shows an overall mixed response to loading in cortical bone, with elements of both osteogenesis (cortical thickening) and osteolysis (lesion formation). As mechanical loading is seen to increase cortical thickness, it must be stimulating osteoblast cells to lay down new bone. One possible explanation for the induction of osteolytic lesion formation by loading is that the stimulus to generate new bone is so great it results in the laying down of large quantities of porous, woven bone in an attempt to quickly increase bone mass to compensate for the increased strain experienced. The structure of woven bone is reported to contain large vascular spaces (Scheuer & Black 2004), and it is possible that these vascular spaces act as templates for osteolytic lesions during later osteoclastic remodelling of woven bone into its more mature, lamellar form.

As in the previous chapter, orthotopic breast tumours were shown to generate a substantial increase in lesion number and area in tumour bearing mice (Fig. 5.8). Mechanical loading of WT tumour bearing mice further increased lesion number and area on top of that already generated by the primary tumour (Figs. 5.7 & 5.8), however the generated increase from loading of tumour bearing mice was not statistically significant when compared to internal non-loaded controls (i.e. the non-loaded limb of the same tumour bearing, loaded mouse). Despite this lack of statistical significance, however, the trend towards increase suggests that mechanical loading is continuing to contribute to lesion formation in tumour bearing mice, but that the magnitude of the increase generated by loading is not great enough to generate a statistically significant increase on top of that already created by the presence of the primary tumour. This shows that the tumour has a far more substantial contribution to osteolytic lesion formation than loading. Future repeats of this experiment may benefit from an increased number of mice, or by prolonging the loading period to 3 weeks to maximise the potential for loading to manifest a statistically significant change in lesion formation in tumour bearing mice.

5.3.2.2 Effect of LOX and Mechanical Loading on Osteolytic Lesion Formation

LOX, secreted from the primary tumour, was found to drive tumour mediated osteolytic lesion formation in this experiment (Fig. 5.8), repeating the observations of the previous chapter (Chapter 4). There was, however, no notable effect of LOX knockdown on the ability of mechanical loading to generate lesions, with both 4T1 and 4T1-shLOX tumour bearing WT mice displaying similar trends towards increased lesion number and area in response to mechanical loading (Fig. 5.8). This suggests that, while mechanical loading is generating osteolytic lesions, it is not dependent upon tumour secreted LOX, as we would expect to see an impaired level of loading mediated osteolytic lesion formation in 4T1-shLOX tumour bearing mice if this were the case. While this does not rule out LOX as a contributory factor in loading mediated lesion formation, as LOX knockdown is only present in cells of the primary tumour and not in the mouse, it suggests that LOX is either unimportant for loading mediated lesion formation, or that only a level already present in the mouse, prior to tumour implantation, is required. In either case, tumour presence does not enhance bone response to loading, and knockdown of LOX in the primary tumour reduces tumour mediated lesion formation, but not loading mediated lesion formation.

While the above hypothesis, that mechanical loading would result in an accumulation of LOX in the bone microenvironment and drive osteolytic lesion formation, is not supported by the observations made in this study, it cannot be entirely ruled out. Thus future research of loading mediated osteolytic lesion formation should aim to quantify LOX in the bone microenvironment and investigate how it is affected by mechanical loading. Furthermore, dosing mice with a LOX inhibitor, such as BAPN, could elucidate whether normal physiological levels of LOX are contributing to loading mediated effects.

5.3.2.3 Effect of P2X7R and Mechanical Loading on Osteolytic Lesion Formation

The interaction of LOX and P2X7R in tumour mediated lesion formation was suggested by observations in the previous chapter (section 4.2.1.3), which showed that lesion formation could be inhibited by interference with either tumour production of LOX or host P2X7R activity. The role of P2X7R in tumour mediated lesion formation was supported by results from the current loading study, showing that knockout of P2X7R significantly reduced lesion formation in tumour bearing mice (Fig. 5.9). Knockout of P2X7R in conjunction with knockdown of LOX in the primary tumour, however, returned some very unexpected results in the loading experiment, showing a large increase in lesion formation in 4T1-shLOX tumour bearing P2X7R$^{-/-}$ mice, returning overall values which rivalled the levels of lesion formation seen in WT mice with 4T1 tumours (i.e. those in which the greatest levels of lesion formation were expected) (Figs. 5.6 & 5.9).

One possibility for the observed increases in lesion number and area fold change in P2X7R$^{-/-}$ mice with 4T1-shLOX tumours is that LOX knockdown in the 4T1 tumour is causing upregulation of some compensatory mechanism, for example LOXL-2, which has previously been shown to drive osteolytic lesion formation (Barker et al. 2011). There is, however, no evidence of an increase in lesion formation in the non-loaded 4T1-shLOX tumour bearing mice analysed in the previous chapter, so it is possible that mechanical loading of one limb is causing some kind of systemic effect in the mouse which may be exploited by the 4T1-shLOX tumour, but not the 4T1 tumour. As it has been previously reported that the effects of mechanical loading are isolated to the loaded limb alone (Sugiyama et al. 2010; De Souza et al. 2005a), however, a systemic effect from mechanical loading in one limb is unlikely.

A final possibility to consider is experimental error. Tumour implantation was achieved by injection of cancer cells in a PBS solution. As all 4T1-shLOX tumour bearing P2X7R$^{-/-}$ mice were injected in the same session, it is possible that the number of 4T1-shLOX cells in the solution used in that session was underestimated, resulting in injection of a higher cell number than anticipated. Further repeats of the experiment would benefit from increased numbers of mice, with tumour implantation staggered over separate sessions to control for this kind of error.

As previously discussed above, mechanical loading was shown to generate a statistically significant increase in lesion formation in WT mice (Fig. 5.7). Mechanical loading in healthy age-matched P2X7R$^{-/-}$ mice did not result in a statistically significant increase in lesion formation, but a trend towards increase in response to loading persisted, suggesting that P2X7R contributes towards some degree of loading mediated lesion formation (Fig. 5.7). The reduced response to loading in P2X7R$^{-/-}$ mice supports previous publications showing reductions of up to 61% in bone response to loading in female mice upon knockout of P2X7R (Li et al. 2005). A role for P2X7R in loading mediated lesion formation is also supported by analysis of fold change data, which

shows no significant differences between age-matched WT and P2X7R$^{-/-}$ mice in fold changes of lesion number or area in response to loading (Fig. 5.9). Thus, taken together, this suggests that loading is driving lesion formation in both WT and P2X7R$^{-/-}$ age-matched mice, but that the effect in P2X7R$^{-/-}$ mice is less pronounced than in WT mice.

While loading induced lesion formation was seen to be inhibited in P2X7R$^{-/-}$ age-matched mice, it appears to be entirely absent in P2X7R$^{-/-}$ tumour bearing mice (Fig. 5.7). Neither 4T1 nor 4T1-shLOX tumour bearing mice showed any notable effect of mechanical loading on lesion formation whatsoever, with mean values for both lesion number and area in loaded and non-loaded limbs remaining almost identical. Direct comparison of lesion number and area fold changes between WT and P2X7R$^{-/-}$ mice revealed that knockout of P2X7R has no statistically significant effect on lesion formation in response to mechanical loading in age-matched mice, but that it did significantly reduce lesion formation in response to tumour bearing (Fig. 5.9), repeating the observations of the previous chapter (Chapter 4). Furthermore, P2X7R$^{-/-}$ mice subjected to both tumour bearing and mechanical loading also showed a significant reduction in lesion formation compared to WT mice (Fig. 5.9), but this is likely more resultant from P2X7R knockout preventing tumour induced lesions, rather than preventing loading induced lesions.

In summary, knockout of P2X7R was observed to inhibit, but not prevent, loading mediated lesion formation when comparing raw values in tumour free mice, but analysis of the magnitude of this effect (by analysing the fold changes in lesion number and area) revealed it to be insignificant in comparison to the lesion causing effect of 4T1 tumours. Taken together, these observations show that while knockout of P2X7R appears to have a small effect on loading mediated lesion formation, it has a much larger effect on tumour mediated lesion formation, identifying P2X7R as a potential target for novel therapies to combat osteolytic lesion formation in metastatic bone disease, and to hinder formation of a pre-metastatic niche in bone.

5.4 Conclusion

Mechanical loading is shown to have a mixed effect on bone remodelling in this study. Analysis of indices of bone volume show that mechanical loading is largely osteogenic, resulting in thicker cortical bone, and thicker trabeculae, supporting previous publications which have reported increases in these parameters in response to mechanical loading (Wang et al. 2012; De Souza et al. 2005a; Robling & Turner 2002; Holguin et al. 2013; Li et al. 2005). At the same time, the same loading regime is shown to contribute to the formation of osteolytic lesions in cortical bone. While a previous publication has shown osteolytic effects of mechanical loading in bone (Fujiki et al. 2013), this was in the hard palate, a bone which is not habitually loaded in the same manner as a long bone, and thus the identification of mechanical loading leading to osteolytic activity in a load bearing long bone is unusual and warrants further investigation, particularly given the role of osteolytic lesion formation in the establishment of the pre-metastatic niche.

P2X7R is confirmed to play a prominent role in bone response to loading, with P2X7R knockout shown to reduce loading mediated osteogenic effects in cortical and trabecular thickness, as well as loading mediated osteolytic effects in lesion formation.

The extent of change induced by mechanical loading is also shown to be sufficient to combat tumour mediated bone loss in a murine breast cancer model, in some cases entirely reversing the process of bone loss and resulting in stronger bone than non-loaded age-matched controls. While mechanical loading was found to also promote osteolytic lesion formation in WT tumour bearing mice, knockout of P2X7R reduced loading mediated lesion formation to such an extent that there was no notable effect whatsoever of mechanical loading on lesion formation in tumour bearing $P2X7R^{-/-}$ mice.

A final important observation to make is that mechanical loading was able to counteract the effects of tumour induced bone loss in a safe manner, without causing fracture. While physical exercise, and strength training in particular, are advised to improve physical and psychological wellbeing in cancer survivors (Schmitz et al. 2010; Rock et al. 2012), clinical trials investigating their effect have thus far excluded patients with bone metastases due to concerns that loading of weakened bone would increase risk of fracture (Courneya & Friedenreich 2011). This study therefore suggests that an appropriately designed regime of mechanical loading, is able to safely counteract tumour induced bone loss with no increase in fracture rate. This supports findings from a study of strength training in prostate cancer patients with confirmed bone lesions, which found that appropriately devised and supervised resistance training was safely tolerated, resulting in improved physical function, activity levels, and lean mass (Cormie et al. 2013). Unfortunately, there is no data on the effect that this training regime had in the bone of the

patients, but it highlights the possibility that meaningful levels of physical exercise can be tolerated while avoiding fracture.

Considering the protective effect of mechanical loading upon tumour induced bone loss as described above, and the absence of any real effect of mechanical loading on osteolytic lesion formation in tumour bearing P2X7R$^{-/-}$ mice, this suggests that mechanical loading can safely be used to combat metastatic bone loss without contribution to pre-metastatic osteolytic lesion formation, especially if it is applied in conjunction with P2X7R antagonism. Thus a combination of suitably devised loading exercises and P2X7R antagonism shows promise as an adjuvant therapy to bisphosphonate treatment of metastatic bone disease, importantly one which may prove to be effective in populations, such as pre-menopausal women, in whom bisphosphonate treatment is less effective.

CHAPTER 6:

GENERAL DISCUSSION

Metastasis to bone is a serious problem in cancer, complicating treatments to the extent that bone metastases are largely considered to be incurable (Roodman 2004; Li et al. 2012). Metastasis to bone is the leading contributor to morbidity in cancer patients (Chambers et al. 2002; Weigelt et al. 2005), where it may result in extremely debilitating reductions in quality of life, resulting from symptoms such as pain, pathological fracture, spinal cord compression, and potentially life-threatening levels of hypercalcaemia (Mercadante 1997; Domchek et al. 2000; Cancer Research UK 2014). In addition, osteolytic bone metastases contribute to the breakdown of bone mineral, fuelling the vicious cycle of bone metastasis by releasing growth factors stored therein (Guise 2010), thus perpetuating metastasis, promoting cancer cell survival, and exponentially increasing bone destruction and disease severity.

Breast and prostate cancers are the most common to metastasise to bone, and ~70% of patients who die from either of these cancers show evidence of metastatic bone disease (Coleman 2006; Rosen 2013). It is estimated that, in the UK alone, around 9000 women with breast cancer develop metastatic bone disease each year, many of whom are likely to survive for more than 2 years (British Association of Surgical Oncology Guidelines 1999), thus highlighting the need for effective preventative and palliative treatments. Current treatment of metastatic bone disease focusses heavily on bisphosphonates, a class of drug which combats bone loss by inhibiting osteoclast cell activity and survival (Drake et al. 2008; Fleisch 2002). There are, however, concerns that bisphosphonates are ineffective in certain populations, including pre-menopausal women, offering only marginal improvements over placebo (Wong et al. 2012; EBCTCG 2015). Furthermore, while bisphosphonates prevent further bone loss, they do not repair bone loss acquired prior to their administration. Thus there is a need to develop alternative, osteogenic treatments to combat metastatic bone disease in a wider range of patients.

Expression of LOX is known to drive the generation of a metastatic phenotype in breast cancer cells (Kirschmann et al. 2002), and has also recently been identified as a contributor to the formation of a pre-metastatic niche in bone by generating osteolytic lesions prior to tumour cell arrival (Cox et al. 2015). While the mechanism by which LOX affects pre-metastatic change in the bone micro-environment is partially understood, there is scope for further investigation of the metabolic pathways involved. One identified potential interactor was P2X7R, which is involved in both cancer and bone biology. In addition, its ligand, ATP, is noted to be released from cells upon mechanical loading, potentially co-localising with LOX, which has also been noted to accumulate at areas of pressure.

This study investigated the effect of tumour secreted LOX on bone in a syngeneic mouse breast cancer model which utilised the 4T1 murine breast cancer cell line and BALB/c mouse strain, including an established $P2X7R^{-/-}$ BALB/c mouse (Chessell et al. 2005; Syberg et al. 2012). Both

orthotopic tumour and cancer cell free models were used to confirm that lesion formation was able to occur prior to metastasis, and that P2X7R was essential for LOX mediated destruction of bone. Furthermore, the role of mechanical loading in LOX/P2X7R related bone loss was investigated by non-invasive axial loading of the tibia and was found to be predominantly osteogenic, dependent upon P2X7R activity, and able to effectively combat tumour induced bone loss.

Validation of the experimental model, detailed in chapter 3, confirmed both LOX knockdown, and P2X7R expression in the 4T1 cell line. Knockdown of LOX in the 4T1 cell line was previously achieved by our collaborators via insertion of shRNA against LOX (Erler et al. 2009). Western Blot of concentrated conditioned medium from 4T1 and 4T1-shLOX cells used in this study confirmed a reduction in secreted LOX in the 4T1-shLOX cell line. This method of analysis, however, is only semi-quantitative, and while it shows knockdown, it could be improved in future by performing a quantitative assay to quantify the extent of LOX knockdown. Quantification of LOX levels in conditioned medium from 4T1 cells, and sera from tumour bearing mice, would also identity potential LOX dose difference effects between the orthotopic and cell-free models used in this study, as well as inform potential thresholds for LOX manipulation of the bone microenvironment which could aid metastatic cancer screening programs.

The 4T1 cell line was shown to express both the (a) and (k) variants of P2X7R, however attempts to ascertain whether this was translated into functional protein were inconclusive. Future research could improve on this by including an assay of P2X7R activity, such as assessment of P2X7R pore formation in 4T1 cells by assessment of YO-PRO-1 uptake, as previously described (Rassendren et al. 1997).

The potential interaction of LOX and P2X7R in tumour modification of bone was investigated *in vivo*, and results are detailed in Chapter 4. Mice bearing 4T1 tumours were shown to generate osteolytic lesions in bone during the pre-metastatic window, before cancer cell arrival was expected. The ability of tumour secreted LOX to generate lesions prior to cancer cell arrival in bone was confirmed in mice injected with conditioned medium from 4T1 cells *in vitro*, which developed osteolytic lesions in the total absence of cancer cell presence. The generation of lesions was also shown to occur at specific foci rather than result from an overall thinning of cortical bone, as there was no significant loss of cortical thickness in WT mice in response to tumour bearing. Furthermore, P2X7R was shown to be necessary for LOX mediated lesion formation, confirming its role in modification of the pre-metastatic niche, and identifying P2X7R as a key factor in the mechanism driving the metastatic affinity for bone noted in LOX expressing cancer cells (Cox et al. 2015). Interestingly P2X7R appears to be less important in LOX mediated

modification of trabecular bone, where knockout failed to prevent LOX induced trabecular bone loss, as it had in cortical bone. Thus there is a possibility for separate site-specific LOX mechanisms in cortical and trabecular bone. One possibility being that LOX/P2X7R activity recruits osteoprogenitor cells to the surface of cortical bone allowing the process of remodelling to commence, something not required in the medullary cavity which houses trabecular bone in close proximity to osteoprogenitor cells from the haematopoietic stem cell niche. It would, therefore, be prudent for future research to investigate how LOX/P2X7R activity affects bone remodelling cell numbers on cortical and trabecular surfaces by histologically processing bone sections and staining for TRAP and alkaline phosphatase to assess osteoclast and osteoblast cell number, respectively, in these regions. Furthermore, assessment of LOX/P2X7R activity in primary osteoclast and osteoblast cell cultures would identify whether there was a direct interaction between LOX and P2X7R in the cell, or whether other intermediaries were required.

Analysis of tumour volumes suggested that LOX production promoted tumour growth, though the mechanism by which this occurs is not currently understood. Investigation of possible LOX and P2X7R interaction at the cellular level in cancer could elucidate LOX/P2X7R effects on primary tumour growth. This potential LOX/P2X7R interaction could be investigated *in vitro* by culturing 4T1 cells with recombinant LOX protein (or even conditioned medium from naïve 4T1 cultures) and a P2X7R inhibitor, such as A 438079 HCl, used previously, to ascertain effects on 4T1 cell growth. Furthermore, RT-PCR of LOX expression in response to P2X7R stimulation, and P2X7R expression in response to LOX stimulation in the 4T1 cell line could ascertain if there were direct stimulation at the transcriptional level and in which direction it occurred. One limitation to consider for a future *in vivo* experiment on tumour growth is the method used to calculate tumour volume. Calliper measurements, used in this study, are subject to inaccuracy and user bias. A previous study investigated 4T1 tumour growth and metastasis in BALB/c mice using the 4T1-Luc (luciferase expressing) cell line, and IVIS imaging (Tao et al. 2008). This model would allow for more accurate quantification of primary tumour growth, as well as allowing assessment of how LOX/P2X7R may be influencing metastasis to other bones, and other tissues.

The potential role of mechanical loading in LOX/P2X7R modification of the bone microenvironment was investigated in chapter 5. Mechanical loading was shown to have mixed osteogenic and osteolytic effects in bone. Loading induced thickening of cortical and trabecular bone, successfully combating tumour induced bone loss in these indices, but also contributed to the formation of osteolytic lesions in the surface of cortical bone. The extent of loading induced lesion formation, however, was much smaller than that of tumour induced lesion formation, to the extent that loading of tumour bearing mice caused no significant increase in total lesion formation on top of that induced by the tumour. Furthermore, P2X7R was found to contribute

to loading response in both thickening of cortical and trabecular bone and in osteolytic lesion formation, suggesting that it is a fundamental component of bone response to loading. Knockout of P2X7R entirely removed loading induced lesion formation in tumour bearing mice, identifying a combination of mechanical loading and P2X7R antagonism as a potential osteogenic treatment for patients with metastatic bone disease.

Mechanical loading in this study had less of an effect on trabecular bone than the same loading regime used in older C57BL/6 mice, which was partly attributed to differences in maturity between the mice. Future research, therefore, could include investigation of the effects of mechanical loading in older BALB/c mice to assess the effects of loading on a mature skeleton, which would provide a more suitable proxy for cancer patients, and patients with age-related bone loss. Investigation of different loading frequencies is also advisable to optimise the osteogenic effect of loading.

Tumour secreted LOX contributed heavily to tumour mediated lesion formation, but had no significant effect on loading mediated lesion formation. It is, however, unclear whether or not physiological levels of LOX from the mouse, accumulating at the area of pressure generated from mechanical loading, may have contributed to lesion formation. Future research could investigate the effect of mechanical loading on LOX accumulation in the mouse by assaying LOX levels from sera of loaded and non-loaded mice for comparison.

There were some limitations in the mechanical loading experiment which should be addressed in future research utilising a similar model. Firstly, having only 6 limbs in each of the loaded and unloaded subsets of each experimental group limits the robustness of the dataset and prevented the use of parametric statistical analyses, which may have been better able to assess significance. Secondly, the non-loaded age-matched $P2X7R^{-/-}$ mouse group showed significant differences between left and right limbs in BV/TV, Tb No., and SMI in trabecular analysis. This suggests that the non-loaded mouse control group may not have been suitable for comparison with the rest of the $P2X7R^{-/-}$ mice used in the trabecular analyses in this loading study, and this is likely related to the low sample size.

Finite element analysis to calculate the required loading force (in newtons) to generate a strain of 5000με in the mouse limb was conducted on the output of a μCT scan of a dissected tibia, which was free from soft tissues. In the living mouse the tibia is surrounded by musculature and connective tissues which will bear a percentage of the mechanical loading, thus reducing the strain experienced by the bone. As such, the strain induced in the mice in this study is likely to have been lower than the 5000με calculated. This study, however, calculated optimal force and applied mechanical force in the same manner as a previous study (Wang et al. 2013), in which

the level of mechanical loading was sufficient to induce significant bone growth, therefore priorly validating this method for design of an osteogenic mechanical loading regime.

Another concern is that the 8.3N loading strength, chosen to engender a strain of 5000με in the loaded limb, may have been too high. Mice were observed avoiding weight bearing on their loaded limb upon conclusion of the loading procedure, as they came round from anaesthesia. This behaviour occurred regularly, after each loading session, though mice were observed to be weight bearing as normal on the loaded limb within minutes of the end of the loading procedure and before they were returned to their cages. There is evidence in the non-loaded limbs of loaded mice, however, to suggest that mice experienced discomfort in their right (loaded) legs, which led to then them bearing more weight on their left legs in between loading sessions, possibly leading to a loading effect in this leg, which was meant to act as a contralateral, non-loaded control. In future it may be prudent to reduce loading force to a level which would not generate this effect.

Finally, 4T1-shLOX tumour bearing P2X7R$^{-/-}$ mice returned abnormally high levels of lesion formation in the experiments conducted for chapter 5, compared to those in chapter 4, and in published literature (Cox et al. 2015). The levels of lesion formation recorded were much higher than expected, and possibly the result of experimental error. As all mice in this group were inoculated with 4T1-shLOX cells from the same cell suspension, on the same day, a miscalculation in the dilution of this suspension could have resulted in mice receiving a higher number of tumour cells than anticipated. Future repeats of this experiment would benefit from staggering tumour inoculations over at least two separate sessions to avoid a repeat of this error.

Taking these considerations together it is apparent that the overall design of the loading experiment performed in this study is sound, but would benefit from an increased sample number, older mice, and possibly from reduction of loading induced strain. Previous research has shown greater osteogenic effects with increased loading waveform frequency and a reduced rest period between cycles (Holguin et al. 2013), and future research to optimise osteogenic loading effect should seek the optimal balance between loading intensity and tolerance for mice with tumour induced bone loss.

To summarise the key findings of this study, P2X7R has been identified as an integral component of the mechanism by which LOX generates a pre-metastatic environment in bone. Mechanical loading did not contribute to tumour secreted LOX modification of bone as had been hypothesised, and did in fact protect against tumour induced bone loss without causing fracture in mice. In addition to future work proposed above as continuations or optimisations of work

already conducted, there are a number of possible research avenues which could build upon the observations herein. First and foremost, the role of LOX and P2X7R at the cellular level should be investigated. While LOX is known to directly affect both osteoclast and osteoblast primary cultures, the role of P2X7R at the cellular level has not been confirmed. Primary culture of calvarial derived osteoblasts, and bone marrow derived osteoclasts from $P2X7R^{-/-}$ mice stimulated with recombinant LOX protein, or LOX containing CM, could confirm interaction of P2X7R and LOX at the cellular level, and also allow closer inspection of the cellular mechanisms by which LOX/P2X7R stimulation mediated its effect upon bone. One particular mechanism of interest is NFATc1 localisation. Both LOX and P2X7R have been shown to drive NFATc1 nuclear localisation, describing part of the mechanism for the increased osteoclastic activity witnessed in mice with LOX producing tumours (Cox et al. 2015). To ascertain if LOX is realising NFATc1 localisation via P2X7R, immunostaining for NFATc1 in LOX treated cultures of primary osteoclasts from $P2X7R^{-/-}$ mice should be conducted. The role of H_2O_2 in LOX modification of bone is also a potentially interesting avenue of research, particularly considering published interactions of reactive oxygen species with both P2X7R (Ficker et al. 2014; Lenertz et al. 2009) and osteoclasts (Ha et al. 2004). Thus cell culture as described above, with the addition of catalase (to rapidly break down H_2O_2) warrants future investigation.

Additionally, while there is a substantial reduction in tumour induced bone loss and lesion formation upon LOX knockdown, neither is entirely prevented. Thus it may be worthwhile developing a true LOX knockout 4T1 cell line (if viable) to ascertain whether the tumour induced lesion formation and bone loss noted in 4T1-shLOX treated mice is the result of residual LOX expression escaping knockdown in the cell line, or other tumour related factors. Investigation of other factors involved in the vicious cycle of metastasis would also contribute to this. Analysis of proteins in the 4T1 secretome, cross-referenced with those known to contribute to the vicious cycle of bone metastasis, could thus identify potential additional targets for treatments to combat tumour induced bone loss.

A final suggested avenue of investigation involves broadening out the purinergic receptors investigated. One exciting target is the $P2Y_2$ receptor ($P2Y_2R$), which is reported to stimulate LOX secretion in response to hypoxia via upregulation of HIF-1α expression, contributing to pre-metastatic niche formation in the lung (Joo et al. 2014). $P2Y_2R$ (formerly known as P2U) expression has been identified in osteoblasts (Bowler et al. 1995), where its activation inhibits mineralisation (Hoebertz et al. 2000), and while it has been shown to be expressed in osteoclasts (Dixon et al. 1997; Bowler et al. 1998), there are no reports of any effect on osteoclast formation or resorptive activity (Orriss et al. 2011), save that direct stimulation of $P2Y_2R$ does not appear to mediate osteoclastic resorption *in vitro* (Bowler et al. 1998). Upregulation of HIF-1α

(potentially via $P2Y_2R$), however, promotes expression of P2X7R (Tafani et al. 2011), suggesting a possible contribution of $P2Y_2R$ to the LOX/P2X7R mechanism discovered in this study.

In short, the present study identifies P2X7R as a crucial component in the mechanism of tumour secreted LOX destruction of bone. Tumour secreted LOX is also shown to generate osteolytic lesions in bone and contribute to trabecular bone loss prior to tumour cell arrival, identifying LOX/P2X7R activity as a contributor to pre-metastatic niche formation. Mechanical loading was found to combat bone loss in cortical and trabecular thickness, but to contribute to the formation of osteolytic lesions, albeit to a much lesser extent than the primary tumour. P2X7R was shown to contribute significantly to bone response to loading, with knockout reducing both the osteogenic and osteoblastic effects. Combining mechanical loading and P2X7R knockout in tumour bearing mice successfully reduced lesion formation and tumour induced bone loss, identifying the combination as a potential new target for strategies to treat and prevent metastatic bone disease in cancer patients.

REFERENCES

Adinolfi E, Capece M, Franceschini A, Falzoni S, Giuliani AL, Rotondo A, Sarti, AC, Bonora M, Syberg S, Corigliano D, Pinton P, Jorgensen NR, Abelli L, Emionite L, Raffaghello L, Pistoia V, and Di Virgilio F. Accelerated Tumor Progression in Mice Lacking the ATP Receptor P2X7. *Cancer Research,* 75(4), 635-44.

Adinolfi E, Raffaghello L, Giuliani AL, Cavazzini L, Capese M, Chiozzi P, Binachni G, Kroemer G, Pistoia V, and Di Virgilio F. (2012) Expression of P2X7 Receptor Increases In Vivo Tumor Growth. *Cancer Research,* 72(12), 2957-69.

Adinolfi E, Callegari MG, Cirillo M, Pinton P, Giorgi C, Cavagna D, Rizzuto R, and Di Virgilio F. (2009) Expression of the P2X7 Receptor Increases the Ca^{2+} Content of the Endoplasmic Reticulum, Activated NFATc1m and Protects from Apoptosis. *Journal of Biological Chemistry,* 284(15), 10120-28.

Adinolfi A, Melchiorri L, Falzoni S, Chiozzi P, Morelli A, Tieghi A, Cuneo A, Castoldi G, Di Virgilio F, and Baricordi OR. (2002) P2X7 receptor expression in evolutive and indolent forms of chronic B lymphocytic leukaemia. *Blood*, 99(2), 706-08.

Agerbaek MO, Eriksen E, Kragstrup J, Mosekilde L, and Melsen F. (1991) A reconstruction of the remodelling cycle in normal human cortical iliac bone. *Bone and Mineral,* 12(2), 101-12.

Agrawal A, Buckley KA, Bowers K, Furber M, Gallagher JA, and Gartland A. (2010) The effects of P2X7 receptor antagonists on the formation and function of human osteoclasts in vitro. *Purinergic Signalling,* 6(3), 307-15.

Agrawal A, and Gartland A. (2015) P2X7 receptors: role in bone cell formation and function. *Journal of Molecular Endocrinology*, 54, R75-R88.

Arai F, Miyamoto T, Ohneda O, Inada T, Sudo T, Brasel K, Miyata T, Anderson DK, and Suda T. (1999) Commitment and Differentiation of Osteoclast Precursor Cells by the Sequential Expression of c-Fms ad Receptor Activator of Nuclear Factor κB (RANK) Receptors. *The Journal of Experimental Medicine,* 190(12), 1741-54.

Baker A-M, Bird D, Lang G, Cox TR, and Erler JT. (2013) Lysyl oxidase enzymatic function increases stiffness to drive colorectal cancer progression through FAK. *Oncogene,* 32(14), 1863-68.

Baker A-M, Cox TR, Bird D, Lang G, Murray GI, Sun X-F, Southall SM, Wilson JR, and Erler JT. (2011) The Role of Lysyl Oxidase in SRC-Dependent Proliferation and Metastasis of Colorectal Cancer. *Journal of the National Cancer Institute,* 103(5), 407-24.

Bakota EL, Aulisa L, Galler KM, and Hartgerink JD. (2011) Enzymatic Cross-Linking of a Nanofibrous Peptide Hydrogel. *Biomacromolecules,* 12(1), 82-7.

Ban Y, Wu Y-Y, Yu T, Geng N, Wang Y-Y, Liu X-G, and Gong P. (2011) Response of osteoblasts to low fluid shear stress is time dependent. *Tissue and Cell,* 43 (5), 311-7.

Barker HE, Chang J, Cox TR, Lang G, Bird D, Nicolau M, Evans HR, Gartland A, and Erler JT. (2011) LOXL2-Mediated Matrix Remodelling in Metastasis and Mammary Gland Involution. *Cancer Research,* 71(5), 1561-72.

Barker HE, Bird D, Lang G, and Erler JT. (2013) Tumor-secreted LOXL2 Activates Fibroblasts Through FAK Signaling. *Molecular Cancer Research,* 11(11), 1425-36.

Bass SL, Saxon L, Daly RM, Turner CH, Robling AG, Seeman E, and Stuckey S. (2002) The Effect of Mechanical Loading on Size and Shape of Bone in Pre-, Peri-, and Postpubertal Girls: A Study in Tennis Players. *Journal of Bone and Mineral Research*, 17(12), 2274-80.

Bax BE, Alam ASMT, Banjeri B, Bax CMR, Bevis PJR, Stevens CR, Moonga BS, Blake DR, and Zaidi M. (1992) Stimulation of Osteoclastic Bone Resorption by Hydrogen Peroxide. *Biochemical and Biophysical Research Communications,* 183(3), 1153-58.

Berman AG, Clauser CA, Wunderlin C, Hammond MA, Wallace JM. (2015) Structural and Mechanical Improvements to Bone Are Strain Dependent with Axial Compression of the Tibia in Female C57BL/6 Mice. *Plos One,* 10(6), 1-16.

Blanchette PS and Pritchard KI. (2015) The Role of Bisphosphonates in Early- and Advanced-Stage Breast Cancer: Have We Finally Optimised Care? *Oncology,* 29(1), 23-30.

Blavier L and Delaissé JM (1995) Matrix metalloproteinases are obligatory for the migration of preosteoclasts to the developing marrow cavity of primitive long bones. *Journal of Cell Science,* 108(1), 3649-59.

Bowler WB, Birch MA, Gallagher JA, and Bilbe G. (1995) Identification and cloning of human P2U purinoceptor present in osteoclastoma, bone, and osteoblasts. *Journal of Bone and Mineral Research,* 10(7), 1137-45.

Bowler WB, Littlewood-Evans A, Bilbe G, Gallagher JA, and Dixon CJ. (1998) P2Y2 Receptors Are Expressed by Human Osteoclasts of Giant Cell Tumor but Do Not Mediate ATP-Induced Bone Resorption. *Bone,* 22(3), 195-200.

Boyce BF, and Xing L. (2007) The RANKL/RANK/OPG Pathway. *Current Osteoporosis Reports,* 5(3), 98-104.

Boyce BF, Xing L, and Chen D. (2005) Osteoprotegerin, the bone protector, is a surprising target for β-catenin signalling. *Cell Metabolism,* 2(6), 344-45.

Boyle WJ, Simonet WS, and Lacey DL. (2003) Osteoclast differentiation and activation. *Nature,* 423(May), 337-342

Brandao-Burch A, Key ML, Patel JJ, Arnett TR, and Orriss IR. (2012) The P2X7 receptor is an important regulator of extracellular ATP levels. *Frontiers in Endocrinology,* 3, 1-9.

British Association of Surgical Oncology Guidelines. (1999) The Management of Metastatic Bone Disease in the United Kingdom. *European Journal of Surgical Oncology,* 25(1), 3-23.

Browne, LE, Jiang L-H, and North RA. (2010) New structure enlivens interest in P2X receptors. *Trends in Pharmacological Sciences,* 31 (5), 229-237.

Burnstock G. (1978) A basis for distinguishing two types of purinergic receptor. *In:* Straub RW, and Bolis L. (eds) *Cell membrane receptors for drugs and hormones: a multidisciplinary approach.* New York, Raven Press. p107-18.

Burnstock G. (2006) Purinergic signalling. *British Journal of Pharmacology,* 147, S172-81.

Bussard KM, Gay CV, and Mastro AM. (2008) The bone microenvironment in metastasis; what is special about bone? *Cancer Metastasis Reviews,* 27(1), 41-55.

Cancer Research UK. (2014) High calcium in people with cancer [online] Available from: http://www.cancerresearchuk.org/about-cancer/coping-with-cancer/coping-physically/calcium/high-calcium-in-people-with-cancer [Accessed 26/05/2015].

Cazzaniga A, Castiglioni S, and Maier JAM. (2014) Conditioned Media from Microvascular Endothelial Cells Cultured in Simulated Microgravity Inhibit Osteoclast Activity. *BioMed Research International,* 2014, 1-9.

Chambers AF, Groom AC, and MacDonald IC. (2002) Dissemination and Growth of Cancer Cells in Metastatic Sites. *Nature Reviews. Cancer,* 2(8), 563-72.

Chang YS, di Tomaso E, MacDonald DM, Jones R, Jain RK, and Munn LL. (2000) Mosaic blood vessels in tumors: Frequency of cancer cells in contact with flowing blood. *Proceedings of the national Academy of Sciences of the United States of America,* 97(26), 14608-13.

Chessell IP, Hatcher JP, Bountra C, Michel AD, Hughes JP, Green P, Egerton J, Murfin M, Richardson J, Peck WL, Grahames CBA, Casula MA, Yiangou Y, Birch R, Anand P, and Buell GN. (2005) Disruption of the P2X7 purinoceptor gene abolishes chronic inflammatory and neuropathic pain. *Pain,* 114(3), 386-96.

Chiozzi P, Sanz JM, Ferrarri D, Falzoni S, Aleotti A, Buell GN, Collo G, and Di Virgilio F (1997) Spontaneous Cell Fusion in Macrophage Cultures Expressing High Levels of P2Z/P2X7 Receptor. *Journal of Cell Biology,* 138(3), 697-706.

Clarke B (2008) Normal bone anatomy and physiology. *Clinical Journal of the American Society of Nephrology,* 3(suppl3), 131-9.

Coleman R, Gnant M, Morgan G, and Clezardin P (2014) Effects of Bone-Targeted Agents on Cancer Progression and Mortality. *Journal of the National Cancer Institute,* 104(14) 1059-67.

Coleman R (2006) Clinical Features of Metastatic Bone Disease and Risk of Skeletal Morbidity. *Clinical Cancer Research,* 12 (20 Pt 2), 6243s-6249s.

Coleman R (2002) The Clinical Use of Bone Resorption Markers in Patients with Malignant Bone Disease. *Cancer,* 94(10), 2521-33.

Conquet (1995) Inactivation In Vivo of Metabotropic Glutamate Receptor 1 by Specific Chromosomal Insertion of Reporter Gene lacZ. *Neuropharmacology,* 34(8), 865-70.

Cormie O, Newton RU, Spry N, Joseph D, Taaffe DR, and Galvão DA. Safety and efficacy of resistance exercise in prostate cancer patients with bone metastases. *Prostate Cancer and Prostatic Diseases,* 16(4), 328-35.

Courneya KS and Friedenreich C (eds) (1995) *Physical Activity and Cancer*. Berlin, Springer.

Coutinho-Silva R, Stahl L, Cheung K-K, Enes de Campos N, de Oliviera Souza C, Ojcius DM, and Burnstock G. (2004) P2X and P2Y purinergic receptors on human intestinal epithelial carcinoma cells: effects of extracellular nucleotides on apoptosis and cell proliferation. *Am J Physiol Gastrointest Liver Physiol,* 288, G1024-G1035.

Cox TR, Rumney RMH, Schoof EM, Perryman L, Høye A, Agrawal A, Bird D, Ab Latif N, Forrest H, Evans HR, Huggins ID, Lang G, Linding R, Gartland A, and Erler JT (2015) The hypoxic cancer secretome induces pre-metastatic bone lesions through lysyl oxidase. *Nature* 522, (7554), 106-110.

Cox TR, and Erler JT. (2013) Lysyl oxidase in colorectal cancer. *American Journal of Physiology, Gastrointestinal, and Liver Physiology,* 305(50), G659-66.

Csiszar K (2001) Lysyl Oxidases: A Novel Multifunctional Amine Oxidase Family. *Progress in Nucleic Acid Research and Molecular Biology,* 70, 1-32.

De Souza RL, Matsuura M, Eckstein F, Rawlinson SCF, Lanyon LE, and Pistillides AA. (2005a) Non-invasive axial loading of mouse tibiae increases cortical bone formation and modifies trabecular organization: A new model to study cortical and cancellous compartments in a single loaded element. *Bone,* 37(6), 810-18.

De Souza RL, Pitsillides AA, Lanyon LE, Skerry TM, and Chenu C. (2005b) Sympathetic nervous system does not mediate the load-induced cortical new bone formation. *Journal of Bone and Mineral Research,* 20(12), 2159-68.

Di Virgilio F, Flazoni S, Chiozzi P, Sanz JM, Ferrari D, and Buell GN. (1999) ATP receptors and giant cell formation. *Journal of Leukocyte Biology,* 66(5), 723-26.

Di Virgilio F, Ferrari D, and Adinolfi E. (2009) P2X7: A growth=promoting receptor – implications for cancer. *Purinergic Signalling,* 5(2), 251-6.

Dixon CJ, Bowler WB, Fleetwood P, Ginty AF, Gallagher JA, and Carron JA (1997) Extracellular nucleotides stimulate proliferation in MCF-7 breats cancer cells via P_2-purinoceptors. *British Journal of Cancer* 75(1), 34-39.

Domchek SM, Younger J, Finkelstein DM, and Seiden MV. (2000) Predictors od skeletal complications in patients with metastatic breast carcinoma. *Cancer* 89(2), 363-68.

Drake MT, Clarke BL, and Khosla S. (2008) Bisphosphonates: Mechanism of Action and Role in Clinical Practice. *Mayo Clinic Proceedings* 83(9), 1032-45.

EBCTCG: Early Breast Cancer Trialists' Collaborative Group (2015) Adjuvant bisphosphonate treatment in early breast cancer: meta-analyses of individual data from randomised trials. *The Lancet* 15, 1-19.

Erben RG (2015) Hypothesis: coupling between resorption and formation in cancellous bone remodelling is a mechanically controlled event. *Frontiers in Endocrinology* 6 (May), 1-5.

Eriksen EF (2010) Cellular mechanisms of bone remodelling. *Reviews in Endocrine and Metabolic Disorders* 11(4), 219-227.

Eriksen EF (1986) Normal and pathological remodelling of human trabecular bone: three dimensional reconstruction of the remodelling sequence in normal and in metabolic bone disease. *Endocrine Reviews* 7(4), 379-408.

Erler JT, Bennewith KL, Cox TR, Lang G, Bird D, Koong A, Le Q-T, and Giaccia AJ. (2009) Hypoxia-induced lysyl oxidase is a critical mediator of bone marrow cell recruitment to form the premetastatic niche. *Cancer Cell* 15(1), 35-44.

Erler JT, Bennewith KL, Nicolau M, Dornhöfer N, Kong C, Le Q-T, Chi J-T A, Jeffrey SS, and Giaccia AJ. (2006) Lysyl oxidase is essential for hypoxia-induced metastasis. *Nature* 440(7088), 1222-226.

Ficker C, Rozmer K, Kató E, Rómeó DA, Schumann L, Krügel U, Franke H, Sperlágh B, Riedel T, and Illes P. (2014) Astrocyte-neuron interaction in the substantia gelatinosa of the spinal cord dorsal horn via P2X7 receptor-mediated release of glutamate and reactive oxygen species. *Glia* 62(10), 1671-86.

Flesich H (2002) Development of bisphosphonates. *Breast Cancer Research* 4(1), 30-4.

Front D, Schneck SO, Frankel A, and Robinson E. (1979) Bone metastases and bone pain in breast cancer. Are they closely associated? *Journal of the American Medical Association* 242(16), 1747-1748.

Fujiki K, Aoki K, Marcián, Borák L, Hudieb M, Ohya K, Igarashi Y, and Wakabayashi N (2012) The influence of mechanical stimulation on osteoclast localization in the mouse maxilla: bone histomorphometry and finite element analysis. *Biomechanics and Modeling in Mechanobiology* 12(2), 325-33.

Garrett IR, Boyce BF, Oreffo ROC, Bonewald L, Poser J, and Mundy GR. (1990) Oxygen-derived free radicals stimulate osteoclastic bone resorption in rodent bone in vitro and in vivo. *Journal of Clinical Investigations* 85(3), 632-639.

Gartland A, Hipskind RA, Gallagher JA, and Bowler WB. (2001) Expression of a P2X7 receptor by a subpopulation of human osteoblasts. *Journal of Bone and Mineral Research* 16(5), 846-56.

Gartland A, Buckley KA, Bowler WB, and Gallagher JA. (2003a) Blockade of the pore-forming P2X7 receptor inhibits formation of multinucleated human osteoclasts in vitro. *Calcified Tissue International* 73(4), 361-69.

Gartland A, Buckley KA, HIpskind RA, Perry MJ, Tobias JH, Buell G, Chessell I, Bowler WB, and Gallagher JA. (2003b) Multinucleated osteoclast formation in vivo and in vitro by P2X7 receptor-deficient mice. *Critical Reviews in Eukaryotic Gene Expression.* 13(2-4), 243-53.

Greig AVH, Linge C, Healy V, Lim P, Clayton E, Rustin MHA, McGrouther DA, and Burnstock G. (2003). Exoression of purinergic receptors in non-melanoma skin cancers and their functional roles in A431 cells. *The Journal of Investigative Dermatology*, 121(2), 315-27.

Guise T, and Mundy G. (1998) Cancer and bone. *Endocrine Reviews,* 19(1), 18-54.

Guise T (2010) Examining the metastatic niche: Targeting the microenvironment. *Seminars in Oncology*, 37 Suppl2 (5), S2-14.

Ha H, Kwak HB, Lee SW, Jin HM, Kim H-M, Kim H-H, and Lee ZH (2004) Reactive oxygen species mediate RANK signalling in osteoclasts. *Experimental Cell Research,* 301(2), 119-127.

Hanahan D and Weinberg RA (2011) Hallmarks of Cancer: The Next Generation. *Cell,* 144(5), 646-74.

Hansen RR, Nielsen CK, Nasser A, Thomsen SIM, Eghorn LF, Pham Y, Schulenberg C, Syberg S, Ding M, Stojilkovic SS, Jorgensen NR, and Heegaard A-M (2011) P2X7 receptor-deficient mice are susceptible to bone cancer pain. *Pain,* 152(8), 1766-76.

Hendrix MJ, Seftor EA, Seftor RE, Gardner LM, Boldt HC, Meyer M, Pe'er J, and Folberg R. (1998) Biologic determinants of uveak mekanoma metastatic phenotype: role of intermediate filaments as predictive markers. *Lab Investigation* 78(2), 153-63.

Heppner GH, Miller FR, and Shekhar PVM (2000) Nontransgenic models of breast cancer. *Breast Cancer Research,* 2, 331-34.

Hill PA, Murphy G, Docherty AJP, Hembry RM, Millican TA, Reynolds JJ, and Meikle MC. (1994) The effects of selective inhibitors of matrix metalloproteinases (MMPs) on bone resorption and the identification of MMPs and TIMP-1 in isolated osteoclasts. *Journal of Cell Science,* 107(1), 3055-3064

Hoebertz A, Townsend-Nicholson A, Glass R, Burnstock G, and Arnett TR. (2000) Expression of P2 receptors in bone and cultured bone cells. *Bone,* 27(4)m 503-10.

Holguin N, Brodt MD, Sanchez ME, Kotiya AA, and Silva MJ. (2013) Adaptation of tibial structure and strength to axial compression depends on loading history in both C57BL.6 and BALB/c mice. *Calcified Tissue International,* 93(3), 211-21.

Humphreys BD, Rice J, Kertesy SB, and Dubyak GR (2000) Stress-activated protein kinase/JNK activation and apoptotic induction by the macrophage P2X7 nucleotide receptor.*Journal of Biological Chemistry,* 275(35), 26792-798.

Hwang YS, Ma G-T, Park K-K, and Chung W-Y (2014) Lysophosphatidic acid stimulates osteoclast fusion through OC-STAMP and P2X7 receptor signaling. *Journal of Bone and Mineral Metabolism,* 32(2), 110-22.

Iotsova V, Caamaño J, Loy J, Yang Y, Lewin A, and Bravo R. (1997) Osteopetrosis in mice lacking NF-κB1 and NF-κB2. *Nature Medicine,* 3(11), 1285-89.

Israel O, Lubushitzky R, Frenkel A, Iosilevsky G, Bettman L, Gips S, Hardoff R, Baron E, Barzilai D, Kolodny GM, and Front D. (1994) Bone turnover in cotical and trevacular bone in normal women and in women with osteoporosis. *Journal of Nuclear Medicine*, 35(7), 1155-58.

Iturbide A, García de Herreros A, and Peiró S. (2015) A new role for LOX and LOXL2 proteins in transcription regulation. *FEBS Journal* 282(9), 1768-73.

Janssens R, and Boeynaems J. (2001) Effects of extracellular nucleotides and nucleosides on prostate carcinoma cells. *British Journal of Pharmacology,* 132(2), 536-46.

Jee WSS, and Ma YF. (1997) The in vivo anabolic actions of prostaglandins in bone. *Bone,* 21(4), 294-304.

Jelassi B, Chantôme A, Alcarez-Pérez F, Baroja-Mazo A, Cayuela ML, Pelegrin P, Suprenant A, and Roger S. (2011) P2X7 receptor activation enhances SK3 channels- and cysteine cathepsin-dependent cancer cells invasiveness. *Oncogene*, 30(18), 2108-22.

Joo YN, Jin H, Eun SY, Park SQ, Chang KC, and Kim HJ. (2014) $P2Y_2R$ activation by nucleotides released from the highly metastatic breast cancer cell contributes to pre-metastatic niche formation by mediating lysyl oxidase secretion, collagen crosslinking, and monocyte recruitment. *Oncotarget,* 5(19), 9322-34.

Jørgensen NR, Henriksen Z, Sørensen OH, Eriksen EF, Civitelli R, and Steinberg TH. (2002) Intercellular calcium signaling occurs between human osteoblasts and osteoclasts and requires activation of osteoclast P2X7 receptors. *The Journal of Biological Chemistry* 277(9), 7574-7580.

Kagan HM, and Li W (2003) Lysyl oxidase: properties, specificity, and biological roles inside and outside of the cell. *Journal of Cellular Biochemistry*, 88(4), 660-72.

Kaplan RN, Riba, RD, Zacharoulis S, Bramley AH, Vincent L, Costa C, MacDonald DD, Jin DK, Shido K, Kerns SA, Zhu Z, Hicklin D, Wu Y, Port JL, Altorki N, Port ER, Ruggero D, Shmelkov SV, Jensen KK, Rafii S, and Lyden D. (2005) *Nature,* 438(7069), 820-7.

Kaplan RN, Psaila B, and Lyden D. (2006) Bone marrow cells in the 'pre-metastatic niche': within bone and beyond. *Cancer Metastasis Reviews,* 25(4), 521-29.

Ke HZ, Qi H, Weidema F, Zhang Q, Panupinthu N, Crawford DT, Grasser WA, Paralkar VM, Li M, Audoly LP, Gabel CA, Jee WSS, Dixon SJ, Sims SM, and Thompson DD. (2003) Deletion of the P2X7 nucleotide receptor reveals its regulatory roles in bone formation and resorption. *Molecular Endocrinology,* 17(7), 1356-67.

Ke HZ (2005) In vivo characterization of skeletal phenotype of genetically modified mice. *Journal of Bone and Mineral Metabolism,* 23(S1), 84-89.

Kirschmann DA, Seftor EA, Fong SFT, Nieva DRC, Sullivan CM, Edwards EM, Sommer P, Csiszar K, and Hendrix MJC. (2002) A molecular role for lysyl oxidase in breast cancer invasion. *Cancer Research,* 62(15), 4478-83.

Knott L, and Bailey AJ. (1998) Collagen cross-links in mineralizing tissues: a review of their chemistry, function, and clinical relevance. *Bone,* 22(3), 181-87.

Korcok J, Raimundo LN, Ke HZ, Sims SM, and Dixon SJ. (2004) Extracellular nucleotides act through P2X7 receptors to activate NF-κB in osteoclasts. *Journal of Bone and Mineral Research,* 19(4), 642-51.

Kramer I, Halleux C, Keller H, Pegurri M, Gooi JH, Weber PB, Feng JQ, Bonewald LF, and Kneissel M. (2010) Osteocyte Wnt/β-catenin signaling is required for normal bone homeostasis. *Molecular and Cellular Biology*, 30(12), 3071-85.

Kurata K, Uemura T, Nemoto A, Tateishi T, Murakami T, Higaki H, Miura H, and Iwamoto Y. (2001) Mechanical strain effect of bone-resorbing activity and messenger RNA expressions of marker enzymes in isolated osteoclast culture. *Journal of Bone and Mineral Research,* 16(4), 722-30.

Lazarus HM, Cruikshank WW, Narasimhan N, Kagan HM, and Center DM (1994) Induction of human monocyte motility by lysyl oxidase. *Matrix Biology*, 14(9), 727-31

Lenertz LY, Gavala ML, Hill LM, and Berties PJ (2009). Cell signaling via the P2X7 nucleotide receptor: linkage to ROS production, gene transcription, and receptor trafficking. *Purinergic Signalling*, 5(2), 175-87.

Li J, Liu D, Ke HZ, Duncan RL, and Turner CH. (2005) The P2X7 nucleotide receptor mediates skeletal mechanotransduction. *The Journal of Biological Chemistry,* 250(52), 42952-9.

Li S, Peng Y, Weinhandl ED, Blaes AH, Cetin K, Chia VM, Stryker S, Pinzone JJ, Acquavella JF, and Arneson TJ. (2012) Estimated number of prevalent cases of metastatic bone disease in the US adult population. *Clinical Epidemiology,* 4(1), 87-93.

Li W, Nellaiappan K, Strassmaier T, Graham L, Thomas KM, and Kagan HM. (1997) Localization and activity of lysyl oxidase within the nuclei of fibrogenic cells. *Proceedings of the national Academy of Sciences of the United Stated of America.* 94(24), 12817-822.

Luo J, Sharma N, Seftor EA, De Larco J, Heidger PM, Hendrix MJC, and Lubaroff DM. (1997) Heterogenous expression of invasive and metastatic properties in a prostate tumour model. *Pathology Oncology Research,* 3(4), 264-71.

Mackenzie AB, Young MT, Adinolfi E, and Suprenant A. (2005) Pseudoapoptosis induced by brief activation of ATP-gated P2X7 receptors. *The Journal of Biological Chemistry*, 280(40, 33968-76.

Meakin LB, Price JS, and Lanyon LE. (2014) The contribution of experimental in vivo models to understanding the mechanisms of adaptation to mechanical loading in bone. *Frontiers in Endocrinology*, 5, 154.

Mercadante, S. (1997) Malignant bone pain: pathophysiology and treatment. *Pain,* 69 (1-2), 1-18.

Miller FR, Miller BE, and Heppner GH. (1983) Characterization of metastatic heterogeneity among subpopulations of a single mouse mammary tumour: heterogeneity in phenotypic stability. *Invasion Metastasis,* 3(1), 22-31.

Mitra SK, and Schlaepfer DD. (2006) Integrin-regulated FAK-Src signaling in normal and cancer cells. *Current Opinions in Cell Biology,* 18(5), 516-23.

Miyamoto T, Arai F, Ohneda O, Takagi K, Anderson DM, and Suda T. (2000) An adherent condition is required for formation of multinuclear osteoclasts in the presence of macrophage colony-stimulating factor and receptor activator of nuclear factor κB ligand. *Blood,* 96, 4335-43.

Molnar J, Fong KS, He QP, Hayashi K, Kim Y, Fong SF, Fogelgren B, Szauter KM, Mink M, and Csiszar K. (2003) Structural and functional diversity of lysyl oxidase and the LOX-like proteins. *Biochimica et biophysica acta,* 1647(1-2), 220-24.

Naemsch LN, Dixon SJ, and Sims SM. (2001) Activity-dependent development of P2X7 current and Ca^{2+} entry in rabbit osteoclasts. *The Journal of Biological Chemistry,* 276(42), 39107-114.

Nguyen DX, Bos PD, and Massagué J. (2009) Metastasis: from dissemination to organ-specific colonization. *Nature Reviews. Cancer,* 9(4), 274-84.

Nicke A, Kuan Y-H, Masin M, Rettinger J, Marquez-Klaka B, Bender O, Górecki DC, Murrell-Lagnado RD, and Soto F. (2009) A functional P2X7 splice variant with an alternative transmembrane domain 1 escaped gene inactivation in P2X7 knock-out mice. *The Journal of Biological Chemistry,* 284(38), 25813-22.

Norrdin RW, Jee WS, and High WB. (1990) The role of prostaglandins in bone in vivo. *Prostaglandins Lekot Essent Fatty Acids,* 41(3), 139-49.

North AR (2002) Molecular physiology of P2X receptors. *Physiological Reviews,* 82(4), 1013-67.

Orriss IR, Knight GE, Ranasinghe S, Burnstock G, and Arnett TR. (2006) Osteoblast responses to nucleotides increase during differentiation. *Bone,* 39(2), 300-09.

Orriss I, Syberg S, Wang N, Robaye B, Gartland A, Jorgensen N, Arnett T, and Boeynaems J-M. (2011) Bone phenotypes displayed by P2 receptor knockout mice. *Frontiers in Bioscience*, 1046, 1038-46.

Orriss IR, Key ML, Hajjawi MOR, and Arnett TR. (2013) Extracellular ATP released by osteoblasts is a key local inhibitor of bone mineralisation. *PLoS ONE,* 8(7), 1-13.

Oxlund H, Barckman M, Ørtoft G, and Andreassen TT. (1995) Reduced concentrations of collagen cross-links are associated with reduced strength of bone. *Bone,* 17(4), 365-371

Paddison PJ, Caudy AA, Bernstein E, Hannon GJ, and Conklin DS. (2015) Short hairpin RNAs (shRNAs) induce sequence-specific silencing in mammalian cells. *Genes and Development,* 16, 949-58.

Panchenko MV, Stetier-Stevenson WG, Trubetskoy OV, Gacheru SN, and Kagan HM (1996). Metalloproteinase activity secreted by fribrinogenic cells in the processing of prolysyl oxidase. *The Journal of Biological Chemistry* 271(12), 7113-19.

Panupinthu N, Zhao L, Possmayer F, Ke HZ, Sims SM, and Dixon SJ. (2007) P2X7 nucleotide receptors mediate blebbing in osteoblasts through a pathway involving lysophosphatidic acid. *The Journal of Biological Chemistry,* 282(5), 3403-12.

Panupinthu N, Rogers JT, Zhao L, Solano-Flores LP, Possmayer F, Sims SM, and Dixon SJ. (2008) P2X7 receptors on osteoblasts couple to production of lysophosphatidic acid: a signalin axis promoting osteogenesis. *The Journal of Cell Biology* 181(5), 859-71.

Peinado H, Lavotshkin S, and Lyden D. (2011) The secreted factors responsible for pre-metastatic niche formation: old sayings and new thoughts. *Seminars in Cancer Biology,* 21(2), 139-46.

Pellegatti P, Falzoni S, Donvito G, Lemaire I, and Di Virgilio F. (2011) P2X7 receptor drives osteoclast fusion by increasing the extracellular adenosine concentration. *The FASEB Journal,* 25(4), 1264-74.

Plunkett TA, Smith P, and Rubens RD. (2000) Risk of complications from bone metastases in breast cancer. Implications for management. *European Journal of Cancer,* 36(4), 476-82.

Psaila B and Lyden D. (2009) The metastatic niche: adapting the foreign soil. *Nature Reviews. Cancer,* 9(4), 285-93.

Rajkumar SV, Dimopolous MA, Palumbo A, Blade K, Merlini G, Mateos M-V, Kumar S, Hillengass J, Kastritis E, Richardson P, Landgren O, Paiva B, Dispenzieri A, Weiss B, Leleu X, Zweegman S, Lonial S, Rosinol L, Zamagni E, Jagannath S, Sezer O, Kristinsson SY, Usmani SZ, Lahuerta JJ, Johnsen HE, Beksac M, Cavo M, Golschmidt H, Terpos E, Kyle RA, Anderson KC, Durie BGM, and San Miguel JF. (2014) International myeloma working group updates criteria for the diagnosis of multiple myeloma. *The Lancet Oncology,* 15(12), e538-48.

Ralevic V, and Burnstock G. (1998) Receptors for purines and pyrimidines. *Pharmacological reviews,* 50(3), 413-92.

Rao DD, Senzer N, Cleary MA, and Nemunaitis J. (2009) Comparative assessment of siRNA and shRNA off target effects: what is slowing clinical development. *Cancer Gene Therapy,* 16(11), 807-09.

Rassendren F, Buell GN, Virginio C, Collo G, North RA, and Suprenant A. (1997) The permeabilizing ATP receptor, P2X7. *The Journal of Biological Chemistry,* 272(9), 5482-86.

Robling AG and Turner CH (2002) Mechanotransduction in bone: Genetic effects on mechanosensitivity in mice. *Bone,* 31(5), 562-69.

Rock CL, Doyle C, Demark-Wahnefried W, Meyerhardt J, Courneya KS, Schwartz AL, Bandera EV, Hamilton KK, Grant B, McCullough M, Byers T, and Gansler T. (2012) Nutrition and physical activity guidelines for cancer survivors. *CA: A Cancer Journal for Clinicians,* 62(2), 243-74.

Roger S, Jelassi B, Couillin I, Pelegrin P, Besson P, and Jiang L-H. (2014) Understanding the rols of the P2X7 receptor in solid tumour progression and therapeutic perspectives. *Biochimica et Biophysica Acta,* 1848(10), 2584-602.

Romanello M, Pani B, Bicego M, and D'Andrea P. (2001) Mechanically induced ATP release from human octeoblastic cells. *Biochemical and biophysical research communications,* 289(5), 1275-81.

Romanello M, Codognotto A, Bicego M, Pines A, Tell G, and D'Andrea P. (2005). Autocrine/paracrine stimulation of purinergic receptors in osteoblasts: Contribution of vesicular ATP release. *Bicohemical and biophysical research communications,* 331(4), 1429-38.

Roodman GD. (2004) Mechanisms of disease: Mechanisms of bone metastasis. *The New England Journal of Medicine,* 350(16), 1655-64.

Rosen C. (2013) Primer on the metabolic bone diseases and disorders of mineral metabolism. *Annals of the rheumatic diseases,* 53(3), 0-1071.

Rubin J, Fan X, Biskobing DM, Taylor WR, and Rubin CT. (1999) Osteoclastogenesis is repressed by mechanical strain in an in vitro model. *Journal of Orthopaedic Research, 17(*25), 639-45.

Ruff C, Holt B, and Trinkaus E. (2006) Who's afraid of the bid bag Wolff? "Wolff's Law" and bone functional adaptation. *American Journal of Physical Anthropology,* 498, 484-98.

Rumney RMH, Agrawal A, Shah K, and Gartland A. (2011) Frontiers: Fluid flow stimulates ATP release form human derived osteoclasts without changing resorption: *Proceedings of the 2011 Joint Meeting of the Bone Research Society and The British Research Society.*

Sato T, Forged NT, and Delaissé J-M (1998) The migration of purified osteoclasts trough collagen is inhibited by matrix metalloproteinase inhibitors. *Journal of Bone and Mineral Research*, 13(1), 59-66.

Schäfer R, Sedehizade F, Welte T, and Resier G. (2003) ATP- and UTP-activated P2Y receptors differently regulate proliferation of human lung epithelial tumor cells. *American Journal of Physiology. Lung Cellular and Molecular Physiology.* 285(2), L376-85.

Scheuer L and Black S (eds) (2004) *The Juvenile Skeleton* 1st ed., Bodmin, Cornwall. Elsevier.

Schmitz KH, Courneya KS, Matthews C, Demark-Wahnefried W, Galvão DA, Pinto BM, Irwin ML, Wolin KY, Segal RJ, Lucia A, Schneider CM, von Gruenigen VE, and Schwartz AL. (2010) American college of sports medicine roundtable on exercise guidelines for cancer survivors. *Medicine and Science in Sports and Exercise*. 42(7), 1409-26.

Schneider G, Voltz R, and Gaertner J (2012) Cancer pain management and bone metastases: AN update for the clinician. *Breast Care*, 7(2), 113-20.

Serrano M, Lin AW, McCurrach ME, Beach D, and Lowe SW. (1997) Oncogenic ras provokes premature cell senescence associated with accumulation of p53 and $p16^{INK4a}$. *Cell,* 88(5), 593-602.

Silva BC and Bilezikian JP (2015) Parathyroid hormone: anabolic and catabolic action on the skeleton. *Current Opinion in Pharmacology,* 22, 41-50.

Sim JA, Young MT, Sung H-Y, North RA, and Suprenant A. (2004) Reanalysis of P2X7 receptor expression in rodent brain. *The Journal of Neuroscience* 24(28), 6307-14.

Simonet WS, Lacey DL, Dunstan CR, Kelley M, Chang M-S, Lüthy R, Nguyen HQ, Wooden S, Bennett L, Boone T, Shimamoto G, DeRose M, Elliott R, Colombero A, Tan H-L, Trail G, Sullivan G, Davy E, Bucay N, Renshaw-Gegg L, Hughes TM, Hill D, Pattison W, Campbell P, Sander S, Van G, Tarpley J, Derby P, Lee R, Amgen EST Program, and Boyle WJ. (1997) Osteoprotegerin: A novel secreted protein involved in the regulation of bone density. *Cell,* 89(2). 309-19.

Singh VA, Haseeb A, and Alkubaisi AAHA. (2014) Incidence and outcome of bone metastatic disease at University Malaya Medical Centre. *Singapore Medical Journal,* 55(10), 539-546.

Slater M, Danieletto S, Pooley M, The LC, Gidley-Baird A, and Barden JA. (2004) Differentiation between the cancerous and normal hyperplastic lobules in breast lesions. *Breast Cancer Research and Treatment*, 83(1), 1-10.

Solle M, Labasi J, Perregaux DG, Stam R, Petrushova N, Koller BH, Griffiths RJ, and Gabel CA. (2001) Altered cytokine production in mice lacking P2X7 receptors. *The Journal of Biological Chemistry,* 276(1), 125-132.

Spessotto P, Rossi FM, Degan M, Di Francia R, Perris R, Colombatti A, and Gattei V. (2002) Hyaluranon-CD44 interaction hampers migration of osteoclast-like cells by down-regulating MMP-9. *Journal of Cell Biology,* 158(6), 1133-44.

Sugiyama T, Price JS, and Lanyon LE. (2010) Functional adaptation to mechanical loading in both cortical and cancellous bone is controlled locally and is confined to the loaded bones. *Bone,* 46(2), 314-21.

Sun J, Liu X, Tong J, Sun L, Xu H, Shi L, and Zhang J. (2014) Fluid sheer stress induces calcium transients in osteoblasts through depolarization of osteoblastic membrane. *Journal of Biomechanics,* 47(16), 3903-08.

Syberg S, Petersen S, Jensen J-E B, Gartland A, Teilmann J, Chessell I, Steinberg TH, Schwarz P, and Jørgensen NR. (2012) Genetic background strongly influences the bone phenotype of P2X7 receptor knockout mice. *Journal of Osteoporosis, 2012, 1-9.*

Tafani M, Schito L, Pellegrini L, Villanova L, Marfe G, Anwar T, Rosa R, Indelicato M, Fini M, Pucci B, and Russo MA. (2011) Hypoxia-increased RAGE and P2X7R expression regulates tumor cell invasion through phosphorylation of Erk1/2 and Akt and nuclear translocation of NF-κB. *Carcinogenesis,* 32(8), 1175-2011.

Takayanagi H, Kim S, Koga T, Nishina H, Isshiki M, Yoshida H, Saiura A, Isove M, Yokochi T, Inoue J, Wagner EF, Mak TW, Kodama T, and Taniguchi T. (2002) Induction and activation of the transcription factor NFATc1 (NFAT2) integrate RANKL signalling in terminal differentiation of osteoclasts. *Developmental Cell,* 3(6), 889-901.

Tao K, Fang M, Alroy J, and Sahagian GG. (2008) Imagable 4T1 model for the study of late stage breast cancer. *BMC Cancer,* 8(228), 1-19.

Taylor MA, Amin JD, Kirschmann DA, and Schiemann WP. (2011) Lysyl oxidase contributes to mechanotransduction-mediated regulation of transforming growth factor-β signaling in breast cancer cells. *Neoplasia,* 13(5), 406-18.

Van Oers RFM, Ruimerman R, Tanck E, Hilbers PAJ, and Huiskes R. (2008) A unified theory of osteonal and hemi-osteonal remodelling. *Bone,* 42(2), 250-59.

Virk MS, and Lieberman JR (2007) Tumor metastasis to bone. *Arthritis Research and Therapy,* 9(Suppl1), S5.

Vora SR, Palamakumbura AH, Mitsi M, Guo Y, Pischon N, Nugent MA, and Trackman PC. (2009) Lysyl oxidase propeptide inhibits FGF-2-induced signaling and proliferation of osteoblasts. *The Journal of Biological Chemistry,* 285(10), 7384-93.

Wang N, Robaye B, Agrawal A, Skerry TM, Boeynaems J-M, and Gartland A. (2012) Reduced bone turnover in mice lacking the P2Y(13) receptor of ADP. *Molecular Endocrinology,* 26(1), 142-52.

Wang N, Rumney RMH, Yang L, Robaye B, Boeynaems J-M, Skerry TM, and Gartland A. (2013) The $P2Y_{13}$ receptor regulates extracellular ATP metabolism and the osteogenic response to mechanical loading. *Journal of Bone and Mineral Research,* 28(6), 1446-56.

Wang Q, Wang L, Feng Y-H, Li X, Zeng R, and Gorodeski GI. (2004) P2X7 receptor-mediated apoptosis of human cervical epithelial cells. *Am J Physiol Cell Physiol,* 287(5), 1349-58.

Wang SX, Mure M, Medzihtadsxky KF, Burlingame AL, Brown DE, Dooley DM, Smith AJ, Kagan HM, and Klinman JP. (1996) A crosslinked cofactor in lysyl oxidase: redox function for amino acid side chains. *Science,* 273(5278), 1078-84.

Weigelt B, Peterse JL, van't Verr LJ. (2005) Breast cancer metastasis: markers and models. *Nature Reviews. Cancer*, 5(8), 591-602.

White N and Burnstock G. (2006) P2 receptors and cancer. *Trends in Pharmacological Sciences,* 27(4), 211-7.

White N, Butler PEM, and Burnstock G. (2005) Human melanomas express functional P2X7 receptors. *Cell and tissue research,* 321(3), 411-8.

Wiel C, Augert A, Vincent DF, Gitenay D, Vindrieux D, Le Calvé B, Arfi V, Lallet-Daher H, Reynaud C, Treilleux I, Bartholin L, Lelievre E, and Bernard D. (2013) Lysyl oxidase activity regulates oncogenic stress response and tumorigenesis. *Cell Death and Disease,* 4, e855.

Willie BM, Birkhold AI, Razi H, Thiele T, Aido M, Kruck B, Schill A, Checa S, Main RP, and Duda GN. (2013) Diminished response to in vivo mechanical loading in trabecular and not cortical bone in adulthood of female C57BL/6 mice coincides with a reduction in deformation to load. *Bone,* 55(2), 335-46.

Willingham MD, Brodt MD, Lee KL, Stephens AL, Ye J, and Silva MJ. (2010) Age-related changes in bone structure and strength in female and male BALB/c mice. *Calcified Tissue International,* 86(6), 470-83.

Wong CC, Gilkes DM, Zhang H, Chen J, Wei H, Chaturvedi P, Fraley SI, Wong C-M, Khoo U-S, Ng IO, Wirtz D, and Semenza GL. (2011) Hypoxia-inducible factor 1 is a master regulator of breast cancer metastatic niche formation. *Proceedings of the National Academy of Sciences of the United States of America,* 108(39), 16369-74.

Wong MHF, Stockler MR, Pavlakis N. (2012) Bisphosphonates and other bone agents for breast cancer (review). *Cochrane Database Syst Rev,* 2(2), 1-140.

Xia J, Yu X, Tang L, Li G, and He T. (2015) P2X7 receptor stimulates breast cancer cell invasion and migration via the AKT pathway. *Oncology Reports,* 34(1), 103-110.

Xu X-Y, Guo C, Yan Y-X, Guo Y, Li R-X, Song M, and Zhang X-Z. (2012) Differential effects of mechanical strain on osteoclastogenesis and osteoclast-related gene expression in RAW264.7 cells. *Molecular Medicine Reports,* 6(2), 409-15.

Yasuda H, Shima N, Nakagawa N, Yamaguchi K, Kinosaki M, Mochizuki S-I, Tomoyasu A, Yano K, Goto M, Murakami A, Tsua E, Morinaga T, Higashio K, Udagawa N, Takahashi N, and Suda T. (1998) Osteoclast differentiation factor is a ligand for osteoprotegerin/osteoclastogenesis-inhibitory factor and is identical to TRANCE/RANKL. *Proceedings of the National Academy of Sciences of the United States of America,* 95(7), 3597-602,

Zheng L-M, Zychlinksy A, Liu C-C, Ojcius DM, and Young JD. (1991) Extracellular ATP as a trigger for apoptosis or programmed cell death. *The Journal of Cell Biology,* 112(20), 279-88.